Petrology, Geochemistry, and Geochronology of the Pikoo Kimberlites, Saskatchewan

by

Denelle Smyth

A thesis submitted in partial fulfillment of the requirements for the degree of

Master of Science

Department of Earth and Atmospheric Sciences

University of Alberta

Abstract

The Pikoo kimberlites of east-central Saskatchewan are a relatively recent discovery, comprising at least ten discreet bodies thought to erupt through the Sask Craton, a small Archean microcontinent enclosed within the Paleoproterozoic Trans-Hudson Orogen. Since the Sask Craton also plays host to the 70+ bodies of the diamondiferous Cretaceous Fort à la Corne kimberlites, which are among the largest kimberlites in the world, significant interest lay in unraveling the genesis of the Pikoo bodies. This study presents the first detailed examination of the petrology and geochronology of the Pikoo kimberlites. A combination of detailed petrography, major and minor element chemistry analyzed by EPMA, and trace element determinations measured via LA-ICP-MS was employed to characterize the Pikoo samples as archetypal coherent (hypabyssal) kimberlite. Traditional criteria for diamond preservation potential were applied to the Pikoo ilmenite by assessing their Fe_2O_3 and MgO contents. The results indicated high MgO and low Fe_2O_3 within the grain interiors and rims with elevated MgO and MnO in PK150, PK151, PK314, and variably in PK312. The high-Fe mineral compositions of PK346 contradict the trends of the other intrusions, suggesting PK346 formed from an oxidized, high-carbonate late pulse of previously fractionated magma. The differences in magma evolution can explain the striking petrographic and chemical distinctions highlighted between the two most significant intrusions of PK150 and PK346, as well as the notably less favourable microdiamond results North Arrow reported for PK346. A robust U-Pb age of 417 ± 14 Ma was determined from PK150 perovskite analyzed *in situ* via LA-ICP-MS. The data were processed using two approaches to confirm the perovskite represented a single population with a uniform common Pb composition. This age is distinctly different from the nearby FALC kimberlites but overlaps with occurrences in the Slave Craton, the United States, Russia, and Namibia. This

may suggest more widespread diamond-bearing kimberlite activity in circa Silurian times. Tracer isotopes were also measured in situ via LA-MC-ICP-MS on PK150 perovskite. The dominant range in εNd_i (+1.8 to -2.0) is near chondritic, suggesting a deep mantle source isolated from contamination.

Acknowledgments

First, I would like to thank Drs Graham Pearson and Larry Heaman. I appreciate that you would always make time for my questions and confusion through undergrad and grad school, your clarifications were always both illuminating and succinct. I would also like to thank Ken Armstrong and Barb Kupsch of North Arrow Minerals for providing the samples (without which this project would not have been possible), details on the geologic context, and impressions of the core. Funding for this project was provided by an NSERC CREATE grant for the Diamond Exploration and Research Training School, which is kept running smoothly by the multi-talented Anetta Banas. Thanks to Dr. Andrew Locock for the reassuring consistency he brought to each EPMA session, Dr. Yan Luo for her infinite patience in helping me not break the LA-ICP-MS, and Dr. Steven Creighton of the Saskatchewan Research Council for graciously offering me the use of their EPMA in my time of need. I would also like to thank Dr. Bruce Kjarsgaard of the Geological Survey of Canada for his invaluable insights on the intricacies of kimberlite. An especially large thanks to Dr. Chiranjeeb Sarkar for his help in extracting precious data from perovskite and for the in-depth discussions of methodology.

Thanks to my friends (Ebberly, Sasiri, Jared, Mike (& Angie), Alix, Calla, Maya, and Brette) who have gone through school with me since undergrad and still think rocks are cool. Ebberly and Sasiri are especially thanked for providing wonderful entertainment for the third floor, particularly with their office hockey extravaganzas. Thank you to my roommate Carl for having a Friends quote for every occasion, for being a true friend himself, and for trying to bring me Gatorade when I got sick. A special thanks to Matt Hardman for being the most encouraging and reassuring sounding board for strange data, an exceptional Pokémon trainer, and most importantly, the best friend anyone could ask for. Thanks to Flapjacks, the fluffy white stuffed

rabbit, for being an excellent listener to concepts I needed to work through. Lastly, I would like to thank Matt Wudrick for too many things to list. University would not have been the same without you.

Table of Contents

List of Tables

List of Figures

List of Abbreviations and Symbols

~	Approximately
σ	Sigma or one standard deviation unit from the mean
amu	Atomic mass unit
BSE	Backscatter electron
ca.	Circa
cf.	*Confer/Conferatur* (Latin, meaning "compare")
C.I.	Clement's Contamination index
CHUR	Chondritic uniform reservoir
cm	Centimeter
cpht	Carats per hundred tonnes
e.g.	For example
EDS	Energy dispersive spectroscopy
EPMA	Electron probe microanalyzer
FALC	Fort à la Corne
Ga	Giga-annum, billion years
Gyr	Billions of years
HFSE	High field strength element
Hz	Hertz
i.e.	That is
kg	Kilogram
km	Kilometer
kv	Kilovolt
KIMs	Kimberlite indicator minerals
J/cm^2	Joules per centimeter squared
LA-ICP-MS	Laser ablation inductively coupled mass spectrometry

LOD	Limit of detection
LOI	Loss on ignition
ln	Natural log
m	Meter
Ma	Mega-annum, million years
MC-ICP-MS	Multi-collector inductively coupled mass spectrometry
mJ	Millijoule
mm	Millimeter
Mg#	Magnesium number, 100Mg/(Mg+Fe)
MORB	Mid-ocean ridge basalt
MUM	Magnesian ulvöspinel—ulvöspinel—magnetite
nA	Nanoamp
OIB	Oceanic Island Basalt
PPL	Plain polarized light
REE	Rare earth element
RSD	Relative standard deviation
s	Second
SEM	Scanning electron microscope
SRC	Saskatchewan Research Council
THO	Trans-Hudson Orogen
TIMAC	Titanian magnesian aluminous chromite
µm	Micrometers
XRF	X-ray fluorescence

1 Introduction

1.1 Background

Kimberlites are small-volume, ultrabasic, volatile-rich (H_2O and CO_2), silica-undersaturated extrusive and intrusive igneous rocks that occur on cratons worldwide and typically exhibit a distinct inequigranular texture (Dawson, 1980; Clement et al., 1984; Mitchell, 1986, 2008; Scott Smith et al., 2018). In general, kimberlites are found in old cratonic regions with thick lithospheric roots. These complex rocks are of great economic interest as they, along with lamproites, serve as the principal mechanism for transporting diamonds from the lithospheric mantle to the surface. As few kimberlites are diamond-bearing, much emphasis is placed on characterising kimberlite discoveries in terms of their field occurrence, mineralogy, chemistry, and eruption history. This information is used to construct genetic models to aid in understanding the economic potential of the various bodies that comprise a field.

Alluvial diamonds had been recovered prior to identification of their source. The first discovery of a kimberlite – the most common host for diamond – occurred in the Kimberley region of South Africa in 1869, from which the name 'kimberlite' was derived. A rush of kimberlite discoveries in the surrounding areas followed and the profusion of southern African kimberlites profoundly shaped the classification of kimberlites, pipe models, and the understanding of geochemical trends associated with economically-promising deposits. This knowledge was applied to subsequent discoveries worldwide for many decades. Early studies (e.g., Wagner, 1914; Williams, 1932) included comprehensive petrographic descriptions of various types of kimberlite that proved influential, paving the way for future considerations of the genesis and evolution of kimberlites (e.g., Dawson, 1962; Hawthorne, 1975). With the

discovery of diverse kimberlite localities and new textural-genetic types of kimberlite in Canada (Field and Scott Smith, 1999), it was recognized that existing terminology established from South African kimberlites could not be adequately applied to all kimberlites without first tailoring the methodologies to each unique occurrence. As the diversity of kimberlite occurrences was realized, a significant challenge arose in effectively communicating the characterization of kimberlites and comparing the economic potential of one body to another in a manner that is consistent with general volcanology terms while also conveying the unique nature of kimberlite rocks. As such, considerable effort has been dedicated to aligning the nomenclature and classification criteria to be useful across industry and academia (e.g., Field and Scott Smith, 1998; Cas et al., 2008a, 2009; Scott Smith et al., 2013; Scott Smith et al., 2018).

Studying kimberlites is difficult not only due to inconsistent terminology but also because of the incredibly diverse nature of the rocks themselves. Kimberlite magma can interact with and entrain fragments of the crust and mantle, which complicates the interpretation of the compositional features of the magma source. Methods have been developed to quantify the degree of contamination in kimberlite by crustal material (Clement, 1982) but the counteracting effects of mantle contaminants (e.g., cratonic peridotite) to typical silicic crustal material is problematic in detecting crustal addition in kimberlites with high peridotite input (Kjarsgaard et al., 2009b). Unraveling the genetic history of kimberlites is also complicated by the hybrid nature of these rocks as they contain primary magmatic material, mantle-derived xenoliths and xenocrysts that may appear similar to phenocrystic kimberlitic components, and country rock fragments (Mitchell, 1986).

Olivine is particularly problematic for kimberlite petrologists. Historically, grain size and morphology were used to distinguish the petrogenetic origin of olivine: phenocrystic olivine

is typically fine- to medium-grained and euhedral to subhedral in shape while xenocrystic olivines are commonly medium- to coarse-grained, rounded disaggregated components of peridotite entrained by the kimberlite, usually referred to as 'macrocrysts' (e.g., Skinner and Clement, 1979; Clement et al., 1984; Mitchell, 1986, 2008). Traditionally, it was considered that ~ 25 vol% of olivine in any given kimberlite crystallizes directly from the kimberlite magma during ascent (Clement, 1982; Harris et al., 2004; Mitchell, 2008). Brett et al. (2009) asserted that this percentage is significantly lower (≤ 5 vol%), implying that kimberlite is dominated by xenocrystic mantle olivine. Recent studies have demonstrated that size and morphology alone are insufficient to differentiate between primary and xenocrystic olivine as many grains exhibit a distinctive core-rim relationship, representing phenocrystic overgrowth on a xenocrystic core (Bussweiler et al., 2015). A positive correlation has also been drawn between olivine and diamond size distributions in kimberlite units, investigated due to their comparable specific gravities and thus the potential for hydraulic equivalence (Field et al., 2009), further emphasizing the need to understand the origin of olivine in kimberlite.

Perhaps the most significant obstacles to the investigation of new kimberlite discoveries is the alteration state of the primary mineral assemblage. Kimberlites can experience an exceptionally diverse array of alteration processes throughout transport and post-emplacement. Among the most common are serpentinization (which can occur in multiple forms) and carbonate replacement (which can impact significant portions of kimberlites with high volatile contents). Most kimberlites exhibit some degree of alteration, which may range in intensity from totally altered to relatively fresh. Understanding the original character of a kimberlite is important in order to construct reliable genetic models and to determine the mantle sources which were sampled by the kimberlite. Using this information, we can assess the diamond

potential of both the unaltered kimberlites and make comparisons with altered kimberlite. As the primary interest in kimberlites is their economic potential as assessed by their diamond populations, it is most important to be able to describe the features, textures, and components of kimberlites prior to alteration. Unfortunately, there is a large bias in the literature towards the description of fresh or moderately fresh kimberlite since it is understandably more straightforward to examine. Numerous examples of altered kimberlite exist but detailed studies into the characteristics of these intrusions are rarely published. However, altered kimberlites can yield a wealth of information pertaining to the nature of the kimberlite and perhaps even their economic potential. The initial discoveries of kimberlite material during exploration usually consist of kimberlite indicator minerals (KIMs) and the most-altered rocks, as fresh material typically occurs preferentially far beneath the surface. It is therefore important to recognize which exploration tools (textural, chemical, or petrologic) are most robust regardless of kimberlite alteration state, and which can consistently provide useful, accurate information.

As exploration programs involve significant capital investment, considerable effort has been devoted to developing methods of distinguishing kimberlite from similar rock types and differentiating economic from barren intrusions. Concentrate minerals are much easier and less expensive to collect than complete samples during exploration programs (e.g., from till samples), so discrimination methods using mineral chemistry have been developed for many of the major phases found in kimberlite. Such trends have been established for garnet (Grutter et al., 2003; Hardman et al., 2018), olivine (see above), Mg-ilmenite/picroilmenite (Gurney and Zweistra, 1995; Wyatt et al., 2004; Carmody et al., 2014), chromite (Nowicki et al., 2007), spinel group minerals (Mitchell., 1986), and phlogopite (Mitchell, 1995). Apatite has only recently been investigated as a potentially useful indicator in diamond exploration (Milligan, 2017); studies

have already shown that trace elements in apatite can have characteristics distinctive of the rocks they are derived from and can adequately distinguish economic igneous deposits (Belousova et al., 2002; Mao et al., 2016). The listed minerals can also be used to assess whether the host rock from which they were derived could be associated with diamond. Some of these discriminatory trends appear to be quite robust and are commonly used in diamond exploration (e.g. Grutter et al., 2003).

1.2 Projective Objectives – The Pikoo kimberlites, Saskatchewan, Canada

This study presents the first detailed petrologic investigation of the Pikoo kimberlites to assess their mineralogy, petrography, mineral chemistry, and geochronology using a variety of analytical techniques. The main objectives of this project can be summarized as 1) confirm the identification of the Pikoo bodies as true archetypal kimberlite, 2) characterize the eruption history of the Pikoo kimberlites in terms of magma source region and determine a relative emplacement age to a reasonable degree of uncertainty, and 3) trace magmatic evolution of the Pikoo kimberlites from magma generation to post-emplacement alteration. To achieve theses objectives, it was necessary to: make thorough descriptions of the mineral textures and relationships; characterize the mineral chemistry and compare it to recognized trends pertaining to kimberlites and similar rock types; and assess the robustness of exploration tools to extreme alteration.

2 Regional Geology

2.1 Trans-Hudson Orogen

The Trans-Hudson Orogen (THO) is one of several Proterozoic orogenic belts arising from the collision and amalgamation of Archean continental fragments and juvenile crust, making it an important component of the continental assembly of North America (Hoffman, 1988). This Himalayan-style belt (St-Onge et al., 2006; Weller and St-Onge, 2017) is continuous from South Dakota, U.S.A. through Saskatchewan and Manitoba, Canada and up to Greenland, marking a well-exposed continent-continent collision zone (Lucas et al., 1993; Lewry et al., 1994; Lucas et al., 1994). The THO *sensu stricto* is divided into four composite lithotectonic zones: the Thompson belt, Reindeer Zone, Wathaman-Chipewyan Batholith, and Cree Lake Zone (Lewry et al., 1994). Zircon U-Pb geochronology was applied extensively to the THO and its significant features (e.g. Ansdell and Norman, 1995; Ashton et al., 1999; Chiarenzelli et al., 1998; Heaman et al., 1992, 1993, 1994; Rayner et al., 2005), constraining its age to 1.8 – 1.9 Ga and peak metamorphism at ~ 1.8 Ga (Ansdell and Norman, 1995; Heaman et al., 1992; Rayner et al., 2005). The closing of the Manikewan Ocean between the Superior and Rae-Hearne provinces (Stauffer, 1984; Chiarenzelli et al., 1998) eventually led to the amalgamation of the Superior and Rae-Hearne cratons into the continent of Laurentia (Hoffman, 1988).

The LITHOPROBE project and later studies carried out extensive seismic work in the THO, elucidating the wide extent of buried Archean crust and highlighting a buried but distinct and "seismically transparent" structure beneath the THO, interpreted to be a microcontinent or craton fragment (Ansdell and Norman, 1995; Bank et al., 1998; Ellis et al., 1996; Hajnal et al., 2005; Hammer et al., 2011; Lewry et al., 1994; Lucas et al., 1993, 1994). This crustal-scale

domal culmination beneath the Glennie Domain (Lucas et al., 1993, 1994; Lewry et al., 1994) was dubbed the Sask Craton (Ansdell et al., 1995). It is now recognized that three major Archean blocks (the Superior, Rae-Hearne, and Sask cratons) were involved in the continental collision that formed the THO (Ashton et al., 2005; Hajnal et al., 2005; Mareschal et al., 2005). The presence of the Sask Craton prevented completed convergence, contributing to the preservation of an unusually large amount of juvenile oceanic material within the THO (Hajnal et al., 2005).

2.2 Sask Craton

Before the Sask Craton was officially recognized, the recovery of zircons from drill core with Proterozoic U-Pb ages but Archean Nd model ages provided evidence that widespread, reworked Archean crust underlaid the Glennie Domain (Collerson et al., 1989, 1990). Geophysical methods, including seismic reflection/refraction studies (Lucas et al., 1993; Ellis et al., 1996; Hajnal et al., 2005; Németh et al., 2005) were employed to estimate the extent of the Sask Craton at depth, with contribution from compositional studies of post-orogenic intrusions (Bickford et al., 2005). We are given insight into the Sask Craton by exposure through three tectonic windows – two in the Glennie Domain (the Nistowiak Lake and Hunter Bay windows; Chiarenzelli et al., 1998; Bickford et al., 2004) and one in the Flin Flon Domain (the Pelican Window; Ashton et al., 1999). As a largely buried Archean microcontinent, several Saskatchewan kimberlites are thought to erupt through the Sask Craton, including the Fort à la Corne (FALC) kimberlite field (Fig. 1a). Until recently, little was known about the crust-mantle boundary beneath the Sask Craton. Evidence gathered from teleseismic work could not identify an anomaly marking a boundary between the Superior/Hearne lithospheric roots from a Sask Craton mantle root (Bank et al., 1998) and later refraction profiles suggest that the Sask's

lithospheric root was either poorly developed, incorporated with the Hearne's root, or detached and recycled (Németh et al., 2005). Recently, Czas (2018a, b) examined mantle xenoliths from the Fort à la Corne kimberlites to asses the origin of the lithospheric mantle and metasomatic processes beneath the Sask Craton and concluded that whereas the crust contains Archean components, the lithospheric mantle underpinning the crust likely formed at ~ 2 Ga.

Several scenarios have been proposed regarding the origins of the Sask Craton. Chiarenzelli et al. (1998) proposed it is a rafted fragment from the bounding Superior and/or Hearne cratons at ca. 2.1 Ga, however, seismic data indicate that the Sask Craton is structurally isolated (e.g. Lewry et al., 1994). The Wyoming Craton has also been put forth as a potential parent block due to the similar elevated $^{206}Pb/^{204}Pb$ ratios and Sm-Nd isotopic signatures between it and the Sask Craton, characteristics which would be atypical of the Superior and Rae-Hearne cratons (Bickford et al., 2005 and references therein). Other authors suggest that the Sask Craton is unlikely to be a product of simple fragmentation from an adjacent Archean province without significant tectonic transport due to the paucity of ca. 2.45 Ga rocks in the margins of the Superior and Rae-Hearne cratons; rocks of this age are common in the exposed sections of the Sask Craton, which has been used as evidence for the proposal that the Sask Craton is exotic in origin (Ashton et al., 1999; Rayner et al., 2005).

2.3 Fort à la Corne Kimberlites

The Fort à la Corne kimberlites were the first to be found in Saskatchewan, discovered by a joint venture between Uranerz Exploration and Mining and Cameco. They identified seven kimberlite pipes based on magnetic anomalies (Lehnert-Thiel et al., 1992). Continued exploration in the FALC region led to the identification of > 70 bodies, some in excess of 350 ha (Lefebvre and Kurszlaukis, 2008; Harvey et al., 2009), of which ~ 75 % have proven

diamondiferous (Harvey, 2004). These occurrences fall in two main clusters, along with isolated bodies and small groupings of isolated bodies. Despite the ~ 100 m overburden of glacial till and unconsolidated sediment (Kjarsgaard and Levinson, 2002) hindering exploration and development, interest in the FALC kimberlites continues due to the attractive diamond population; macrodiamonds are present in 50 % of the FALC kimberlites (Harvey et al., 2004) and approximately 70 % of recovered diamonds are of gem quality (Jellicoe et al., 1998). Based on current economic estimates of 14 carats per hundred tonnes (cpht) for a 38-year project life, the preliminary economic assessment for the Star – Orion South Diamond Project predicts the recovery of 66 million carats over the Life of Mine (Leroux et al., 2018). The other significant kimberlite discoveries in the area are at Sturgeon Lake, where two rafted kimberlite blocks were glacially transported to their present location (Gent, 1992; Kjarsgaard, 1996), and Candle Lake, two bodies whose relationship to FALC is unknown (Harvey, 2004). The C29/30 kimberlite of the Candle Lake cluster, however, is noted to have similarities to the FALC kimberlites regarding pipe morphology, textural characteristics, and country rock setting (Verigeanu et al., 2009).

The FALC field represents exceptionally well-preserved and complete examples of primary pyroclastic kimberlite, extra-crater volcaniclastic kimberlite, and re-worked/re-sedimented kimberlite along with feeder vents, tuff rings/cones, and associated craters (Leahy, 1997, 2001; Leckie et al., 1997; Zonneveld et al., 2004; Lefebvre and Kurszlaukis, 2008; Harvey et al., 2009; Kjarsgaard et al., 2008; Pitarri et al., 2008). In most known kimberlite occurrences, the upper and external volcanic edifices have been removed by erosion but the transgressional marine sediments at FALC aided their preservation (Zonneveld et al., 2004; Kjarsgaard et al., 2007). The internal geology of the field is extremely complex due to extensive interstratification

with approximately 200 m of contemporaneous continental to marginal marine and marine sedimentary material (Leckie et al., 1997; Zonneveld et al., 2004; Harvey et al., 2009; Kjarsgaard et al., 2007, 2009; Pittari et al., 2008). These authors have discussed the relationship between kimberlite and sedimentary stratigraphy, as well as detailed descriptions of the depositional environment of the Western Canadian Sedimentary Basin. Kimberlite was emplaced into the Mannville Group (Cantuar and Pense formations) through shallow marine sediments of the Lower Colorado Group (Joli Fou, Viking, Westgate, and Belle Fourche formations). Subaerial pyroclastic deposition followed by marine reworking and resedimentation comprise the major emplacement processes. Evidence suggests that fluctuations in the hydrologic environment over the course of the eruptive history led to varying degrees of interaction between the magma and sea/groundwater, thus producing an array of eruptive styles, including magmatic, wet phreatomagmatic, dry phreatomagmatic, and submarine (Lefebvre and Kurszlaukis, 2008; Harvey et al., 2009; Kjarsgaard et al., 2009).

One model (Scott Smith et al., 1995, 1998; Field and Scott Smith, 1999; Berryman et al., 2004) posits that the FALC kimberlites were emplaced through a two-stage formation process — initial phreatomagmatic crater excavation and subsequent rapid in-filling by pyroclastic material. This model was initially proposed to account for the undisturbed nature of the sediments and overall shape of the kimberlite bodies as 'champagne glass' (Scott Smith et al., 1995, 1998; Jellicoe et al., 1998; Field and Scott Smith, 1999; Leahy, 2001; Berryman et al., 2004). In accordance with this model, Berryman et al. (2004) suggest Orion South contains a younger "nested crater" in its central region. Other authors (e.g. Kjarsgaard et al., 2007, 2009) have outlined problems with the two-stage excavation and infill model, citing an incorrect interpretation of the depositional environment and hence the relationship between the

sedimentary host rock and eruptive kimberlite. They suggest that the FALC bodies instead represent domal tephra cones, tuff rings, and associated feeder vents that formed over multiple eruptive events (Zonneveld et al., 2004; Harvey et al., 2009; Kjarsgaard et al., 2007). Initial infill of the crater was by kimberlite deposited during the same eruptive event (Harvey et al., 2009). Other recent studies have provided a thorough examination of the geochemistry and petrologic history of the FALC kimberlites (Chalapathi Rao et al., 2017), their geochronology (Kjarsgaard et al., 2017), and the origin of the lithospheric mantle and metasomatic processes beneath the Sask Craton (Czas 2018a, b).

Magmatism ranged from 115 to 92 Ma (Heaman et al., 2004; Kjarsgaard et al., 2017) and is described as long-lived but episodic volcanism punctuated by sedimentary deposition and kimberlite re-working (Zonneveld et al., 2004; Kjarsgaard et al., 2009a; Harvey et al., 2009). A combination of direct radiometric dating and biostratigraphic markers were employed to constrain the eruptive history, indicating that most of the bodies are older than ~ 99 Ma (Kjarsgaard et al., 2007 and references therein; Kjarsgaard et al., 2017; cf. Scott Smith et al., 1998).

2.4 Pikoo Kimberlites

The Pikoo kimberlites are situated in east central Saskatchewan, approximately 140 km east of La Ronge, 90 km northwest of Flin Flon, and 10 km north of Deschambault Lake (Fig. 1). Exploration claims in the Pikoo area were staked in 2011 with North Arrow Minerals Inc. acquiring 100% of interests in the project by January 2017 from the former joint venture with Stornoway Diamond Corporation (North Arrow Minerals Inc., 2017). Following initial till sampling, two distinct KIM trains (North Pikoo and South Pikoo) were targeted for diamond drilling, leading to the first discovery of kimberlite on the property in 2013 (North Arrow

Minerals Inc., 2013). After this success, further exploration commenced, including a magnetic geophysical survey, two more seasons of drilling, additional till sampling, and microdiamond sampling.

Like the FALC field, the Pikoo kimberlites erupt through the Precambrian Shield of the THO and the underlying Sask Craton. The property is dominantly comprised of Paleoproterozoic granites, granodiorites, and tonalites of the Glennie Domain (Precambrian) with lesser amounts of intermediate to basic volcanics and granitic to mafic gneisses (Kupsch, 2017). The surficial geology can be characterized as a combination of glaciolacustrine veneer, till veneer, and exposed bedrock (Kupsch, 2017). As of 2017, North Arrow has identified ten discrete kimberlite bodies (PK150, PK151, PK311, PK312, PK314, PK315, PK346, PK347, PK350, PK386) largely occurring as dykes. Five of these bodies were sampled for microdiamond analysis (PK150, PK311, PK312, PK314, PK346) and all proved to be diamondiferous (North Arrow Minerals Inc., 2015, 2016a). Additionally, till sampled down ice of the North Pikoo area contains abundant pyrope garnet yet this phase is absent in samples from PK314 and PK346, which North Arrow interprets as evidence of the existence of at least one unidentified kimberlite body (North Arrow Minerals Inc., 2016b).

Approximate dimensions/orientations for several of the Pikoo bodies are described by Kupsch (2016, 2017) for PK150 (10 to 15 m wide and 150 m in strike length, and traceable to nearly 200 m depth), PK151 (90 cm east-west trending dyke), PK312 (near-vertical dyke, strike length >150 m), PK314 (rough surface dimensions of 20 x 30 m), and PK346 (apparent width of 15 m and a minimum strike length of 55 m, open along strike). Microdiamond analysis performed thus far indicates far more favourable results for PK150 than PK346. For PK150, a total of 487 stones were recovered from 321.4 kg of dry material and a later sample of 582.05 kg

of dry material returned 1,308 total stones while for PK346, 22 stones were recovered from 157.3 kg of dry material (http://www.northarrowminerals.com/projects/pikoo/). PK150 also has a coarser size distribution than PK314; 0.673 carats > 0.85 mm size were recovered of 1355 total stones from PK150 (Kupsch, 2017). As of 2018, the PK150 body remains the most significant discovery on the property in terms of both size and diamond content. The PK346 body, approximately 25 m north of PK314, is the next most significant discovery but it has yielded considerably less promising microdiamond results in terms of quantity and size distribution.

3 Samples

Based on detailed core logging and petrographic descriptions carried out between 2013 and 2016, North Arrow Minerals has classified the Pikoo bodies as ilmenite-rich hypabyssal kimberlite (HK). PK150 is described as macrocryst- and mantle nodule-rich HK in contrast to the paucity of mantle material and macrocryst-poor nature of PK346 and PK314 (Kupsch, 2017). The PK312 occurrence in East Pikoo is unusual compared to many of the other Pikoo bodies due its high proportion of KIMs and mantle nodules (Kupsch, 2017). KIM analysis in 2015 and 2016 for PK150, PK151, PK311, PK312, PK314 and PK346 recovered virtually no chrome diopside, chromite, or olivine from any sample, but ilmenite was abundant in all these intrusions (Kupsch, 2017).

North Arrow initially provided samples from the Pikoo kimberlites in the form of unprocessed core (one sample from PK150 and two from PK346) and KIM-processed core (four samples from PK150, four from PK314, and two from PK346). Initial work on these samples was limited due to the pervasive and severe alteration. North Arrow provided additional material in the form of slab samples and off cuttings from existing thin sections. From the unprocessed core, sections free of carbonate veining and with the least amount of alteration were selected to make four thick (100 μm) polished thin sections from each sample. The finest fraction (-0.25 mm) of each disaggregated core sample was cleaned via an ultrasonic bath to liberate clays on the surface, then processed with a Wilfley Table to separate out light, medium, and heavy fractions. A hand magnet was used to remove the magnetics from the heavy fraction rather than a Frantz Isodynamic Separator to minimize sample loss. The magnetics-free heavy fractions of each sample were examined carefully and thoroughly with a stereo-microscope to search for any perovskite that could be hand-picked for geochemical and geochronological work.

The second set of samples sent by North Arrow permitted a more representative cross-section of the Pikoo bodies to be examined because thin sections could be created from PK151, PK312, and PK314 to supplement the work completed on PK150 and PK346. The slab samples were especially useful as they could be examined in greater detail with a hand lens along the cut surface; only samples with areas exhibiting minimal alteration and features of interest were flagged. A rock saw was then used to cut out these sections to make polished thin sections. The off-cuttings from PK151 and PK314 were used to make new thick polished thin sections as these were the only available sample material for these two bodies. In total, 36 thick (100 μm) polished thin sections were produced in-house at the University of Alberta Thin Section Laboratory.

4 Analytical Methods

4.1 Petrography

Initial observations were made from core and cut slab samples using a hand lens and binocular microscope. Unfortunately, the high degree of alteration, fine grain size of some samples, and overall dark colour of the kimberlite rendered it difficult to identify individual phases and features. Therefore, thin sections were critical for developing accurate petrographic descriptions of the samples. All thin sections were examined using a petrographic microscope. When necessary, a Zeiss Sigma 300 VP-FESEM Scanning Electron Microscope (SEM) connected to a Bruker energy dispersive x-ray spectroscopy (EDS) system was used to make EDS point analyses and take backscatter electron (BSE) images to identify ambiguous mineral phases and better describe textures, respectively.

While all thin sections were inspected to assess the degree of alteration in each sample, not all were suitable for detailed study. Since all samples exhibited considerable alteration, more complex criteria were established in selecting thin sections for more detailed work. At least one thin section was selected from each of the five Pikoo bodies (PK150, PK151, PK312, PK314, PK346) to make the best possible effort to compare all the occurrences. As mentioned above, only one thin section was available for PK151 and PK314. After all mineral phases were identified, the thin sections containing the grains least affected by alteration for each phase (olivine, spinel, ilmenite, etc.) were selected for future work. Additional thin sections for the two major bodies (PK150 and PK346) were also selected if they exhibited significantly different textures from the other sections already selected. Petrographic descriptions used Stage 1 of the

systematic framework for the description, classification, and interpretation of kimberlites established by Scott Smith et al. (2013) as a guide.

4.2 Whole rock geochemistry

Only one sample from PK150 (44813) and two samples from PK346 (44834 and 44848) were selected for whole rock major and minor element geochemistry due to limited sample availability and the high probability of crustal contamination. Fragments of core were carefully examined to determine whether any areas exhibited less pervasive alteration or were lacking in visible crustal material. Pervasive alteration was apparent in drill core and confirmed by thin section analysis. Samples taken from core were manually pre-crushed into ~ 2 to 3 cm pieces with a small alumina crusher. To prevent contamination, the crusher components were rinsed with distilled water and ethanol before each sample was crushed. The pre-crushed pieces were then pulverized into a fine powder using an agate puck mill. The puck mill components were cleaned in the same manner described above to prevent possible contamination. The powders were stored in clean plastic containers.

One gram of each powder was measured out using an electronic balance and sent to Franklin and Marshall College, Pennsylvania, USA. Whole rock major and minor element geochemistry was determined through X-ray fluorescence (XRF) using fused $Li_2B_2O_7$ glass discs per the procedure outlined by Boyd and Mertzman (1987). Measurements were made for the oxides SiO_2, TiO_2, Al_2O_3, Fe_2O_3 (expressed from total Fe), MnO, MgO, CaO, Na_2O, K_2O, and P_2O_5, and elemental concentrations for Sr, Zr, V, Ni, Cr, Co, and Rb.

4.3 Major and Minor Element Mineral Chemistry

Based on petrographic examination of polished thin sections, a subset of thin sections from each body were selected for detailed mineralogical study. Emphasis was placed on the minerals olivine, ilmenite, spinel, and phlogopite due to their relative importance in kimberlite characterization. Grains with minimal alteration were identified by BSE imaging and targeted for mineral chemistry. Major and minor element mineral chemistry was analyzed using a CAMECA SX100 and a JEOL JXA-8900R electron probe microanalyzer (EPMA) at the University of Alberta, and a CAMECA SX100 EPMA at the Saskatchewan Research Council (SRC). Two thin sections were analyzed at both institutions as an evaluation of analytical quality and inter-machine data comparability.

Elemental concentrations were determined quantitatively using Probe for EPMA software (Donovan et al., 2015) and wavelength-dispersive spectrometry (WDS) operating with conditions of: 20 kV accelerating voltage, 20 nA beam current, and a beam diameter between 'fully focused' and 5 μm (the larger diameters employed for more friable samples). Count times were 20 to 60 s for both peak and background. When grains were large enough, multiple points were set; the median value is reported for grains that did not exhibit heterogeneity. Sessions were calibrated using both natural and synthetic materials (note: sessions run at the SRC were calibrated using the materials of their default kimberlite set up). A complete summary of analytical settings, including count times and standards, can be found in Table 1. Matrix corrections were performed using ZAF or φ (ρZ) calculations (Armstrong, 1998). Interference corrections were applied when appropriate, including: Ti for interference by Ba, Mn for interference by Cr, F for interference by Fe, Sr for interference by Ca and Si, and Na for interference by Zn. Iron data was collected as FeO_T (total Fe as FeO).

Major element concentrations in ilmenite, spinel group minerals, garnet, rutile, and pseudo-rutile were determined for the oxides SiO_2, TiO_2, Al_2O_3, Cr_2O_3, FeO_T, NiO (ilmenite only), MnO, MgO, CaO, and Na_2O. Oxides of Nb_2O_5, ZnO, NiO, BaO, and K_2O were also analyzed in some sessions when possible with the analytical set up (e.g., standard block availability, time constraints). Thirteen oxides were analyzed in phlogopite (Nb_2O_5, SiO_2, TiO_2, Al_2O_3, Cr_2O_3, FeO_T, NiO, MnO, MgO, CaO, BaO, Na_2O, K_2O) and thirteen in olivine (SiO_2, TiO_2, ZnO, Al_2O_3, Cr_2O_3, FeO_T, NiO, MnO, MgO, CaO, Na_2O, and K_2O). All apatite was analyzed in one session for SiO_2, FeO_T, MnO, CaO, SrO, Na_2O, P_2O_5, SO_3, Cl, and F. V_2O_3 in ilmenite and phlogopite was analyzed at the SRC as part of their default method setup.

Oxide analyses below the instruments limit of detection (bld) are indicated, along with oxides not analyzed (n.a.). For all phases, iron was analyzed as FeO_T. Components FeO and Fe_2O_3 were calculated stoichiometrically (Droop, 1987) from FeO_T for ilmenite and spinel.

4.4 Trace Element Geochemistry

In situ trace element analysis of ilmenite and apatite was conducted by laser ablation inductively coupled plasma mass spectrometry (LA-ICP-MS) via a RESOlution 193 nm ArF Excimer Laser Ablation system coupled with a Thermo Element II XR ICP-MS. SEM images were used to target areas least affected by fractures, alteration, and compositional inhomogeneity.

Ilmenite trace elements were measured at spot sizes of 50, 130, or 190 µm with ablation settings as follows: 30 s of background time, 50 s of ablation time, a repetition rate of 5 Hz, laser energy of 120 mJ, an attenuator value of 26 %T, and a fluence of ~ 2.6 J/cm^2. In total, 22 elements were measured: ^{45}Sc, ^{47}Ti, ^{49}Ti, ^{51}V, ^{55}Mn, ^{57}Fe, ^{59}Co, ^{60}Ni, ^{66}Zn, ^{68}Zn, ^{69}Ga, ^{71}Ga, ^{90}Zr,

^{91}Zr, ^{93}Nb, ^{178}Hf, ^{180}Hf, ^{180}Ta, ^{181}Ta, ^{182}W, ^{183}W, and ^{238}U. GSE reference glass was used as the primary standard while the reference glasses BCR-2G, GSC, and BIR-1G were employed as secondary standards to monitor instrument performance and data quality. GSE and BCR-2G were analyzed at the start and end of each run, while GSC and BIR-1G were analyzed after every three to five unknowns. Apatite trace elements were measured at a spot size of 23 or 33 μm with 40 s of background time, 50 s of ablation time, a repetition rate of 5 Hz, laser energy of 120 mJ, an attenuator value of 26 %T, and a fluence of ~ 2.7 J/cm^2. In total, 35 elements were measured: ^{29}Si, ^{42}Ca, ^{43}Ca, ^{47}Ti, ^{49}Ti, ^{51}V, ^{52}Cr, ^{53}Cr, ^{60}Ni, ^{85}Rb, ^{88}Sr, ^{89}Y, ^{90}Zr, ^{93}Nb, ^{137}Ba, ^{139}La, ^{140}Ce, ^{141}Pr, ^{146}Nd, ^{147}Sm, ^{153}Eu, ^{157}Gd, ^{159}Tb, ^{163}Dy, ^{165}Ho, ^{166}Er, ^{169}Tm, ^{172}Yb, ^{175}Lu, ^{178}Hf, ^{181}Ta, ^{204}Pb, ^{208}Pb, ^{232}Th, and ^{238}U. NIST612 reference glass was used as the primary standard and Bancroft apatite was used as a matrix-matched secondary standard. Bancroft was analyzed after every five unknowns; NIST612 was analyzed at the start and end of each run as well as after every five unknowns. To monitor oxide generation, ThO/Th was also measured.

Data reduction was performed off-line using the Iolite software (version 3.32). Internal standards of ^{57}Fe for ilmenite trace elements and ^{42}Ca for apatite trace elements were employed, as determined by previous EPMA analysis. Time resolved spectra were inspected individually to remove erroneous spikes caused by analysis of micro-inclusions. Values measured for standard reference materials were compared to the preferred values given by the GeoReM database (Geological and Environmental Reference Materials) or the in-house accepted values; the measured values generally agreed within ~ 10% (see Appendix C for comparisons of internal and secondary standards).

4.5 Geochronology

LA-ICP-MS was also used for *in situ* U-Pb geochronology on apatite and perovskite, employing the same analytical setup (RESOlution 193 nm ArF Excimer Laser Ablation system coupled with a Thermo Element II XR ICP-MS) that was used for trace element analysis. The same SEM images of apatite fans used in trace-element analyses were also used to locate elongate, wide, and pristine apatite grains suitable for positioning raster lines. Perovskite can experience cation leaching and replacement by other Ti-rich minerals in late-stage kimberlite evolution, most commonly by TiO_2 phases (Chakhmouradian and Mitchell, 2000), as it is unstable under CO_2-rich, weakly acidic conditions (Mitchell and Chakhmouradian, 1998). In kimberlites, this TiO_2 polymorph is commonly the more stable phase of rutile (Chakhmouradian and Mitchell, 2000), though anatase alteration has also been noted (Mitchell and Chakhmouradian, 1998). Replacement of perovskite by a TiO_2 phase is a common feature of Pikoo. As such, significant time was devoted to examining the BSE images to locate both the largest possible perovskite grains and to carefully examine each individual grain to position spots in areas without alteration. When the BSE images were taken, the grains were also analyzed with EDS point spectra to confirm the identification as perovskite. Data reduction was performed offline using the Iolite software (version 3.32); age calculations were performed with Isoplot (version 4.15).

4.5.1 Apatite

Prior to apatite geochronology measurements, the ICP-MS cones were replaced to ensure peak instrument functioning to gather the highest quality data possible. The largest pure apatite portions of the fans were selected for the geochronology portion and 50 μm raster lines of 30 s duration were plotted, using settings of: 70 s of background time, a repetition rate of 13 Hz, laser energy of 120 mJ, an attenuator value of 11.4 %T, and fluence of ~ 1.1 J/cm^2. A combination of

apatite standards (Bancroft, Durango, Madagascar, and AP401) were used to monitor instrument performance and data quality.

4.5.2 Perovskite

As a common groundmass but rarely xenocrystic phase in kimberlite that crystallizes directly from the magma, perovskite is a valuable kimberlite geochronology tool (Heaman and Parrish, 1991). Based on petrographic analysis, unaltered perovskite is only present in the freshest areas of select samples from PK150. Due to the very fine size distribution (mostly ranging from <15 to ~ 25 μm), the perovskite was not ideal for hand picking. Samples were ablated for 48 s with 30 s of background. Measurements were performed *in* situ at spot sizes of 23 or 33 μm at a repetition rate of 5 Hz, laser energy of 120 mJ, an attenuator value of 11.4 %T, and a fluence of ~ 3.88 J/cm^2. Given the small size, there was only room for one spot per perovskite grain. A total of three thin sections from two different samples were analyzed, two from 47517 and one from 47504. The extremely fine size fraction of grains meant that the risk of ablating through grains was high. Time-resolved spectra were scrutinized in Iolite for signs of the ablation progressing beyond the thickness of the crystal and to remove any anomalous spikes or potentially erroneous signal.

Three analyses of both Ice River and Afrikanda perovskite standards were made at the start and end of each run, as well as bracketing every six Pikoo analyses to monitor data quality and instrument drift. These results are tabulated in Table 2. However, it should be noted the concentrated nature of the data for both the standards prevents the same treatment data that was employed for the Pikoo analyses (discussed below), thus a weighted average of the $^{206}Pb/^{238}U$ ages was calculated for both Ice River and Afrikanda. The weighted average of the 48 spot analyses of the Ice River standard analyzed concurrently with the Pikoo samples (Fig. 2a)

yielded an age of 356.7 ± 1.8 Ma (95 % confidence, MSWD = 0.53), which is in good agreement with previous studies (356.5 ± 1.0 Ma of Heaman, 2009 and 357.17 ± 0.27 Ma of Burgess et al., 2012). Similarly, the weighted average of the 43 perovskite spot analyses of the Afrikanda standard (Fig. 2b) yielded an age of 376.2 ± 2.6 Ma (95 % confidence, MSWD = 0.65), in good agreement with other geochronology studies of the Afrikanda complex (371 to 374 Ma, Reguir et al., 2010; 376 Ma, Wu et al., 2013). The high-quality data from the standards indicates a high degree of confidence can be placed in the quality of the data for unknown samples.

Once collected, the treatment of perovskite U-Pb data required careful consideration. Unlike zircon, perovskite contains Pb formed from both the decay of U and Th as well as non-radiogenic Pb ("common Pb") incorporated into the structure during crystallization. This common Pb portion can comprise as much as 80 % of the total Pb (Heaman and Parrish, 1991). It is crucial to make an accurate estimate of the common Pb composition since small changes can have a significant impact on the accuracy and uncertainties associated with the $^{207}Pb/^{206}Pb$ and $^{207}Pb/^{235}U$ ages. The $^{206}Pb/^{238}U$ ages are least sensitive to common Pb corrections and are thus the most frequently reported perovskite ages (Heaman, 2009). One common method of correcting for common Pb employs the Stacey-Kramers two-stage evolution model (Stacey and Kramers, 1975). However, this method is not appropriate for all cases such as when the U/Pb ratio is low and a high proportion of common Pb is present that deviates from the model Stacey-Kramers composition. As well, relying on model Pb compositions requires certain assumptions regarding the nature of the (kimberlite) magma, its source region, and interactions between the two. The Pb isotopic composition derived from the model may not reflect the true nature of the sample in question. In such instances, it is more suitable to derive the common Pb compositions from the sample itself rather than relying on a model-driven estimate. Often, a low-U phase

cogenetic with perovskite is used to directly measure the Pb isotopic composition and the results are applied to age calculation. Such cogenetic phases include ulvöspinel-magnetite in kimberlite (e.g., Stamm et al., 2018) or feldspar, clinopyroxene, nepheline, and magnetite in alkaline rock types (e.g. Corfu and Dahlgren, 2007). Most of these phases are absent in kimberlite. The extensive alteration of the Pikoo kimberlites severely limits the choice of other phases for this purpose. It is possible to use the $^{207}Pb/^{206}Pb$ ratio of the perovskite to estimate the initial common Pb isotopic composition and this is more reliable in ICP-MS methods owing to the isobaric interference of ^{204}Hg from the Ar plasma gas on ^{204}Pb (Cox and Wilton, 2006).

On a Tera-Wasserburg diagram, uncertainty of the calculated age arises from the spread in uncorrected data points (or lack thereof) and the proximity of the data relative to the concordia intercept, itself a reflection of the common Pb proportion within each individual data point. Lower intercept ages can underestimate a sample's true age if the data does not have sufficient spread, therefore, some studies take a weighted average, nominally improving the uncertainty by considering a large number of analyses. Since LA-ICP-MS can generate a large quantity of data quickly and cost-efficiently, this method has been recently utilized to assess kimberlite eruption histories effectively by calculating weighted average $^{206}Pb/^{238}U$ ages (e.g. Wu et al., 2010; Guarino et al., 2013). However, individual uncertainties are not always correctly propagated through the weighted average calculation and the data need careful consideration to see if they fit the criteria to be treated as a single population. Often the weighted mean uncertainties are not reflective of the true uncertainty (Spencer et al., 2016).

The significant variation between radiogenic and common Pb in the Pikoo samples is advantageous because the spread is sufficiently large to anchor a reasonable extrapolation, meaning no weighted average was taken. In this study, the common Pb composition was derived

by intersection with the y-axis ($^{207}Pb/^{206}Pb$) on a Tera-Wasserburg diagram and the perovskite crystallization age from the intersection with the concordia curve (lower intercept age). This method will hence be referred to as the semi-total Pb isochron approach.

To confirm whether this was a reasonable estimation from which to base age calculations, the total-Pb/U isochron approach, hereafter referred to as the total Pb method, outlined by Ludwig (1998) was also utilized. Measurements for ^{204}Pb must be made with reasonable precision in order to apply the total Pb method, but this method provides a more stringent test on the fundamental assumption that the perovskite is reflective of a single concordant population with the same common Pb composition. Such a distinction is important because two (or more) populations of perovskite can appear very similar when plotted on a Tera-Wasserburg concordia but have different common Pb compositions. The data, without correcting for common Pb, is input into a regression involving the $^{238}U/^{206}Pb$ and $^{207}Pb/^{206}Pb$ ratios plus an extra dimension of $^{204}Pb/^{206}Pb$. If the data is linearly covariant in both $^{238}U/^{206}Pb$ – $^{207}Pb/^{206}Pb$ and $^{204}Pb/^{206}Pb$ – $^{207}Pb/^{206}Pb$ space, the data forms a plane, with a vertex falling on the concordia curve at the sample age. For samples that do not satisfy the fundamental assumption, the regression will fail or present no physical meaning (Ludwig, 1998). For easier graphical representation, the data are usually transformed to Tera-Wasserburg ratios and errors and displayed in two dimensions.

This method is a useful built-in check but, like the Stacey-Kramers approach, certain criteria must be met. The total Pb approach is not useful when the mineral in question has insufficient quantities of common Pb for direct measurement (e.g. zircons) or for young samples as adequate time is needed for radiogenic Pb to accumulate. Usually, ~ 400 to 500 Ma is considered the cut off point for young samples, beyond which there is no improvement to the precision (Ludwig, 1998). The more rigorous criteria for defining a satisfactory total Pb

isochron compared to a semi-total Pb isochron can be beneficial as the system is less susceptible to distortion resulting from disturbances to the isotopic composition of multi-component systematics (Ludwig, 1998). Both the semi-total Pb and total Pb methods were applied to the Pikoo data in determining the sample age.

4.6 Tracer Isotopes

Perovskite is especially useful for unravelling the magmatic evolution of kimberlites as it a relatively early-crystallizing groundmass (but rarely xenocrystic) phase that is sensitive the initial isotopic composition of the magma prior to crustal entrainment (Heaman, 1989). Furthermore, Sr-Nd isotopic systematics are recorded more robustly in unaltered perovskite compared to other kimberlitic minerals and whole rock powders (Heaman, 1989; Paton et al., 2007; Woodhead et al., 2009; Yang et al., 2009; Malarkey et al., 2010). This approach to determining the magma source region is applied increasingly often as instrumentation advances are achieved (e.g. Paton et al., 2007, Yang et al., 2009; Woodhead et al., 2009; Wu et al., 2010, 2013a, b; Chalapathi Rao et al., 2012; Sarkar et al., 2018).

Isotope ratios of Sr and Nd in perovskite were analyzed by multicollector inductively coupled plasma mass spectrometry (MC-ICP-MS) *in situ* via a RESOlution 193 nm ArF Excimer Laser Ablation system connected to a Thermo Neptune Plus Multicollector Inductively Coupled Plasma Mass Spectrometer. Due to the fine size fraction, a single grain could only support one analysis for either geochronology or tracer isotopic composition. Unaltered grains were targeted from the same BSE images used earlier for perovskite geochronology. Measurements were made in static mode at a laser spot size of 23 (Sr) or 33 (Nd) μm with ablation conditions as follows: 30 s of background time, 48 s of ablation time, a repetition rate of 7 Hz, and a fluence of ~ 5.5 J/cm^2. The Faraday cup configurations are presented in Table 3. Three analyses of both

Ice River and Afrikanda perovskite bracketed each group of three to four unknown analyses in order to monitor instrument performance and assess data accuracy for both isotope systems. Data processing was performed offline using the Iolite software (version 3.32). Ice River was used as the primary reference material for both Sr and Nd isotope analyses. Oxides can cause interference (e.g., Ba oxides on Nd) and if oxide production of the mass spectrometer is high, the mass bias correction will no longer follow exponential law. Prior to running unknowns, the instrument was meticulously tuned and sessions consisting only of standard analyses were performed, monitoring the invariant ratios, to mitigate these effects.

In order to generate accurate Nd isotopic data via LA-MC-ICP-MS, several factors must be considered during data collection and processing – the isobaric interference of ^{144}Sm on ^{144}Nd, instrumental mass bias correction factors required for MC-ICP-MS studies, and the accuracy of the ^{147}Sm/^{144}Nd ratio determination (which is increasingly important with sample age in order to calculate the radiogenic growth of ^{143}Nd). The total 144 atomic mass unit (amu) signal, comprising ^{144}Sm and ^{144}Nd, was measured and the natural abundance of Sm was used to correct for the interference of Sm in the 144 signal using Iolite. This interference is especially important as it is standard practice to normalize to ^{144}Nd. There is a slight disparity in the ionisation potential between Sm and Nd, triggering laser induced elemental fractionation of ~ 3 % at 20 μm in previous studies (Fisher et al., 2011). A downhole fractionation correction was applied during data processing, using ^{146}Nd as the index channel (Fisher et al., 2017). A robust determination of ^{147}Sm/^{144}Nd is necessary to calculate initial Nd isotopic values, therefore, it must be determined if a further correction factor is necessary after interference corrections are applied. This was achieved by comparing measurements of the primary standard (Ice River) bracketing the unknowns to the accepted values. If the difference is not within uncertainty, this

correction factor must be applied to the $^{147}Sm/^{144}Nd$ and $^{143}Nd/^{144}Nd$ ratios of the unknowns as well. The mass bias correction was determined using the invariant ratio of $^{146}Nd/^{144}Nd = 0.7219$ and monitored with the ratio of $^{145}Nd/^{144}Nd = 0.348415$. The initial Nd isotopic values were calculated using the $^{238}U/^{206}Pb$ age determined by this study (see 5.5.2).

The extremely low Rb/Sr ratio (< 0.001) inherent to perovskite is beneficial to Sr isotopic determinations as a correction for the radiogenic growth of Sr is unnecessary (Paton et al., 2007). However, multiple isobaric interferences have the potential to affect Sr values. The basis of these corrections is summarized below, and thorough discussions are presented by Ramos et al. (2004) and Paton et al. (2007). Carrier gases have the potential to introduce interference by Kr, though it was determined a correction was unnecessary due to the purity of the Ar carrier gas utilized. A two-stage process is required to apply corrections for doubly charged REEs and Rb. When doubly charged, Er and Yb occur at half of their isotopic mass, interfering with Rb. The signal on masses 83.5 and 86.5 were composed solely of Er^{2+} and Yb^{2+}, respectively. The law of natural abundances could thus be applied to subtract the interference of $^{167}Er^{2+}$ and $^{176}Yb^{2+}$ on the mass 85 signal. Following this subtraction, the mass 85 signal was interpreted to consist solely of ^{85}Rb. The natural abundance of $^{85}Rb/^{87}Rb = 0.3856$ was then used to address the isobaric interference by ^{87}Rb and finally resolve ^{87}Sr. Deviation from the invariant ratio of $^{86}Sr/^{88}Sr = 0.1194$ was used to correct for instrument mass bias following exponential law and subsequently applied to all other measurements. The invariant ratio of $^{84}Sr/^{88}Sr$ was then used to assess the quality of this correction.

5 Results

5.1 Petrography/Mineralogy

While there are distinct differences in mineralogy and textural characteristics between the Pikoo bodies, the following characteristics are ubiquitous in all five bodies examined in this study unless otherwise specified. The basic character can be summarized as altered olivine macro/microcrysts and abundant ilmenite (>1.5 cm to ~ 40 μm) set in a well crystalline groundmass of serpentine, calcite, phlogopite, and spinel group minerals ± apatite. Spinel group minerals often exhibit atoll textures to varying degrees of development, but others can lack an atoll entirely. Segregations of serpentine and calcite comprise a significant proportion of the interstices and can reach several hundred microns across. Late-stage, cross-cutting carbonate veins are also common, with less frequent serpentine veins. Based on petrographic observation of mineral relationships, textures, and inclusions (described in detail below), a magmatic crystallization sequence of olivine, spinel group minerals + perovskite, apatite, phlogopite, and calcite is interpreted (Fig. 3). Sulfide droplets are unique to a subset of PK346 samples but the timing of formation appears similar to the MUM (magnesian ulvöspinel—ulvöspinel—magnetite) spinel. While large mantle xenoliths have been documented by North Arrow, particularly in PK150, the samples available to this study lacked such mantle material entirely.

All Pikoo kimberlite samples are pervasively altered, dominated by serpentinization and calcite replacement, which can obscure differences in groundmass textural characteristics within a body. The proportions of serpentinization and carbonate replacement vary between intrusions, but both are observed in all cases. Minor iddingsite or talc alteration occasionally affects fractures and edges of olivine macrocrysts. Several varieties of serpentine described by Mitchell

(2008) for hypabyssal kimberlites, both primary and secondary, are observed. Primary fine-grained serpentine occurs in the mesostasis as segregations and plate-like crystals (often referred to as serpophite). Retrograde serpentine, likely derived from deuteric fluids (Mitchell, 2008) or a mixture of hydrothermal fluids (deuteric and external fluids ± groundwaters; Giuliani et al., 2017), occurs as pseudomorphs of olivine macro- and microcrysts or as mantles on relict olivine. Carbonate segregations can be partially replaced by fine-grained serpentine, particularly around the peripheries of affected segregations. Virtually all olivine has been completely altered by serpentinization, with or without calcite/clay replacement to grain interiors. Secondary opaque oxides are commonly associated with serpentine alteration in olivine. Minerals typically considered physically and chemically robust to weathering (e.g., ilmenite; Mitchell, 1986) have also been impacted to some degree of alteration, primarily by serpentine. Spinel, phlogopite, apatite, and primary tabular calcite are affected to varying degrees.

5.1.1 PK150

Core from PK150 exhibits uniform to segregationary textures. Typically, the degree of alteration is intense and pervasive, though three thin sections contain irregular pools of partially fresh material (44804 and 47517; Fig. 4). It is only in these areas that partially fresh olivine and perovskite (unaltered to a high-Ti phase) can be found. Unaltered olivine and perovskite are absent in all other available samples. Occasional country rock xenoliths are present but pervasive alteration often precludes detailed description. The groundmass consists of (in order of decreasing abundance) interstitial/segregations of serpentine and calcite, phlogopite, apatite, spinel group minerals, and perovskite/high-Ti pseudomorphs of perovskite (Fig. 5a).

Fine plate-like or needles of serpentine occur in the groundmass, separate from the segregations, often in association with phlogopite and spinel. Serpentine after olivine is pale

yellow to green-brown and present as vein-like textures to patchy or complete replacement of olivine. A thin rim of pale yellow-green serpentine mantles most former olivine. Nearly 100 % of olivine (macrocrysts and phenocrysts) are fully altered, dominantly by serpentinization from the rim inwards with subordinate calcite replacement in the grain interiors. In the most heavily altered areas, the original groundmass assemblage is dominantly replaced by fine-grained secondary serpentine, most obviously impacting apatite, spinel, and perovskite. Partial replacement by calcite or overgrowth by fine flecks of magnetite is also possible. One sample (44804) exhibits minor barite alteration in the interior of former olivines macrocrysts as well. In general, olivine is evenly distributed and olivine macrocrysts (subangular to rounded) up to 9 mm are common. A significant proportion of microcrysts still have easily discernable boundaries despite the alteration, exhibiting a euhedral prismatic morphology.

Using BSE images to highlight compositional differences, a portion of the partially fresh olivine grains exhibit a sharp distinction between the core and rim compositions. These grains exhibited a darker (more Mg-rich) core surrounded by a lighter (more Fe-rich) rim of variable thickness (20 to 100 μm). Similar variations between olivine core and rim are described in other kimberlites (e.g., Lac de Gras) and are interpreted as representing kimberlitic overgrowths on inherited cores (Bussweiler et al., 2015). In rare instances, a relatively smooth transition occurs between the core and rim as the Fe content changes; such a relationship has been referred to as patchy zoning and attributed to diffusional equilibration within a crystal (Streck, 2008). The degree of serpentinization along the edge of a grain had a significant impact on the amount of rim material still present (e.g., Fig. 6a), in some cases masking whether a rim was ever present. A portion of grains with minimal serpentinization along the majority their margins appear to lack

rims entirely (Fig. 6b), suggesting a population of olivine with homogeneous composition is present or that the grains re-equilibrated with the kimberlite magma.

Large (100 to 400 μm) late-stage acicular radial apatite fans occur frequently in portions of PK150, often grading into calcite segregations and enclosing spinel and (former) perovskite in the groundmass (Fig. 7). This habit is inferred to be indicative of relatively rapid cooling (Mitchell, 2008). Some portions of these fans are grown over by calcite segregations, indicating they crystallized within the magmatic sequence of the kimberlite and did not precipitate post-emplacement. Additionally, fine (~ 20 to 30 μm) euhedral prisms and singular acicular grains of apatite occur in the groundmass, often in calcite-rich portions. These textural descriptions are typical of kimberlitic apatite (Mitchell, 1986, 2008; Malarkey et al., 2010; Soltys et al., 2017).

Groundmass phlogopite tends to form elongate laths or tabular grains (Fig. 8a and b). Most groundmass phlogopite exhibits minor alteration and zoning. Phlogopite macrocrysts are uncommon but can be found in thin section. BSE images reveal very little intragrain compositional variation in the macrocrysts beyond partial serpentine replacement.

Spinel group minerals occur as discrete grains (~ 10 to 30 μm across, relatively equidimensional), spread throughout the groundmass or rimming ilmenite macrocrysts. Many grains exhibit an atoll texture, with an Fe-rich rim separated from the core by a 'lagoon' of serpentine and/or calcite. No easily discernible compositional relationship is observed between atoll and non-atoll spinels in PK150 or other intrusions.

Perovskite presents as subhedral cubes in the groundmass, 'necklacing' olivine/ilmenite, or intergrown with spinel. The perovskite population is very fine, ranging from <10 μm to 40 μm with average size of 20 μm. Unaltered perovskite is found in samples 44804 and 47517 in

the same areas as the partially fresh olivine. Replacement of perovskite by rutile can be recognized in moderately altered areas. It is possible for two generations of perovskite to be present in a single kimberlite, e.g. through mingling of compositionally distinct magmas (Castillo-Oliver et al., 2016). Furthermore, pristine secondary hydrothermal perovskite in addition to replacement by both anatase and kassite was described in kimberlites from the Eastern Dharwar craton (Xu et al., 2018). Petrographic analysis is therefore a vital step in U-Pb dating as this variety of alteration (e.g., arising from subaerial weathering or late-stage hydrothermal processes) can reset the U-Pb crystallization age. This is an important consideration when taking concentrates if thin sections are not available of the sampled material. Thorough examination of BSE images of the Pikoo perovskite indicates that all grains selected for analysis were magmatic in origin and free of secondary alteration that may act to re-set the U-Pb age recorded by the perovskite (cf. trends identified by Xu et al., 2018).

Ilmenite ranges in size from ~ 70 μm to 1.5 cm in diameter, with most grains on the order of 200 to 300 μm. Smaller grains are likely the by-product of the disaggregation process as true kimberlitic groundmass ilmenite is rare (Pasteris, 1980). The majority of ilmenite exhibits an interconnected fracture texture. The largest grains may be polycrystalline but homogeneous in composition, also exhibiting fractures. The ilmenite is very texturally complex under BSE imaging, from rim to interior. The outermost margins are relatively smooth but the majority of rims exhibit a symplectic texture and are composed of many intergrown phases, dominantly rutile, magnetite, and serpentine (Fig. 9). Fine flecks of magnetite form a fringe along the outermost margin and infill fractures, occasionally lining the boundary between the ilmenite and the rim as well. Interior to the magnetite border is a rim of rutile of irregular thickness. Discrete patches of rutile can also occur in the interior of the ilmenite, adjacent to a significant fracture in

fine grains. Serpentine exploits fractures to replace significant proportions of the rutile rims in addition to large sections of the ilmenite itself (Fig. 9c). In the absence of a thick rutile rim, the edges of the ilmenite exhibit moderate corrosion by the groundmass and overgrowth by a mantle of MUM spinel ± perovskite. The outermost ilmenite can occasionally exhibit minor (though inconsistent) compositional changes, dominantly an increase in MnO relative to the core, which is distinct from the major compositional changes to ilmenite rims in PK346 (see below). The interior of grains ranges from relatively pristine to demonstrating abundant irregular exsolution lamellae (Fig. 9a, e, and f), which are relatively Fe-enriched as assessed by WDS point analyses. The interior of some ilmenite lack visible zonation under BSE imaging, but most grains have variations in Mg content that lend an irregular appearance to the grain.

Garnet and its kelyphite rim, where present, are often fractured or disaggregated. Accessory angular xenocrystic magnetite is partially replaced by serpentine near grain edges or by exploiting planes of weakness. The grain peripheries are irregular and patchy due to partial corrosion/dissolution (Fig. 10).

Features resembling "magmaclasts" were observed in a small subset PK150 samples in this study (Fig. 11). Use of the term magmaclast is somewhat controversial as it can apply to features arising from the disruption of unsolidified magma by any process, including both melt fragmentation (e.g. pelletal lapilli, melt-bearing pyroclasts) and melt segregations, such as in hypabyssal intrusions (e.g. Webb, 2006; Webb and Hetman, 2017). Some have argued to abandon the term (e.g. Cas et al., 2008b, 2009) but it is retained in Scott Smith et al.'s (2013) updated kimberlite terminology and classification scheme. Unfortunately, the different types can develop very similar characteristics, making the interpretation of an emplacement process difficult to distinguish. Terminology for describing magmaclasts is after Webb and Hetman

(2017) and Scott Smith et al. (2013). The features observed in Pikoo ranged in size from ~ 4 mm to 1.7 cm and have vast differences in irregularity (examples of amoeboid, curvilinear, and regular morphologies have been identified). These features occur as both cored and uncored varieties. The cored examples can have complete symmetrical or asymmetrical rims or incomplete rims. The groundmass is well crystalline with diffuse margins. Identifiable components include groundmass/macrocrystic olivine and phlogopite in addition to ilmenite. Olivine within the rim of the magmaclast is comparable in size and morphology to the olivine of the surrounding kimberlite. As well, the olivine and phlogopite macrocryst frequency and crystallinity is similar between the rim and the rest of the sample.

North Arrow Minerals reports coherent magmaclasts in the eastern half of the PK150 body (Kupsch, 2016). However, thinner-cut sections permit a more detailed petrographic examination of the groundmass, which reveals a gradational change and diffuse boundaries between the darker and lighter serpentine alteration of the magmaclast rim and surrounding kimberlite, respectively. Furthermore, small patches of material resembling the magmaclast rim occur as interconnected patches throughout interstices in the groundmass. It is likely that these features are pseudomagmaclasts, arising from inhomogeneous patchy serpentine and clay alteration of portions of the groundmass. Similar pseudomagmaclasts and associated boundaries, formed by inhomogeneous replacement of the groundmass, were described from the hypabyssal Rat kimberlite at Ekati (Webb et al., 2008). No definitive magmaclasts were identified in this study, but more definitive examples of true coherent magmaclasts may exist in other areas, as reported by North Arrow.

5.1.2 PK346

Drill core from PK346 is dominantly matrix-supported and segregationary in texture. The groundmass consists of (in order of decreasing abundance) segregations of calcite and serpentine, phlogopite, apatite, spinel group minerals, and sulfides (Fig. 5b and 7c). Only one possible country rock inclusion is present in any of the samples, though the degree of alteration masks the original characteristics. This lack of country rock dilution is similar to the findings of North Arrow, who estimated dilution by country rock fragments at ~ 3 % (Kupsch, 2017). Most olivine is fine- to medium-grained and macrocrysts are less common, irregular and elongate to rounded in shape. As such, PK346 is more fine-grained than PK150 and has a significantly higher proportion of large calcite segregations (Fig. 12). Calcite is also present in veins and as the dominant replacement phase of olivine, with easily discernable euhedral calcite rhombs in the cores of some grains. No fresh olivine is observed in thin section due to thorough carbonate replacement. Serpentinization of the olivine is concentrated around the outer margins with lesser amounts of patchy replacement and cross-cutting veins. Secondary cryptocrystalline dark brown-green serpentine alteration in the rest of the groundmass is intense, often overgrowing the calcite segregations and variably masking euhedral olivine boundaries. Irregular serpentine segregations, distinct by the olive-green colour, fill the interstices of other areas. In the areas least impacted by secondary serpentine, dendritic serpentine grains are preserved.

Groundmass minerals have subtle differences compared to PK150. Apatite dominantly occurs as fine (~ 20 to 30 μm) euhedral or stubby prisms scattered throughout the groundmass. Large arrays (up to 200 μm) or acicular radial apatite are rare but can be found in sample 44864, associated with carbonate-rich areas. The groundmass phlogopite typically occurs as zoned, ragged, poikilitic plates with chadacrysts of spinel group minerals and sulfides (Fig. 5b and 7c) or in a decussate texture of stubby but irregularly-edged grains. Spinel group minerals tend to

occur as aggregates (usually 90 to 175 μm across) in the groundmass, within ilmenite rims, or occasionally as discrete isolated grains (Fig. 13a – c). All varieties can be atoll or non-atoll.

Ilmenite is abundant and presents an overall smaller size fraction (usually < 2 mm) than PK150. Representative textures of ilmenite in PK346 are presented in Fig. 13. The interiors of ilmenite grains typically lack the texture seen in ilmenite from other bodies (i.e., exsolution, compositional variation); rarely is there significant exsolution bands. The margins of ilmenite macro- and macrocrysts exhibit complex morphologies due to resorption and reaction-related spinel group minerals, which can contain crystallized sulfide droplets. The lighter interior portions of the ilmenite rims correspond to a distinctly different Fe composition from the core composition (see section 5.3.5). The ilmenite population with small size fraction tends to be significantly subjected to serpentine overgrowth and have much of the grain converted to the PK346 rim-specific composition. Rutile is rarely found in PK346 ilmenite rims (only in 44860 and 44864) and these rims are texturally distinct for from the rutile-rimmed ilmenites of PK150. The ilmenite in PK346 have a much higher proportion of spinel, leaving a very jagged arrangement of the outer periphery when compared to the relatively smooth rutile rims in PK150.

In all studied samples of PK346 are abundant selvages of solidified melt on crystals and uncored melt pockets occurring in drill core from depths of 37.5 to 87 m (Fig. 14). Most examples in PK346 are spherical to ellipsoidal with regular to irregular and curvilinear rim morphologies. The selvages can form complete or partial, symmetrical or asymmetrical single rims on olivine and ilmenite macrocrysts. The dark green serpentine throughout the groundmass commonly coats the microcrysts and obscures the relationship between the apparent crystallized melt and the surrounding kimberlite. Though there are superficial similarities between the magmaclast rim and groundmass in certain areas, examination of thinner-cut sections does not

demonstrate the gradational changes from the fine-grained rim components to the groundmass as described in the pseudo-magmaclasts of PK150. Some of the large cored magmaclasts have well-defined boundaries with the surrounding kimberlite while others have less distinct, diffuse margins. The selvages dominantly consist of intergrown serpentine and calcite with opaque oxide minerals. Very fine-grained olivine and phlogopite are sparsely distributed in some examples but comprise approximately 10 % in others, with a large proportion equivalent size to the microcrysts of the surrounding kimberlite. The selvage groundmass is poorly to well crystalline; faint concentric orientations are present in a small number of the cored examples. The characteristics of these selvages are reflective of the basic character of hypabyssal kimberlite.

5.1.3 PK151

The PK151 thin section is the most heavily altered sample (Fig. 15). The groundmass is composed of intergrown serpentine and calcite, phlogopite laths, apatite, and spinel group minerals. The initial character may have been more calcite-rich, then was extensively overgrown by secondary serpentine. Olivine macrocrysts are common but they (and microcrysts) are completely altered by serpentine, with associated magnetite comprising a significant portion of grain interior and forming a fine rim (<6 μm) around some relict olivines. Other olivine contains fractures infilled by calcite. Groundmass phlogopite occurs as square to rectangular prisms and have experienced considerable alteration (Fig. 15a). Fe-rich lenses are present in the groundmass in calcite segregations and phlogopite as well as olivine; no EPMA analysis was possible due to extreme compositional variations of these lenses, which appear “fuzzy” on BSE imaging. Between the Fe-rich lenses and alteration, very little phlogopite remains to analyze by EPMA. Apatite is a minor groundmass phase, forming small (<25 μm) stubby hexagonal prisms.

Spinel (with or without atolls) occur as isolated grains in the groundmass, in clusters, or necklacing olivine/ilmenite. Rutile reaction rims on ilmenite like those seen in PK150 are present. Ilmenite is also typically rimmed by (magnesian) ulvöspinel and portions of the rim contain elevated MnO contents based on EDS spectra.

5.1.4 PK312

The singular slab of core from PK312 contains abundant irregular or angular olivine macrocrysts (up to 7 mm) and microcrysts. Olivine is completely altered by serpentine and clays, with a higher proportion of the latter than other samples, and is poorly sorted. A portion of the calcite segregations remain quite pristine while carbonate laths show a greater degree of alteration. The groundmass consists of serpentine + calcite, phlogopite, and spinel group minerals. Phlogopite macrocrysts are considerably rounded (Fig. 16a). Garnet with kelyphite rims are relatively common. Groundmass spinel group minerals have similar morphologies to the samples described above. Groundmass phlogopite can become significantly coarser in comparison to the other bodies (single laths up to 160 μm). These grains exhibit minor zoning but frequent serpentine and spinel chadacrysts, occurring as isolated or interlocking laths. The ilmenite in this sample has a similar overall texture to the above bodies but exhibits some of the most complete serpentine alteration of any ilmenite examined. For example, Fig. 16b displays a considerable portion of a large ilmenite grain replaced by serpentine, itself crosscut by a thin calcite vein. The bright phase shown by BSE commonly surrounding ilmenite macrocrysts is magnesian ulvöspinel. The darker portions of the ilmenite rim shown by BSE are an irregular, multiphase assemblage that could not be analyzed. Faintly zoned zircon associated with magnetite is also present as an accessory phase (Fig. 16c and d).

5.1.5 PK314

Samples are more fine-grained overall, dominated my microcrysts rather than macrocrysts (maximum olivine size ~ 1 mm), though olivine is distributed approximately evenly through the samples in thin section. The groundmass varies between serpentine- and carbonate-rich areas with phlogopite, apatite, and spinel group minerals. Olivine alteration is dominated by serpentinization with associated secondary magnetite fringes/inclusions and minor clays. Pale yellow to green serpentine surrounds the former olivine and forms networks through the brown interiors. Groundmass phlogopite laths (minorly zoned) are most commonly observed in areas adjacent to ilmenite. Groundmass spinel group minerals occur with and without atolls. Minor amounts (< 5 vol%) of acicular radial apatite is present in the groundmass, significantly overgrown by serpentine. The interiors of certain ilmenite exhibit signs of considerable alteration, including multiphase patches, pocked surfaces, and compositional variations. As such, it is difficult to distinguish primary textures in ilmenite of PK314 (Fig. 17). Reaction between kimberlite and ilmenite resulted in the formation of rutile in the rims, partially altered to pseudorutile in some areas. Remnants of the grain edges appear similar to those of PK346, with abundant very well-developed atoll-textured spinel group minerals. Accessory chlorite, fine-grained dolomite and Fe-bearing dolomite are also present.

5.2 Whole Rock Geochemistry

Whole rock geochemistry results indicate PK150 has relatively high SiO_2 (40.8 wt%) compared to other archetypal (Group I) kimberlites (Table 4; Fig. 18). High TiO_2 in PK150 and PK346 (4.24 and 4.77 – 4.97 wt%, respectively) as compared to archetypal kimberlite is consistent with the high modal percentage of megacryst suite ilmenite. The FeO content is also

elevated at 15.3 wt% (PK150) and 13.6 wt% (PK346), slightly above the upper range found for fresh hypabyssal kimberlite from Kimberley, South Africa (~ 10 wt%; le Roex et al., 2003). The other oxides measured are within expected ranges of archetypal kimberlite. The slightly elevated Al contents of PK150 and PK346 (approximately 2.21 and 2.85 wt% Al_2O_3, respectively) also suggest crustal contamination when compared to low Al_2O_3 (< 2 wt%) in uncontaminated archetypal kimberlites (Pearson et al., in press). The PK346 samples have 4 wt% more CaO, reflective of the greater frequency of carbonate segregations observed in thin section. PK150 and PK346 have similar levels of TiO_2 (~ 4.5 wt%), Al_2O_3 (~ 2.5 wt%), and MgO (~ 29 wt%). PK150 has a Mg# (100Mg/(Mg+Fe)) of 77 while PK346 is slightly higher at 80. The two samples of PK346 have approximately equivalent values for the major oxides, Zr, Co, and Rb but appreciable differences in Sr and Ni. Due to the limited number of data points, no bulk rock trends or systematic variation can be identified within Pikoo.

Quantifying the degree of contamination can prove incredibly important to the economic assessment of kimberlites as less crustal dilution allows for higher potential diamond grades. Commonly, the Clement's Contamination Index (C.I.), where

$$\text{C.I.} = \frac{SiO_2 + Al_2O_3 + Na_2O}{MgO + K_2O}$$

is used to compare the relative contributions of tectosilicates and clay minerals (sediments introduced during contamination and alteration) to Mg-silicates and phlogopite (Clement, 1982). Traditionally, a C.I. of < 1 indicates fresh/uncontaminated kimberlite while a C.I. > 1 implies more significant weathering and contamination. The Pikoo samples have C.I.s of 1.5 (PK150) and 1.2 (PK346), hence 'contaminated'. These values are supported by petrographic evidence of crustal xenoliths (~ 15 to 20 vol%, albeit heavily altered) found in PK150 samples. However,

the utility of the C.I. is limited due to its lack of sensitivity. The presence of mantle material in kimberlite counteracts the effects of crustal material on the C.I. value – i.e., it decreases the C.I. value – meaning it is not possible to identify small volumes of crustal contamination when significant quantities of mantle peridotite are present using this index (Kjarsgaard et al., 2009; Pearson et al., in press).

Kjarsgaard et al. (2009b) added the parameter of natural log (Si/Al) to aid in distinguishing contaminated kimberlite from non-contaminated samples. This screen effectively partitions Lac de Gras kimberlite samples into discrete clusters, one of which was influenced by Al-rich crustal material (Fig. 19). The PK346 samples mildly overlap the 'non-contaminated' field in Fig. 19 (Kjarsgaard et al., 2009b) with a small proportion plotting towards high ln(Si/Al) and C.I. While additional screens such as ln (Si/Al) discriminate PK346 samples from PK150, little confidence can be placed on the discrimination as there are only three data points generated by this study. It should be noted that no visible mantle xenoliths are observed in any core samples involved in this study.

5.3 Mineral Chemistry

Mineral chemistry results are compiled in Tables 3 through 9. When examining compositional trends, it is useful to bear in mind that the PK151 and PK314 intrusions occur in close spatial proximity to PK150 and PK346, respectively.

5.3.1 Olivine

Core (n = 70) and rim (n = 47) EPMA analyses were performed on partially fresh olivine from PK150 (Table 5). BSE imaging reveals a sharp core to rim zonation corresponding to changes in composition, primarily decreasing in Mg#. The rims have distinctly lower Mg#'s

(80.4 to 88.4, 85.9 median) than most core analyses (maximum 91.5). The relationship of asymmetric rims on angular cores (Fig. 6) suggests that the higher Mg# cores reflect an inherited origin rather than representing the "normal zoning" process induced by fractional crystallization (cf. Streck, 2008). Values of CaO for both cores and rims are between 0.01 and 0.25 wt% (generally < 0.10 wt%; Fig 19a). The majority of core analyses form a tight cluster in NiO vs Mg# space (Fig. 20b). These grains contain 0.36 – 0.39 NiO wt% and <0.08 wt% CaO, consistent with mantle values (Foley et al., 2013). The rims (and a lesser portion of the cores) are well separated from this cluster, exhibiting a positive correlation between Mg# and NiO content (Fig. 20b) and spanning a much greater range in Ni content (0.05 to 0.34 wt% NiO). Plotted for reference are 12 olivine analyses from partially fresh FALC olivine (Leahy, 1996); Mg# generally ranges from 88 to 94, NiO ranges from 0.11 to 0.42 wt%, and CaO is ≤ 0.40 wt%. The two olivines with particularly low Mg#'s (79 and 82) were attributed to a crustal origin, possibly derived from metabasic basement rocks (Leahy, 1996). Olivine from peridotite xenoliths of the Sask Craton have Mg#'s ranging from 87.6 to 92.8, mode 91.5 (Czas et al., submitted).

5.3.2 Phlogopite

EPMA analyses for groundmass phlogopite are reported in Table 6 and the results essentially follow two distinct trends (Fig. 21) in the discriminatory scheme of Mitchell (1995). The data for all the bodies, originate within the kimberlite groundmass mica field, overlapping with previous FALC analyses (Leahy, 1996; Chalapathi Rao et al., 2017). The phlogopite from PK150 and PK151 are spread along the typical kimberlitic groundmass mica trend of Al enrichment without Ti enrichment and minimal increase in Fe. Conversely, groundmass phlogopite from PK346 exhibits a marked decrease in Al_2O_3 and increase in FeO_T, more akin to

the lamproite trend. Analyses of PK312 (intrusion of close spatial proximity to PK346) exhibits minor Al depletion and Fe enrichment relative PK346. This could be indicative of the tetraferriphlogopite or biotite trend, though a larger dataset is necessary to confidently associate a trend. Groundmass phlogopite compositions from PK314 are more intermediate between the two major Pikoo trends but are most comparable to the kimberlite trend. Kimberlitic groundmass phlogopite also commonly exhibits zoning due to the substitution of Ba for K, from barian phlogopite cores through solid solution of phlogopite-kinoshitalite towards the rim (Mitchell, 1995). The groundmass mica of PK150 exhibits greater Ba enrichment (up to 13 wt% BaO) relative to PK346, which generally contains less than 3 wt% BaO (Fig. 22). Analyses from PK151 and PK314 display moderate levels of BaO (generally up to 5 wt%) while data for PK312 is below 1.5 wt% BaO. Groundmass phlogopite from FALC is also low in Ba (< 0.88 wt% BaO; Chalapathi Rao et al., 2017).

Relatively unaltered phlogopite macrocrysts were analyzed in samples from PK150, PK151, and PK312 (Table 7). The most significant difference between macrocrystic and groundmass phlogopite is the lack of zoning in the macrocrysts. The macrocrysts lack detectable Ba; only in one macrocryst (found in PK150) was BaO above the limit of detection (~ 0.18 wt% BaO).

5.3.3 Spinel

The spinel group comprises a range of minerals of the structure AB_2X_4 (A octahedral coordination, B tetrahedral coordination). In this study, the term 'spinel' will encompass all oxides of the spinel group of minerals commonly found in kimberlites (i.e., spinel, pleonaste, magnetite, ulvöspinel, chromite). Spinel EPMA results are reported in Table 8. The spinel rimming ilmenite (formed by reaction between ilmenite and the kimberlite magma) are referred

to here as 'rim spinel'. Groundmass atoll spinel has Fe-rich outermost rims unsuitable for WDS. The small size fraction of spinel combined with its common replacement by serpentine and/or calcite limits analysis. Chemical zonation on spinels is very fine (< 5 – 10 μm), which precludes EPMA analysis owing to secondary fluorescence issues.

Virtually all spinels are represented by a single EPMA point, excepting two grains able to accommodate multiple points: chromite rimmed by titanian magnesian aluminous chromite (TIMAC) spinel (in PK150) and magnetite overgrown by MUM spinel (in PK312). Groundmass spinel in PK346 is low in TiO_2 (< 5 wt%) in comparison to other Pikoo bodies (up to 25 wt%) and PK346 rim spinel (15 to 21 wt%). In addition to a larger range in TiO_2, groundmass spinel from the other bodies also have a greater spread in Fe_2O_3 (< 10 wt% to ~ 65 wt%) in comparison to the more restricted range in PK346 (generally between 35 and 50 wt%). The composition of spinels found in ilmenite reaction rims tend to be higher in TiO_2 (Fig. 23).

Most spinel from Pikoo corresponds most closely with Trend 1 spinel with a portion of PK151 analyses corresponding to Trend 2 (Fig. 24) in the discrimination outlined by Mitchell (1986) and Roeder and Schulze (2008). While a large portion of PK150 and PK314 analyses fall within or near the Chr field, nearly all spinel analyses from PK346 and PK312 overlap the MUM field of Roeder and Schulze (2008). Some analyses falling near the Mag field likely formed from late metasomatic fluids consistent with their occurrence within relict olivine or infilling fractures in ilmenite.

5.3.4 Apatite

Due to the fine grain size of groundmass apatite, major and minor elements were only measured for large apatite fans in PK150 (Table 9). Beyond the major constituents, they only

contain appreciable amounts of F (3.22 to 2.56 wt%), SrO (1.34 to 1.70 wt%), and SiO_2 (0.18 to 1.03 wt%); Cl is nearly always below the limit of detection. The results from Pikoo are in good agreement with other kimberlitic apatite (Fig. 25), which other studies have found to mostly comprise fluorapatite with comparatively low chorine and hydroxy components (e.g., Mitchell, 1986; Malarkey et al., 2010; Solty et al., 2017; Milligan, 2017; Milligan et al., 2017).

5.3.5 Ilmenite

Ilmenite from Pikoo (Table 10) are Mg-rich (generally > 9 wt% MgO), plotting within the kimberlitic ilmenite field of Wyatt et al. (2004) and overlapping with Mg-ilmenite globally (Kaminsky et al., 2004; Fig. 26). Though ilmenite from the two largest bodies (PK150 and PK346) are texturally distinct, they demonstrate complete overlap in their major element chemistry. Ilmenite from PK151 deviates slightly from most of the samples, exhibiting increasing MgO with very little change in TiO_2 compared to the general correlation of these components in other ilmenites. Nevertheless, differences between PK150 and PK346 do exist in the minor element composition, with PK150 ilmenite exhibiting a greater enrichment in Cr_2O_3 (Fig. 27a). Ilmenite from PK312 follows a similar trend to PK346 with maximum values of Cr_2O_3 and MgO of approximately 2 wt% and 13 wt%, respectively. The few ilmenite analyses for PK314 follow the parabolic relationship between Cr_2O_3 and MgO reported by Haggerty (1975). PK151 ilmenite can become quite enriched in Cr_2O_3 (up to 6.25 wt%) but systematic covariation between Cr_2O_3 and MgO is absent (Fig. 27b). Ilmenite from PK150 are enriched in MnO relative to ilmenite from PK346, with maximum values of 3.26 and 1.17 wt% MnO, respectively (Fig. 27c). The rims exhibit higher MnO enrichment relative the cores of PK150 and PK346, up to 7.44 and 2.00 wt% MnO, respectively. Data for PK151 exhibits comparable MnO levels to PK150 cores, as does PK312 to PK346 (Fig. 27d). The highest Mn content

measured in an ilmenite core was from PK314 at 5.75 wt% MnO. Ilmenite from FALC displays similar MnO levels to PK346.

Ilmenite from Pikoo plots dominantly in the intermediate to ultimate preservation fields defined by Gurney and Zweistra (1995), except for the rims of ilmenite from PK346, which plot completely off the array (Fig. 28). Ilmenite from PK151 exhibit approximately invariant Fe_2O_3 abundance with increasing MgO contents compared the negative relationship typically exhibited. The rim compositions of ilmenite from PK346 are chemically distinct from the main body of the grains, composed of similar levels of TiO_2 but very little MgO (< 0.6 wt%, median 0.07 wt%) and thus fall within the non-kimberlitic boundary shown in Fig. 26. While the grain interior is composed of a roughly 3:1 ratio of $FeO:Fe_2O_3$, the Fe^{3+} component in the rims is minimal and Fe compositions are almost entirely of comprised FeO (generally < 1 wt% Fe_2O_3). Slight to substantial decreases in the Fe_2O_3 contents of ilmenite rims in comparison to cores is observed in many other kimberlite localities (Schulze et al., 1995).

5.3.6 Miscellaneous

Lesser numbers of analyses for rutile, pseudorutile, garnet, and perovskite were performed. Rare garnet in PK150 have chemistry indicating derivation from megacryst or Ti-metasomatized suites outlined by (Grütter et al., 2004; Table 11). Only the major elements were analyzed in perovskite rather than a complete REE analysis (Table 12). Results for rutile and pseudorutile are tabulated in Table 13 and Table 14, respectively.

5.4 Trace Element Geochemistry

5.4.1 Apatite

Apatite trace elements for Pikoo were analyzed from the large acicular radial fans of 44813, the results of which are tabulated in Table 15. Larger fans permitted larger spot sizes to analyze for trace elements. The REE patterns display many of characteristics associated with kimberlitic apatite with negative slopes displaying greater depletion in the LREE in comparison to crustal apatites and a distinct lack of Eu anomaly (Fig. 29a). Pikoo apatite contained high Ba and Sr (57,500 and 1,700 ppm, respectively), low Y (14.6 ppm), and Th > U (Fig. 29b). Apatite from other kimberlites share the above characteristics with Pikoo apatite (Fig. 29c and d) though Pikoo overall tends to contain lesser amounts of REE and many other trace elements. Apatite derived from granitoid and entrained by the Leslie kimberlite is also plotted to highlight distinctive geochemical characteristics (Milligan, 2017; Milligan et al., 2017). In comparison to crustal apatite, kimberlite-derived apatite possessed steep negative REE slopes, lack of Eu and Ce anomalies, enrichment in Sr and Ba, low Y, and Th > U.

5.4.2 Ilmenite

Trace elements were measured in a small subset of ilmenite from PK150 and PK346, reported in Table 16. The concentration of textural features (e.g., exsolution lamellae) in PK150 ilmenite grains complicated ablation of pure ilmenite, leading to possible ablation overlap of exsolution lamellae. While differences are evident in the minor element chemistry, PK150 (n = 19) and PK346 (n = 18) display almost complete overlap in their trace element composition (Fig.29). The trace element chemistry of Pikoo ilmenite is consistent with Mg ilmenite of other kimberlites (e.g. Moore et al., 1992; Carmody et al., 2014; Castillo-Oliver et al., 2017), typically containing relatively high amounts of many HFSEs, particularly Ta (50 to 270 ppm, median 120 pp) and Nb (335 to 2660 ppm, median 1300 ppm) in comparison to other rock types (Jang and Naslund, 2003; Kryvdik, 2014). Carbonatitic ilmenite, however, can exhibit similar or higher Nb

and Ta values (Kryvdik, 2014). The Nb/Ta ratio at Pikoo is relatively low, ranging 6.7 to 18 (median 9.8), similar to narrow range of Angolan kimberlites (Castillo-Oliver et al., 2017). The Fe^{3+}-ilmenite found in Angolan kimberlites (Castillo-Oliver et al., 2017) retain higher Nb contents at relatively similar HFSE levels compared to Mg- and Mn-rich ilmenite.

5.5 Geochronology

5.5.1 Apatite

For the large apatite fans of PK150, U-Pb isotopic data were collected using relatively large beam diameters (50 µm raster lines of 30 s duration) to enhance sensitivity, but unfortunately, no radiogenic Pb was detected (Table 17). This could suggest a very young crystallization age for the apatite, i.e. the apatite grains crystallized long after emplacement of the kimberlite or the kimberlite itself is very young. Neither of these options seem likely. Petrographic observations (overgrowth by calcite, chadacrysts of spinel and perovskite, etc.) indicate that the apatite is crystallized magmatically with other kimberlite minerals. These results suggest that the apatite fans are composed almost solely of common Pb, from which it is impossible to determine an age. Trace element analyses indicate that both U and Pb are contents low (< 0.5 and < 1 ppm, respectively).

5.5.2 Perovskite

A comparison was first made between the U-Pb data (standards and unknowns) acquired at a 23 versus a 33 µm spot size from the first two analytical sessions. Both data sets returned consistent data, with no obvious bias and were thus data from both spot sizes were combined for the final regression. The perovskites from Pikoo have high but variable U contents, ranging from 23 to 395 ppm, which is favourable for U-Pb geochronology (Table 18). The data exhibit a

large range in $^{238}U/^{206}Pb$ from 4.3 up to 13.6 and the $^{207}Pb/^{206}Pb$ ratios range from 0.42 to 0.12. The common Pb composition was estimated by plotting the uncorrected data on a Tera-Wasserburg diagram and determining the intersection with the y-axis. Both the semi-total and total Pb approaches were employed in the age determination of Pikoo, with two outliers excluded from the calculations on the basis of a 2σ rejection outside of the error envelope. Two additional analyses were excluded from the total Pb approach calculations due to negative $^{204}Pb/^{206}Pb$ ratios. The former approach returned a lower intercept age of 416 ± 18 Ma (MSWD = 8.7; Fig. 31). Using the total Pb approach, the data should fall along the radiogenic plane with the vertex at the sample age. From this, an age of 417 ± 14 Ma (MSWD = 5.6) is returned. The two ages are within error and have very similar uncertainties, lending greater confidence to the age determination. Fulfilling the 3D regression of the total Pb approach indicates that the Pikoo perovskites likely represent a single population of perovskite that incorporated a uniform common Pb isotopic composition. As the total Pb approach is a more stringent test of this fundamental assumption, this age and associated uncertainty of 417 ± 14 Ma is taken to be the best estimate of the age of the Pikoo samples.

5.6 Tracer Isotopes

Several perovskite grains were analyzed for their Sr isotopic compositions but the uncertainties on the measurements were too great to yield any meaningful results. This is due in part to the small spot size (23 μm) and short ablation time (48 s) necessitated by the fine-grained perovskite population. A larger size fraction of perovskite could improve the internal precision by supporting a larger spot size and longer ablation duration.

Much more success was achieved in analyzing the Nd isotopic composition of another 15 grains as the concentration of Nd in perovskite is 2300 – 9000 ppm (median 5550 ppm), much

higher than Sr (generally 1000 – 2000 ppm). Despite this, it is typically more difficult to generate quality Nd data, suggesting the 33 μm spot size threshold is critical for isotopic determinations of perovskite via LA-MC-ICP-MS. A degree of caution is advised, however, as it cannot be definitively proven that crustal contamination did not influence Nd as well. Secondary matrix-matched perovskite standards of Afrikanda (n = 14) and Ice River (n = 17) were analyzed concurrently with the unknowns. The primary standard (Ice River) measurements differ slightly from accepted values and are thus corrected to the accepted values. This factor is also used to correct the measured ratios of $^{147}Sm/^{144}Nd$ and $^{143}Nd/^{144}Nd$ for Pikoo and Afrikanda. Repeated analyses measured the $^{143}Nd/^{144}Nd$ ratio at 0.512552 for Afrikanda (accepted values of 0.512540 ± 24 for 25-AF and 0.512575 ± 12 for 10AFK3; Wu et al., 2013a) and 0.512530 for Ice River (accepted value of 0.512581 ± 32, 2σ; Tappe and Simonetti, 2012).

The final Pikoo values for $^{147}Sm/^{144}Nd$ and $^{143}Nd/^{144}Nd$ range from 0.0682 to 0.0775 (median 0.0719) and from 0.51215 to 0.51246 (median 0.51224), respectively (Table 19). The value of $^{143}Nd/^{144}Nd_{CHUR}(t)$ was calculated using values of $^{143}Nd/^{144}Nd_{CHUR}(0) = 0.512630 \pm 11$ and $^{147}Sm/^{144}Nd_{CHUR}(0)$ $0.1960 = \pm 4$ (Bouvier et al., 2008) according to the equation:

$$\frac{^{143}Nd}{^{144}Nd}_{CHUR}(t) = \frac{^{143}Nd}{^{144}Nd}_{CHUR}(0) - \frac{^{147}Sm}{^{144}Nd}_{CHUR}(0)x\left(e^{\lambda t} - 1\right)$$

where λ is 6.54 x 10^{-12} and t represents 417 Ma, as determined experimentally (see above). From this, εNd_{417} was determined from:

$$\varepsilon_{Nd}(t) = \left(\frac{\left(\frac{^{143}Nd}{^{144}Nd}\right)_{sample(t)}}{\left(\frac{^{143}Nd}{^{144}Nd}\right)_{CHUR(t)}} \right) x\ 10^4$$

There is an appreciable range in $\varepsilon_{Nd}(t)_{417}$ values of approximately +3.3 to -3.0, though this range is consistent with archetypal kimberlites (Fig. 32). Removing the most extreme positive and negative value narrows the range to +1.83 to -1.97 (median -0.87), very similar to chondritic values. This range is also distinct from South African lamproites (var. Kaapvaal) and typical olivine lamproites.

6 Discussion

6.1 Are the Pikoo intrusive bodies kimberlite?

Textural characteristics, mineralogy, and mineral chemistry are considered in classifying the intrusive rocks from Pikoo. Chemical and textural evidence gathered is consistent with North Arrow's identification of the Pikoo bodies as bonafide archetypal kimberlite. Based on petrographic study of thin sections, the samples can be described as altered olivine macro/microcrysts and abundant ilmenite set in a groundmass of serpentine, calcite, phlogopite, and spinel group minerals (± perovskite, sulfides, and apatite), imparting an inequigranular appearance. A magmatic crystallization sequence of olivine, spinel group minerals + perovskite, apatite, phlogopite, and calcite is interpreted from petrographic and EPMA studies. Apatite is often intergrown with or pseudomorphed by calcite. These characteristics are typical of archetypal hypabyssal kimberlite (Mitchell, 1986, 2008).

Major, minor, and trace element chemistry of the dominant phases found in Pikoo samples are consistent with recognized kimberlitic compositions. Olivine cores and phenocrystic overgrowths overlap well with the NiO and CaO content of the melt trend (Bussweiler et al., 2015). Ilmenite plots well within the kimberlitic field defined by Wyatt et al. (2004) shown in Fig. 26.

REE patterns and trace elements in apatite from PK150 were compared to other kimberlitic apatite and crustally-derived apatite entrained by kimberlite. These characteristics of the Pikoo samples are reflective of apatite crystallizing directly from the kimberlite magma. These features include steep negative REE slopes, lack of Eu and Ce anomalies, enrichment in Sr and Ba, low Y, and Th > U (Milligan, 2017; Milligan et al., 2017). Trace elements measured in

ilmenite are consistent with Mg ilmenite found in other kimberlites, containing relatively high amounts HFSE such as Nb and Ta (Castillo-Oliver et al., 2017 and references therein). Calculated values of εNd_i (mostly +1.8 to -2.0) for PK150 perovskite overlap well with the typical range exhibited by archetypal kimberlites (Nowell et al., 2004; Pearson et al., in press) and values previously reported for the FALC kimberlites in Saskatchewan (Kjarsgaard et al., 2017). Groundmass phlogopite analyses dominantly correspond to the kimberlitic groundmass mica trend (Mitchell, 1995), excluding PK346. This evidence alone is insufficient to discount PK346 as true kimberlite. For example, Lac de Gras is known to consist of archetypal hypabyssal kimberlite but mica from one body (Porpoise) instead follows the tetraferriphlogopite trend more often associated with lamproites (Armstrong et al., 2004).

Spinel chemistry is more complicated to interpret. Based on extensive study of kimberlitic spinel, Roeder and Schulze (2008) concluded that the morphology and composition of spinel in kimberlite can vary due to rapid shifts in pressure and temperature in addition to the generally recognized role of melt composition. The high levels of carbonate (groundmass/segregations) in archetypal kimberlites, allowing for a high Mg activity at low $Fe^{2+}/(Mg + Fe^{2+})$, is thought to influence the moderately oxidizing and magnesian nature of Trend 1 (Roeder and Schuzle, 2008). These authors note the similarity between the increasing Ti and Fe^{3+} with increasing $Fe^{2+}/(Mg + Fe^{2+})$ of their Trend 2 to chemical zonation in basalts. This relative enrichment is due to a depletion in Al and Mg from co-crystallization of other silicates (e.g., olivine and phlogopite). Progressive compositional evolution of spinel from chromite/TIMAC to MUM to magnetite (Trend 1) is observed in kimberlites from diverse localities (Mitchell, 1986; Roeder and Schulze, 2008; Giuliani et al., 2017; Soltys et al., 2018) and is the dominant trend of Pikoo spinel. While the spinel of PK346 is comparable in

composition to that from carbonatites, i.e. high $Fe^{3+}/(Fe^{3+} + Al + Cr)$ at mid- to high-levels of $Fe^{2+}/(Fe^{2+} + Mg)$ (Roeder and Schulze), the ilmenite chemistry is not reflective of carbonatites, particularly in terms of the low MnO content (Mitchell, 1986). As such, Pikoo spinel is most consistent with a kimberlitic origin.

With reasonable certainty that the Pikoo bodies constitute archetypal kimberlite, an effort must be made to assign a textural-genetic classification. Given the well-crystalline groundmass and overall sample texture, it must be determined if the bodies represent hypabyssal or extrusive coherent kimberlite. Two important features to consider in this step is the origin of the magmaclasts and the abundant amoeboid/irregular segregations in the groundmass. The latter is typical for many hypabyssal kimberlites (Mitchell, 1986).

Definitive identification of the features reported as magmaclasts in PK346 by North Arrow is impeded both by the intense alteration and the overlap in characteristics describing autoliths and different types of magmaclasts (melt-bearing pyroclasts and melt segregations). The categorization of these feature has important implications for textural-genetic classification of kimberlite and can significantly impact interpretation of potential economics. The processes generating the magma disruption may also impact the diamond population and the extent of physical processes (sorting, removal of fines, etc.) are often reflected by melt-bearing pyroclasts populations in terms of size, distribution, and physical attributes (Webb and Hetman, 2017). 'Magmaclast' is a general descriptive term applied to fluidal-shaped, physically distinct bodies of magma formed from magma disruption prior to solidification either by fragmentation (melt-bearing pyroclasts, discussed above) or non-explosive segregation processes (Webb and Hetman, 2017; Scott Smith et al., 2018). It is intended as an interim term to be followed by more detailed interpretation and while it is recognized that its use is not ideal due to diverse modes of

formation, it is currently the recommended terminology (Scott Smith et al., 2018). Classification as melt-bearing pyroclasts indicates a pyroclastic origin, typically associated with what is now referred to as Kimberley-type pyroclastic kimberlite (formerly diatreme facies or tuffisitic kimberlite; Scott Smith et al., 2018). Melt segregations tend to form in near-surface environments (subvolcanic to subsurface), commonly in hypabyssal intrusions and other coherent bodies. Conversely, autoliths can both form from and occur in either volcaniclastic or coherent kimberlite.

Many of the characteristics displayed by the features in PK346 (Fig. 14) are commonly described of autoliths, which are fragments produced by disrupting consolidated kimberlite of an earlier body (Scott Smith et al., 2018). The large example shown in Fig. 14a has features different from the surrounding kimberlite. The alteration style of the core is distinctly different from other olivine macrocrysts. The olivine core also shows thick yellow serpentine bands and moderate iddingsite alteration compared to the dominantly calcite-replaced olivine macrocrysts within the main kimberlite. The rim components are not as coarse or abundant as the groundmass but the whole of the cored magmaclast still possessing the main characteristics of kimberlite. However, the faint tangential arrangement of rim components about a core is atypical of most autoliths (Mitchell, 1986). Autoliths are also usually described as angular to subangular, though if rounding occurred during emplacement, it could be impossible to differentiate sub-rounded autoliths from melt-bearing pyroclasts with faint tangential arrangement (Mitchell, 1986, 1995; Scott Smith et al., 2018). North Arrow interprets the PK346 body as one phase of kimberlite (Kupsch, 2017), meaning fragmentation and final inclusion would have to occur in the same body.

Ambiguity in the literature also arises from use of the term ‘nucleated autolith’ (e.g., Danchin et al., 1975) to describe spherical to ellipsoidal bodies of fine-grained kimberlite produced by magmatic crystallization on mineral/rock fragment nuclei. However, it has long been suggested that this term (sensu Danchin et al., 1975) be abandoned due to the incorrect genetic relationships implied for what are considered fluidal, juvenile bodies (Mitchell, 1995; Scott Smith et al., 2018); Scott Smith et al. (2018) suggest that these features be termed cored magmaclasts.

The rounding of many of the magmaclasts, cored and uncored, may indicate melt-bearing pyroclasts. The term melt-bearing pyroclasts is suggested as replacement term for pelletal lapilli (Scott Smith et al., 2018). Common characteristics of these features include pronounced sphericity, large cores of euhedral crystals or fragments of crystals, kimberlitic groundmass of amorphous dark material that is often optically unresolvable, and margins subjected to alteration/replacement by secondary minerals or serpentine (Mitchell, 1986). These cores are often pseudomorphed olivine or occasionally other macrocrysts (e.g., phlogopite) but seldom consist of country rock (Mitchell, 1986). Rim components with a faint concentric orientation are present in a small portion of the cored magmaclast, which is more common in melt-bearing pyroclasts than autoliths. It should be noted that the presence of autoliths does not preclude the presence of melt-bearing pyroclasts (pelletal lapilli) as they can occur in association. If these magmaclasts are indeed melt-bearing pyroclasts, it would necessitate fragmentation and re-welding of the bodies, such as in a spatter dyke. Examples of melt-bearing pyroclasts in extrusive coherent kimberlite can be seen in economic kimberlite deposits (e.g., van Straaten et al., 2011). However, no discernible evidence of welding has yet been seen in thin section or core (Kupsch, personal communication). The selvages are typically somewhat coarser than the

amorphous brown material in melt-bearing pyroclasts, with some optically resolvable portions, and contain rounded components.

North Arrow reported the presence of coherent magmaclasts in the form of melt segregations. Many descriptors of autoliths can also be applied to magmaclasts, but can be distinguished by fluidal shapes, concentric arrangement of components, and frequent protrusion of macrocrysts when cored (Scott Smith et al., 2018). The distribution of serpentine and carbonate throughout the section is heterogeneous, with lighter green serpentine segregations dominating some areas of the groundmass while darker green serpentine covers other portions and coats both the macrocrysts and nearly all microcrysts. In carbonate-rich sections, there are significant distinctions between calcite pools and serpentine, suggesting strong immiscibility between the phases during crystallization (e.g., Fig. 14e – g). Immiscibility or surface tension effects in near-surface environments may have led to coalescence of carbonate into distinct segregations and wrapping of macro- and microcrysts by late-stage kimberlite melt. Magmaclasts identified as melt segregations from the Wales Island hypabyssal kimberlite (shown in Webb and Hetman, 2017) bear similar appearance to the coating of kimberlite material on the macro- and microcrysts of PK346. As well, irregular olivine cores often protrude out of the selvage (Fig. 14b). Given these observations, the most likely identification at present is melt segregations, which would mean the Pikoo bodies, including PK346, are comprised of hypabyssal kimberlite. However, it should be stressed that the material available for this study can only provide snapshots of the Pikoo bodies. A more detailed understanding of the body morphology and additional context from longer lengths of drill core are necessary to confidently identify the magmaclast-like features of PK346. This can be an important step in assigning a

textural-genetic classification and re-evaluation is recommended should additional information become available.

6.1.2 Implications of Alteration

Most kimberlites are highly altered, impacting both mineralogical and textural characteristics. Alteration can mask contamination of country rock xenoliths, impact discriminatory trends, and re-set geochronometers. While no visible mantle xenoliths are observed in any core samples available for this study, North Arrow has documented a considerable population in PK150. The C.I. of the samples sent for whole rock geochemistry reflects 'contaminated' or borderline contaminated kimberlite though it is difficult to estimate crustal fragment inclusion using thin sections. Given this information and the alteration state of the kimberlite, it is likely that, despite carefully selecting core free of calcite veins or visible xenoliths, contaminants (crustal and/or mantle) were included in the crushed sample. The extensive alteration at Pikoo can thus mask the true extent of contamination. Though severe alteration renders the application of several conventional exploration tools (e.g., whole rock geochemistry) impractical, the rocks can still be assessed by new analytical methods (e.g., geochronology and tracer isotope studies of perovskite via LA-ICP-MS), proving that the existing samples do have a wealth of information to offer.

Ilmenite chemistry is well-preserved, even after extreme alteration. The sample (PK151) that appears to have altered chemical systematics, particularly the lack of covariation between FeO content and other oxides displayed by other bodies, also had significant petrographic evidence to suggest secondary Fe-rich phases crystallized post-emplacement. The profusion of Fe-rich lenses (Fig. 15) scattered throughout the groundmass and relict phases of PK151 may be accounted for by an Fe-rich fluid, supported by the lack of systematic variation in ilmenite

chemistry and elevated Fe levels in the spinel (shifting to Trend 2). This was the most-altered sample examined in this study and as only one thin section was available, it is unknown whether the disrupted systematics are widespread throughout the body or a localized feature. The robustness of ilmenite chemistry overall has positive implications for exploration programs, as it is a common kimberlite component that is easily collected in till samples and isolated from heavy concentrate.

Groundmass phlogopite chemistry is also well-preserved despite the pervasive alteration. The compositional variation between PK150 (promising microdiamond results) and PK346 (poor microdiamond results) can perhaps be useful in future studies to distinguish bodies of poor economic potential. The Al-depleted, Fe-enriched phlogopite tended to be associated with more oxidized, highly differentiated late batches of magma.

6.2 Magmatic Evolution

Kimberlites, by definition, are hybrid rocks that contain crustal- and mantle-derived xenoliths/xenocrysts in addition to primary magmatic components. Ascertaining the nature of the components is important as they can offer a valuable perspective into conditions within the mantle and evolution of the kimberlite magma during ascent. Important xenocrystic phases considered in the Pikoo samples are olivine and ilmenite. Xenocrystic olivine, recognized as the darker angular cores of rimmed grains with high Mg# (~ 90) and NiO (0.3 – 0.4 wt%), was entrained from the mantle or peridotite disaggregated during transport. Olivine is also the earliest-crystallizing phase from the kimberlite magma; phenocrystic overgrowths on inherited cores are a common characteristic of many kimberlites globally (e.g., Fedortchouk and Canil, 2004; Kamentsky et al., 2008, 2009; Nielsen and Sand, 2008; Brett et al., 2009; Arndt et al., 2010; Pilbeam et al., 2013; Bussweiler et al., 2015; Giuliani et al., 2017). Therefore, it is

suggested that size and morphology alone are not sufficient to distinguish between populations of olivine (Arndt et al., 2010; Bussweiler et al., 2015). Instead, Bussweiler et al. (2015) proposed that both macrocrystic and groundmass olivine define two distinct trends, the mantle trend (angular cores, low CaO < 0.1 wt%, high NiO of 0.3 to 0.4 wt% at Mg#'s ranging 86 to 93) and the melt trend (thin rims, increasing CaO up to 1.0 wt% and decreasing NiO down to 0.1 wt% at relatively constant Mg# of ~ 91.5), shown in Fig. 20.

Core analyses of Pikoo olivine overlap well with the mantle trend (Fig. 20). Conversely, the decrease in NiO content of the rims falls along a much greater spread in Mg# (from 80.4 to 88.4) than is found in most other kimberlites (Fig 19b). A quarter of core analyses (often identifiable as unrimmed olivine) overlap with rim analyses, far removed from the tight cluster formed by most cores at comparably low Mg#s. Given the complete overlap of rims and unrimmed cores, it is more likely there is a sizeable phenocrystic population in PK150 as opposed substantial entrainment of olivine of xenolithic crustal magmatic origin. Compared to recent suggestions that only a very small percentage (5 vol%) of olivine crystallizes directly from the kimberlite magma (Brett et al., 2008), the proportion of magmatic olivine observed in the Pikoo kimberlites is more similar to early estimates of primary olivine (e.g., Clement, 1982). The wide range in Mg# and protracted melt trend shown in Fig. 20 suggests continued crystallization over an appreciable duration.

The compositional variation recorded by ilmenite can provide useful information of the evolution of the kimberlite magma. Variations in Mg content, exsolution lamellae, and fine-grained reaction zones where ilmenite is in contact with the host kimberlite indicate disequilibrium in the magma. These reaction zones often contain Ti-rich phases such as rutile, perovskite, and spinel and have been noted in other kimberlites (e.g. Schulze et al., 1995;

Kamenetsky et al., 2014). The dominant composition recorded by unaltered, untextured cores is high MgO with FeO:Fe_2O_3 in roughly 3:1 proportions. Traditionally, ilmenite in kimberlite is often thought to contain lesser amounts of Fe_2O_3 in comparison with other igneous rocks (Pasteris, 1981). True Fe^{3+}-rich ilmenite nodules, containing 30 to 40 wt% Fe_2O_3, were found in studies of Angolan kimberlites but the grains were compositionally homogenized to higher Mg contents due to interaction with kimberlitic magma or related fluids (Robles-Cruz et al., 2009, Castillo-Oliver et al., 2017). The elevated MgO and low Fe_2O_3 of Pikoo ilmenite indicate a reduced environment, which has positive implications for the diamond preservation. There is an inferred relationship between oxygen fugacity and diamond preservation potential (Gurney and Zweistra, 1995), with high oxidation states corresponding to high potential for diamond resorption. It should be noted that this preservation potential model is based on South African kimberlites and cannot be universally applied to kimberlites of other localities as exceptions have been documented (e.g., Schulze et al., 1995). The ilmenite at Pikoo likely originated as mantle megacrystic material and later experienced further enrichment in MgO ± MnO.

Suggested origins for this enrichment include reaction with a high-Mg fluid under reducing conditions (Robles-Cruz et al., 2009) or interaction with the kimberlite magma (Pasteris, 1981). Castillo-Oliver et al. (2017) similarly interpret the high levels of Ta, Zr, and Hf associated with Mg-rich ilmenite to indicate interaction with carbonate-bearing kimberlite melt, which can have high contents HFSEs in comparison to similar rock types (e.g., carbonatites; Tappe et al., 2017). Agee et al. (1982) and Schulze et al. (1995) suggest that the higher Mg content of ilmenite rims arose from a sudden increase in the magma's Mg/Fe ratio, caused by incorporation of mantle wall rock (e.g., carbonated peridotite) or the decomposition of magnesite megacrysts during ascent, respectively. High levels of Mg (> 11 wt% MgO) are often

widespread through the interior of the grain. The pervasive nature and variable Mg levels suggest a greater (but variable) contribution of magma interaction during ascent. Analysis of ilmenite rim compositions (rather than the cores) may provide a more reliable indication of potential diamond resorption as the rims would better reflect the redox conditions of the kimberlite with which they were equilibrated. The presence of pseudorutile ($Fe_2Ti_3O_9$), a transitional phase intermediate between ilmenite and rutile, in PK314 indicates an oxidation process to convert Fe^{2+} to Fe^{3+}, with up to one third of Fe^{3+} leached from the original grain (Teufer et al., 1966; Grey and Reid, 1975). This reaction can occur by the diffusion of Fe across an unaltered oxygen lattice, meaning pseudorutile itself can be a stable phase (Grey and Reid, 1975). Pseudorutile was identified in the Horton diamond area (northwest of Great Bear Lake) though it is thought to be related to paleo-lateritic weathering (Davies and Davies, 2019).

The origin of Mn enrichment along ilmenite boundaries/fractures and fine platy grains in the groundmass in kimberlites is similarly debated, with suggestions ranging from primary late-crystallization products of the kimberlite magma (Tompkins and Haggerty, 1985), reaction with a high-CaO fluid (Agee et al., 1982), interaction with late CO_2-rich fluids or hydrothermal fluids related to serpentinization (Robles-Cruz et al., 2009), or a combination of magma and hydrothermal fluid interaction (Castillo-Oliver et al., 2017). Preferential enrichment along grain boundaries and fractures would be expected if fluids played a dominant role. The Pikoo bodies (excluding PK346) do display frequent Mn enrichment in ilmenite rims and along discontinuities. However, PK150, PK151, and PK314 additional exhibit significant Mn enrichment within the interior of the grains (up to 4 wt% MnO). MnO contents reaching similar levels in primary, unaltered ilmenite recovered from kimberlite and as diamond inclusions has

previously been linked to the superdeep diamond population (Kaminsky and Belousova, 2009; Kaminsky et al., 2009).

While ilmenite from other Pikoo bodies have rims easily attributed to reaction with the kimberlite magma, PK346 ilmenite rims are atypical. The grain interiors have an equivalent composition to the other bodies but the rims exhibit a dramatic compositional shift. Analyses (n = 16) taken across four different thin sections of PK346 from three depths (at approximately 38, 55, and 87 m) all recorded near-perfect endmember ilmenite compositions with very little variability (1 – 2 wt% at most). The PK346 ilmenite rims are mainly composed of TiO_2 (50.4 – 51.9 wt%) and FeO (43.1 – 45.3 wt%) with marginal contribution of Fe_2O_3 (0.4 – 2.2 wt%, median 0.5 wt%). These rims record the highest enrichment of MnO (1 – 2 wt%) of any PK346 ilmenite analyses. In contrast to typical kimberlitic ilmenite, the rims in PK346 are depleted in Mg (0.03 – 0.61 wt% MgO, median 0.07 wt%). Other minor elements are either below detection or negligible. Haggerty et al. (1979) refer to ilmenite margins from the Monastery kimberlite with similar compositions (high FeO with enrichment in MnO) as the kimberlitic reaction trend, shifting compositions towards ilmenite in a ternary of ilmenite-geikielite-hematite. The compositional shift, however, was not of the same magnitude as seen in PK346. The extremely narrow compositional range of near-perfect endmember ilmenite across a significant distance indicate the ilmenite was affected by the same process.

High-Ti assemblages (rutile, spinel, and perovskite) are present in ilmenite margins due to magmatic reaction at interfaces with the kimberlite. Much of the major components of these fine-grained reaction products can be sourced from the ilmenite, with contribution of Ca for perovskite available from the carbonatite portion of the magma (Kamentsky et al., 2014). The reaction had an especially corrosive effect on ilmenite in PK346 and PK314, as evidenced by the

margin morphology, with less intense effects within the other bodies. These reaction phases form coeval with their groundmass counterparts, evidenced by the similar compositions of the rim titanomagnetite and groundmass spinel (barring TiO_2). Furthermore, the total Pb approach indicated that the perovskite consists of a single concordant population of the same common Pb composition. Chemical abrasion of ilmenite megacrysts resulting in rims of Ti-Fe oxides and perovskite that formed at a similar time to groundmass perovskite is also evident at Monastery (Kamenetsky et al., 2014).

The earliest phases of spinel to crystallize from the kimberlite magma are chromite/TIMAC spinels, sequestering Cr and, to a lesser extent, Mg and Al. The latter two elements are also taken in by olivine and subsequently crystallising phlogopite. Progressive evolution of the kimberlite magma led to the crystallization of MUM spinel followed by magnetite, as is common in archetypal kimberlites (Mitchell, 1986, 1995; Roeder and Schulze, 2008). The entirety of this trend is exhibited by PK150, PK151, and PK314 while PK346 and PK312 only appear within the MUM field. This suggests that spinel in these intrusions was confined to later portions of the crystallization sequence. Apatite and phlogopite crystallization follow or partially overlap with the MUM spinel, with the final stage of spinel (dominantly consisting of magnetite) forming late in the crystallization sequence, possibly below the kimberlite magma's solidus temperature. This population may derive from the fluids involved in developing carbonate segregations or the serpentinization of olivine (Roeder and Schulze, 2008). The final stages of magmatic crystallization involve the precipitation of carbonate from evolved kimberlitic melt into the mesostasis or as distinct segregations of irregular or embayed morphology. As well, primary serpentine forms additional segregations or develops as plate-like crystals.

In summary, the Pikoo kimberlites were formed from a primary kimberlite magma formed deep within the mantle that entrained olivine, garnet, and ilmenite prior to or during ascent. The ilmenite reacted with the magma during ascent to become enriched in Mg, indicative of a reducing environment. Magma evolution progressed in a manner typical of archetypal kimberlites in PK150, PK151, PK314, and potentially PK312. Conversely, the ilmenite, phlogopite, and spinel chemistry of PK346 suggests that it formed from a batch of magma that already experienced a high degree of differentiation to form an evolved, oxidized fraction of melt with high Fe^{3+} and carbonate content. The oxidizing nature of the magma forming PK346 could account for poor microdiamond results. This magma fraction may be related to PK312, which is in close spatial proximity to PK346. This fundamental difference can account for the distinct disparity in textural, mineralogical, chemical, and alteration features identified by in-depth study of PK150 and PK346. However, given the lack of a dateable mineral population in PK346, an episode of temporally distinct kimberlite emplacement cannot be discounted at this time.

6.3 Age and Regional Implications

Heaman et al. (2003, 2004) examined the geographic and temporal distribution of numerous kimberlite occurrences across North America and their relationship to regional tectonics. The authors identified five broad temporal domains, often connected with probable mantle heat sources. Potential links were drawn between some of these domains and mantle plumes related to the Great Meteor hotspot track and others to changing plate geometry throughout subduction of the Kula-Farallon plate (Heaman et al., 2004). Part of this model consists of a > 4000 km central mid-Cretaceous corridor of kimberlite magmatism, stretching from the Canadian Arctic through central Saskatchewan and into Kansas, USA. The Cretaceous FALC kimberlites are one of the three main kimberlite fields comprising this corridor.

Kjarsgaard et al. (2017) suggest that decompression melting of the transition zone/overlying asthenosphere was triggered by edge-driven convection within the corridor, enabled by the proximity to strongly attenuated lithosphere. The authors then posit that a hot protokimberlite melt (rich in CO_2 and H_2O) was generated from a combination of metasomatism and wet partial melting, with H_2O liberated during the inversion of high-pressure polymorph phases (i.e., ringwoodite/wadsleyite). Local tectonic features were crucial in subsequently emplacing small volume melts in the lithosphere.

The U-Pb perovskite age of 417 Ma is taken to be the most reliable age estimate of PK150, and by extension the diamondiferous magmatic activity at Pikoo. In absence of a dateable phase in a suitable condition (e.g., abundance of inclusions in groundmass phlogopite is unfavourable) in the other samples, this age is applied to the other Pikoo bodies, though it is possible that temporally distinct eruptive events transpired. In the context of North America, circa Silurian kimberlites are not uncommon. The Slave Craton hosts several Siluro-Ordovician kimberlites (Orion 435.4 ± 2.8 Ma, DryBones Bay 441.4 ± 0.8 Ma, Cross 450.4 ± 2.2 Ma, and Ursa 463.0 ± 16.0 Ma) of broadly similar age to Pikoo (Heaman et al., 2003). South of Saskatchewan is the State Line field, from which Iron Mountain is dated as 408.4 ± 2.6 Ma (Heaman et al., 2003). Globally, there was kimberlite activity in Namibia at circa 400 Ma and older (Griffin et al., 2014) and in Russia from 419 to 410 Ma (Sun et al., 2014). Slightly older are the Mengyin kimberlites of China with an emplacement age of ~ 470 Ma (Yang et al., 2009). The modest proliferation of similarly-aged kimberlites may suggest a more widespread period of diamondiferous magmatic activity across North America in circa Silurian to Devonian times than was previously recognized.

6.4 Source Region

Radiogenic isotope systematics are valuable tools for geochemists in their endeavors to model the structure and evolution of the mantle. Kimberlite melts offer an invaluable perspective into the Earth's interior as they are derived from deeper portions of the mantle (> 200 km). They also are less influenced by shallow melt sources (cf. basaltic magmas) owing to the thick lithosphere of the cratons into which they erupt. While perovskite can be unstable under CO_2-rich, weakly acidic conditions (Mitchell and Chakhmouradian, 1998), it can more effectively retain its isotopic composition than other kimberlitic minerals or whole rock samples, as discussed above. While the processes governing the formation and emplacement of kimberlites has been the subject of extensive and ongoing debate, certain characteristics regarding the magma source are agreed upon. Archetypal kimberlites, orangeites (lamproite var. Kaapvaal; Scott Smith et al., 2018), and lamproites magmas can be traced to deep sources with variable lithospheric/asthenospheric contribution. Kimberlites are thought to be derived from a relatively primitive source in terms of their radiogenic isotope systematics, though the potential for mixing of MORB (mid-ocean ridge basalt) and enriched components must be considered (Tachibana et al., 2006). Interaction with the lithosphere can also impart distinct characteristics of the cratons through which the magmas erupt (Tappe et al., 2011).

The range in εNd_i calculated for Pikoo does overlap with the kimberlites of central mid-Cretaceous corridor and the lower range of the OIB (oceanic island basalt) field, as well a selection of northern Canada kimberlites (Fig. 33). The lack of distinctly narrow isotopic range and vastly different age indicate Pikoo was not a product of the same event that generated the mid-Cretaceous kimberlite corridor, despite its spatial association. However, a subducted slab of oceanic basalt in the transition zone or lower mantle could still be a potential source, as has been

proposed for the kimberlites of the mid-Cretaceous corridor and other localities (e.g., Nowell et al., 2004; Carlson et al., 2006; Tachibana et al., 2006; Tappe et al., 2011; Kjarsgaard et al., 2017).

Woodhead et al. (2019) examined the trend of εNd and εHf values of globally distributed kimberlites through > 2 Gyr of time to assess potential evolution of the source reservoir(s) for kimberlites. Their findings indicate that older (> 200 Ma) populations of kimberlites fit a linear isotopic trajectory spanning > 2 billion years. The authors suggest that the abrupt negative deviation from this trajectory seen in select post-200 Ma kimberlites arose from significant contamination by exogenic material into their deep mantle source, possibly in relation to subduction peripheral to Pangea, thereby initiating changes to large-scale mantle regimes. The pre-200 Ma occurrences (termed 'primitive' kimberlites) have much more restricted, close to chondritic Hf and Nd isotope compositions that appear to be derived from a long-lived undifferentiated reservoir occurring deep within the mantle, isolated from crustal recycling to preserve the homogeneous, near-chondritic compositions (Woodhead et al., 2019).

Given the small sample size, fine-grained population of perovskite, and potential effects of crustal contamination on the overall isotopic signatures in the P150 Pikoo body, it is not possible to make definitive claims regarding the source region. Most perovskite Nd isotope analyses fall within a range of εNd_i of +1.8 to -2.0, distinct from MORB but scattering around the composition proposed for the chondritic uniform reservoir (CHUR), potentially indicative of a relatively pristine, undifferentiated reservoir. The available evidence therefore suggests the magma forming Pikoo originated deep within in the mantle, possibly sourced from a single homogeneous reservoir reflecting primitive mantle compositions (Woodhead et al., 2019). More refined isotopic results, i.e., an assessment of $^{87}Sr/^{86}Sr_i$ to allow more thorough assessment of

potential crustal contamination, and more precise Nd analyses, are necessary to better constrain the Pikoo kimberlite source region. Regardless of source, the area surrounding Pikoo hosts a plethora of complex tectonic structures related to the Trans-Hudson Orogen that may have experienced reactivation, facilitating small volume magma emplacement.

7 Conclusions

Based on geochemical, textural, and mineralogical considerations, the Pikoo rocks described here are archetypal coherent kimberlites, with available samples best described as hypabyssal. Characteristically, the Pikoo kimberlites comprise abundant rounded olivine and ilmenite macrocrysts set in a well-crystalline groundmass of olivine phenocrysts, phlogopite, apatite, spinel group minerals ± perovskite (or TiO_2 pseudomorphs), calcite, and sulfides. Given traditional criteria of kimberlitic ilmenite, the Pikoo kimberlites yield positive indications for diamond preservation (enrichment in MgO and MnO, relatively low Fe_2O_3 contents, rims reflective of decreased oxygen fugacity), though caveats for the use of ilmenite in diamond exploration exist (see Robles-Cruz et al., 2009 and Castillo-Oliver et al., 2017 for thorough discussion). For PK150, 151, PK314 and potentially PK312, magma evolution began in a relatively reducing environment and progressed in a manner similar to many other archetypal kimberlites, e.g., the De Beers dyke of Kimberley, South Africa (Soltys et al., 2018). Conversely, PK346 likely formed from an oxidized, high-carbonate, late pulse of magma that had already undergone significant fractionation. This difference could explain the striking distinction in textural, mineralogical, chemical, and alteration properties in comparison to PK150 along with the notably less favourable microdiamond results of PK346.

Through rigorous examination of perovskite U-Pb measurements and the application of two approaches (semi total Pb and total Pb) to age calculations, a robust age of 417 ± 14 Ma was determined for PK150. This age is significantly different from the nearby FALC kimberlites but overlaps the emplacement times of several Slave kimberlite localities within error, which may suggest more widespread diamond-bearing kimberlite activity across North America in circa Silurian times. The range in εNd_i (+3.3 to -3.0) determined from PK150 perovskite is

characteristic of archetypal kimberlite, overlapping with the central mid-Cretaceous corridor and the lower end of the OIB field. The vastly different age and lack of narrow isotopic ranges reported for the mid-Cretaceous corridor bodies implies Pikoo was not formed within the same event as the FALC, Somerset, and Kansas kimberlites. More refined isotopic results are necessary to confidently tie the Pikoo kimberlites to a source region, but current evidence is consistent with a pristine, deep mantle source, possibly reflective of a 'primitive' composition.

References

Agee, J. J., Garrison, J. R., & Taylor, L. A. (1982). Petrogenesis of oxide minerals in kimberlite, Elliott County, Kentucky. *American Mineralogist*, *67*(1-2), 28-42.

Ansdell, K. M., & Norman, A. R. (1995). U-Pb geochronology and tectonic development of the southern flank of the Kisseynew Domain, Trans-Hudson Orogen, Canada. *Precambrian Research*, *72*(1-2), 147-167.

Armstrong, J. P., Wilson, M., Barnett, R. L., Nowicki, T., & Kjarsgaard, B. A. (2004). Mineralogy of primary carbonate-bearing hypabyssal kimberlite, Lac de Gras, Slave province, Northwest Territories, Canada. *Lithos*, *76*(1-4), 415-433.

Armstrong, J. T. (1988). Quantitative analysis of silicate and oxide minerals: Comparison of Monte Carlo, ZAF and φ (ρZ) procedures: in Newbury, DE, ed., Analysis microbeam: San Francisco, California.

Arndt, N. T., Guitreau, M., Boullier, A. M., Le Roex, A., Tommasi, A., Cordier, P., & Sobolev, A. (2010). Olivine, and the origin of kimberlite. *Journal of Petrology*, *51*(3), 573-602.

Ashton, K. E., Heaman, L. M., Lewry, J. F., Hartlaub, R. P., & Shi, R. (1999). Age and origin of the Jan Lake Complex: a glimpse at the buried Archean craton of the Trans-Hudson Orogen. *Canadian Journal of Earth Sciences*, *36*(2), 185-208.

Ashton, K. E., Lewry, J. F., Heaman, L. M., Hartlaub, R. P., Stauffer, M. R., & Tran, H. T. (2005). The Pelican Thrust Zone: basal detachment between the Archean Sask Craton and Paleoproterozoic Flin Flon–Glennie Complex, western Trans-Hudson Orogen. *Canadian Journal of Earth Sciences*, *42*(4), 685-706.

Bank, C. G., Bostock, M. G., Ellis, R. M., Hajnal, Z., & VanDecar, J. C. (1998). Lithospheric mantle structure beneath the Trans-Hudson Orogen and the origin of diamondiferous kimberlites. *Journal of Geophysical Research: Solid Earth*, *103*(B5), 10103-10114.

Belousova, E. A., Griffin, W. L., O'Reilly, S. Y., & Fisher, N. I. (2002). Apatite as an indicator mineral for mineral exploration: trace-element compositions and their relationship to host rock type. *Journal of Geochemical Exploration*, *76*(1), 45-69.

Berryman, A. K., Smith, B. H. S., & Jellicoe, B. C. (2004). Geology and diamond distribution of the 140/141 kimberlite, Fort à la Corne, central Saskatchewan, Canada. *Lithos*, *76*(1-4), 99-114.

Bickford, M. E., Mock, T. D., Steinhart Iii, W. E., Collerson, K. D., & Lewry, J. F. (2005). Origin of the Archean Sask craton and its extent within the Trans-Hudson orogen: evidence from Pb and Nd isotopic compositions of basement rocks and post-orogenic intrusions. *Canadian Journal of Earth Sciences*, *42*(4), 659-684.

Bouvier, A., Vervoort, J. D., & Patchett, P. J. (2008). The Lu–Hf and Sm–Nd isotopic composition of CHUR: constraints from unequilibrated chondrites and implications for the bulk composition of terrestrial planets. *Earth and Planetary Science Letters*, *273*(1-2), 48-57.

Boyd, F. R., & Mertzman, S. A. (1987). Composition and structure of the Kaapvaal lithosphere, southern Africa. *Magmatic processes: physicochemical principles*, *1*, 3-12.

Brett, R. C., Russell, J. K., & Moss, S. (2009). Origin of olivine in kimberlite: Phenocryst or impostor?. *Lithos*, *112*, 201-212.

Burgess, S. D., Bowring, S. A., & Heaman, L. M. (2012, December). High-precision U-Pb geochronology of Ice River perovskite: a possible interlaboratory and intertechnique EARTHTIME standard. In *AGU Fall Meeting Abstracts*.

Bussweiler, Y., Foley, S. F., Prelević, D., & Jacob, D. E. (2015). The olivine macrocryst problem: new insights from minor and trace element compositions of olivine from Lac de Gras kimberlites, Canada. *Lithos*, *220*, 238-252.

Carlson, R. W., Czamanske, G., Fedorenko, V., & Ilupin, I. (2006). A comparison of Siberian meimechites and kimberlites: Implications for the source of high-Mg alkalic magmas and flood basalts. *Geochemistry, Geophysics, Geosystems*, *7*(11).

Carmody, L., Taylor, L. A., Thaisen, K. G., Tychkov, N., Bodnar, R. J., Sobolev, N. V., Pokhilenko, L.N., & Pokhilenko, N. P. (2014). Ilmenite as a diamond indicator mineral in the Siberian craton: a tool to predict diamond potential. *Economic Geology*, *109*(3), 775-783.

Cas, R. A. F., Hayman, P., Pittari, A., & Porritt, L. (2008a). Some major problems with existing models and terminology associated with kimberlite pipes from a volcanological perspective, and some suggestions. *Journal of Volcanology and Geothermal Research*, *174*(1-3), 209-225.

Cas, R. A. F., Porritt, L., Pittari, A., & Hayman, P. C. (2009). A practical guide to terminology for kimberlite facies: A systematic progression from descriptive to genetic, including a pocket guide. *Lithos*, *112*, 183-190.

Cas, R., Porritt, L., Pittari, A., & Hayman, P. (2008b). A new approach to kimberlite facies terminology using a revised general approach to the nomenclature of all volcanic rocks and deposits: descriptive to genetic. *Journal of Volcanology and Geothermal Research*, *174*(1-3), 226-240.

Castillo-Oliver, M., Galí, S., Melgarejo, J. C., Griffin, W. L., Belousova, E., Pearson, N. J., Watangua, M., & O'Reilly, S. Y. (2016). Trace-element geochemistry and U–Pb dating of perovskite in kimberlites of the Lunda Norte province (NE Angola): petrogenetic and tectonic implications. *Chemical geology*, *426*, 118-134.

Castillo-Oliver, M., Melgarejo, J. C., Galí, S., Pervov, V., Gonçalves, A. O., Griffin, W. L., Pearson, N.J., & O'Reilly, S. Y. (2017). Use and misuse of Mg-and Mn-rich ilmenite in diamond exploration: a petrographic and trace element approach. *Lithos*, *292*, 348-363.

Chakhmouradian, A. R., & Mitchell, R. H. (2000). Occurrence, alteration patterns and compositional variation of perovskite in kimberlites. *The Canadian Mineralogist*, *38*(4), 975-994.

Chalapathi Rao, N. V., Lehmann, B., Belyatsky, B., & Warnsloh, J. M. (2017). The Late Cretaceous diamondiferous pyroclastic kimberlites from the Fort à la Corne (FALC) field, Saskatchewan craton, Canada: petrology, geochemistry and genesis. *Gondwana Research*, *44*, 236-257.

Chalapathi Rao, N. V., Wu, F. Y., Mitchell, R. H., Li, Q. L., & Lehmann, B. (2013). Mesoproterozoic U–Pb ages, trace element and Sr–Nd isotopic composition of perovskite

from kimberlites of the Eastern Dharwar craton, southern India: distinct mantle sources and a widespread 1.1 Ga tectonomagmatic event. *Chemical Geology*, *353*, 48-64.

Chiarenzelli, J., Aspler, L., Villeneuve, M., & Lewry, J. (1998). Early Proterozoic evolution of the Saskatchewan Craton and its allochthonous cover, Trans-Hudson Orogen. *The Journal of Geology*, *106*(3), 247-268.

Clement, C. R. (1982). *A comparative geological study of some major kimberlite pipes in the Northern Cape and Orange Free State* (Doctoral dissertation). University of Cape Town, South Africa.

Clement, C. R., Skinner, E. M. W., & Scott Smith, B. H. (1984). Kimberlite redefined. *The Journal of Geology*, *92*(2), 223-228.

Collerson, K. D., Lewry, J. F., Bickford, M. E., & Van Schmus, W. R. (1990). Crustal evolution of the buried Precambrian of southern Saskatchewan: implications for diamond exploration. In: Beck, L.S. & Harper, C.T. (Eds). *Modern Exploration Techniques: Saskatchewan Geological Society*, 150-165.

Collerson, K. D., Van Schmus, R. W., Lewry, J. F., & Bickford, M. E. (1989). Sm-Nd isotopic constraints on the age of the buried basement in central and southern Saskatchewan: Implications for diamond exploration. *Summary of Investigations 1989, Saskatchewan Geological Survey, Miscellaneous Report 89–4*, 168-171.

Corfu, F., & Dahlgren, S. (2008). Perovskite U–Pb ages and the Pb isotopic composition of alkaline volcanism initiating the Permo-Carboniferous Oslo Rift. *Earth and Planetary Science Letters*, *265*(1-2), 256-269.

Cox, R. A., & Wilton, D. H. (2006). U–Pb dating of perovskite by LA-ICP-MS: an example from the Oka carbonatite, Quebec, Canada. *Chemical Geology*, *235*(1-2), 21-32.

Czas, J., Pearson, D.G., Stachel, T., Kjarsgaard, B.A., & Read, G. H. (submitted). A Paleoproterozoic diamond-bearing lithospheric mantle root beneath the Archean Sask Craton, Canada. *Lithos*.

Czas, J., Stachel, T., Pearson, D. G., Stern, R. A., & Read, G. H. (2018b). Diamond brecciation and annealing accompanying major metasomatism in eclogite xenoliths from the Sask Craton, Canada. *Mineralogy and Petrology*, *112*(1), 311-323.

Czaz, J. (2018a). *The quandary of the Sask Craton: Origin and evolution of the lithospheric mantle beneath the Sask Craton* (Unpublished doctoral dissertation). University of Alberta, Edmonton, Canada.

Danchin, R. V., Ferguson, J., McIver, J. R., & Nixon, P.H. (1975). The composition of late stage kimberlite liquids as revealed by nucleated autoliths. *Physics and Chemistry of the Earth*, 9, 235-245.

Davies, R., & Davies, A.W. (2019, March). Mn-ilmenite and alteration products in Horton River Area of Lena West. Poster brochure presented at PEDAC, Toronto, Canada.

Dawson, J. B. (1962). Basutoland kimberlites. *Geological Society of America Bulletin*, *73*(5), 545-560.

Dawson, J. B. (1980). *Kimberlites and Their Xenoliths.* Berlin, Heidelberg: Springer Berlin Heidelberg.

Dawson, J.B. (1967). A review of the geology of kimberlite. In: P.J. Wyllie (Ed.) *Ultramafic and related rocks* (241-251). New York: John Wiley.

Donovan, J. J., Kremser, D., Fournelle, J. H., & Goemann, K. (2015). Probe for EPMA: Acquisition, automation and analysis, version 11: Eugene, Oregon, Probe Software. *Inc., http://www. probesoftware. com*.

Droop, G. T. R. (1987). A general equation for estimating Fe 3+ concentrations in ferromagnesian silicates and oxides from microprobe analyses, using stoichiometric criteria. *Mineralogical magazine*, *51*(361), 431-435.

Ellis, R. M., Hajnal, Z., & Bostock, M. G. (1996). Seismic studies on the Trans-Hudson Orogen of western Canada. *Tectonophysics*, *262*(1-4), 35-50.

Fedortchouk, Y., & Canil, D. (2004). Intensive variables in kimberlite magmas, Lac de Gras, Canada and implications for diamond survival. *Journal of Petrology*, *45*(9), 1725-1745.

Field, M., & Scott Smith, B. H. (1998, April). Textural and genetic classification schemes for kimberlites: a new perspective. In *International Kimberlite Conference: Extended Abstracts*, *7*(1), 214-216.

Field, M., & Scott Smith, B. H. (1999, October). Contrasting geology and near-surface emplacement of kimberlite pipes in southern Africa and Canada. In Gurney, J.J., Gurney, J.J., Pascoe, M.D., & Richardson, S.H. (Eds.), *Proceedings of the 7th international kimberlite conference* (Vol. 1, pp. 214-237). Cape Town: Red Roof Design.

Field, M., Gernon, T. M., Mock, A., Walters, A., Sparks, R. S. J., & Jerram, D. A. (2009). Variations of olivine abundance and grain size in the Snap Lake kimberlite intrusion, Northwest Territories, Canada: A possible proxy for diamonds. *Lithos*, *112*, 23-35.

Fisher, C. M., McFarlane, C. R., Hanchar, J. M., Schmitz, M. D., Sylvester, P. J., Lam, R., & Longerich, H. P. (2011). Sm–Nd isotope systematics by laser ablation-multicollector-inductively coupled plasma mass spectrometry: Methods and potential natural and synthetic reference materials. *Chemical Geology*, *284*(1-2), 1-20.

Fisher, C. M., Paton, C., Pearson, D. G., Sarkar, C., Luo, Y., Tersmette, D. B., & Chacko, T. (2017). Data Reduction of Laser Ablation Split-Stream (LASS) Analyses Using Newly Developed Features Within Iolite: With Applications to Lu-Hf+ U-Pb in Detrital Zircon and Sm-Nd+ U-Pb in Igneous Monazite. *Geochemistry, Geophysics, Geosystems*, *18*(12), 4604-4622.

Foley, S. F., Prelevic, D., Rehfeldt, T., & Jacob, D. E. (2013). Minor and trace elements in olivines as probes into early igneous and mantle melting processes. *Earth and Planetary Science Letters*, *363*, 181-191.

Gent, M. R. (1992). Diamonds and precious gems of the Phanerozoic Basin. *Saskatchewan: preliminary investigations, Saskatchewan Energy and Mines Open File Report*, 92-2.

Giuliani, A., Soltys, A., Phillips, D., Kamenetsky, V. S., Maas, R., Goemann, K., Woodhead, J.D., Drysdale, R.N., & Griffin, W. L. (2017). The final stages of kimberlite petrogenesis: petrography, mineral chemistry, melt inclusions and Sr-CO isotope geochemistry of the Bultfontein kimberlite (Kimberley, South Africa). *Chemical Geology*, *455*, 342-356.

Grey, I. E., & Reid, A. F. (1975). The structure of pseudorutile and its role in the natural alteration of ilmenite. *American Mineralogist: Journal of Earth and Planetary Materials*, *60*(9-10), 898-906.

Griffin, W. L., & Ryan, C. G. (1995). Trace elements in indicator minerals: area selection and target evaluation in diamond exploration. *Journal of geochemical Exploration*, *53*(1-3), 311-337.

Griffin, W. L., Batumike, J. M., Greau, Y., Pearson, N. J., Shee, S. R., & O'Reilly, S. Y. (2014). Emplacement ages and sources of kimberlites and related rocks in southern Africa: U–Pb ages and Sr–Nd isotopes of groundmass perovskite. *Contributions to Mineralogy and Petrology*, *168*(1), 1032.

Grütter, H. S., Gurney, J. J., Menzies, A. H., & Winter, F. (2004). An updated classification scheme for mantle-derived garnet, for use by diamond explorers. *Lithos*, *77*(1-4), 841-857.

Guarino, V., Wu, F. Y., Lustrino, M., Melluso, L., Brotzu, P., de Barros Gomes, C., ... & Svisero, D. P. (2013). U–Pb ages, Sr–Nd-isotope geochemistry, and petrogenesis of kimberlites, kamafugites and phlogopite-picrites of the Alto Paranaíba Igneous Province, Brazil. *Chemical Geology*, *353*, 65-82.

Gurney, J. J., & Zweistra, P. (1995). The interpretation of the major element compositions of mantle minerals in diamond exploration. *Journal of Geochemical Exploration*, *53*(1-3), 293-309.

Haggerty, S. E. (1975). The chemistry and genesis of opaque minerals in kimberlites. In *Physics and Chemistry of the Earth*, 9, 295-307.

Haggerty, S. E., Hardie, R. B., & McMahon III, B. M. (1979). The Mineral Chemistry of Ilmenite Nodule Associations from the Monastery Diatreme. In Boyd, F.R. & Meyer, H.A. (Eds.), *The Mantle Sample* (pp. 249-256). Washington, DC: American Geophysical Union.

Hajnal, Z., Lewryb, J., White, D., Ashton, K., Clowes, R., Stauffer, M., Gyorfi, I., & Takacs, E. (2005). The Sask Craton and Hearne Province margin: seismic reflection studies in the western Trans-Hudson Orogen. *Canadian Journal of Earth Sciences*, *42*(4), 403-419.

Hammer, P. T., Clowes, R. M., Cook, F. A., Vasudevan, K., & van der Velden, A. J. (2011). The big picture: A lithospheric cross section of the North American continent. *GSA Today*, *21*(6), 4-10.

Hardman, M. F., Pearson, D. G., Stachel, T., & Sweeney, R. J. (2018). Statistical approaches to the discrimination of crust-and mantle-derived low-Cr garnet–major-element-based methods and their application in diamond exploration. *Journal of Geochemical Exploration*, *186*, 24-35.

Harris, M., le Roex, A., & Class, C. (2004). Geochemistry of the Uintjiesberg kimberlite, South Africa: petrogenesis of an off-craton, group I, kimberlite. *Lithos*, *74*(3-4), 149-165.

Harvey, S. (2004). Synthesis of diamond recoveries from the Fort à la Corne kimberlite field, east-central Saskatchewan. *Summary of Investigations*, *2*, 2004-4.

Harvey, S., Kjarsgaard, B., McClintock, M., Shimell, M., Fourie, L., Du Plessis, P., & Read, G. (2009). Geology and evaluation strategy of the Star and Orion South kimberlites, Fort à la Corne, Canada. *Lithos*, *112*, 47-60.

Hawthorne, J. B. (1975). Model of a kimberlite pipe. *Physics and Chemistry of the Earth*, *9*, 1-15.

Heaman, L. M. (1989). The nature of the subcontinental mantle from SrNdPb isotopic studies on kimberlitic perovskite. *Earth and Planetary Science Letters*, *92*(3-4), 323-334.

Heaman, L. M. (2009). The application of U–Pb geochronology to mafic, ultramafic and alkaline rocks: an evaluation of three mineral standards. *Chemical Geology*, *261*(1-2), 43-52.

Heaman, L. M., & Kjarsgaard, B. A. (2002). A Cretaceous corridor of kimberlite magmatism: U–Pb results from the Fort à la Corne Field, central Saskatchewan. In *Geological Association of Canada/Mineralogical Association of Canada Annual Convention,* Abstracts 27, 17.

Heaman, L. M., Kjarsgaard, B. A., & Creaser, R. A. (2003). The timing of kimberlite magmatism in North America: implications for global kimberlite genesis and diamond exploration. *Lithos*, *71*(2-4), 153-184.

Heaman, L. M., Kjarsgaard, B. A., & Creaser, R. A. (2004). The temporal evolution of North American kimberlites. *Lithos*, *76*(1-4), 377-397.

Heaman, L. M., Maxeiner, R. O. & Slimmon, W. L. (1994). 1993-94 U–Pb Geochronological Investigations in the Trans-Hudson Orogen, Saskatchewan. *Summary of Investigations 1994, Saskatchewan Geological Survey, Saskatchewan Energy and Mines, Miscellaneous Report*, 92(4), 96-99.

Heaman, L.M., & Parrish, R. R. (1991). U-Pb geochronology in accessory minerals. In L.M. Heaman & J.N. Ludden (Eds.), *Applications of Radiogenic Isotope Systems to Problems in Geology: Short Course Handbook on Applications…* (pp. 59-102). Toronto: Mineralogical Association of Canada.

Heaman, L.M., Ashton, K.E., Reilly, B.A., Sibbald, T.I.I., Slimmon, W.L., & Thomas, D.J. 1993. 1992-93 U-Pb geochronological investigations in the Trans-Hudson orogen, Saskatchewan. *Summary of investigations 1993. Saskatchewan Geological Survey, Saskatchewan Energy and Mines, Miscellaneous Report*, 93(4), 109-111.

Heaman, L.M., Kamo, S.L., Ashton, K.E., Reilly, B.A., Slimmon, W.L., & Thomas, D.J. (1992). U-Pb geochronological investigations in the Trans-Hudson Orogen, Saskatchewan. *Summary of Investigations 1992, Saskatchewan Geological Survey, Saskatchewan Energy and Mines, Miscellaneous Report,* 92(4), 120-123.

Hoffman, P. F. (1988). United plates of America, the birth of a craton: Early Proterozoic assembly and growth of Laurentia. *Annual Review of Earth and Planetary Sciences*, *16*(1), 543-603.

Jang, Y. D., & Naslund, H. R. (2003). Major and trace element variation in ilmenite in the Skaergaard Intrusion: petrologic implications. *Chemical Geology*, *193*(1-2), 109-125.

Jellicoe, B. C., Robertshaw, P., Williamson, P., & Murphy, J. (1998). Summary of exploration activities and results for the Fort à la Corne diamond project, Saskatchewan. *Summary of investigations*, *Report 98-4*, 144-157.

Kamenetsky, V. S., Belousova, E. A., Giuliani, A., Kamenetsky, M. B., Goemann, K., & Griffin, W. L. (2014). Chemical abrasion of zircon and ilmenite megacrysts in the Monastery

kimberlite: implications for the composition of kimberlite melts. *Chemical Geology*, *383*, 76-85.

Kamenetsky, V. S., Kamenetsky, M. B., Sobolev, A. V., Golovin, A. V., Demouchy, S., Faure, K., Victor, V., & Kuzmin, D. V. (2008). Olivine in the Udachnaya-East kimberlite (Yakutia, Russia): types, compositions and origins. *Journal of Petrology*, *49*(4), 823-839.

Kamenetsky, V. S., Kamenetsky, M. B., Weiss, Y., Navon, O., Nielsen, T. F., & Mernagh, T. P. (2009). How unique is the Udachnaya-East kimberlite? Comparison with kimberlites from the Slave Craton (Canada) and SW Greenland. *Lithos*, *112*, 334-346.

Kaminsky, F. V., & Belousova, E. A. (2009). Manganoan ilmenite as kimberlite/diamond indicator mineral. *Russian Geology and Geophysics*, *50*(12), 1212-1220.

Kaminsky, F. V., Khachatryan, G. K., Andreazza, P., Araujo, D., & Griffin, W. L. (2009). Super-deep diamonds from kimberlites in the Juina area, Mato Grosso State, Brazil. *Lithos*, *112*, 833-842.

Kaminsky, F. V., Sablukov, S. M., Sablukova, L. I., & Channer, D. M. D. (2004). Neoproterozoic 'anomalous' kimberlites of Guaniamo, Venezuela: mica kimberlites of 'isotopic transitional' type. *Lithos*, *76*(1-4), 565-590.

Kjarsgaard, B. A. (1996). Prairie kimberlites. In A.N. Lecheminant, D.G. Richardson, R.W. Diablo, & K.A. Richardson (Eds.), *Searching for diamonds in Canada*, (67-72). Geological Survey of Canada, Open File Report 3228.

Kjarsgaard, B. A., & Levinson, A. A. (2002). Diamonds in Canada. *Gems and Gemology*, *38*(3), 208-238.

Kjarsgaard, B. A., Harvey, S., McClintock, M., Zonneveld, J. P., Du Plessis, P., McNeil, D., & Heaman, L. (2009a). Geology of the Orion South kimberlite, Fort à la Corne, Canada. *Lithos*, *112*, 600-617.

Kjarsgaard, B. A., Heaman, L. M., Sarkar, C., & Pearson, D. G. (2017). The North America mid-Cretaceous kimberlite corridor: Wet, edge-driven decompression melting of an OIB-type deep mantle source. *Geochemistry, Geophysics, Geosystems*, *18*(7), 2727-2747.

Kjarsgaard, B. A., Leckie, D. A., & Zonneveld, J. P. (2007). Discussion of "Geology and diamond distribution of the 140/141 kimberlite, Fort à la Corne, central Saskatchewan, Canada", by A. Berryman, BH Scott-Smith and BC Jellicoe (Lithos v. 76, p. 99–114). *Lithos*, *97*(3-4), 422-428.

Kjarsgaard, B. A., Pearson, D. G., Tappe, S., Nowell, G. M., & Dowall, D. P. (2009b). Geochemistry of hypabyssal kimberlites from Lac de Gras, Canada: comparisons to a global database and applications to the parent magma problem. *Lithos*, *112*, 236-248.

Kjarsgaard, B.A. (2007). Kimberlite diamond deposits. In Goodfellow, W.D. (Ed.), *Mineral Deposits of Canada: A Synthesis of Major Deposit-Types, District Metallogeny, the Evolution of Geological Provinces, and Exploration Methods*. Geological Association of Canada, Mineral Deposits, Special Publications, 245-272.

Kryvdik, S. G. (2014). Geochemical features of ilmenites from the alkaline complexes of the Ukrainian Shield: LA-ICP MS data. *Geochemistry International*, *52*(4), 287-295.

Kupsch, B. (2016, November). *Pikoo diamond project – 2016 exploration update*. Presented at the 2016 Saskatchewan Geological Open House, Saskatoon, Canada.

Kupsch, B. (2017). Assessment report, Pikoo Project, Saskatchewan: Report on exploration activities (diamond drilling, ground geophysics, airborne geophysics). North Arrow Minerals Inc. Saskatchewan Ministry of Energy and Resource, Assessment work number MAW2098.

Le Roex, A. P., Bell, D. R., & Davis, P. (2003). Petrogenesis of group I kimberlites from Kimberley, South Africa: evidence from bulk-rock geochemistry. *Journal of Petrology*, *44*(12), 2261-2286.

Leahy, K. (1996). *The geology of kimberlites from the Fort à la Corne area, Saskatchewan, Canada* (Doctoral dissertation). University of Leeds, Leeds, United Kingdom.

Leahy, K. (1997). Discrimination of reworked pyroclastics from primary tephra-fall tuffs: a case study using kimberlites of Fort a la Corne, Saskatchewan, Canada. *Bulletin of Volcanology*, *59*(1), 65-71.

Leahy, K. (2001). Post-eruptive processes in kimberlites—implications for diamond exploration. *Applied Earth Science*, *110*(1), 1-4.

Leckie, D. A., Kjarsgaard, B. A., Bloch, J., McIntyre, D., McNeil, D., Stasiuk, L., & Heaman, L. (1997). Emplacement and reworking of Cretaceous, diamond-bearing, crater facies kimberlite of central Saskatchewan, Canada. *Geological Society of America Bulletin*, *109*(8), 1000-1020.

Lefebvre, N., & Kurszlaukis, S. (2008). Contrasting eruption styles of the 147 Kimberlite, Fort à la Corne, Saskatchewan, Canada. *Journal of Volcanology and Geothermal Research*, *174*(1-3), 171-185.

Lehnert-Thiel, K., Loewer, R., Orr, R. G., & Robertshaw, P. (1992). Diamond-bearing kimberlites in Saskatchewan, Canada: the Fort à la Corne case history. *Exploration and Mining Geology*, *1*(4), 391-403.

Leroux, D., Roy, W., van Niekerk, L., Wilkie, G. & McGarry, L. (2018). *Preliminary economic assessment of the Star - Orion South diamond project, Fort a la Corne, Saskatchewan*.

Lewry, J. F., Hajnal, Z., Green, A., Lucas, S. B., White, D., Stauffer, M. R., Ashton, K.E., Weber, W., & Clowes, R. (1994). Structure of a Paleoproterozoic continent-continent collision zone: a LITHOPROBE seismic reflection profile across the Trans-Hudson Orogen, Canada. *Tectonophysics*, *232*(1-4), 143-160.

Lucas, S. B., Green, A., Hajnal, Z., White, D., Lewry, J., Ashton, K., Weber, W., & Clowes, R. (1993). Deep seismic profile across a Proterozoic collision zone: surprises at depth. *Nature*, *363*(6427), 339.

Lucas, S. B., White, D., Hajnal, Z., Lewry, J., Green, A., Clowes, R., Zwanzig, H., Ashton, K., Schledewitz, D., Stauffer, M., & Norman, A. (1994). Three-dimensional collisional structure of the Trans-Hudson Orogen, Canada. *Tectonophysics*, *232*(1-4), 161-178.

Ludwig, K. R. (1998). On the treatment of concordant uranium-lead ages. *Geochimica et Cosmochimica Acta*, *62*(4), 665-676.

Malarkey, J., Pearson, D. G., Kjarsgaard, B. A., Davidson, J. P., Nowell, G. M., Ottley, C. J., & Stammer, J. (2010). From source to crust: tracing magmatic evolution in a kimberlite and a

melilitite using microsample geochemistry. *Earth and Planetary Science Letters*, *299*(1-2), 80-90.

Mao, M., Rukhlov, A. S., Rowins, S. M., Spence, J., & Coogan, L. A. (2016). Apatite trace element compositions: A robust new tool for mineral exploration. *Economic Geology*, *111*(5), 1187-1222.

Mareschal, J. C., Jaupart, C., Rolandone, F., Gariépy, C., Fowler, C. M., Bienfait, G., Carbonne, C. & Lapointe, R. (2005). Heat flow, thermal regime, and elastic thickness of the lithosphere in the Trans-Hudson Orogen. *Canadian Journal of Earth Sciences*, *42*(4), 517-532.

McDonough, W. F., & Sun, S. S. (1995). The composition of the Earth. *Chemical geology*, *120*(3-4), 223-253.

Milligan, R. S. (2017). *Features of apatite in kimberlite from Ekati Diamond Mine and Snap Lake: modelling kimberlite composition* (Master's thesis). Dalhousie University, Halifax, Canada.

Milligan, R., Fedortchouk, Y., Normandeau, P. X., Fulop, A., & Robertson, M. (2017, September). Features of apatite in kimberlites from Ekati Diamond Mine and Snap Lake, Northwest Territories, Canada: modelling of kimberlite composition. In *International Kimberlite Conference: Extended Abstracts* (Vol. 11).

Mitchell, R. H. (1986). *Kimberlites: mineralogy, geochemistry, and petrology*. New York: Plenum Publishing Company.

Mitchell, R. H. (1995). *Kimberlites, orangeites, and related rocks*. New York: Plenum Publishing Company.

Mitchell, R. H. (2008). Petrology of hypabyssal kimberlites: relevance to primary magma compositions. *Journal of Volcanology and Geothermal Research*, *174*(1-3), 1-8.

Mitchell, R. H., & Chakhmouradian, A. R. (1998). Instability of perovskite in a CO 2-rich environment; examples from carbonatite and kimberlite. *The Canadian Mineralogist*, *36*(4), 939-951.

Németh, B., Clowes, R. M., & Hajnal, Z. (2005). Lithospheric structure of the Trans-Hudson Orogen from seismic refraction–wide-angle reflection studies. *Canadian Journal of Earth Sciences*, *42*(4), 435-456.

Nielsen, T. F., & Sand, K. K. (2008). The Majuagaa kimberlite dike, Maniitsoq region, West Greenland: constraints on an Mg-rich silicocarbonatitic melt composition from groundmass mineralogy and bulk compositions. *The Canadian Mineralogist*, *46*(4), 1043-1061.

North Arrow Minerals Inc. (2013, August 7). North Arrow drills kimberlite in nine of ten holes at the Pikoo Diamond Project, Saskatchewan [Press release]. Retrieved from http://www.northarrowminerals.com/news/press_releases/2013/index.php?content_id=129.

North Arrow Minerals Inc. (2015, October 20). North Arrow confirms four diamondiferous kimberlites at Pikoo Diamond Project, Saskatchewan [Press release]. Retrieved from http://www.northarrowminerals.com/news/press_releases/2015/index.php?content_id=190

North Arrow Minerals Inc. (2016a, May 31). North Arrow confirms new diamondiferous kimberlites at Pikoo, Saskatchewan [Press release]. Retrieved from http://www.northarrowminerals.com/news/press_releases/2016/index.php?content_id=200

North Arrow Minerals Inc. (2016b, July 25). North Arrow reports microdiamond results and completion of till sampling program at Pikoo, Saskatchewan [Press release]. Retrieved from http://www.northarrowminerals.com/news/press_releases/2016/index.php?content_id=201

North Arrow Minerals Inc. (2017, January 18). North Arrow acquires remaining interests in Qilalugaq (Nunavut) and Pikoo (Saskatchewan) diamond projects from Stornoway [Press release]. Retrieved from http://www.northarrowminerals.com/news/press_releases/2017/index.php?content_id=208

Nowell, G. M., Pearson, D. G., Bell, D. R., Carlson, R. W., Smith, C. B., Kempton, P. D., & Noble, S. R. (2004). Hf isotope systematics of kimberlites and their megacrysts: new constraints on their source regions. *Journal of Petrology*, *45*(8), 1583-1612.

Nowicki, T. E., Moore, R. O., Gurney, J. J., & Baumgartner, M. C. (2007). Diamonds and associated heavy minerals in kimberlite: a review of key concepts and applications. *Developments in Sedimentology*, *58*, 1235-1267.

Pasteris, J. D. (1980). The significance of groundmass ilmenite and megacryst ilmenite in kimberlites. *Contributions to Mineralogy and Petrology*, *75*, 315-325.

Paton, C., Woodhead, J. D., Hergt, J. M., Phillips, D., & Shee, S. (2007). Strontium isotope analysis of kimberlitic groundmass perovskite via LA-MC-ICP-MS. *Geostandards and Geoanalytical Research*, *31*(4), 321-330.

Pearson, D.G., Woodhead, J., & Janney, P.E. (in press). Kimberlites as geochemical probes of Earth's mantle. *Elements*.

Pilbeam, L. H., Nielsen, T. F. D., & Waight, T. E. (2013). Digestion fractional crystallization (DFC): an important process in the genesis of kimberlites. Evidence from olivine in the Majuagaa kimberlite, southern West Greenland. *Journal of Petrology*, *54*(7), 1399-1425.

Pittari, A., Cas, R. A. F., Lefebvre, N., Robey, J., Kurszlaukis, S., & Webb, K. (2008). Eruption processes and facies architecture of the Orion Central kimberlite volcanic complex, Fort à la Corne, Saskatchewan; kimberlite mass flow deposits in a sedimentary basin. *Journal of Volcanology and Geothermal Research*, *174*(1-3), 152-170.

Ramos, F. C., Wolff, J. A., & Tollstrup, D. L. (2004). Measuring 87Sr/86Sr variations in minerals and groundmass from basalts using LA-MC-ICPMS. *Chemical Geology*, *211*(1-2), 135-158.

Rayner, N. M., Stern, R. A., & Bickford, M. E. (2005). Tectonic implications of new SHRIMP and TIMS U Pb geochronology of rocks from the Sask Craton, Peter Lake Domain, and Hearne margin, Trans-Hudson Orogen, Saskatchewan. *Canadian Journal of Earth Sciences*, *42*(4), 635-657.

Reguir, E. P., Camacho, A., Yang, P., Chakhmouradian, A. R., Kamenetsky, V. S., & Halden, N. M. (2010). Trace-element study and uranium-lead dating of perovskite from the Afrikanda plutonic complex, Kola Peninsula (Russia) using LA-ICP-MS. *Mineralogy and Petrology*, *100*(3-4), 95-103.

Robles-Cruz, S. E., Watangua, M., Isidoro, L., Melgarejo, J. C., Galí, S., & Olimpio, A. (2009). Contrasting compositions and textures of ilmenite in the Catoca kimberlite, Angola, and implications in exploration for diamond. *Lithos*, *112*, 966-975.

Robles-Cruz, S. E., Watangua, M., Melgarejo i Draper, J. C., & Galí Medina, S. (2008). New insights into the concept of ilmenite as an indicator for diamond exploration, based on kimberlite petrographic analysis. *MACLA. Revista de la Sociedad Española de Mineralogía, 2008, num. 9, p. 205-206*.

Sarkar, C., Kjarsgaard, B. A., Pearson, D. G., Heaman, L. M., Locock, A. J., & Armstrong, J. P. (2018). Geochronology, classification and mantle source characteristics of kimberlites and related rocks from the Rae Craton, Melville Peninsula, Nunavut, Canada. *Mineralogy and Petrology*, *112*(2), 653-672.

Schulze, D. J., Anderson, P. F., Hearn Jr, B. C., & Hetman, C. M. (1995). Origin and significance of ilmenite megacrysts and macrocrysts from kimberlite. *International Geology Review*, *37*(9), 780-812.

Scott Smith, B. H., Nowicki, T. E., Russell, J. K., Webb, K. J., Mitchell, R. H., Hetman, C. M., Harder, M., Skinner, E.W., & Robey, J. A. (2013). Kimberlite terminology and classification. In Pearson, D. G., Grütter, H. S., Harris, J. W., Kjarsgaard, B. A., O'Brien, H., Chalapathi Rao, N. V., & Sparks, S. (Eds.), *Proceedings of 10th International Kimberlite Conference* (pp. 1-17). New Delhi: Springer.

Scott Smith, B. H., Orr, R. G., Robertshaw, P., & Avery, R. W. (1998, April). Geology of the Fort a la Corne kimberlites, Saskatchewan. In *International Kimberlite Conference: Extended Abstracts*, 7(1), 772-774.

Scott Smith, B. H., Orr, R. G., Robertshaw, P., & Avery, R. W. (1995, September). Geology of the Fort a la Come kimberlites Saskatchewan. In *International Kimberlite Conference: Extended Abstracts*, 6, 543-545.

Scott Smith, B. H., Russell, J. K., Webb, K.J., Mitchell, R. H., Hetman., Robey, J.V. (2018). *A glossary of kimberlite and related terms*. North Vancouver: Scott-Smith Petrology Inc.

Skinner, E. M. W., & Clement, C. R. (1977, September). Mineralogical classification of southern African kimberlites. In *International Kimberlite Conference: Extended Abstracts*, 2, 304-306.

Soltys, A., Giuliani, A., & Phillips, D. (2017, September). Apatite from the Kimberley kimberlites (South Africa): petrography and mineral chemistry. In *International Kimberlite Conference: Extended Abstracts*, 11.

Soltys, A., Giuliani, A., & Phillips, D. (2018). Crystallisation sequence and magma evolution of the De Beers dyke (Kimberley, South Africa). *Mineralogy and Petrology*, *112*(2), 503-518.

Spencer, C. J., Kirkland, C. L., & Taylor, R. J. (2016). Strategies towards statistically robust interpretations of in situ U–Pb zircon geochronology. *Geoscience Frontiers*, *7*(4), 581-589.

Stamm, N., Schmidt, M. W., Szymanowski, D., von Quadt, A., Mohapi, T., & Fourie, A. (2018). Primary petrology, mineralogy and age of the Letšeng-la-Terae kimberlite (Lesotho, Southern Africa) and parental magmas of Group-I kimberlites. *Contributions to Mineralogy and Petrology*, *173*(9), 76.

Stauffer, M. R. (1984). Manikewan: an early Proterozoic ocean in central Canada, its igneous history and orogenic closure. *Precambrian Research*, *25*(1-3), 257-281.

St-Onge, M. R., Searle, M. P., & Wodicka, N. (2006). Trans-Hudson Orogen of North America and Himalaya-Karakoram-Tibetan Orogen of Asia: Structural and thermal characteristics of the lower and upper plates. *Tectonics*, *25*(4).

Streck, M. J. (2008). Mineral textures and zoning as evidence for open system processes. *Reviews in Mineralogy and Geochemistry*, *69*(1), 595-622.

Sun, J., Liu, C. Z., Tappe, S., Kostrovitsky, S. I., Wu, F. Y., Yakovlev, D., Yang, Y.H., & Yang, J. H. (2014). Repeated kimberlite magmatism beneath Yakutia and its relationship to Siberian flood volcanism: insights from in situ U–Pb and Sr–Nd perovskite isotope analysis. *Earth and Planetary Science Letters*, *404*, 283-295.

Tachibana, Y., Kaneoka, I., Gaffney, A., & Upton, B. (2006). Ocean-island basalt–like source of kimberlite magmas from West Greenland revealed by high 3He/4He ratios. *Geology*, *34*(4), 273-276.

Tappe, S., & Simonetti, A. (2012). Combined U–Pb geochronology and Sr–Nd isotope analysis of the Ice River perovskite standard, with implications for kimberlite and alkaline rock petrogenesis. *Chemical Geology*, *304*, 10-17.

Tappe, S., Pearson, D. G., Nowell, G., Nielsen, T., Milstead, P., & Muehlenbachs, K. (2011). A fresh isotopic look at Greenland kimberlites: cratonic mantle lithosphere imprint on deep source signal. *Earth and Planetary Science Letters*, *305*(1-2), 235-248.

Tappe, S., Romer, R. L., Stracke, A., Steenfelt, A., Smart, K. A., Muehlenbachs, K., & Torsvik, T. H. (2017). Sources and mobility of carbonate melts beneath cratons, with implications for deep carbon cycling, metasomatism and rift initiation. *Earth and Planetary Science Letters*, *466*, 152-167.

Teufer, G., & Temple, A. K. (1966). Pseudorutile—a new mineral intermediate between ilmenite and rutile in the N alteration of ilmenite. *Nature*, *211*(5045), 179.

Tompkins, L. A., & Haggerty, S. E. (1985). Groundmass oxide minerals in the Koidu kimberlite dikes, Sierra Leone, West Africa. *Contributions to Mineralogy and Petrology*, *91*(3), 245-263.

van Straaten, B. I., Kopylova, M. G., Russell, J. K., & Smith, B. S. (2011). A rare occurrence of a crater-filling clastogenic extrusive coherent kimberlite, Victor Northwest (Ontario, Canada). *Bulletin of Volcanology*, *73*(8), 1047-1062.

Verigeanu, D., Hetman, C. M., Jellicoe, B., & Baumgartner, M. C. (2009). Preliminary geology, mineral chemistry and diamond results from the C29/30 Candle Lake volcanic complex, Saskatchewan, Canada. *Lithos*, *112*, 529-540.

Wagner, A.P., (1914). *The diamond fields of Southern Africa.* Johannesburg: Transvaal Leader.

Webb, K. J. (2006, September). Juvenile clasts in kimberlites: Standardized comprehensive description towards unravelling emplacement mechanisms. In *Long Abstract Volume, Kimberlite Emplacement Workshop, Saskatoon, Canada*.

Webb, K. J., & Hetman, C. M. (2017, September). Magmaclasts in kimberlite. In *International Kimberlite Conference: Extended Abstracts* (Vol. 11).

Webb, K., Crawford, B., Nowicki, T., Hetman, C., & Carlson, J. (2008, October). Coherent kimberlite at EKATI, Northwest Territories, Canada: textural and geochemical variations and implications for emplacement. In *International Kimberlite Conference: Extended Abstracts* (Vol. 9).

Weller, O. M., & St-Onge, M. R. (2017). Record of modern-style plate tectonics in the Palaeoproterozoic Trans-Hudson orogen. *Nature Geoscience*, *10*(4), 305.

Williams, A. F. (1932). *The genesis of the diamond* (2 volumes). London: Ernest Benn Ltd.

Woodhead, J., Hergt, J., Giuliani, A., Maas, R., Phillips, D., Pearson, D.G., & Nowell., G.M. (2019) Kimberlites reveal 2.5-billion-year evolution of a deep, isolated mantle reservoir. *Nature*, *573(7775)*, 578-587.

Woodhead, J., Hergt, J., Phillips, D., & Paton, C. (2009). African kimberlites revisited: in situ Sr-isotope analysis of groundmass perovskite. *Lithos*, *112*, 311-317.

Wu, F. Y., Arzamastsev, A. A., Mitchell, R. H., Li, Q. L., Sun, J., Yang, Y. H., & Wang, R. C. (2013a). Emplacement age and Sr–Nd isotopic compositions of the Afrikanda alkaline ultramafic complex, Kola Peninsula, Russia. *Chemical Geology*, *353*, 210-229.

Wu, F. Y., Mitchell, R. H., Li, Q. L., Sun, J., Liu, C. Z., & Yang, Y. H. (2013b). In situ UPb age determination and SrNd isotopic analysis of perovskite from the Premier (Cullinan) kimberlite, South Africa. *Chemical Geology*, *353*, 83-95.

Wu, F. Y., Yang, Y. H., Mitchell, R. H., Li, Q. L., Yang, J. H., & Zhang, Y. B. (2010). In situ U–Pb age determination and Nd isotopic analysis of perovskites from kimberlites in southern Africa and Somerset Island, Canada. *Lithos*, *115*(1-4), 205-222.

Wyatt, B. A., Baumgartner, M., Anckar, E., & Grutter, H. (2004). Compositional classification of “kimberlitic” and “non-kimberlitic” ilmenite. *Lithos*, *77*(1-4), 819-840.

Xu, J., Melgarejo, J., & Castillo-Oliver, M. (2018). Styles of alteration of Ti oxides of the kimberlite groundmass: implications on the petrogenesis and classification of kimberlites and similar rocks. *Minerals*, *8*(2), 51.

Yang, Y. H., Wu, F. Y., Wilde, S. A., Liu, X. M., Zhang, Y. B., Xie, L. W., & Yang, J. H. (2009). In situ perovskite Sr–Nd isotopic constraints on the petrogenesis of the Ordovician Mengyin kimberlites in the North China Craton. *Chemical Geology*, *264*(1-4), 24-42.

Zonneveld, J. P., Kjarsgaard, B. A., Harvey, S. E., Heaman, L. M., McNeil, D. H., & Marcia, K. Y. (2004). Sedimentologic and stratigraphic constraints on emplacement of the Star Kimberlite, east–central Saskatchewan. *Lithos*, *76*(1-4), 115-138.

Appendix A – Tables

Table 1a – EPMA (CAMECA) analytical settings and standards for Session 1 (ilmenite, phlogopite, spinel, rutile)

Element/Line	Crystal	Standard	On-Peak Time	Background	Kilovolts	Beam Current	Beam Size
			s	s	kV	nA	um
Si ka	LTAP	Fo90.5	20	20	20	20, 30	0, 1, 2
Na ka	TAP	NaAlSi3O8 albite VA 131705	20	20	20	20, 30	0, 1, 2
Fe ka	LLIF	Fe2SiO4 fayalite Rockport, FeTiO3 Ilmenite 96189	20	20	20	20, 30	0, 1, 2
Al ka	TAP	Frank Smith pyrope garnet	20	20	20	20, 30	0, 1, 2
Ti ka	PET	TiO2 Rutile MTI, FeTiO3 Ilmenite 96189	20	20	20	20, 30	0, 1, 2
Mn ka	LLIF	(Mn,Fe)3Al2Si3O12 spessartine, Navegadora Mine	20	20	20	20, 30	0, 1, 2
Mg ka	LTAP	Frank Smith pyrope garnet, Fo90.5	20	20	20	20, 30	0, 1, 2
Cr ka	PET	Cr2O3 chromium oxide Alfa	20	20	20	20, 30	0, 1, 2
Ni ka	LLIF	Ni nickel Alfa	20	20	20	20, 30	0, 1, 2
Ca ka	PET	CaMgSi2O6 diopside Wakefield	20	20	20	20, 30	0, 1, 2
Zn ka	LLIF	ZnAl2O4 gahnite H111989	30	30	20	30	0, 1
K ka	LPET	KAlSi3O8 sanidine Itrongay	30	30	20	20, 30	0, 1, 2

Table 1b – EPMA (CAMECA) analytical settings and standards for Session 2 (phlogopite, spinel)

Element/Line	Crystal	Standard	On-Peak Time	Background	Kilovolts	Beam Current	Beam Size
			s	s	kV	nA	um
Si ka	LTAP	Frank Smith pyrope garnet	30	30	15	20	3
Na ka	TAP	NaAlSi3O8 albite VA 131705	30	30	15	20	3
Fe ka	LLIF	Fe2SiO4 fayalite Rockport	30	30	15	20	3
Ti ka	PET	TiO2 Rutile MTI	30	30	15	20	3
K ka	LPET	KAlSi3O8 sanidine Itrongay	30	30	15	20	3
Al ka	LTAP	Frank Smith pyrope garnet	30	30	15	20	3
Mg ka	TAP	Frank Smith pyrope garnet	30	30	15	20	3
Mn ka	LLIF	(Mn,Fe)3Al2Si3O12 spessartine, Navegadora Mine	30	30	15	20	3
Cr ka	PET	Cr2O3 chromium oxide Alfa	30	30	15	20	3
Ca ka	LPET	CaMgSi2O6 diopside Wakefield	30	30	15	20	3
Ba lb	LPET	BaSi2O5 Sanbornite, Fresno	30	30	15	20	3

Table 1c – EPMA (CAMECA) analytical settings and standards for Session 3 (ilmenite, phlogopite, spinel, rutile, garnet)

Element/Line	Crystal	Standard	On-Peak Time	Background	Kilovolts	Beam Current	Beam Size
			s	s	kV	nA	um
Si ka	LTAP	Frank Smith pyrope garnet	30	30	15	20	0, 3
Na ka	TAP	NaAlSi3O8 albite VA 131705	30	30	15	20	0, 3
Fe ka	LLIF	Fe2SiO4 fayalite Rockport	30	30	15	20	0, 3
Ti ka	PET	TiO2 Rutile MTI	30	30	15	20	0, 3
K ka	LPET	KAlSi3O8 sanidine Itrongay	30	30	15	20	0, 3
Al ka	LTAP	Frank Smith pyrope garnet	30	30	15	20	0, 3
Mg ka	TAP	Frank Smith pyrope garnet	30	30	15	20	0, 3
Mn ka	LLIF	(Mn,Fe)3Al2Si3O12 spessartine, Navegadora Mine	30	30	15	20	0, 3
Cr ka	PET	Cr2O3 chromium oxide Alfa	30	30	15	20	0, 3
Ca ka	LPET	Plagioclase (labradorite) 115900	30	30	15	20	0, 3
Ba lb	LPET	BaSi2O5 Sanbornite, Fresno	30	30	15	20	0, 3
Ni ka	LLIF	Ni nickel Alfa	30	30	15	20	0, 3

Table 1d – EPMA (CAMECA) analytical settings and standards for Session 4 (apatite)

Element/Line	Crystal	Standard	On-Peak Time	Background	Kilovolts	Beam Current	Beam Size
			s	s	kV	nA	um
P ka	LPET	Fluorapatite Ca5(PO4)3F JH	30	30	15	20	5
Cl ka	PET	Tugtupite	40	40	15	20	5
Ca ka	LPET	Fluorapatite Ca5(PO4)3F JH	30	30	15	20	5
F ka	PC0	Topaz	60	60	15	20	5
Mn ka	LLIF	Tephroite synth JH block Mn2SiO4	40	40	15	20	5
Na ka	LTAP	Tugtupite	30	30	15	20	5
S ka	PET	Anhydrite ON CaSO4	35	35	15	20	5
S ka	LPET	Anhydrite ON CaSO4	0	0	15	20	5
Fe ka	LLIF	Fe metal	40	40	15	20	5
Si ka	LTAP	Topaz	30	30	15	20	5
Sr la	LTAP	SrTiO3	30	30	15	20	5

Table 1e – EPMA (JEOL) analytical settings and standards for Session 5 (ilmenite, phlogopite, spinel, rutile, garnet, olivine, perovskite)

Element/Line	Crystal	Standard	On-Peak Time	Background	Kilovolts	Beam Current	Beam Size
			s	s	kV	nA	um
Ti ka	PET	TiO2 Rutile MTI	30	30	20	20	0
Si ka	TAP	Frank Smith pyrope garnet	30	30	20	20	0
K ka	PETH	KAlSi3O8 sanidine Itrongay	30	30	20	20	0
Na ka	TAP	NaAlSi3O8 albite VA 131705	30	30	20	20	0
Fe ka	LIFH	Fe2SiO4 fayalite Rockport	30	30	20	20	0
Cr ka	PET	Cr2O3 chromium oxide Alfa	30	30	20	20	0
Mg ka	TAP	Frank Smith pyrope garnet	30	30	20	20	0
Ca ka	PETH	Plagioclase (labradorite) 115900	30	30	20	20	0
Al ka	TAP	Frank Smith pyrope garnet	30	30	20	20	0
Mn ka	LIFH	(Mn,Fe)3Al2Si3O12 spessartine, Navegadora Mine	20	20	20	20	0
Ni ka	LIFH	Ni nickel Alfa	20	20	20	20	0
Zn ka	LIFH	ZnAl2O4 gahnite H111989	20	20	20	20	0
Nb la	PETH	Niobium, Nb - ESPI	30	30	20	20	0
Ba lb	PET	BaSi2O5 Sanbornite, Fresno	30	30	20	20	0

Table 1f – EPMA (CAMECA) analytical settings and standards for Session 5 (ilmenite, phlogopite, spinel, rutile, pseudorutile, garnet)

Element/Line	Crystal	Standard	On-Peak Time	Background	Kilovolts	Beam Current	Beam Size
			s	s	kV	nA	um
Si ka	LTAP	Frank Smith pyrope garnet	30	30	15	20	0
Na ka	TAP	NaAlSi3O8 albite VA 131705	30	30	15	20	0
Fe ka	LLIF	Hematite SK block	30	30	15	20	0
Ti ka	PET	FeTiO3 Ilmenite 96189	30	30	15	20	0
K ka	LPET	KAlSi3O8 sanidine Itrongay	30	30	15	20	0
Al ka	LTAP	Frank Smith pyrope garnet	30	30	15	20	0
Mg ka	TAP	Frank Smith pyrope garnet	30	30	15	20	0
Mn ka	LLIF	(Mn,Fe)3Al2Si3O12 spessartine, Navegadora Mine	30	30	15	20	0
Cr ka	PET	Cr2O3 chromium oxide Alfa	30	30	15	20	0
Ca ka	LPET	Plagioclase (labradorite) 115900	30	30	15	20	0
Ba lb	LPET	BaSi2O5 Sanbornite, Fresno	30	30	15	20	0
Ni ka	LLIF	Ni nickel Alfa	30	30	15	20	0
Nb la	PET	Niobium, Nb - ESPI	30	30	15	20	0

Table 1g – EPMA (CAMECA) analytical settings and standards for Session 5 (olivine)

Element/Line	Crystal	Standard	On-Peak Time	Background	Kilovolts	Beam Current	Beam Size
			s	s	kV	nA	um
Si ka	LTAP	Fo90.5	30	30	20	20	0
Na ka	TAP	KAlSi3O8 sanidine Itrongay	30	30	20	20	0
Fe ka	LLIF	Fe2SiO4 fayalite Rockport	30	30	20	20	0
Al ka	TAP	Frank Smith pyrope garnet	30	30	20	20	0
Mn ka	LLIF	(Mn,Fe)3Al2Si3O12 spessartine, Navegadora Mine	30	30	20	20	0
Mg ka	LTAP	Fo90.5	30	30	20	20	0
Cr ka	PET	Cr2O3 chromium oxide Alfa	30	30	20	20	0
K ka	LPET	KAlSi3O8 sanidine ltrongay	30	30	20	20	0
Ca ka	LPET	CaMgSi2O6 diopside Wakefield	30	30	20	20	0
Ti ka	PET	TiO2 Rutile MTI	30	30	20	20	0
Ni ka	LLIF	Ni nickel Alfa	30	30	20	20	0

Table 2 – Perovskite U-Pb geochronology isotopic data for standards; decay constants of 1.55125E-10 for ^{238}U and 9.8485E-10 for ^{235}U

Standard	Spot Size	U	Pb	$^{238}U/^{206}Pb$	2σ	$^{207}Pb/^{206}Pb$	2σ	^{204}Pb	^{206}Pb	^{207}Pb	^{238}U
	µm	ppm	ppm					cps	cps	cps	cps
Ice River	23	143	41	17.513	0.736	0.0538	0.0000	126	22810	1227	332000
Ice River	23	143	41	17.746	0.724	0.0538	0.0000	73	22450	1208	329000
Ice River	23	138	41	17.483	0.734	0.0538	0.0000	114	21960	1182	315000
Ice River	23	142	41	17.532	0.707	0.0538	0.0000	81	21480	1156	305000
Ice River	23	147	40	17.794	0.760	0.0538	0.0000	70	21860	1176	314000
Ice River	23	134	42	17.483	0.734	0.0538	0.0000	71	20240	1089	286000
Ice River	23	144	43	17.668	0.718	0.0538	0.0000	45	19960	1074	286000
Ice River	23	144	38	17.627	0.715	0.0538	0.0000	60	20120	1083	285000
Ice River	23	142	41	17.486	0.703	0.0538	0.0000	64	19780	1064	277000
Ice River	23	150	42	17.637	0.747	0.0538	0.0000	72	16150	869	249000
Ice River	23	134	40	17.575	0.772	0.0538	0.0000	87	15750	847	220300
Ice River	23	139	40	17.513	0.736	0.0538	0.0000	110	15670	843	221000
Ice River	23	142	41	17.452	0.761	0.0538	0.0000	94	15830	852	225000
Ice River	23	148	42	17.857	0.797	0.0538	0.0000	112	15990	860	235000
Ice River	23	148	41	17.452	0.731	0.0538	0.0000	94	16390	882	229000
Ice River	23	140	42	18.018	0.779	0.0538	0.0000	49	15170	816	216000
Ice River	23	135	39	17.422	0.759	0.0538	0.0000	114	14880	801	208000
Ice River	23	123	46	17.606	0.744	0.0538	0.0000	75	14300	770	202200
Ice River	23	156	38	17.606	0.744	0.0538	0.0000	125	18500	996	260000
Ice River	23	162	42	17.544	0.800	0.0538	0.0000	55	19640	1057	275000
Ice River	23	140	41	18.116	0.624	0.0541	0.0032	58	11420	607	176300
Ice River	23	136	41	17.007	0.550	0.0537	0.0032	45	11700	615	171700
Ice River	23	137	41	17.637	0.529	0.0535	0.0032	50	11340	610	171600
Ice River	23	138	41	17.483	0.581	0.0542	0.0031	59	11610	625	173200

Table 2 continued

Standard	Spot Size µm	U ppm	Pb ppm	$^{238}U/^{206}Pb$	2σ	$^{207}Pb/^{206}Pb$	2σ	^{204}Pb cps	^{206}Pb cps	^{207}Pb cps	^{238}U cps
Ice River	23	139	41	17.331	0.541	0.0534	0.0029	51	11540	618	171800
Ice River	23	176	44	17.921	0.674	0.0540	0.0058	63	12680	682	217900
Ice River	23	113	38	17.575	0.710	0.0530	0.0042	28	10520	541	139300
Ice River	23	141	41	17.867	0.511	0.0539	0.0031	36	11240	605	171400
Ice River	23	139	41	17.668	0.562	0.0539	0.0025	54	11130	593	169000
Ice River	23	138	41	17.483	0.520	0.0540	0.0029	48	11180	601	167500
Ice River	23	140	41	17.690	0.501	0.0538	0.0027	59	11100	597	167300
Ice River	23	139	41	17.575	0.525	0.0542	0.0030	60	11100	598	166100
Ice River	23	143	42	17.640	0.498	0.0538	0.0027	46	11350	611	171000
Ice River	23	142	41	17.301	0.509	0.0534	0.0034	68	11360	605	168600
Ice River	33	142	49	17.241	0.892	0.0537	0.0051	137	25510	1350	388000
Ice River	33	140	41	17.422	0.728	0.0534	0.0023	114	21570	1143	347000
Ice River	33	141	40	17.953	0.709	0.0541	0.0025	126	20750	1118	339000
Ice River	33	141	47	16.722	0.783	0.0543	0.0047	153	23130	1245	338400
Ice River	33	141	41	17.721	0.691	0.0544	0.0024	118	21680	1173	355000
Ice River	33	141	40	17.584	0.711	0.0540	0.0022	95	21660	1165	358000
Ice River	33	141	42	17.857	0.733	0.0533	0.0025	111	22220	1196	368000
Ice River	33	141	42	17.452	0.701	0.0539	0.0022	142	23040	1240	383000
Ice River	33	140	40	17.606	0.713	0.0531	0.0022	135	22290	1189	373000
Ice River	33	141	41	17.391	0.696	0.0539	0.0027	130	23090	1241	379000
Ice River	33	141	43	17.153	0.706	0.0538	0.0026	144	23880	1285	387000
Ice River	33	141	41	17.606	0.682	0.0537	0.0019	110	22210	1195	374000
Ice River	33	141	41	17.662	0.686	0.0543	0.0021	107	22100	1189	366000
Ice River	33	141	40	17.787	0.696	0.0537	0.0023	82	21290	1145	362000

Table 2 continued

Standard	Spot Size	U	Pb	$^{238}U/^{206}Pb$	2σ	$^{207}Pb/^{206}Pb$	2σ	^{204}Pb	^{206}Pb	^{207}Pb	^{238}U
	µm	ppm	ppm					cps	cps	cps	cps
Afrikanda	23	50	19	14.881	0.642	0.1262	0.0040	41	9310	1170	112800
Afrikanda	23	65	19	15.385	0.639	0.1385	0.0041	73	11800	1628	146300
Afrikanda	23	57	16	15.015	0.631	0.1322	0.0031	30	10530	1391	127600
Afrikanda	23	51	10	14.948	0.626	0.1328	0.0038	47	8840	1173	106900
Afrikanda	23	60	9	14.025	0.570	0.1729	0.0039	135	10930	1888	125400
Afrikanda	23	52	9	15.083	0.637	0.1301	0.0037	26	8950	1155	109900
Afrikanda	23	55	17	14.903	0.644	0.1436	0.0061	72	9020	1279	106500
Afrikanda	23	69	13	14.970	0.650	0.1529	0.0062	52	11120	1710	131600
Afrikanda	23	77	17	14.144	0.600	0.1727	0.0040	79	12800	2227	144500
Afrikanda	23	79	8	13.405	0.557	0.1619	0.0040	103	11020	1781	128000
Afrikanda	23	83	7	13.298	0.584	0.1574	0.0056	60	10890	1711	135100
Afrikanda	23	75	10	13.387	0.591	0.1820	0.0120	88	10500	1940	120100
Afrikanda	23	67	10	14.514	0.674	0.1317	0.0039	32	8290	1097	106900
Afrikanda	23	68	10	14.184	0.604	0.1221	0.0031	58	8870	1081	106800
Afrikanda	23	62	7	13.966	0.644	0.1444	0.0039	62	9500	1368	98500
Afrikanda	23	64	9	14.388	0.621	0.1670	0.0060	57	9690	1619	98200
Afrikanda	23	72	8	14.815	0.615	0.1342	0.0057	61	9180	1229	112700
Afrikanda	23	65	26	15.267	0.629	0.1219	0.0035	43	9380	1137	113600
Afrikanda	23	63	217	15.129	0.641	0.1269	0.0037	83	9350	1192	111800
Afrikanda	23	53	-25	14.771	0.611	0.1372	0.0048	41	8090	1105	94300
Afrikanda	23	78	9	14.771	0.502	0.1541	0.0043	63	7800	1204	97900
Afrikanda	23	88	10	14.265	0.468	0.1464	0.0041	79	8970	1318	109900

Table 2 continued

Standard	Spot Size	U	Pb	$^{238}U/^{206}Pb$	2σ	$^{207}Pb/^{206}Pb$	2σ	^{204}Pb	^{206}Pb	^{207}Pb	^{238}U
	µm	ppm	ppm					cps	cps	cps	cps
Afrikanda	23	72	9	14.144	0.460	0.1425	0.0042	56	7350	1052	89400
Afrikanda	23	69	9	14.793	0.525	0.1497	0.0044	42	6580	982	84500
Afrikanda	23	94	10	14.706	0.454	0.1464	0.0039	70	9160	1360	115200
Afrikanda	23	71	9	14.184	0.443	0.1538	0.0038	55	7160	1102	86900
Afrikanda	23	95	10	14.793	0.481	0.1507	0.0039	50	9040	1356	114700
Afrikanda	23	81	9	14.641	0.450	0.1331	0.0033	27	7790	1051	98000
Afrikanda	23	98	10	14.577	0.446	0.1472	0.0038	53	9580	1413	118600
Afrikanda	23	100	10	14.859	0.442	0.1431	0.0033	59	9400	1340	119100
Afrikanda	23	90	9	14.793	0.503	0.1359	0.0033	53	8440	1148	107200
Afrikanda	33	101	11	14.025	0.669	0.1652	0.0075	187	18650	3110	243500
Afrikanda	33	83	10	15.038	0.678	0.1474	0.0033	134	14240	2084	201700
Afrikanda	33	87	13	14.144	0.580	0.1842	0.0064	145	16210	3000	210500
Afrikanda	33	90	10	14.993	0.629	0.1402	0.0030	138	16740	2346	239700
Afrikanda	33	69	10	15.221	0.672	0.1362	0.0032	73	13080	1767	188800
Afrikanda	33	63	12	14.948	0.626	0.1495	0.0046	122	12180	1836	173400
Afrikanda	33	84	11	14.837	0.594	0.1379	0.0030	78	15760	2184	228000
Afrikanda	33	99	10	14.409	0.623	0.1672	0.0054	164	19740	3300	275500
Afrikanda	33	77	9	15.038	0.633	0.1441	0.0024	89	14940	2157	216500
Afrikanda	33	111	10	14.706	0.606	0.1780	0.0088	189	19790	3570	282500
Afrikanda	33	100	11	13.423	0.595	0.1967	0.0078	174	19090	3780	246800
Afrikanda	33	70	10	14.472	0.628	0.1460	0.0110	104	11720	1680	164800

Table 3a – Configuration of Faraday cups on Thermo Neptune Plus MC-ICP-MS and relevant interferences for Nd tracer isotope collection

Collector	**L4-F**	**L3-F**	**L2-F**	**L1-F**	**C-F**	**H1-F**	**H2-F**	**H3-F**	**H4-F**
Analyte	^{142}Nd	^{143}Nd	^{144}Nd	^{145}Nd	^{146}Nd	^{147}Sm	^{148}Nd	^{149}Sm	^{150}Nd
Interference			^{144}Sm						

Table 3b – Configuration of Faraday cups on Thermo Neptune Plus MC-ICP-MS and relevant interferences for Sr tracer isotope collection

Collector	**L4-F**	**L3-F**	**L2-F**	**L1-F**	**C-F**	**H1-F**	**H2-F**	**H3-F**	**H4-F**
Analyte/Mass	83Kr	83.5	84Sr	85Rb	85.47	86Sr	86.5	87Sr	88Sr
Double mass	166	167	168	170		172	173	174	176
Interference	166Er	167Er		170Er 170Yb					176Yb

Table 4 – Whole rock geochemistry of powdered core samples

	PK150 44813	**PK346 44834**	**PK346 44848**
wt%			
SiO_2	40.78	35.15	34.77
TiO_2	4.24	4.77	4.97
Al_2O_3	2.20	2.81	2.91
FeO*	15.26	13.55	13.63
MnO	0.18	0.15	0.16
MgO	28.66	29.68	30.31
CaO	7.66	11.82	11.69
Na_2O	0.11	0.17	0.16
K_2O	0.22	0.99	0.78
P_2O_5	0.68	0.91	0.61
Total	100	100	100
LOI	14.04	14.39	14.24
Mg#	77.0	79.6	79.9
ppm			
Sr	586	814	680
Zr	123	128	134
V	223	209	262
Ni	1034	1006	722
Cr	1205	830	856
Co	50	100	109
Rb	14	34	32
ln(Si/Al)	2.80	2.40	2.36
C.I.	1.49	1.24	1.22
K_2O/TiO_2	0.05	0.21	0.16

*Total Fe expressed as FeO; LOI = loss on ignition

Table 5 – Olivine major and minor elements (wt%)

	47504 core	47504 core	47504 core	47504 core	47504 core	47504 core	47504 core	47517a core	47517a core	47517a core	47517a core	47517a core	47517a core
Major element analysis (wt%)													
SiO_2	40.69	40.57	39.62	40.76	40.66	40.73	40.72	40.57	40.40	40.89	39.62	40.65	40.63
TiO_2	0.01	0.03	bld	0.02	0.02	bld	bld	bld	0.03	0.01	0.03	bld	bld
ZnO	n.a.	n.a.	n.a.	n.a.	n.a.	n.a.	n.a.	n.a.	bld	n.a.	0.03	n.a.	n.a.
Al_2O_3	bld	bld	bld	bld	bld	bld	bld	bld	0.02	bld	0.02	bld	bld
Cr_2O_3	0.05	bld	bld	0.04	0.02	bld	bld	0.04	0.04	0.06	bld	0.05	0.06
FeO	9.33	9.64	16.07	8.98	9.65	9.23	9.90	9.59	8.87	8.28	14.61	9.09	9.45
NiO	0.34	0.32	0.21	0.38	0.33	0.35	0.39	0.37	0.38	0.39	0.17	0.39	0.37
MnO	0.12	0.15	0.27	0.11	0.15	0.15	0.29	0.11	0.11	0.10	0.16	0.11	0.12
MgO	49.24	49.11	44.04	49.44	48.99	49.04	48.70	48.69	49.83	49.81	45.11	49.02	48.95
CaO	0.05	0.02	0.03	0.06	0.02	0.01	0.01	0.06	0.05	0.05	0.04	0.07	0.06
Na_2O	bld	bld	bld	bld	bld	bld	bld	bld	0.02	bld	bld	bld	bld
Total	99.82	99.84	100.24	99.79	99.84	99.51	100.00	99.42	99.75	99.58	99.79	99.38	99.64
Number of cation (apfu) on the basis of 4 oxygen atoms and 3 cations													
Si	0.998	0.996	0.998	0.999	0.998	1.001	1.000	1.000	0.991	1.000	0.996	1.000	0.999
Ti	0.000	0.001	0.000	0.000	0.000	0.000	0.000	0.000	0.001	0.000	0.001	0.000	0.000
Zn	0.000	0.000	0.000	0.000	0.000	0.000	0.000	0.000	0.000	0.000	0.001	0.000	0.000
Al	0.000	0.000	0.000	0.000	0.000	0.000	0.000	0.000	0.001	0.000	0.001	0.000	0.000
Cr	0.001	0.000	0.000	0.001	0.000	0.000	0.000	0.001	0.001	0.001	0.000	0.001	0.001
Fe	0.191	0.198	0.339	0.184	0.198	0.190	0.203	0.198	0.182	0.169	0.307	0.187	0.194
Ni	0.007	0.006	0.004	0.007	0.007	0.007	0.008	0.007	0.007	0.008	0.003	0.008	0.007
Mn	0.002	0.003	0.006	0.002	0.003	0.003	0.006	0.002	0.002	0.002	0.003	0.002	0.002
Mg	1.800	1.798	1.654	1.806	1.793	1.797	1.783	1.790	1.822	1.817	1.690	1.799	1.794
Ca	0.001	0.001	0.001	0.002	0.001	0.000	0.000	0.002	0.001	0.001	0.001	0.002	0.002
Na	0.000	0.000	0.000	0.000	0.000	0.000	0.000	0.000	0.000	0.000	0.000	0.000	0.000
sum	3.001	3.003	3.002	3.001	3.001	2.999	3.000	2.999	3.008	2.999	3.003	2.999	3.000
100Mg/(Mg+Fe)	90.40	90.08	83.01	90.75	90.05	90.45	89.77	90.05	90.92	91.47	84.62	90.58	90.23

Table 5 continued

	47517a core	47517a core	47517a core	47517a core	47517a core	47517a core	47517a core	47517a core	47517a core	47517a core	47517a core	47517a core	47517a core
Major element analysis (wt%)													
SiO_2	39.18	40.74	40.71	39.89	40.95	39.72	39.31	40.27	39.47	39.57	40.72	40.53	40.83
TiO_2	0.03	0.01	0.02	0.04	bld	0.04	bld	0.03	0.03	0.03	0.02	0.04	0.02
ZnO	bld	n.a.	bld	n.a.	0.02	n.a.	bld	bld	n.a.	bld	n.a.	n.a.	n.a.
Al_2O_3	0.02	bld	0.02	bld	0.01	bld	bld	0.03	bld	bld	bld	bld	bld
Cr_2O_3	0.00	0.04	0.04	bld	0.02	bld	bld	bld	bld	bld	0.07	0.03	0.02
FeO	16.46	8.98	9.17	12.28	8.85	14.70	16.81	9.45	16.15	13.60	8.85	8.96	9.79
NiO	0.14	0.36	0.36	0.25	0.35	0.17	0.09	0.37	0.10	0.25	0.37	0.37	0.36
MnO	0.16	0.11	0.11	0.11	0.12	0.13	0.18	0.12	0.17	0.14	0.13	0.10	0.11
MgO	43.62	49.31	49.70	46.53	49.63	44.65	43.28	48.87	43.76	45.51	49.37	48.88	48.70
CaO	0.05	0.06	0.05	0.04	0.05	0.04	0.04	0.06	0.03	0.05	0.06	0.06	0.07
Na_2O	0.03	bld	0.02	bld	0.02	bld	0.01	0.02	bld	0.02	bld	bld	bld
Total	99.67	99.60	100.20	99.14	100.00	99.45	99.70	99.22	99.71	99.17	99.58	98.96	99.90
Number of cation (apfu) on the basis of 4 oxygen atoms and 3 cations													
Si	0.995	1.000	0.994	0.998	1.000	1.001	0.999	0.995	0.999	0.997	0.999	1.001	1.002
Ti	0.000	0.000	0.000	0.001	0.000	0.001	0.000	0.001	0.001	0.001	0.000	0.001	0.000
Zn	0.000	0.000	0.000	0.000	0.000	0.000	0.000	0.000	0.000	0.000	0.000	0.000	0.000
Al	0.001	0.000	0.001	0.000	0.000	0.000	0.000	0.001	0.000	0.000	0.000	0.000	0.000
Cr	0.000	0.001	0.001	0.000	0.000	0.000	0.000	0.000	0.000	0.000	0.001	0.001	0.000
Fe	0.349	0.184	0.187	0.257	0.181	0.310	0.357	0.195	0.342	0.286	0.182	0.185	0.201
Ni	0.003	0.007	0.007	0.005	0.007	0.003	0.002	0.007	0.002	0.005	0.007	0.007	0.007
Mn	0.003	0.002	0.002	0.002	0.002	0.003	0.004	0.003	0.004	0.003	0.003	0.002	0.002
Mg	1.651	1.804	1.810	1.736	1.807	1.678	1.639	1.800	1.652	1.709	1.806	1.800	1.782
Ca	0.001	0.001	0.001	0.001	0.001	0.001	0.001	0.002	0.001	0.001	0.002	0.002	0.002
Na	0.000	0.000	0.000	0.000	0.000	0.000	0.000	0.000	0.000	0.000	0.000	0.000	0.000
sum	3.004	3.000	3.004	3.001	2.999	2.998	3.001	3.004	3.000	3.002	3.000	2.998	2.997
100Mg/(Mg+Fe)	82.53	90.73	90.62	87.10	90.91	84.41	82.11	90.21	82.85	85.64	90.87	90.68	89.87

Table 5 continued

	47517a core	47517a core	47517a core	47517a core	47517b core	47517b core	47517b core	47517b core	47517b core	47517b core	47517b core	47517b core	47517b core
Major element analysis (wt%)													
SiO_2	40.52	39.76	39.78	40.61	40.55	40.28	40.72	41.12	40.62	40.91	40.32	39.73	39.94
TiO_2	bld	bld	bld	0.02	0.02	0.04	bld	0.01	0.02	bld	0.05	0.04	0.02
ZnO	n.a.	n.a.	n.a.	n.a.	n.a.	bld	n.a.	bld	n.a.	bld	n.a.	n.a.	bld
Al_2O_3	bld	bld	bld	bld	bld	0.02	bld	0.03	bld	0.02	bld	0.08	bld
Cr_2O_3	0.09	0.00	0.00	0.05	0.05	0.02	0.04	0.07	0.08	0.03	bld	bld	bld
FeO	9.96	13.65	14.62	8.86	10.28	12.34	8.97	8.69	10.22	9.15	12.43	14.77	14.95
NiO	0.35	0.16	0.17	0.37	0.37	0.21	0.35	0.36	0.37	0.33	0.17	0.18	0.20
MnO	0.12	0.14	0.20	0.12	0.12	0.12	0.11	0.12	0.12	0.10	0.12	0.12	0.17
MgO	48.58	45.67	44.95	49.36	48.17	46.77	49.43	49.87	48.32	49.44	46.57	44.92	44.62
CaO	0.05	0.05	0.02	0.04	0.06	0.07	0.04	0.06	0.07	0.06	0.06	0.06	0.04
Na_2O	bld	bld	bld	bld	bld	0.03	bld	0.03	bld	0.02	bld	bld	0.02
Total	99.67	99.43	99.73	99.41	99.59	99.87	99.66	100.34	99.81	100.06	99.72	99.90	99.96
Number of cation (apfu) on the basis of 4 oxygen atoms and 3 cations													
Si	0.998	0.998	1.000	0.998	1.001	1.000	0.999	1.000	1.000	1.000	1.003	0.998	1.003
Ti	0.000	0.000	0.000	0.000	0.000	0.001	0.000	0.000	0.000	0.000	0.001	0.001	0.000
Zn	0.000	0.000	0.000	0.000	0.000	0.000	0.000	0.000	0.000	0.000	0.000	0.000	0.000
Al	0.000	0.000	0.000	0.000	0.000	0.001	0.000	0.001	0.000	0.001	0.000	0.002	0.000
Cr	0.002	0.000	0.000	0.001	0.001	0.000	0.001	0.001	0.001	0.001	0.000	0.000	0.000
Fe	0.205	0.287	0.307	0.182	0.212	0.256	0.184	0.177	0.211	0.187	0.259	0.310	0.314
Ni	0.007	0.003	0.003	0.007	0.007	0.004	0.007	0.007	0.007	0.006	0.003	0.004	0.004
Mn	0.003	0.003	0.004	0.002	0.002	0.003	0.002	0.002	0.003	0.002	0.003	0.003	0.004
Mg	1.784	1.709	1.684	1.809	1.773	1.731	1.807	1.808	1.774	1.801	1.727	1.682	1.670
Ca	0.001	0.001	0.001	0.001	0.001	0.002	0.001	0.001	0.002	0.002	0.002	0.002	0.001
Na	0.000	0.000	0.000	0.000	0.000	0.000	0.000	0.000	0.000	0.000	0.000	0.000	0.000
sum	3.001	3.002	3.000	3.001	2.998	2.998	3.001	2.998	2.999	2.999	2.996	3.000	2.996
100Mg/(Mg+Fe)	89.68	85.64	84.57	90.85	89.31	87.11	90.76	91.10	89.39	90.59	86.98	84.43	84.18

Table 5 continued

	47517b core	47517b core	47517b core	47517b core	47517b core	47517b core	47517b core	47517b core	47517b core	47517b core	47517b core	47517b core	47517b core
Major element analysis (wt%)													
SiO_2	40.84	40.65	40.76	40.25	40.67	39.87	40.56	40.87	40.69	40.71	40.75	40.92	40.76
TiO_2	0.03	bld	0.01	0.02	0.02	0.02	0.03	bld	0.02	0.02	0.03	0.05	0.02
ZnO	n.a.	bld	n.a.	0.03	n.a.	bld	n.a.	bld	n.a.	n.a.	n.a.	n.a.	n.a.
Al_2O_3	bld	0.03	0.01	0.02	bld	bld	0.03	0.03	bld	bld	bld	bld	bld
Cr_2O_3	0.06	0.04	0.06	0.05	0.07	0.03	0.06	0.05	0.04	0.05	0.03	0.07	0.03
FeO	8.46	9.72	9.28	9.30	9.13	13.62	10.12	9.76	9.18	9.97	9.03	8.25	8.95
NiO	0.36	0.36	0.38	0.34	0.36	0.24	0.36	0.36	0.34	0.35	0.38	0.36	0.36
MnO	0.11	0.12	0.11	0.12	0.11	0.16	0.11	0.11	0.11	0.12	0.11	0.11	0.11
MgO	49.74	48.64	49.28	49.21	49.05	45.75	48.64	48.93	49.01	48.52	49.46	50.07	49.41
CaO	0.04	0.07	0.07	0.07	0.06	0.08	0.06	0.06	0.05	0.06	0.05	0.06	0.05
Na_2O	bld	0.03	bld	0.03	bld	bld	bld	bld	bld	bld	bld	bld	bld
Total	99.63	99.66	99.94	99.44	99.46	99.76	99.96	100.17	99.44	99.79	99.82	99.89	99.68
Number of cation (apfu) on the basis of 4 oxygen atoms and 3 cations													
Si	1.000	1.000	0.998	0.992	1.000	0.998	0.997	1.000	1.001	1.001	0.998	0.998	0.999
Ti	0.000	0.000	0.000	0.000	0.000	0.000	0.001	0.000	0.000	0.000	0.001	0.001	0.000
Zn	0.000	0.000	0.000	0.001	0.000	0.000	0.000	0.000	0.000	0.000	0.000	0.000	0.000
Al	0.000	0.001	0.000	0.001	0.000	0.000	0.001	0.001	0.000	0.000	0.000	0.000	0.000
Cr	0.001	0.001	0.001	0.001	0.001	0.000	0.001	0.001	0.001	0.001	0.001	0.001	0.001
Fe	0.173	0.200	0.190	0.192	0.188	0.285	0.208	0.200	0.189	0.205	0.185	0.168	0.184
Ni	0.007	0.007	0.007	0.007	0.007	0.005	0.007	0.007	0.007	0.007	0.007	0.007	0.007
Mn	0.002	0.003	0.002	0.003	0.002	0.003	0.002	0.002	0.002	0.002	0.002	0.002	0.002
Mg	1.815	1.784	1.799	1.808	1.798	1.707	1.783	1.786	1.797	1.779	1.806	1.821	1.806
Ca	0.001	0.002	0.002	0.002	0.001	0.002	0.001	0.002	0.001	0.001	0.001	0.002	0.001
Na	0.000	0.000	0.000	0.000	0.000	0.000	0.000	0.000	0.000	0.000	0.000	0.000	0.000
sum	2.999	2.998	3.001	3.006	2.999	3.001	3.001	2.999	2.998	2.998	3.001	3.000	3.000
100Mg/(Mg+Fe)	91.29	89.92	90.44	90.41	90.55	85.69	89.55	89.94	90.49	89.66	90.71	91.54	90.77

Table 5 continued

	47517b core	47517b core	47517b core	47517b core	47517b core	47517b core	47517b core	47517b core	47517b core	47517b core	47517b core	47517b core	47517b core
Major element analysis (wt%)													
SiO_2	40.84	40.78	40.81	39.57	40.90	40.52	40.50	40.35	40.68	40.63	40.65	40.63	40.62
TiO_2	0.02	0.03	0.03	0.03	0.04	bld	0.02	bld	0.02	0.03	0.03	0.02	0.01
ZnO	n.a.	n.a.	n.a.	n.a.	n.a.	n.a.	n.a.	n.a.	n.a.	n.a.	n.a.	n.a.	n.a.
Al_2O_3	bld	bld	bld	bld	bld	0.03	bld	bld	bld	bld	bld	bld	bld
Cr_2O_3	0.06	0.05	0.07	0.00	0.05	0.04	0.06	0.07	0.07	0.05	0.06	0.06	0.05
FeO	9.24	9.27	8.46	15.83	8.73	10.08	9.87	9.74	8.84	9.79	9.64	9.51	9.14
NiO	0.37	0.36	0.39	0.10	0.38	0.34	0.33	0.35	0.36	0.37	0.36	0.37	0.35
MnO	0.12	0.12	0.11	0.16	0.12	0.12	0.10	0.10	0.12	0.11	0.13	0.11	0.11
MgO	49.29	49.27	49.83	44.02	49.59	48.30	48.51	48.43	49.49	48.77	48.81	49.14	49.25
CaO	0.07	0.05	0.06	0.04	0.04	0.07	0.06	0.07	0.05	0.07	0.07	0.07	0.06
Na_2O	bld	bld	bld	bld	bld	bld	bld	bld	bld	bld	bld	bld	bld
Total	99.99	99.93	99.74	99.73	99.82	99.50	99.45	99.11	99.63	99.79	99.75	99.91	99.57
Number of cation (apfu) on the basis of 4 oxygen atoms and 3 cations													
Si	1.000	0.999	0.998	1.000	1.000	1.000	0.999	0.999	0.998	0.999	0.999	0.997	0.998
Ti	0.000	0.001	0.000	0.000	0.001	0.000	0.000	0.000	0.000	0.000	0.001	0.000	0.000
Zn	0.000	0.000	0.000	0.000	0.000	0.000	0.000	0.000	0.000	0.000	0.000	0.000	0.000
Al	0.000	0.000	0.000	0.000	0.000	0.001	0.000	0.000	0.000	0.000	0.000	0.000	0.000
Cr	0.001	0.001	0.001	0.000	0.001	0.001	0.001	0.001	0.001	0.001	0.001	0.001	0.001
Fe	0.189	0.190	0.173	0.335	0.178	0.208	0.204	0.202	0.181	0.201	0.198	0.195	0.188
Ni	0.007	0.007	0.008	0.002	0.007	0.007	0.007	0.007	0.007	0.007	0.007	0.007	0.007
Mn	0.002	0.002	0.002	0.003	0.002	0.003	0.002	0.002	0.002	0.002	0.003	0.002	0.002
Mg	1.798	1.799	1.817	1.658	1.808	1.778	1.785	1.787	1.810	1.788	1.789	1.797	1.804
Ca	0.002	0.001	0.002	0.001	0.001	0.002	0.002	0.002	0.001	0.002	0.002	0.002	0.001
Na	0.000	0.000	0.000	0.000	0.000	0.000	0.000	0.000	0.000	0.000	0.000	0.000	0.000
sum	3.000	3.000	3.001	3.000	2.999	2.999	3.000	3.000	3.001	3.000	3.000	3.002	3.001
100Mg/(Mg+Fe)	90.48	90.45	91.31	83.21	91.02	89.52	89.76	89.86	90.89	89.88	90.03	90.21	90.57

Table 5 continued

	47517b core	47517b core	47517b core	47517b core	47517b core	47504 rim	47504 rim	47504 rim	47504 rim	47504 rim	47504 rim	47517a rim	47517a rim
Major element analysis (wt%)													
SiO_2	40.60	40.80	40.60	40.41	39.99	39.98	40.50	40.19	40.13	40.57	40.48	39.90	39.70
TiO_2	0.00	0.00	0.02	0.02	0.02	0.03	bld	0.03	0.03	0.05	bld	0.03	0.05
ZnO	n.a.	n.a.	n.a.	n.a.	n.a.	n.a.	n.a.	n.a.	n.a.	bld	n.a.	n.a.	n.a.
Al_2O_3	bld	bld	bld	0.04	bld	bld	bld	bld	bld	0.02	bld	bld	bld
Cr_2O_3	0.05	0.05	0.06	0.04	0.05	0.04	0.03	0.03	bld	bld	bld	0.04	0.02
FeO	9.61	9.09	8.85	10.27	13.20	12.91	11.17	12.83	14.00	12.12	12.07	13.30	13.26
NiO	0.35	0.37	0.38	0.35	0.31	0.33	0.31	0.26	0.20	0.29	0.34	0.19	0.22
MnO	0.12	0.10	0.11	0.11	0.15	0.15	0.15	0.12	0.14	0.13	0.17	0.13	0.13
MgO	48.90	49.36	49.14	48.05	45.82	46.05	47.92	46.18	46.00	47.19	47.14	45.85	45.39
CaO	0.06	0.04	0.07	0.05	0.05	0.07	0.05	0.04	0.04	0.06	0.04	0.05	0.13
Na_2O	bld	bld	bld	bld	bld	bld	bld	bld	bld	0.03	bld	bld	bld
Total	99.69	99.81	99.23	99.34	99.57	99.54	100.13	99.68	100.54	100.46	100.24	99.49	98.88
Number of cation (apfu) on the basis of 4 oxygen atoms and 3 cations													
Si	0.999	1.000	1.000	1.000	1.001	1.000	0.998	1.002	0.998	1.001	1.001	0.999	1.001
Ti	0.000	0.000	0.000	0.000	0.000	0.000	0.000	0.001	0.001	0.001	0.000	0.001	0.001
Zn	0.000	0.000	0.000	0.000	0.000	0.000	0.000	0.000	0.000	0.000	0.000	0.000	0.000
Al	0.000	0.000	0.000	0.001	0.000	0.000	0.000	0.000	0.000	0.001	0.000	0.000	0.000
Cr	0.001	0.001	0.001	0.001	0.001	0.001	0.001	0.001	0.000	0.000	0.000	0.001	0.000
Fe	0.198	0.186	0.182	0.213	0.276	0.270	0.230	0.268	0.291	0.250	0.250	0.279	0.280
Ni	0.007	0.007	0.008	0.007	0.006	0.007	0.006	0.005	0.004	0.006	0.007	0.004	0.004
Mn	0.002	0.002	0.002	0.002	0.003	0.003	0.003	0.003	0.003	0.003	0.004	0.003	0.003
Mg	1.793	1.803	1.804	1.773	1.709	1.717	1.761	1.717	1.705	1.735	1.737	1.712	1.706
Ca	0.002	0.001	0.002	0.001	0.001	0.002	0.001	0.001	0.001	0.002	0.001	0.001	0.004
Na	0.000	0.000	0.000	0.000	0.000	0.000	0.000	0.000	0.000	0.000	0.000	0.000	0.000
sum	3.001	3.000	2.999	2.999	2.998	2.999	3.001	2.997	3.002	2.998	2.999	3.000	2.998
100Mg/(Mg+Fe)	90.07	90.64	90.82	89.29	86.09	86.41	88.44	86.52	85.42	87.41	87.44	86.00	85.92

Table 5 continued

	47517a rim	47517a rim	47517a rim	47517a rim	47517a rim	47517a rim	47517a rim	47517a rim	47517a rim	47517b rim	47517b rim	47517b rim	47517b rim
Major element analysis (wt%)													
SiO_2	39.79	39.75	39.96	39.99	39.69	39.89	39.88	39.60	40.12	39.23	39.85	40.12	39.96
TiO_2	0.02	0.04	0.06	0.05	0.03	0.03	0.04	0.03	0.03	0.06	0.02	0.04	0.04
ZnO	n.a.	n.a.	n.a.	n.a.	n.a.	n.a.	n.a.	n.a.	n.a.	n.a.	n.a.	bld	n.a.
Al_2O_3	bld	bld	bld	bld	bld	bld	bld	bld	bld	bld	0.01	0.03	bld
Cr_2O_3	0.03	bld	0.03	bld	0.04	0.04	0.03	0.04	0.04	bld	0.03	0.05	0.02
FeO	13.38	12.99	12.75	13.00	13.55	13.71	12.73	14.87	13.27	16.82	13.50	11.85	13.37
NiO	0.27	0.21	0.27	0.23	0.18	0.14	0.26	0.13	0.20	0.05	0.19	0.29	0.24
MnO	0.15	0.12	0.13	0.12	0.16	0.17	0.11	0.24	0.15	0.17	0.15	0.13	0.13
MgO	45.58	45.75	46.15	46.25	45.66	45.55	45.85	44.60	46.09	43.05	45.71	47.05	45.89
CaO	0.08	0.05	0.06	0.04	0.06	0.08	0.06	0.11	0.06	0.25	0.05	0.06	0.06
Na_2O	bld	bld	bld	bld	bld	bld	bld	bld	bld	bld	bld	0.03	bld
Total	99.30	98.91	99.38	99.68	99.37	99.60	98.96	99.62	99.95	99.72	99.49	99.65	99.69
Number of cation (apfu) on the basis of 4 oxygen atoms and 3 cations													
Si	1.000	1.000	1.000	0.998	0.997	1.000	1.002	0.998	1.000	0.998	0.999	0.997	0.999
Ti	0.000	0.001	0.001	0.001	0.001	0.001	0.001	0.001	0.001	0.001	0.000	0.001	0.001
Zn	0.000	0.000	0.000	0.000	0.000	0.000	0.000	0.000	0.000	0.000	0.000	0.000	0.000
Al	0.000	0.000	0.000	0.000	0.000	0.000	0.000	0.000	0.000	0.000	0.000	0.001	0.000
Cr	0.001	0.000	0.000	0.000	0.001	0.001	0.001	0.001	0.001	0.000	0.001	0.001	0.000
Fe	0.281	0.273	0.267	0.271	0.285	0.287	0.267	0.314	0.277	0.358	0.283	0.246	0.280
Ni	0.005	0.004	0.005	0.005	0.004	0.003	0.005	0.003	0.004	0.001	0.004	0.006	0.005
Mn	0.003	0.003	0.003	0.003	0.003	0.004	0.002	0.005	0.003	0.004	0.003	0.003	0.003
Mg	1.707	1.716	1.721	1.721	1.710	1.702	1.717	1.676	1.713	1.632	1.709	1.744	1.711
Ca	0.002	0.001	0.001	0.001	0.002	0.002	0.002	0.003	0.001	0.007	0.001	0.002	0.002
Na	0.000	0.000	0.000	0.000	0.000	0.000	0.000	0.000	0.000	0.000	0.000	0.000	0.000
sum	3.000	2.999	2.999	3.001	3.002	2.999	2.997	3.001	2.999	3.001	3.000	3.001	3.000
100Mg/(Mg+Fe)	85.86	86.26	86.59	86.38	85.73	85.55	86.52	84.24	86.09	82.02	85.79	87.62	85.95

Table 5 continued

	47517b rim	47517b rim	47517b rim	47517b rim	47517b rim	47517b rim	47517b rim	47517b rim	47517b rim	47517b rim	47517b rim	47517b rim	47517b rim
Major element analysis (wt%)													
SiO_2	39.57	39.85	39.81	40.14	39.74	39.57	39.90	39.88	40.04	39.84	39.83	39.99	39.86
TiO_2	0.03	0.05	0.05	bld	0.04	0.05	0.02	0.09	0.04	0.03	0.05	0.05	0.05
ZnO	bld	n.a.	n.a.	bld	n.a.	n.a.	n.a.	n.a.	n.a.	n.a.	n.a.	n.a.	n.a.
Al_2O_3	0.03	bld	bld	bld	bld	bld	bld	bld	bld	bld	bld	0.01	bld
Cr_2O_3	0.03	0.05	0.04	bld	0.03	0.05	0.02	0.05	0.04	0.05	0.02	0.03	0.04
FeO	13.11	13.80	13.55	13.20	13.53	14.21	13.72	13.42	13.63	13.48	13.48	13.47	14.46
NiO	0.20	0.17	0.22	0.21	0.21	0.15	0.20	0.26	0.16	0.19	0.21	0.19	0.13
MnO	0.14	0.17	0.17	0.16	0.15	0.18	0.17	0.13	0.14	0.15	0.15	0.15	0.20
MgO	45.91	45.55	45.53	45.83	45.52	44.89	45.58	45.73	45.87	45.79	45.76	45.80	45.05
CaO	0.06	0.06	0.09	0.05	0.06	0.12	0.06	0.08	0.07	0.06	0.06	0.06	0.09
Na_2O	bld	bld	bld	bld	bld	bld	bld	bld	bld	bld	bld	bld	bld
Total	99.05	99.70	99.44	99.59	99.28	99.22	99.65	99.64	99.99	99.55	99.53	99.74	99.88
Number of cation (apfu) on the basis of 4 oxygen atoms and 3 cations													
Si	0.995	0.999	0.999	1.004	0.999	0.999	1.000	0.999	0.999	0.998	0.998	1.000	1.000
Ti	0.001	0.001	0.001	0.000	0.001	0.001	0.000	0.002	0.001	0.000	0.001	0.001	0.001
Zn	0.000	0.000	0.000	0.000	0.000	0.000	0.000	0.000	0.000	0.000	0.000	0.000	0.000
Al	0.001	0.000	0.000	0.000	0.000	0.000	0.000	0.000	0.000	0.000	0.000	0.000	0.000
Cr	0.000	0.001	0.001	0.000	0.001	0.001	0.000	0.001	0.001	0.001	0.000	0.000	0.001
Fe	0.276	0.289	0.284	0.276	0.284	0.300	0.288	0.281	0.284	0.282	0.282	0.282	0.303
Ni	0.004	0.003	0.004	0.004	0.004	0.003	0.004	0.005	0.003	0.004	0.004	0.004	0.003
Mn	0.003	0.004	0.004	0.003	0.003	0.004	0.004	0.003	0.003	0.003	0.003	0.003	0.004
Mg	1.722	1.702	1.704	1.708	1.706	1.689	1.703	1.707	1.706	1.710	1.710	1.707	1.685
Ca	0.001	0.002	0.002	0.001	0.002	0.003	0.001	0.002	0.002	0.001	0.001	0.001	0.002
Na	0.000	0.000	0.000	0.000	0.000	0.000	0.000	0.000	0.000	0.000	0.000	0.000	0.000
sum	3.003	3.000	3.000	2.996	3.000	3.000	3.000	2.999	3.000	3.001	3.001	2.999	2.999
100Mg/(Mg+Fe)	86.20	85.47	85.69	86.09	85.71	84.92	85.55	85.86	85.71	85.83	85.82	85.84	84.74

Table 5 continued

	47517b rim	47517b rim	47517b rim	47517b rim	47517b rim	47517b rim	47517b rim	47517b rim	47517b rim	47517b rim	47517b rim	47517b rim	47517b rim
Major element analysis (wt%)													
SiO_2	40.06	39.78	40.23	40.18	39.65	39.88	39.80	39.68	39.57	39.16	39.24	39.86	40.25
TiO_2	0.03	0.05	0.04	0.04	0.05	0.04	0.03	0.03	0.03	0.03	0.02	0.03	0.05
ZnO	n.a.	n.a.	n.a.	n.a.	n.a.	n.a.	n.a.	n.a.	n.a.	n.a.	n.a.	n.a.	n.a.
Al_2O_3	bld	bld	bld	bld	bld	bld	bld	bld	bld	bld	bld	bld	bld
Cr_2O_3	0.03	0.04	0.03	0.04	0.03	0.03	0.03	bld	bld	bld	bld	0.05	0.03
FeO	13.60	13.54	13.31	13.32	13.64	13.26	13.46	13.69	13.35	18.10	17.61	13.60	13.17
NiO	0.18	0.14	0.19	0.20	0.18	0.24	0.19	0.13	0.20	0.12	0.23	0.16	0.23
MnO	0.16	0.15	0.14	0.15	0.16	0.14	0.13	0.16	0.13	0.31	0.31	0.15	0.12
MgO	46.02	45.40	46.15	45.99	45.17	45.93	45.86	45.57	45.54	41.72	42.12	45.91	46.24
CaO	0.06	0.07	0.05	0.05	0.06	0.05	0.05	0.08	0.05	0.19	0.18	0.07	0.04
Na_2O	bld	bld	bld	bld	bld	bld	bld	bld	bld	bld	bld	bld	bld
TOTAL	100.14	99.17	100.14	99.97	98.94	99.55	99.55	99.34	98.85	99.63	99.68	99.83	100.13
Number of cation (apfu) on the basis of 4 oxygen atoms and 3 cations													
Si	0.998	1.001	1.001	1.001	1.001	0.998	0.997	0.998	0.998	1.002	1.002	0.997	1.001
Ti	0.001	0.001	0.001	0.001	0.001	0.001	0.001	0.001	0.001	0.001	0.000	0.001	0.001
Zn	0.000	0.000	0.000	0.000	0.000	0.000	0.000	0.000	0.000	0.000	0.000	0.000	0.000
Al	0.000	0.000	0.000	0.000	0.000	0.000	0.000	0.000	0.000	0.000	0.000	0.000	0.000
Cr	0.001	0.001	0.001	0.001	0.001	0.001	0.001	0.000	0.000	0.000	0.000	0.001	0.001
Fe	0.283	0.285	0.277	0.278	0.288	0.278	0.282	0.288	0.282	0.387	0.376	0.284	0.274
Ni	0.004	0.003	0.004	0.004	0.004	0.005	0.004	0.003	0.004	0.002	0.005	0.003	0.005
Mn	0.003	0.003	0.003	0.003	0.003	0.003	0.003	0.003	0.003	0.007	0.007	0.003	0.003
Mg	1.710	1.703	1.711	1.709	1.699	1.714	1.713	1.708	1.713	1.592	1.603	1.711	1.714
Ca	0.002	0.002	0.001	0.001	0.002	0.001	0.001	0.002	0.001	0.005	0.005	0.002	0.001
Na	0.000	0.000	0.000	0.000	0.000	0.000	0.000	0.000	0.000	0.000	0.000	0.000	0.000
sum	3.001	2.998	2.998	2.998	2.998	3.001	3.002	3.002	3.001	2.997	2.998	3.002	2.998
100Mg/(Mg+Fe)	85.78	85.67	86.07	86.02	85.51	86.06	85.86	85.58	85.88	80.43	81.00	85.75	86.22

Table 6 – Groundmass phlogopite major and minor elements (wt%)

Body	Sample	Nb_2O_5	SiO_2	TiO_2	Al_2O_3	Cr_2O_3	FeO_T	NiO	MnO	MgO	CaO	V_2O_3	BaO	Na_2O	K_2O	Total
PK150	**47513-1**	0.02	29.05	2.19	20.44	bld	5.12	bld	0.11	26.88	0.54	0.02	5.38	0.68	2.83	93.26
PK150	**47513-2**	bld	35.92	1.52	15.46	bld	4.70	bld	0.04	31.45	0.14	0.03	5.06	0.06	5.15	99.52
PK150	**47513-2**	bld	39.77	0.44	5.19	0.04	9.19	0.06	0.16	37.36	0.24	0.01	0.50	0.01	1.49	94.46
PK150	**47513-3**	bld	37.43	1.11	14.92	0.04	5.99	bld	0.09	30.87	0.15	0.04	2.31	0.03	6.45	99.43
PK150	**47513-3**	0.01	35.77	0.78	13.15	bld	6.81	bld	0.04	32.72	0.13	0.01	1.50	0.02	4.24	95.19
PK150	**47513-4**	bld	33.05	1.25	13.82	bld	7.62	bld	0.04	30.97	0.11	0.01	2.34	0.05	3.95	93.22
PK150	**47513-4**	bld	36.07	1.85	14.75	bld	4.49	bld	0.06	27.67	0.13	0.03	4.06	0.05	7.27	96.43
PK150	**47513-5**	bld	27.88	2.08	21.20	bld	3.62	bld	0.08	26.44	0.71	0.03	10.37	0.53	2.01	94.94
PK150	**47513-5**	bld	26.65	2.32	21.19	bld	4.22	bld	0.09	25.31	0.48	0.03	10.93	0.57	1.68	93.46
PK150	**47513-5**	bld	30.43	2.74	18.82	bld	4.88	bld	0.14	28.60	0.61	0.01	4.30	0.41	2.79	93.73
PK150	**47513-6**	bld	34.42	1.75	16.63	bld	3.80	bld	0.05	28.75	0.07	0.03	4.62	0.11	6.71	96.92
PK150	**47513-6**	bld	36.51	1.75	15.86	bld	3.32	bld	0.05	28.18	0.12	0.03	3.83	0.04	7.96	97.64
PK150	**47513-6**	0.01	27.91	3.68	20.88	0.02	5.68	bld	0.18	26.00	0.84	0.01	3.95	0.72	3.99	93.86
PK150	**47513-7**	bld	36.61	1.53	16.27	bld	3.56	bld	0.06	28.19	0.04	0.04	5.49	0.04	7.38	99.20
PK150	**47513-9**	bld	32.74	2.29	17.27	0.01	5.09	bld	0.04	31.74	0.07	0.02	6.30	0.07	3.62	99.27
PK150	**47513-9**	bld	32.49	1.77	16.12	0.04	6.22	bld	0.05	32.03	0.06	0.01	4.12	0.05	3.73	96.69
PK150	**47513-10**	bld	30.59	2.86	17.49	0.05	6.89	bld	0.12	29.75	0.64	0.02	3.53	0.38	2.93	95.25
PK150	**47513-10**	bld	26.86	2.96	21.01	0.01	4.71	bld	0.12	24.04	3.35	0.02	7.32	0.53	2.88	93.82
PK150	**47513-11**	bld	35.70	1.51	16.18	bld	3.51	bld	0.03	27.71	0.13	0.03	4.81	0.05	7.15	96.80
PK150	**47513-12**	0.02	30.21	2.34	22.42	0.03	5.99	bld	0.16	26.16	0.57	0.04	0.40	0.79	4.88	93.98
PK150	**47513-12**	bld	27.61	2.03	22.57	bld	3.17	bld	0.08	29.27	1.06	0.03	9.06	1.64	1.17	97.68
PK150	**47513-12**	bld	31.69	1.52	16.45	0.03	6.99	bld	0.13	32.35	0.32	0.01	1.22	0.66	1.71	93.09
PK150	**47513-12**	0.02	28.75	2.68	21.15	bld	6.21	0.01	0.11	26.67	0.54	bld	2.62	0.78	3.68	93.23
PK150	**47513-12**	bld	36.87	1.31	16.40	bld	3.46	bld	0.04	29.50	0.25	0.03	4.05	0.08	6.92	98.92
PK150	**47513-13**	bld	26.71	1.88	22.09	bld	2.52	bld	0.06	25.12	0.86	0.04	12.76	0.78	1.26	94.09
PK150	**47513-13**	0.02	31.30	3.02	18.61	bld	6.51	bld	0.46	28.11	0.67	0.03	1.75	0.64	3.83	94.94
PK150	**44813a-1**	n.a.	31.72	1.02	15.69	0.21	6.67	n.a.	0.04	26.55	0.02	n.a.	6.24	0.04	5.86	94.06

Table 6 continued

Body	Sample	Nb_2O_5	SiO_2	TiO_2	Al_2O_3	Cr_2O_3	FeO_T	NiO	MnO	MgO	CaO	V_2O_3	BaO	Na_2O	K_2O	Total
PK150	**44813a-1**	n.a.	34.14	1.10	15.46	0.16	4.06	n.a.	0.06	26.06	0.01	n.a.	6.25	bld	7.31	94.61
PK150	**44813a-2**	n.a.	33.39	0.32	15.69	bld	4.37	n.a.	0.03	28.29	0.06	n.a.	6.10	0.04	6.00	94.29
PK150	**44813a-3**	n.a.	34.02	0.55	14.89	bld	6.95	n.a.	0.07	27.54	0.05	n.a.	2.72	bld	6.34	93.13
PK150	**44813a-4**	n.a.	35.22	0.78	15.97	bld	3.90	n.a.	0.06	25.40	0.03	n.a.	3.94	bld	8.45	93.75
PK150	**44813a-5**	n.a.	36.04	0.53	15.97	bld	3.42	n.a.	0.04	26.72	0.07	n.a.	3.72	bld	8.88	95.39
PK150	**44813a-5**	n.a.	35.33	0.45	16.29	bld	4.50	n.a.	0.04	26.20	0.08	n.a.	3.43	bld	8.22	94.54
PK150	**44813a-6**	n.a.	35.08	1.01	15.83	bld	4.28	n.a.	0.04	26.71	0.06	n.a.	3.53	0.03	8.01	94.58
PK150	**44813b-1**	n.a.	36.75	0.93	14.71	bld	4.21	bld	0.07	25.21	0.13	n.a.	3.90	0.04	7.89	93.84
PK150	**44813b-1**	n.a.	33.09	1.39	16.45	bld	3.65	bld	0.06	24.44	bld	n.a.	8.14	bld	7.40	94.62
PK150	**44813b-1**	n.a.	32.95	1.34	15.64	bld	5.11	0.04	0.07	25.57	0.01	n.a.	5.68	bld	6.63	93.04
PK150	**44813b-2**	n.a.	35.62	1.15	15.00	0.07	4.02	bld	0.05	26.02	0.02	n.a.	3.52	bld	8.30	93.77
PK150	**44813b-3**	n.a.	36.48	0.30	14.59	bld	3.76	0.04	bld	27.68	0.02	n.a.	2.95	bld	7.83	93.65
PK150	**44813b-3**	n.a.	36.27	1.00	14.97	bld	4.76	bld	0.06	25.96	0.05	n.a.	3.54	bld	6.92	93.53
PK150	**44813c-1**	n.a.	34.45	0.94	15.66	bld	4.46	0.12	0.04	26.84	0.02	n.a.	5.69	0.02	6.71	94.95
PK150	**44813d-1**	n.a.	34.80	0.95	15.13	bld	4.66	bld	0.05	26.54	0.04	n.a.	3.33	bld	7.51	93.01
PK150	**44813d-1**	n.a.	33.06	0.85	15.92	0.05	5.09	bld	0.07	26.04	0.03	n.a.	5.94	0.03	6.42	93.50
PK150	**44813d-2**	n.a.	34.21	1.22	15.49	0.07	5.36	bld	0.07	25.81	0.06	n.a.	5.82	0.03	7.32	95.46
PK150	**44813d-2**	n.a.	35.87	1.23	15.89	bld	3.38	bld	0.05	25.71	bld	n.a.	4.12	bld	8.76	95.01
PK150	**44813d-3**	n.a.	35.41	1.09	15.32	bld	4.40	bld	0.05	25.98	0.02	n.a.	3.97	bld	7.73	93.97
PK150	**39249b-1**	bld	36.24	0.90	14.69	0.06	6.57	0.03	0.06	26.06	0.12	n.a.	1.13	0.14	7.26	93.26
PK150	**39249b-2**	0.02	38.59	1.43	14.46	0.02	4.85	0.02	0.06	27.54	0.09	0.02	1.64	0.11	8.19	97.04
PK150	**39249b-3**	bld	37.74	1.83	14.09	bld	5.72	0.02	0.16	27.46	0.05	0.02	1.45	0.09	7.34	95.97
PK150	**39249b-3**	bld	40.11	1.53	13.07	0.01	4.82	bld	0.08	27.50	0.07	0.02	0.90	0.11	9.26	97.49
PK150	**39249b-3**	0.02	38.68	1.24	15.36	0.07	4.39	bld	0.09	27.39	0.07	0.02	1.04	0.07	8.40	96.85
PK150	**39249b-5**	bld	37.65	1.57	11.50	0.01	6.63	0.01	0.08	28.29	0.16	0.02	1.00	0.11	6.92	93.95
PK150	**39249b-6**	0.02	39.39	0.49	5.87	0.03	12.12	0.04	0.10	32.54	0.19	0.01	0.22	0.05	3.23	94.29
PK150	**39249b-7**	0.02	38.92	0.53	9.86	0.03	8.05	0.09	0.14	34.06	0.08	0.04	0.86	0.04	3.36	96.09

Table 6 continued

Body	Sample	Nb_2O_5	SiO_2	TiO_2	Al_2O_3	Cr_2O_3	FeO_T	NiO	MnO	MgO	CaO	V_2O_3	BaO	Na_2O	K_2O	Total
PK150	**39249b-7**	0.02	41.04	0.45	7.12	0.07	7.28	0.07	0.08	33.57	0.25	0.03	0.86	0.03	3.00	93.86
PK150	**39249b-8**	bld	36.99	1.15	10.81	0.03	7.90	0.01	0.06	31.30	0.60	0.01	0.41	0.07	4.38	93.72
PK150	**39249b-9**	bld	38.25	1.93	14.82	0.05	4.21	bld	0.10	26.21	0.67	0.02	1.69	0.14	9.26	97.37
PK150	**39249b-9**	0.01	37.08	2.18	13.32	0.06	5.90	0.03	0.06	27.52	0.06	0.02	1.72	0.08	7.17	95.22
PK150	**39249b-9**	bld	39.45	1.12	10.12	0.07	6.35	0.01	0.03	29.89	0.07	0.03	1.00	0.07	5.61	93.84
PK150	**47517a-1**	bld	39.75	0.71	11.29	bld	4.46	bld	0.09	26.50	0.13	n.a.	1.19	0.10	9.02	93.24
PK150	**47517a-2**	bld	39.97	0.76	10.44	bld	4.80	0.03	0.06	26.43	0.04	n.a.	0.96	0.09	9.54	93.12
PK150	**47517a-3**	bld	39.00	1.09	11.37	bld	4.18	bld	0.08	26.67	0.33	n.a.	2.31	0.07	8.77	93.87
PK150	**47517b1**	bld	37.85	0.97	12.78	0.04	4.86	bld	0.08	25.36	0.07	n.a.	2.74	0.07	8.92	93.74
PK150	**47517b-1**	bld	39.08	0.54	13.31	bld	3.28	bld	0.09	25.94	0.08	n.a.	1.84	0.08	9.72	93.96
PK150	**47517b-1**	bld	38.30	0.69	13.70	bld	3.54	bld	0.09	25.10	0.15	n.a.	2.83	0.09	9.40	93.89
PK150	**47517b-2**	bld	37.23	0.71	13.16	bld	4.50	bld	0.08	25.87	0.05	n.a.	2.81	0.06	8.55	93.02
PK150	**47517b-3**	bld	37.03	1.04	13.66	bld	3.79	bld	0.07	24.98	0.10	n.a.	4.69	0.05	8.54	93.95
PK150	**47517b-3**	bld	36.79	2.17	10.54	0.13	7.66	bld	0.14	27.59	0.85	n.a.	0.17	0.05	7.43	93.52
PK150	**47517b-3**	bld	37.12	0.93	13.25	bld	4.30	bld	0.09	25.45	0.11	n.a.	3.11	0.07	8.77	93.20
PK150	**47517b-4**	bld	37.19	0.78	13.50	0.12	5.92	bld	0.17	25.45	0.10	n.a.	2.42	0.08	9.20	94.93
PK150	**47517b-4**	bld	38.42	0.50	13.76	bld	3.35	bld	0.10	25.45	0.08	n.a.	2.89	0.08	9.50	94.13
PK150	**47517b-4**	bld	38.51	0.56	13.94	bld	3.35	bld	0.08	25.95	0.09	n.a.	2.65	0.09	9.52	94.74
PK150	**47517b-5**	bld	38.24	0.96	13.65	bld	3.46	bld	0.07	25.24	0.03	n.a.	2.47	0.07	9.44	93.63
PK150	**47517b-5**	bld	37.91	0.96	13.81	bld	3.54	bld	0.10	24.97	0.03	n.a.	2.74	0.07	9.57	93.70
PK150	**47517b-5**	bld	36.33	0.81	13.55	bld	3.95	0.03	0.08	25.36	0.02	n.a.	4.79	0.08	8.05	93.05
PK150	**47517b-6**	bld	37.40	1.20	13.43	bld	5.36	bld	0.06	26.93	0.03	n.a.	2.89	0.00	8.16	95.46
PK150	**47517b-6**	bld	40.02	1.30	11.56	bld	4.85	bld	0.06	27.57	0.03	n.a.	1.26	0.00	8.56	95.21
PK150	**47517b-7**	bld	38.38	0.66	12.18	bld	4.79	bld	0.10	28.90	0.01	n.a.	1.82	0.00	7.96	94.80
PK150	**44803-1**	bld	39.50	1.10	12.43	bld	4.73	bld	0.07	28.34	0.03	0.05	1.82	0.06	8.10	96.24
PK150	**44803-1**	bld	39.34	0.73	10.38	0.03	7.75	0.01	0.11	30.87	0.05	0.02	1.66	0.08	5.00	96.04
PK150	**44803-2**	bld	42.06	0.43	9.64	0.02	4.36	bld	0.08	31.75	0.09	0.01	0.36	0.07	6.79	95.66

Table 6 continued

Body	Sample	Nb_2O_5	SiO_2	TiO_2	Al_2O_3	Cr_2O_3	FeO_T	NiO	MnO	MgO	CaO	V_2O_3	BaO	Na_2O	K_2O	Total
PK150	**44803-4**	bld	39.69	0.63	12.61	0.01	4.92	0.01	0.08	28.96	0.03	0.05	1.46	0.06	7.59	96.11
PK150	**44803-5**	bld	39.96	0.96	12.51	bld	3.75	bld	0.05	27.66	0.06	0.04	2.37	0.08	8.69	96.14
PK150	**44803-6**	bld	37.43	1.56	13.48	0.12	5.43	0.01	0.12	26.30	0.04	0.08	3.87	0.07	7.47	95.98
PK150	**44803-7**	bld	41.27	0.88	14.57	bld	3.35	bld	0.08	29.07	0.02	0.05	0.07	0.05	10.01	99.42
PK150	**44803-8**	bld	41.21	0.97	12.09	bld	4.38	bld	0.10	30.11	0.04	0.05	2.61	0.07	7.31	98.93
PK150	**44803-8**	0.01	43.56	0.59	8.19	0.03	6.75	0.02	0.10	30.16	0.11	0.02	1.10	0.08	7.30	98.01
PK150	**44803-9**	0.01	35.72	1.42	12.71	0.10	9.14	0.01	0.14	27.78	0.13	0.09	1.97	0.08	6.01	95.32
PK150	**44803-9**	bld	38.12	1.03	12.81	0.02	5.50	bld	0.08	28.38	0.08	0.05	1.84	0.08	7.56	95.55
PK150	**44803-10**	bld	41.55	0.69	10.48	0.01	3.86	0.01	0.09	30.89	0.05	0.05	0.50	0.07	7.06	95.30
PK150	**44803-12**	bld	37.76	0.71	13.76	0.03	4.39	bld	0.08	27.68	0.02	0.04	2.01	0.11	7.95	94.56
PK150	**44803-12**	bld	39.09	0.73	11.47	0.03	5.41	bld	0.06	30.88	0.05	0.02	1.18	0.09	6.08	95.09
PK150	**44803-13**	bld	40.36	1.00	14.08	bld	2.96	bld	0.05	28.78	0.01	0.04	2.61	0.07	8.98	98.94
PK150	**44803-13**	bld	38.45	1.54	14.36	bld	2.84	bld	0.06	27.55	0.01	0.05	4.35	0.06	9.02	98.30
PK150	**44803-13**	bld	39.76	1.53	14.74	bld	2.78	bld	0.05	27.37	0.01	0.06	3.60	0.06	9.41	99.36
PK150	**44803-14**	bld	40.83	0.68	12.94	0.03	3.16	bld	0.07	28.60	0.03	0.02	1.48	0.07	9.34	97.23
PK150	**44803-14**	bld	39.72	1.40	14.46	bld	2.76	bld	0.05	27.45	0.02	0.05	3.94	0.06	9.38	99.29
PK150	**44803-14**	bld	40.63	1.33	14.00	bld	2.90	bld	0.06	27.62	0.03	0.06	2.48	0.06	9.96	99.13
PK150	**44803-14**	0.02	42.02	0.80	13.19	0.01	3.09	bld	0.07	29.19	0.04	0.04	2.00	0.08	9.35	99.89
PK150	**44803-14**	bld	41.46	0.66	14.00	bld	2.69	bld	0.08	28.75	0.05	0.03	1.82	0.06	10.05	99.66
PK150	**44803-14**	bld	42.65	0.49	13.83	0.02	2.56	bld	0.08	29.70	0.06	0.04	0.03	0.06	10.49	99.99
PK150	**44803-14**	0.04	37.57	1.57	12.31	0.02	4.99	bld	0.08	27.48	0.08	0.03	1.58	0.06	7.71	93.52
PK150	**44803-14**	bld	38.07	0.96	12.99	0.17	8.00	0.02	0.16	29.10	0.05	0.09	1.86	0.09	7.16	98.75
PK150	**44803-14**	bld	39.57	1.19	13.31	0.01	3.83	bld	0.08	28.06	0.03	0.04	1.99	0.08	8.92	97.11
PK150	**44803-15**	bld	40.13	1.14	13.08	0.03	3.74	bld	0.08	28.08	0.03	0.05	2.07	0.08	8.99	97.49
PK150	**44803-15**	bld	38.68	1.39	14.88	bld	3.34	bld	0.07	27.08	0.03	0.05	4.57	0.09	8.70	98.87
PK346	**44848a-1**	n.a.	40.29	2.41	7.42	0.05	9.22	bld	0.07	25.56	0.05	n.a.	n.a.	0.32	7.65	93.04
PK346	**44848a-2**	n.a.	32.22	10.91	6.71	0.09	17.43	bld	0.37	28.44	0.41	n.a.	n.a.	0.26	2.04	98.88

Table 6 continued

Body	Sample	Nb_2O_5	SiO_2	TiO_2	Al_2O_3	Cr_2O_3	FeO_T	NiO	MnO	MgO	CaO	V_2O_3	BaO	Na_2O	K_2O	Total
PK346	**44848a-3**	n.a.	41.53	1.38	7.59	0.07	8.57	bld	0.10	24.77	0.06	n.a.	n.a.	0.51	9.52	94.10
PK346	**44848a-4**	n.a.	41.58	1.14	8.10	0.00	8.05	bld	0.14	25.72	0.05	n.a.	n.a.	0.39	9.03	94.20
PK346	**44848a-5**	n.a.	40.85	1.11	7.62	0.08	8.79	0.02	0.06	25.57	0.02	n.a.	n.a.	0.53	8.64	93.29
PK346	**44848a-6**	n.a.	40.38	1.33	8.35	0.05	8.59	bld	0.07	25.75	0.19	n.a.	n.a.	0.41	8.46	93.58
PK346	**44848a-7**	n.a.	41.12	1.18	7.33	0.05	8.97	bld	0.08	25.91	0.02	n.a.	n.a.	0.54	8.35	93.55
PK346	**44848a-8**	n.a.	40.11	2.62	8.80	0.00	8.35	0.02	0.07	24.03	0.02	n.a.	n.a.	0.31	9.56	93.89
PK346	**44848a-9**	n.a.	41.01	0.89	6.66	0.04	9.54	bld	0.08	26.21	bld	n.a.	n.a.	0.56	8.14	93.13
PK346	**44848a-10**	n.a.	40.74	0.96	9.34	0.09	6.51	bld	0.22	26.23	0.03	n.a.	n.a.	0.30	8.91	93.33
PK346	**44848a-11**	n.a.	41.06	1.44	7.29	0.06	8.95	bld	0.11	26.49	0.07	n.a.	n.a.	0.39	8.18	94.04
PK346	**44848a-12**	n.a.	41.33	0.76	7.22	0.00	8.61	bld	0.10	26.36	0.06	n.a.	n.a.	0.58	8.13	93.15
PK346	**44848a-13**	n.a.	41.60	0.73	7.74	0.06	7.75	bld	0.13	26.34	0.03	n.a.	n.a.	0.52	8.60	93.50
PK346	**44848a-14**	n.a.	42.38	0.97	7.59	0.04	8.32	bld	0.11	25.55	0.03	n.a.	n.a.	0.48	9.53	95.00
PK346	**44848a-15**	n.a.	40.98	2.05	7.14	0.05	9.79	bld	0.09	24.82	0.05	n.a.	n.a.	0.55	8.37	93.89
PK346	**44848a-16**	n.a.	43.20	0.77	6.69	0.05	8.34	bld	0.09	24.91	0.04	n.a.	n.a.	0.68	10.09	94.86
PK346	**44848a-17**	n.a.	41.89	1.20	6.41	0.04	9.42	bld	0.07	25.03	0.08	n.a.	n.a.	0.63	9.00	93.77
PK346	**44848a-18**	n.a.	40.69	0.68	7.53	0.06	9.45	bld	0.12	27.32	0.14	n.a.	n.a.	0.43	7.34	93.76
PK346	**44848b-1**	n.a.	40.43	2.69	8.50	0.05	8.43	bld	0.06	24.76	0.03	n.a.	n.a.	0.37	8.87	94.19
PK346	**44848b-2**	n.a.	40.65	0.92	7.55	0.05	9.03	bld	0.12	26.49	0.03	n.a.	n.a.	0.31	8.22	93.37
PK346	**44848b-3**	n.a.	41.54	1.65	7.86	0.04	8.27	bld	0.08	25.51	0.03	n.a.	n.a.	0.42	9.43	94.83
PK346	**44848b-4**	n.a.	40.06	0.93	7.77	0.06	8.86	bld	0.14	27.50	0.02	n.a.	n.a.	0.30	7.49	93.13
PK346	**44848b-5**	n.a.	40.85	1.35	8.28	0.06	8.34	bld	0.12	26.37	bld	n.a.	n.a.	0.35	8.52	94.24
PK346	**44848b-6**	n.a.	41.82	0.76	6.76	0.05	8.82	bld	0.08	26.26	bld	n.a.	n.a.	0.63	8.46	93.64
PK346	**44848b-7**	n.a.	41.59	0.79	7.45	0.06	8.11	bld	0.12	27.38	0.06	n.a.	n.a.	0.48	8.17	94.21
PK346	**44848b-8**	n.a.	40.33	0.84	8.13	0.00	8.40	bld	0.13	27.96	0.04	n.a.	n.a.	0.30	7.30	93.43
PK346	**44848b-9**	n.a.	39.42	1.50	7.10	0.00	10.79	bld	0.17	29.13	0.15	n.a.	n.a.	0.30	5.10	93.66
PK346	**44848b-10**	n.a.	41.32	0.75	7.83	0.05	8.07	bld	0.14	26.58	0.02	n.a.	n.a.	0.46	8.39	93.61
PK346	**44848b-11**	n.a.	39.92	1.08	7.78	0.00	9.94	bld	0.12	26.65	0.03	n.a.	n.a.	0.30	7.60	93.42

Table 6 continued

Body	Sample	Nb_2O_5	SiO_2	TiO_2	Al_2O_3	Cr_2O_3	FeO_T	NiO	MnO	MgO	CaO	V_2O_3	BaO	Na_2O	K_2O	Total
PK346	**44848b-12**	n.a.	42.02	0.64	8.13	0.05	7.46	bld	0.15	26.34	0.03	n.a.	n.a.	0.43	9.28	94.53
PK346	**44848b-13**	n.a.	41.47	1.09	6.98	0.04	9.48	0.03	0.09	24.98	0.02	n.a.	n.a.	0.55	9.28	94.01
PK346	**44848b-14**	n.a.	42.01	0.70	7.16	0.06	8.62	bld	0.11	26.44	bld	n.a.	n.a.	0.53	8.77	94.40
PK346	**44848b-15**	n.a.	41.60	0.65	7.72	0.07	7.68	0.03	0.12	27.27	bld	n.a.	n.a.	0.55	7.93	93.62
PK346	**44848b-16**	n.a.	39.99	1.13	8.89	0.08	9.04	bld	0.18	26.84	0.09	n.a.	n.a.	0.25	7.58	94.07
PK346	**44848b-17**	n.a.	40.55	3.70	8.45	0.06	8.10	bld	0.07	23.45	0.04	n.a.	n.a.	0.37	9.78	94.57
PK346	**44848b-18**	n.a.	40.02	1.09	7.75	0.05	9.22	bld	0.09	27.59	0.17	n.a.	n.a.	0.47	6.56	93.01
PK346	**44848b-19**	n.a.	42.45	0.77	6.91	0.00	8.24	bld	0.17	26.95	0.02	n.a.	n.a.	0.60	8.54	94.65
PK346	**44848b-20**	n.a.	41.72	1.12	7.22	0.09	8.84	bld	0.09	26.19	0.03	n.a.	n.a.	0.50	8.66	94.46
PK346	**44848b-21**	n.a.	41.24	0.77	6.89	0.04	9.58	bld	0.14	25.38	0.13	n.a.	n.a.	0.52	8.86	93.55
PK346	**44848b-22**	n.a.	41.58	1.05	7.65	0.05	9.24	bld	0.09	24.68	0.03	n.a.	n.a.	0.50	9.68	94.55
PK346	**44848b-23**	n.a.	41.61	1.64	8.45	0.04	8.06	bld	0.07	24.34	0.04	n.a.	n.a.	0.43	10.10	94.78
PK346	**44848b-24**	n.a.	40.26	2.49	9.04	0.07	8.50	0.02	0.08	23.96	0.05	n.a.	n.a.	0.33	9.69	94.49
PK346	**44848b-25**	n.a.	41.03	2.52	9.28	0.00	8.20	bld	0.07	24.15	0.04	n.a.	n.a.	0.33	10.00	95.62
PK346	**44848b-26**	n.a.	41.87	1.73	7.92	0.06	8.09	bld	0.07	24.40	0.03	n.a.	n.a.	0.46	10.14	94.77
PK346	**44848b-27**	n.a.	40.10	2.77	9.18	0.05	8.37	bld	0.08	23.37	0.06	n.a.	n.a.	0.29	9.99	94.26
PK346	**44848b-28**	n.a.	41.52	2.06	8.75	0.00	7.86	0.04	0.05	24.55	0.08	n.a.	n.a.	0.39	9.96	95.26
PK346	**44834a-1**	n.a.	37.66	0.74	11.38	0.05	8.90	bld	0.22	25.13	0.10	n.a.	1.67	0.10	8.05	94.00
PK346	**44834a-1**	n.a.	40.07	0.52	8.96	0.05	8.00	bld	0.32	26.38	0.25	n.a.	0.59	0.14	8.23	93.51
PK346	**44834a-1**	n.a.	39.05	0.80	10.98	bld	6.41	bld	0.18	26.04	0.03	n.a.	1.31	0.08	8.13	93.01
PK346	**44834b-1**	n.a.	38.88	1.29	10.66	0.05	8.11	n.a.	0.08	26.19	0.12	n.a.	0.22	0.10	7.57	93.27
PK346	**44834b-2**	n.a.	38.25	1.48	11.82	0.07	6.65	n.a.	0.06	26.26	0.05	n.a.	1.02	0.10	7.94	93.70
PK346	**44834b-3**	n.a.	40.11	2.22	7.34	bld	11.16	n.a.	0.07	23.92	0.07	n.a.	0.34	0.25	8.82	94.30
PK346	**44834b-3**	n.a.	39.08	1.10	9.58	bld	8.03	n.a.	0.12	27.41	0.08	n.a.	0.75	0.13	6.72	93.00
PK346	**44834b-4**	n.a.	38.55	1.27	10.84	bld	7.63	n.a.	0.06	26.44	0.05	n.a.	0.48	0.10	7.86	93.28
PK346	**44864-1**	bld	40.17	0.17	10.65	bld	4.11	bld	0.06	29.85	0.11	n.a.	1.40	bld	8.67	95.19
PK346	**44864-1**	bld	39.40	0.24	10.34	bld	4.57	bld	0.05	30.40	0.06	n.a.	3.36	bld	7.99	96.41

Table 6 continued

Body	Sample	Nb_2O_5	SiO_2	TiO_2	Al_2O_3	Cr_2O_3	FeO_T	NiO	MnO	MgO	CaO	V_2O_3	BaO	Na_2O	K_2O	Total
PK346	**44864-1**	0.09	39.85	0.21	8.29	bld	6.80	bld	0.05	31.53	0.06	n.a.	0.62	bld	6.88	94.38
PK346	**44864-1**	bld	38.56	0.42	10.62	0.04	4.31	bld	0.04	31.04	0.02	n.a.	2.55	bld	6.99	94.59
PK346	**44864-1**	bld	32.62	0.54	16.48	0.04	4.55	bld	0.04	27.23	0.02	n.a.	8.87	0.06	5.06	95.51
PK346	**44864-1**	bld	40.69	1.57	8.28	0.07	6.22	bld	0.06	29.30	0.01	n.a.	0.52	0.09	7.53	94.34
PK346	**44864-1**	bld	39.24	1.64	11.25	bld	5.92	bld	0.07	28.32	bld	n.a.	0.99	bld	8.12	95.55
PK346	**44864-1**	bld	39.44	0.30	9.82	bld	5.86	0.04	bld	31.23	bld	n.a.	1.11	bld	7.13	94.93
PK346	**44864-2**	bld	39.02	0.18	8.67	bld	7.08	bld	0.06	31.33	0.03	n.a.	0.65	bld	6.33	93.35
PK346	**44864-2**	bld	40.18	0.42	7.99	0.04	6.07	bld	bld	32.04	0.02	n.a.	0.50	bld	6.66	93.92
PK346	**44864-2**	bld	40.07	0.27	8.65	bld	5.38	bld	0.04	31.49	0.02	n.a.	1.14	bld	7.17	94.23
PK346	**44864-2**	bld	41.12	0.16	7.23	bld	6.23	bld	0.04	31.42	0.04	n.a.	0.65	bld	7.66	94.55
PK346	**44864-3**	bld	41.22	1.84	9.50	bld	5.98	bld	0.06	29.39	0.01	n.a.	0.36	0.07	8.18	96.61
PK346	**44864-3**	bld	41.20	1.71	8.69	0.13	5.80	bld	0.06	29.71	0.03	n.a.	0.53	0.10	7.72	95.68
PK346	**44864-3**	bld	40.92	1.73	9.68	0.14	5.29	bld	0.06	29.17	0.02	n.a.	0.68	0.10	8.28	96.07
PK346	**44864-4**	bld	41.33	0.19	10.50	bld	4.92	bld	0.06	30.55	0.04	n.a.	0.69	bld	9.76	98.04
PK346	**44864-4**	bld	40.79	0.08	8.89	bld	5.47	0.04	bld	31.91	0.03	n.a.	1.14	bld	7.99	96.34
PK346	**44864-4**	bld	40.95	0.12	8.61	bld	5.34	bld	0.04	33.41	0.02	n.a.	0.58	bld	7.48	96.55
PK346	**44864-4**	bld	36.94	0.41	12.59	bld	5.45	bld	0.09	29.20	0.04	n.a.	2.87	bld	7.24	94.83
PK346	**44864-1**	bld	42.30	1.93	10.20	0.02	4.76	bld	0.06	28.47	0.02	0.01	0.46	0.08	8.46	96.76
PK346	**44864-1**	bld	41.95	1.42	11.17	0.01	4.41	bld	0.05	29.00	0.02	0.02	0.74	0.08	8.01	96.88
PK346	**44864-1**	bld	42.08	1.31	11.26	bld	3.89	bld	0.05	30.06	0.02	0.02	1.08	0.07	7.45	97.28
PK346	**44864-2**	bld	38.51	0.48	11.95	bld	5.81	bld	0.06	31.64	0.06	0.04	1.91	0.11	5.76	96.34
PK346	**44864-2**	bld	39.29	0.31	10.09	bld	6.51	bld	0.05	31.95	0.04	0.01	0.75	0.01	6.18	95.18
PK346	**44864-2**	bld	40.47	1.31	13.23	bld	4.13	bld	0.04	28.92	0.05	0.02	1.30	0.07	8.62	98.17
PK346	**44864-2**	bld	40.08	1.47	12.75	bld	4.43	bld	0.06	28.46	0.03	0.04	1.32	0.06	8.37	97.08
PK346	**44864-2**	bld	42.65	1.97	9.41	0.06	4.84	bld	0.03	29.60	0.04	bld	0.70	0.11	8.20	97.62
PK346	**44864-3**	bld	39.12	0.55	12.46	0.01	4.90	0.01	0.02	30.22	bld	bld	2.14	0.03	7.61	97.07
PK346	**44864-3**	bld	41.69	1.96	11.36	0.14	4.44	bld	0.06	27.93	bld	0.01	0.75	0.08	9.37	97.80

Table 6 continued

Body	Sample	Nb_2O_5	SiO_2	TiO_2	Al_2O_3	Cr_2O_3	FeO_T	NiO	MnO	MgO	CaO	V_2O_3	BaO	Na_2O	K_2O	Total
PK346	**44864-3**	bld	42.74	1.75	10.42	0.06	4.96	bld	0.05	28.39	0.05	0.01	0.66	0.12	9.47	98.68
PK346	**44864-3**	bld	42.00	1.89	11.28	0.06	4.56	bld	0.05	27.27	bld	0.01	0.69	0.09	10.26	98.15
PK346	**44864-4**	bld	41.20	1.02	8.08	bld	5.38	bld	0.04	32.69	0.02	bld	0.76	0.05	4.56	93.80
PK346	**44864-4**	bld	41.97	0.26	8.23	bld	4.91	0.01	0.03	32.00	0.01	bld	0.99	0.02	6.75	95.18
PK346	**44864-4**	bld	41.88	0.28	7.44	bld	4.71	0.01	0.03	32.74	0.02	bld	1.05	0.03	5.53	93.71
PK346	**44864-5**	bld	41.25	0.27	10.56	bld	4.91	0.02	0.02	31.78	0.01	bld	0.98	0.02	6.51	96.33
PK346	**44864-5**	bld	41.62	0.29	11.76	bld	3.40	0.02	0.01	30.83	0.01	bld	1.99	0.04	8.08	98.03
PK346	**44864-5**	0.01	42.50	0.17	9.89	bld	3.96	0.01	0.03	30.63	0.01	bld	0.72	0.02	8.69	96.64
PK346	**44864-5**	bld	43.03	0.10	9.23	bld	4.42	0.01	0.02	31.65	0.01	bld	0.71	0.01	7.97	97.17
PK346	**44864-6**	bld	43.12	0.29	9.07	bld	4.41	bld	0.04	32.00	0.04	bld	1.17	0.02	7.05	97.21
PK346	**44864-6**	bld	42.78	0.28	9.29	bld	4.45	0.03	0.03	31.42	0.02	bld	1.15	0.03	6.90	96.37
PK346	**44864-7**	bld	41.17	0.24	9.25	bld	4.71	0.01	0.04	30.47	0.02	bld	1.11	0.02	7.19	94.21
PK346	**44864-7**	bld	41.04	2.01	11.85	0.19	3.43	bld	0.05	28.73	0.01	bld	1.35	0.06	8.40	97.12
PK346	**44864-7**	0.02	40.40	2.09	10.00	0.05	5.44	bld	0.05	28.35	0.01	0.01	0.99	0.08	7.90	95.39
PK346	**44864-8**	0.02	38.74	0.09	10.33	bld	7.08	0.01	0.02	31.88	0.01	bld	0.68	bld	5.99	94.85
PK346	**44864-8**	bld	40.34	0.59	11.04	0.04	4.98	0.01	0.03	30.80	0.01	bld	1.27	0.02	7.26	96.39
PK346	**44864-8**	bld	39.51	0.16	13.05	bld	2.94	bld	0.01	30.43	0.01	0.01	3.30	0.01	7.71	97.14
PK346	**44864-10**	bld	39.42	0.25	15.07	bld	2.73	bld	0.03	29.66	bld	0.02	4.28	0.01	8.11	99.58
PK346	**44864-10**	bld	39.48	1.01	12.44	0.04	5.04	bld	0.04	29.86	bld	bld	2.16	0.03	7.83	97.93
PK346	**44864-11**	bld	40.49	0.45	13.53	bld	2.94	bld	0.03	30.38	0.01	0.03	3.20	0.01	8.35	99.43
PK346	**44864-12**	bld	39.80	0.50	12.77	bld	3.80	bld	0.06	30.53	bld	0.02	2.73	0.02	7.93	98.17
PK346	**44864-12**	0.02	41.47	0.83	11.41	bld	3.64	bld	0.03	31.19	0.01	0.01	2.34	0.04	7.66	98.65
PK346	**44864-12**	bld	41.91	0.20	10.22	bld	4.56	0.01	0.04	30.69	0.02	bld	1.00	0.02	8.54	97.20
PK346	**44860-1**	bld	42.44	0.57	4.48	0.03	7.04	0.01	0.07	31.56	0.09	0.04	0.64	0.14	7.45	94.55
PK346	**44860-1**	bld	43.32	0.57	3.80	0.02	7.14	0.02	0.18	32.71	0.09	0.13	0.64	0.08	6.03	94.74
PK346	**44860-1**	0.02	43.26	0.72	4.25	0.01	7.83	0.02	0.06	30.64	0.07	0.02	0.99	0.20	9.18	97.26
PK346	**44860-2**	bld	41.99	0.36	7.48	0.01	5.72	0.01	0.08	30.94	0.08	0.04	1.85	0.07	6.96	95.60

Table 6 continued

Body	Sample	Nb_2O_5	SiO_2	TiO_2	Al_2O_3	Cr_2O_3	FeO_T	NiO	MnO	MgO	CaO	V_2O_3	BaO	Na_2O	K_2O	Total
PK346	**44860-3**	bld	37.63	0.39	13.17	bld	4.65	0.09	0.03	28.68	0.08	0.02	6.07	0.07	7.69	98.56
PK346	**44860-3**	0.01	44.19	0.80	2.29	bld	7.12	bld	0.12	31.55	0.47	0.03	0.94	0.17	8.59	96.28
PK346	**44860-4**	bld	44.48	0.22	3.22	0.01	5.14	0.02	0.07	35.04	0.23	0.01	0.72	0.03	4.62	93.81
PK346	**44860-4**	bld	44.54	0.27	2.80	bld	5.63	0.02	0.12	36.16	0.08	bld	0.58	0.04	4.33	94.58
PK346	**44860-4**	bld	45.18	0.33	2.53	bld	5.38	0.01	0.12	36.66	0.08	0.01	0.58	0.03	4.14	95.06
PK346	**44860-5**	bld	36.75	0.12	12.19	0.02	4.96	0.10	0.02	28.78	0.05	0.03	8.74	bld	6.72	98.48
PK346	**44860-5**	bld	39.38	0.17	8.87	0.01	5.11	0.05	0.04	30.67	0.06	0.03	3.35	0.02	5.73	93.49
PK346	**44860-6**	bld	41.18	0.34	6.61	bld	6.79	0.03	0.11	31.95	0.09	0.01	0.84	0.31	5.54	93.80
PK346	**44860-7**	bld	35.41	0.30	14.08	bld	6.13	bld	0.06	31.72	0.16	0.01	2.14	0.72	3.64	94.39
PK346	**44860-7**	bld	37.94	0.19	11.06	bld	4.12	bld	0.04	30.74	0.05	0.01	4.20	0.05	6.21	94.60
PK346	**44838-1**	bld	44.24	3.08	7.29	0.08	6.72	bld	0.06	25.71	0.10	0.01	0.28	0.51	10.23	98.31
PK346	**44838-1**	bld	44.22	1.68	4.40	0.05	6.08	bld	0.04	31.88	0.07	0.01	0.10	0.31	5.95	94.79
PK346	**44838-2**	0.02	45.02	2.58	8.27	0.09	5.82	bld	0.09	26.66	0.07	0.02	0.21	0.40	10.13	99.36
PK346	**44838-2**	bld	44.70	1.95	6.82	0.10	6.92	bld	0.06	27.98	0.24	0.01	0.19	0.44	8.64	98.05
PK346	**44838-3**	0.03	42.82	2.84	7.07	0.11	7.49	bld	0.09	26.22	1.33	0.01	0.24	0.40	8.55	97.20
PK346	**44838-4**	0.02	43.10	2.25	7.57	0.14	5.31	bld	0.10	25.77	3.30	0.02	0.16	0.43	9.49	97.66
PK346	**44838-5**	0.01	44.63	1.77	8.50	0.05	5.97	bld	0.09	29.32	0.05	0.03	0.29	0.34	8.86	99.91
PK346	**44838-5**	bld	43.39	2.54	8.06	0.07	6.66	bld	0.11	27.21	0.30	0.01	0.28	0.32	9.50	98.44
PK346	**44838-6**	0.02	43.39	2.44	8.24	0.13	6.53	0.01	0.10	26.74	0.58	0.03	0.21	0.43	9.87	98.71
PK346	**44838-6**	bld	42.25	1.65	5.83	0.08	6.83	bld	0.06	29.74	0.06	0.02	0.15	0.18	6.30	93.17
PK346	**44838-6**	bld	43.42	2.37	6.17	0.06	7.10	bld	0.07	29.05	0.18	0.02	0.20	0.23	7.70	96.58
PK346	**44838-6**	bld	42.41	2.42	7.50	0.07	6.19	bld	0.13	27.09	1.41	0.02	0.18	0.25	8.56	96.23
PK346	**44838-7**	0.02	42.78	2.78	6.77	0.06	7.20	bld	0.06	27.11	0.09	0.01	0.35	0.30	8.45	95.96
PK346	**44838-7**	bld	42.73	3.06	7.83	0.06	7.31	bld	0.10	25.68	0.08	0.01	0.35	0.34	10.08	97.65
PK346	**44838-8**	0.02	45.05	1.49	7.26	0.08	4.46	bld	0.10	29.26	0.13	0.18	0.74	0.38	8.16	97.31
PK346	**44838-11**	bld	42.95	3.13	8.55	0.12	7.11	bld	0.09	25.38	0.15	0.01	0.37	0.36	10.02	98.25
PK346	**44838-13**	bld	44.21	1.16	7.89	0.20	8.21	bld	0.05	32.35	0.79	0.03	0.11	0.17	4.73	99.91

Table 6 continued

Body	Sample	Nb_2O_5	SiO_2	TiO_2	Al_2O_3	Cr_2O_3	FeO_T	NiO	MnO	MgO	CaO	V_2O_3	BaO	Na_2O	K_2O	Total
PK346	**44838-13**	0.01	41.73	0.99	6.58	0.15	8.57	bld	0.07	29.88	0.80	0.02	0.05	0.12	4.92	93.87
PK346	**44838-14**	bld	42.71	1.73	6.57	0.11	5.18	bld	0.10	30.41	0.12	0.08	0.48	0.15	6.16	93.78
PK346	**44838-15**	bld	44.85	1.50	4.68	0.03	6.71	bld	0.06	32.81	0.07	0.01	0.14	0.22	5.63	96.71
PK346	**44838-15**	0.02	46.27	2.59	5.36	0.05	6.43	bld	0.05	29.14	0.09	0.01	0.21	0.55	8.58	99.33
PK346	**44838-16**	bld	45.25	1.79	6.07	0.09	6.38	bld	0.05	31.69	0.06	0.02	0.13	0.34	6.55	98.42
PK346	**44838-16**	bld	46.04	0.95	3.17	0.03	5.44	bld	0.01	36.71	0.05	bld	0.03	0.19	3.59	96.23
PK346	**44838-16**	bld	46.84	0.50	2.89	0.11	7.14	bld	0.04	38.93	0.14	0.02	0.02	0.07	1.91	98.60
PK346	**44838-17**	bld	46.70	1.74	5.89	0.07	5.33	bld	0.06	30.54	0.12	0.02	0.12	0.47	8.44	99.50
PK346	**44838-17**	0.02	45.86	2.28	4.45	0.07	7.31	bld	0.06	32.16	0.12	0.07	0.29	0.18	5.86	98.73
PK346	**44838-17**	bld	44.03	2.37	5.35	0.02	6.38	bld	0.05	31.08	0.07	bld	0.20	0.26	7.04	96.85
PK151	**47514-1**	bld	38.04	1.25	16.35	0.02	6.14	0.01	0.09	28.27	0.22	bld	0.94	0.10	7.36	98.79
PK151	**47514-3**	bld	33.66	1.43	20.59	bld	4.30	bld	0.08	25.08	0.22	0.01	4.00	0.14	7.40	96.91
PK151	**47514-3**	bld	37.78	4.96	15.10	1.21	5.83	0.08	0.05	22.26	0.04	0.02	0.22	0.42	9.15	97.12
PK151	**47514-3**	bld	38.49	5.43	15.21	1.18	5.27	0.07	0.04	21.01	0.03	0.03	0.12	0.38	9.82	97.08
PK151	**47514-5**	bld	36.27	1.38	18.00	0.01	4.62	0.01	0.06	25.32	0.08	0.01	2.18	0.16	7.89	95.99
PK151	**47514-5**	0.02	38.41	1.12	15.53	0.04	5.64	0.05	0.06	26.07	0.06	bld	0.98	0.22	6.66	94.85
PK151	**47514-5**	0.02	36.21	1.40	14.60	0.05	8.01	0.01	0.15	28.58	0.19	0.01	1.06	0.13	5.43	95.85
PK151	**47514-5**	bld	34.05	1.30	18.11	bld	6.06	0.01	0.07	26.74	0.22	0.01	2.92	0.19	5.09	94.76
PK151	**47514-7**	bld	38.05	1.03	15.75	0.01	4.96	bld	0.20	27.14	0.11	0.01	0.67	0.15	7.83	95.93
PK151	**47514-7**	bld	35.73	1.01	15.19	0.01	6.59	bld	0.06	27.46	0.13	bld	0.61	0.10	6.63	93.51
PK151	**47514-8**	bld	35.90	1.95	18.74	bld	4.68	bld	0.08	24.27	0.10	0.01	2.90	0.23	7.82	96.67
PK151	**47514-8**	0.01	34.78	1.40	19.79	bld	4.22	0.02	0.07	24.45	0.16	0.02	3.71	0.23	7.24	96.08
PK151	**47514-9**	0.03	32.85	1.51	17.08	bld	9.33	0.02	0.12	22.21	0.39	0.02	1.74	0.20	7.61	93.11
PK312	**47553b-2**	bld	38.44	1.49	11.79	bld	7.25	0.08	0.06	25.82	0.06	n.a.	0.36	0.08	8.59	94.02
PK312	**47553b-3**	bld	36.89	1.48	10.95	bld	8.96	0.04	0.07	26.38	0.06	n.a.	0.21	0.04	6.30	91.38
PK312	**47553b-4**	bld	37.76	1.82	12.60	0.12	6.41	0.06	bld	24.48	0.06	n.a.	1.11	0.10	8.02	92.54
PK312	**47553b-4**	bld	35.94	2.72	10.34	0.12	10.93	0.06	0.04	24.83	0.08	n.a.	0.34	0.07	6.19	91.66

Table 6 continued

Body	Sample	Nb_2O_5	SiO_2	TiO_2	Al_2O_3	Cr_2O_3	FeO_T	NiO	MnO	MgO	CaO	V_2O_3	BaO	Na_2O	K_2O	Total
PK312	**47553b-4**	bld	36.04	1.49	11.50	0.09	9.11	0.07	0.04	26.51	0.08	n.a.	0.33	0.06	6.18	91.50
PK312	**47553b-5**	bld	38.04	1.94	12.55	0.08	5.73	0.07	0.03	23.38	0.13	n.a.	1.29	0.13	8.75	92.12
PK312	**47553b-6**	bld	39.05	1.60	11.88	0.04	6.87	0.05	0.04	25.80	0.06	n.a.	0.32	0.07	8.67	94.45
PK312	**47553b-6**	bld	37.38	1.57	12.71	0.11	7.02	bld	0.05	26.17	0.02	n.a.	0.60	0.07	7.70	93.40
PK312	**47553b-6**	bld	39.36	1.74	11.71	0.11	6.54	0.08	0.05	25.57	0.02	n.a.	0.28	0.11	8.80	94.37
PK312	**47553b-6**	bld	38.18	4.99	15.39	1.13	6.56	0.09	0.03	20.46	0.02	n.a.	bld	0.15	9.64	96.64
PK312	**47553b-6**	bld	37.12	1.78	12.20	0.11	7.85	0.05	0.03	26.29	0.02	n.a.	0.47	0.09	7.35	93.36
PK312	**47553b-6**	bld	37.22	1.03	11.21	bld	8.24	0.05	0.03	26.66	0.14	n.a.	0.14	0.06	6.96	91.74
PK312	**47553b-7**	bld	38.62	5.15	14.77	1.16	6.40	0.07	0.03	20.47	0.02	n.a.	bld	0.39	9.69	96.77
PK312	**47553b-7**	bld	38.34	5.13	15.24	1.11	6.10	0.08	0.03	19.92	0.01	n.a.	bld	0.29	9.85	96.10
PK312	**47553b-7**	bld	38.25	5.11	15.31	1.18	6.10	0.09	0.03	19.78	0.02	n.a.	bld	0.32	9.75	95.94
PK312	**47553b-7**	bld	39.56	1.54	13.70	0.14	4.90	0.08	0.04	24.97	0.01	n.a.	0.87	0.13	9.99	95.93
PK312	**47553b-7**	bld	36.65	1.37	12.93	0.10	7.26	0.05	0.03	26.36	0.06	n.a.	0.65	0.08	7.27	92.81
PK312	**47553b-7**	bld	38.73	1.51	13.85	0.05	5.42	0.07	bld	25.11	0.03	n.a.	1.00	0.09	9.48	95.34
PK312	**47553b-7**	bld	40.36	1.48	11.72	0.06	5.82	0.08	0.03	25.51	0.03	n.a.	0.24	0.09	9.89	95.31
PK312	**47553b-7**	bld	41.48	0.12	8.67	bld	9.36	bld	0.70	25.22	0.07	n.a.	0.10	bld	9.16	94.88
PK312	**47553b-7**	bld	37.67	1.39	12.33	0.05	7.31	0.06	bld	26.55	0.01	n.a.	0.41	0.07	7.62	93.47
PK312	**47553b-8**	bld	38.55	1.43	11.08	bld	7.55	0.06	0.04	26.04	0.18	n.a.	0.29	0.08	7.61	92.91
PK312	**47553b-9**	bld	38.75	1.34	8.85	0.13	8.31	0.06	0.05	28.51	0.08	n.a.	0.09	0.07	5.49	91.73
PK312	**47553b-9**	bld	38.94	1.75	10.47	0.13	7.09	0.05	0.07	26.03	0.04	n.a.	0.25	0.07	7.76	92.65
PK312	**47553b-9**	bld	37.57	0.94	11.18	bld	7.91	0.06	0.07	26.99	0.13	n.a.	0.14	0.05	6.75	91.79
PK314	**47547-1**	bld	37.72	1.51	15.44	bld	3.35	bld	0.06	25.42	0.02	n.a.	4.08	0.07	9.25	96.92
PK314	**47547-1**	bld	40.86	1.94	12.36	0.05	3.72	bld	0.05	26.43	0.02	n.a.	1.04	0.09	10.29	96.85
PK314	**47547-2**	bld	37.70	1.97	15.17	bld	3.19	bld	0.06	25.07	0.02	n.a.	4.18	0.07	9.01	96.44
PK314	**47547-2**	bld	37.55	1.54	15.57	bld	3.06	bld	0.04	25.51	0.03	n.a.	4.46	0.04	9.04	96.84
PK314	**47547-2**	bld	39.02	1.94	14.27	bld	3.13	bld	0.07	25.88	0.02	n.a.	2.66	0.05	9.65	96.69
PK314	**47547-2**	bld	38.43	1.97	13.08	0.06	4.29	bld	0.09	24.66	0.06	n.a.	1.97	0.05	9.05	93.71

Table 6 continued

Body	Sample	Nb_2O_5	SiO_2	TiO_2	Al_2O_3	Cr_2O_3	FeO_T	NiO	MnO	MgO	CaO	V_2O_3	BaO	Na_2O	K_2O	Total
PK314	**47547-2**	bld	38.28	1.10	12.40	0.05	6.34	bld	0.05	26.56	0.12	n.a.	1.45	0.05	7.68	94.08
PK314	**47547-3**	bld	37.11	1.38	15.98	bld	3.54	bld	0.06	24.80	0.02	n.a.	4.64	0.06	8.73	96.32
PK314	**47547-4**	0.06	38.63	1.49	13.69	bld	3.73	0.04	0.04	25.61	0.12	n.a.	3.39	0.07	9.06	95.93
PK314	**47547-5**	bld	37.15	1.48	14.49	0.04	3.72	bld	0.05	24.98	0.02	n.a.	4.42	0.05	8.84	95.24
PK314	**47547-5**	bld	38.40	1.57	13.90	bld	3.66	0.05	0.08	24.99	0.03	n.a.	3.05	0.00	9.12	94.85
PK314	**47547-5**	bld	30.93	0.45	21.41	bld	4.85	bld	0.07	23.64	0.07	n.a.	10.48	0.05	5.38	97.33
PK314	**47547-5**	bld	40.14	0.76	11.22	0.06	4.84	0.04	0.07	26.22	0.10	n.a.	0.55	0.08	9.27	93.35
PK314	**47547-6**	bld	36.07	1.41	14.63	bld	5.97	bld	0.06	26.25	0.06	n.a.	3.35	0.00	6.95	94.75
PK314	**47547-7**	bld	40.14	1.34	11.90	bld	4.09	bld	0.06	26.21	0.10	n.a.	1.58	0.07	8.85	94.34
PK314	**47547-7**	bld	41.08	1.37	12.21	bld	4.39	bld	0.05	27.13	0.09	n.a.	1.36	0.06	8.91	96.65
PK314	**47547-7**	bld	40.35	3.48	11.65	bld	4.90	bld	0.07	24.64	0.04	n.a.	1.49	0.15	9.85	96.62
PK314	**47547-7**	bld	41.69	2.23	9.50	0.06	5.41	bld	0.04	26.13	0.10	n.a.	0.64	0.07	7.78	93.65
PK314	**47547-7**	bld	39.77	1.66	13.32	0.06	3.65	bld	0.06	25.46	0.07	n.a.	1.73	0.05	9.78	95.61
PK314	**47547-8**	bld	40.91	0.89	9.76	0.04	8.97	0.06	0.18	30.90	0.21	0.01	1.81	0.11	4.10	97.94
PK314	**47547-9**	bld	38.56	2.14	11.13	0.03	6.04	0.10	0.04	27.22	0.16	0.01	1.50	0.07	7.22	94.21
PK314	**47547-10**	bld	40.41	0.79	11.53	bld	5.92	0.11	0.11	30.22	0.13	0.06	1.23	0.11	6.94	97.55
PK314	**47547-11**	bld	39.83	2.03	9.17	0.13	9.34	0.08	0.14	26.46	0.16	0.04	1.75	0.09	5.85	95.05

Table 7 – Phlogopite macrocryst major and minor elements (wt%)

Body	Sample	Nb_2O_5	SiO_2	TiO_2	ZnO	Al_2O_3	Cr_2O_3	FeO_T	NiO	MnO	MgO	CaO	BaO	Na_2O	K_2O	Total
PK150	**39249b**	bld	38.29	3.60	bld	13.70	0.13	7.47	0.05	0.05	20.89	0.05	0.13	0.57	9.60	94.53
PK150	**39249b**	bld	38.49	3.64	bld	13.62	0.14	7.49	0.05	0.05	20.82	bld	0.23	0.51	9.57	94.61
PK150	**39249b**	bld	38.95	3.46	0.03	13.37	0.11	7.65	0.05	0.03	20.98	bld	0.17	0.55	9.64	94.99
PK150	**39249b**	bld	38.44	3.70	bld	13.76	0.16	7.32	0.05	0.06	20.76	bld	0.11	0.55	9.63	94.54
PK150	**39249b**	bld	39.07	3.69	bld	14.09	0.14	7.26	0.06	0.04	21.21	bld	0.29	0.56	9.50	95.91
PK150	**39249b**	bld	38.23	3.65	bld	13.98	0.16	7.41	0.05	0.04	21.34	bld	0.18	0.26	9.84	95.14
PK150	**39249b**	bld	38.88	5.15	bld	14.21	1.22	5.89	0.10	0.04	19.90	bld	bld	0.55	9.64	95.58
PK150	**39249b**	bld	39.03	5.18	bld	14.28	1.40	5.88	0.07	0.03	19.82	bld	bld	0.51	9.72	95.92
PK150	**39249b**	bld	38.72	5.25	bld	14.22	1.52	5.98	0.09	0.00	19.73	bld	bld	0.55	9.74	95.80
PK150	**39249b**	bld	38.41	5.32	bld	14.55	1.39	5.81	0.11	0.02	19.72	bld	bld	0.55	9.52	95.40
PK150	**39249b**	bld	39.17	5.27	bld	14.56	1.44	5.83	0.08	0.03	20.08	bld	bld	0.56	9.66	96.68
PK150	**39249b**	bld	38.94	4.77	bld	13.25	1.36	6.12	0.12	0.03	21.10	0.02	bld	0.44	8.91	95.06
PK150	**47517a**	bld	41.19	1.57	0.03	10.45	bld	7.69	bld	0.08	21.33	bld	bld	0.36	10.47	93.17
PK150	**47517a**	bld	41.66	1.59	bld	10.68	bld	7.84	bld	0.10	21.23	bld	bld	0.38	10.36	93.84
PK150	**47517a**	bld	41.64	1.07	0.03	10.64	bld	7.56	bld	0.08	22.40	bld	bld	0.26	10.34	94.02
PK150	**47517a**	bld	40.93	0.96	0.04	10.97	bld	9.99	bld	0.07	20.68	bld	bld	0.19	10.41	94.24
PK150	**47517b**	bld	39.08	4.60	bld	12.65	0.19	6.97	0.08	0.05	20.86	bld	bld	0.28	9.51	94.27
PK150	**47517b**	bld	39.29	4.72	bld	13.03	0.24	6.91	0.08	0.02	20.33	bld	bld	0.54	9.33	94.49
PK150	**47517b**	bld	38.72	4.98	bld	13.49	0.25	6.89	0.08	0.03	19.57	bld	bld	0.54	9.74	94.29
PK150	**47517b**	bld	38.64	4.97	bld	13.50	0.23	6.82	0.09	0.04	19.57	bld	bld	0.53	9.76	94.15
PK150	**47517b**	bld	38.46	5.53	bld	13.44	0.34	6.89	0.09	0.03	19.53	bld	bld	0.32	10.09	94.72
PK151	**47514**	bld	38.51	5.26	0.03	13.45	1.48	5.99	0.08	0.04	19.64	bld	bld	0.53	9.61	94.62
PK151	**47514**	bld	38.48	5.22	bld	13.96	1.54	5.89	0.11	0.03	19.50	bld	bld	0.57	9.80	95.10
PK151	**47514**	bld	38.31	5.23	0.03	14.09	1.50	6.00	0.10	0.04	19.55	bld	bld	0.55	9.74	95.14
PK151	**47514**	bld	38.30	5.10	bld	14.11	1.60	5.88	0.11	0.03	19.49	bld	bld	0.58	9.65	94.85
PK151	**47514**	bld	36.64	4.91	bld	14.08	1.49	7.07	0.12	0.04	19.67	0.02	bld	0.46	8.84	93.34
PK312	**47553b**	n.a.	39.33	4.83	n.a.	14.22	0.58	6.28	0.10	bld	21.40	0.01	bld	0.52	9.44	96.71
PK312	**47553b**	n.a.	39.23	4.83	n.a.	13.92	0.54	6.25	0.08	0.03	21.36	bld	bld	0.47	9.34	96.05
PK312	**47553b**	n.a.	39.02	5.26	n.a.	13.56	0.57	6.20	0.06	0.03	20.98	0.02	bld	0.52	9.49	95.71

Table 8 – Spinel group major and minor elements (wt%); g.m. = groundmass, ilm rim = within ilmenite rim; xeno = xenocrystic magnetite, alt = alteration, ol = olivine

Intrusion	PK150	PK150	PK150	PK150	PK150	PK150	PK150	PK150	PK150
Sample	39249b-1	39249b-2	44803-1	44803-2	44803-3	44813a-1	44813a-2	44813a-3	44813a-4
	g.m.	g.m.	g.m.	g.m.	g.m.	g.m.	g.m.	g.m.	g.m.
Major element analysis (wt%)									
Nb_2O_5	bld	bld	n.a.	n.a.	n.a.	n.a.	n.a.	n.a.	n.a.
SiO_2	bld	bld	0.07	0.07	0.04	0.46	0.16	0.42	0.29
TiO_2	9.90	6.05	12.09	5.92	9.16	13.57	5.69	1.79	0.81
ZnO	0.04	0.05	0.02	0.05	0.01	0.06	n.a.	n.a.	n.a.
Al_2O_3	7.75	8.43	7.98	14.78	9.05	7.81	17.46	0.37	0.14
Cr_2O_3	27.80	43.25	15.57	30.70	27.01	12.91	31.90	0.38	0.35
FeO	24.66	21.35	24.35	20.04	22.52	22.03	19.67	26.59	23.74
Fe_2O_3	16.23	7.78	24.53	13.05	16.96	26.37	10.96	65.61	68.97
NiO	0.16	0.23	0.07	0.11	0.13	0.22	n.a.	n.a.	n.a.
MnO	0.41	0.21	0.77	0.51	0.46	0.72	0.28	1.19	1.01
MgO	10.00	10.61	11.57	11.64	11.21	13.80	12.77	3.55	4.79
CaO	0.46	0.02	0.02	0.08	0.19	1.06	0.17	0.05	0.11
BaO	n.a.	n.a.	n.a.	0.01	n.a.	n.a.	bld	bld	bld
Na_2O	bld	bld	0.02	0.00	0.01	bld	bld	bld	bld
K_2O	0.01	bld	0.02	0.04	0.01	n.a.	bld	bld	bld
V_2O_3	n.a.	n.a.	0.15	0.25	0.22	n.a.	n.a.	n.a.	n.a.
Total	97.42	97.98	97.23	97.28	96.96	99.01	99.06	99.94	100.21
Number of cations (apfu) on the basis of 3 oxygen atoms and 2 cations									
Nb	-	-	-	-	-	-	-	-	-
Si	-	-	0.002	0.002	0.001	0.015	0.005	0.016	0.011
Ti	0.256	0.154	0.310	0.147	0.234	0.337	0.136	0.050	0.023
Zn	0.001	0.001	0.000	0.001	0.000	0.001	-	-	-
Al	0.314	0.336	0.321	0.573	0.363	0.304	0.654	0.016	0.006
Cr	0.755	1.157	0.420	0.799	0.726	0.337	0.802	0.011	0.010
Fe^{2+}	0.709	0.604	0.695	0.552	0.640	0.608	0.523	0.829	0.734
Fe^{3+}	0.420	0.198	0.630	0.323	0.434	0.655	0.262	1.841	1.917
Ni	0.004	0.006	0.002	0.003	0.004	0.006	-	-	-
Mn	0.012	0.006	0.022	0.014	0.013	0.020	0.008	0.038	0.032
Mg	0.512	0.535	0.588	0.571	0.568	0.679	0.605	0.197	0.264
Ca	0.017	0.001	0.001	0.003	0.007	0.037	0.006	0.002	0.004
Ba	-	-	-	0.000	-	-	-	-	-
Na	-	-	0.000	0.000	0.000	-	-	-	-
K	0.000	-	0.000	0.000	0.000	-	-	-	-
V	-	-	0.004	0.007	0.006	-	-	-	-
sum	3.000	3.000	2.997	2.996	2.997	3.000	3.000	3.000	3.000

Table 8 continued

Intrusion	PK150	PK150	PK150	PK150	PK150	PK150	PK150	PK150	PK150
Sample	44813a-5	44813a-6	44813b-1	44813c-1	44813c-2	44813c-2	44813d-1	47513-1	47513-2
	xeno	xeno	incl-ilm	g.m.	core	rim	xeno	g.m.	g.m.
Major element analysis (wt%)									
Nb_2O_5	n.a.	n.a.	n.a.	n.a.	n.a.	n.a.	n.a.	n.a.	n.a.
SiO_2	0.09	0.12	0.13	0.20	0.07	0.12	bld	0.01	0.21
TiO_2	1.41	1.13	18.27	8.63	1.48	10.62	0.86	17.93	12.62
ZnO	0.02	0.02	n.a.	n.a.	n.a.	n.a.	n.a.	0.01	0.01
Al_2O_3	0.06	0.10	6.68	11.28	0.46	8.15	bld	2.15	3.75
Cr_2O_3	bld	0.02	9.03	29.46	55.07	22.79	0.54	0.94	1.45
FeO	28.93	27.47	29.35	18.72	24.00	23.92	30.36	24.31	18.34
Fe_2O_3	67.67	68.21	21.43	16.32	8.47	19.90	66.21	38.03	47.84
NiO	0.03	0.02	0.15	0.18	0.05	0.12	n.a.	0.11	0.12
MnO	0.29	0.32	0.57	0.5	0.42	0.69	0.19	1.11	0.63
MgO	2.19	2.94	12.18	14.47	4.74	11.27	0.58	14.25	15.88
CaO	0.05	0.02	0.01	0.02	0.06	0.03	bld	0.15	0.40
BaO	n.a.	n.a.	bld	bld	bld	bld	bld	0.04	n.a.
Na_2O	bld	bld	bld	bld	bld	bld	bld	0.04	0.03
K_2O	n.a.	n.a.	bld	bld	bld	bld	bld	n.a.	0.01
V_2O_3	n.a.	n.a.	n.a.	n.a.	n.a.	n.a.	n.a.	0.11	0.07
Total	100.75	100.35	97.81	99.78	94.82	97.61	98.74	99.21	101.36
Number of cations (apfu) on the basis of 3 oxygen atoms and 2 cations									
Nb	-	-	-	-	-	-	-	-	-
Si	0.003	0.004	0.004	0.006	0.003	0.004	-	0.000	0.007
Ti	0.040	0.032	0.467	0.209	0.042	0.272	0.025	0.458	0.311
Zn	0.001	0.000	-	-	-	-	-	0.000	0.000
Al	0.003	0.004	0.267	0.427	0.021	0.327	-	0.086	0.145
Cr	-	0.000	0.242	0.748	1.648	0.613	0.017	0.025	0.038
Fe^{2+}	0.908	0.861	0.834	0.503	0.760	0.680	0.985	0.690	0.503
Fe^{3+}	1.911	1.923	0.548	0.395	0.241	0.509	1.933	0.971	1.180
Ni	0.001	0.001	0.004	0.005	0.002	0.003	-	0.003	0.003
Mn	0.009	0.010	0.016	0.014	0.013	0.020	0.006	0.032	0.017
Mg	0.123	0.164	0.617	0.693	0.268	0.571	0.034	0.721	0.776
Ca	0.002	0.001	0.000	0.001	0.002	0.001	-	0.005	0.014
Ba	-	-	-	-	-	-	-	0.001	-
Na	-	-	-	-	-	-	-	0.001	0.000
K	-	-	-	-	-	-	-	-	0.000
V	-	-	-	-	-	-	-	0.003	0.002
sum	3.000	3.000	3.000	3.000	3.000	3.000	3.000	2.997	2.998

Table 8 continued

Intrusion	PK150 47513-3	PK150 47513-4	PK150 47513-5	PK150 47513-6	PK150 47513-7	PK150 47513-8	PK150 47517a-1	PK150 47517a-2	PK150 47517a-3
Sample	g.m.	g.m.	g.m.	g.m.	g.m.	xeno	g.m.	g.m.	alt-ol
Major element analysis (wt%)									
Nb_2O_5	n.a.	n.a.	n.a.	n.a.	n.a.	n.a.	bld	bld	bld
SiO_2	0.04	0.05	0.05	0.28	0.29	0.04	0.42	0.11	0.87
TiO_2	16.48	15.33	16.26	15.20	14.53	5.44	15.24	16.85	16.62
ZnO	n.a.	0.03	n.a.	n.a.	n.a.	n.a.	0.05	0.04	0.06
Al_2O_3	2.34	3.91	2.79	4.94	3.48	0.08	5.77	3.85	4.64
Cr_2O_3	1.05	0.46	1.09	0.62	0.64	0.03	0.55	1.07	2.71
FeO	19.61	21.60	20.06	19.19	18.90	28.10	27.14	30.20	27.94
Fe_2O_3	41.21	41.32	41.11	41.06	44.43	59.32	35.75	34.83	32.02
NiO	0.15	0.10	0.15	0.15	0.15	0.02	0.11	0.09	0.12
MnO	0.86	1.03	0.95	0.86	0.84	0.57	0.93	0.9	0.93
MgO	16.49	14.73	16.07	16.71	16.39	4.51	11.16	10.1	11.88
CaO	0.23	0.11	0.30	0.12	0.28	0.04	0.14	0.12	0.36
BaO	n.a.	n.a.	n.a.	n.a.	n.a.	0.04	bld	bld	bld
Na_2O	0.03	0.02	0.03	0.03	0.03	0.02	bld	bld	0.03
K_2O	0.01	n.a.	0.00	0.00	n.a.	n.a.	0.14	0.02	0.02
V_2O_3	0.13	0.09	0.11	0.09	0.11	0.09	n.a.	n.a.	n.a.
Total	98.62	98.79	98.98	99.26	100.07	98.29	97.40	98.18	98.20
Number of cations (apfu) on the basis of 3 oxygen atoms and 2 cations									
Nb	-	-	-	-	-	-	-	-	-
Si	0.001	0.002	0.002	0.009	0.009	0.002	0.015	0.004	0.030
Ti	0.416	0.389	0.410	0.377	0.361	0.154	0.397	0.444	0.428
Zn	-	0.001	-	-	-	-	0.001	0.001	0.002
Al	0.092	0.156	0.110	0.192	0.136	0.003	0.236	0.159	0.187
Cr	0.028	0.012	0.029	0.016	0.017	0.001	0.015	0.030	0.073
Fe^{2+}	0.551	0.609	0.562	0.529	0.522	0.884	0.786	0.884	0.801
Fe^{3+}	1.042	1.049	1.036	1.018	1.105	1.679	0.932	0.917	0.826
Ni	0.004	0.003	0.004	0.004	0.004	0.001	0.003	0.003	0.003
Mn	0.025	0.030	0.027	0.024	0.024	0.018	0.027	0.027	0.027
Mg	0.826	0.741	0.803	0.821	0.807	0.253	0.576	0.527	0.607
Ca	0.008	0.004	0.011	0.004	0.010	0.001	0.005	0.005	0.013
Ba	-	-	-	-	-	0.001	-	-	-
Na	0.000	0.000	0.001	0.000	0.000	0.000	-	-	0.000
K	0.000	-	0.000	0.000	-	-	0.002	0.000	0.000
V	0.003	0.003	0.003	0.002	0.003	0.003	-	-	-
sum	2.997	2.998	2.997	2.998	2.998	3.000	2.995	2.999	2.998

Table 8 continued

Intrusion	PK150	PK150	PK150	PK150	PK150	PK150	PK150	PK150	PK150
Sample	47517a-4	47517b-1	47517b-2	47517b-3	47517b-4	47517b-5	47517b-6	47517b-7	47517b-8
	xeno	g.m.	g.m.	g.m.	g.m.	g.m.	g.m.	g.m.	g.m.
Major element analysis (wt%)									
Nb_2O_5	bld	bld	bld	bld	bld	bld	bld	bld	bld
SiO_2	0.09	bld	0.04	0.15	0.42	0.06	bld	0.06	0.06
TiO_2	2.78	14.42	14.55	17.81	16.13	10.60	8.86	18.40	17.16
ZnO	0.02	0.05	0.07	0.05	0.06	0.09	0.07	0.04	0.05
Al_2O_3	0.07	5.64	6.16	4.50	5.05	6.50	7.63	4.30	4.23
Cr_2O_3	bld	8.46	8.89	0.58	0.89	16.32	29.32	2.74	0.59
FeO	30.49	25.42	22.94	26.94	29.68	17.00	24.22	28.46	30.12
Fe_2O_3	64.66	30.43	30.62	34.35	35.14	29.93	17.13	31.46	34.53
NiO	n.a.	0.11	0.11	0.14	0.09	0.10	0.17	0.10	0.08
MnO	0.27	0.92	0.95	0.95	0.90	0.83	0.59	1.06	1.05
MgO	2.00	11.70	13.49	12.89	10.43	14.88	9.93	12.27	10.18
CaO	bld	0.14	0.34	0.07	0.32	0.25	0.08	0.09	0.16
BaO	bld	bld	bld	bld	bld	bld	bld	bld	bld
Na_2O	bld	bld	bld	bld	bld	bld	bld	bld	bld
K_2O	bld	0.02	0.01	0.04	0.02	0.03	0.01	0.02	0.04
V_2O_3	n.a.	n.a.	n.a.	n.a.	n.a.	n.a.	n.a.	n.a.	n.a.
Total	100.37	97.31	98.18	98.47	99.13	96.59	98.01	99.00	98.25
Number of cations (apfu) on the basis of 3 oxygen atoms and 2 cations									
Nb	-	-	-	-	-	-	-	-	-
Si	0.003	-	0.001	0.005	0.014	0.002	-	0.002	0.002
Ti	0.079	0.375	0.369	0.457	0.417	0.270	0.228	0.472	0.450
Zn	0.000	0.001	0.002	0.001	0.002	0.002	0.002	0.001	0.001
Al	0.003	0.230	0.245	0.181	0.205	0.259	0.308	0.173	0.174
Cr	-	0.231	0.237	0.016	0.024	0.437	0.794	0.074	0.016
Fe^{2+}	0.961	0.734	0.647	0.768	0.853	0.481	0.694	0.811	0.879
Fe^{3+}	1.833	0.791	0.777	0.881	0.909	0.762	0.442	0.807	0.907
Ni	-	0.003	0.003	0.004	0.002	0.003	0.005	0.003	0.002
Mn	0.008	0.027	0.027	0.027	0.026	0.024	0.017	0.031	0.031
Mg	0.112	0.602	0.678	0.655	0.534	0.750	0.507	0.623	0.529
Ca	-	0.005	0.012	0.003	0.012	0.009	0.003	0.003	0.006
Ba	-	-	-	-	-	-	-	-	-
Na	-	-	-	-	-	-	-	-	-
K	-	0.000	0.000	0.000	0.000	0.000	0.000	0.000	0.000
V	-	-	-	-	-	-	-	-	-
sum	3.000	2.999	3.000	2.999	2.999	2.999	3.000	2.999	2.999

Table 8 continued

Intrusion	PK150 47517b-9	PK150 47513-9	PK150 47513-10	PK150 47517a-5	PK150 47517a-6	PK150 47517a-7	PK150 47517a-8	PK150 47517a-9	PK150 47517b-10
Sample	g.m.	ilm rim	ilm rim	ilm rim	ilm rim	ilm rim	ilm rim	ilm rim	ilm rim
Major element analysis (wt%)									
Nb_2O_5	bld	n.a.	n.a.	bld	bld	bld	bld	bld	bld
SiO_2	0.09	n.a.	n.a.	0.62	0.44	0.08	0.89	0.16	0.07
TiO_2	13.79	23.39	20.74	18.81	18.81	18.36	18.07	19.49	19.26
ZnO	n.a.	n.a.	n.a.	0.05	0.07	0.05	0.06	0.04	0.06
Al_2O_3	5.40	2.66	3.45	4.31	3.96	3.75	3.18	3.09	3.70
Cr_2O_3	0.21	3.25	4.25	2.69	3.56	2.26	2.20	3.19	2.96
FeO	29.78	23.90	21.62	28.88	29.73	29.59	31.25	32.14	31.41
Fe_2O_3	41.23	26.87	30.49	29.85	28.84	33.02	30.76	29.60	29.77
NiO	0.05	0.14	0.13	0.12	0.13	0.15	0.08	0.10	0.12
MnO	0.87	1.00	0.96	0.88	0.82	0.94	1.10	0.91	0.89
MgO	9.14	18.10	18.26	10.97	10.91	11.52	10.69	10.61	10.82
CaO	0.37	0.02	0.03	2.76	1.51	0.16	0.10	bld	0.14
BaO	bld	n.a.	0.02	bld	bld	bld	bld	bld	bld
Na_2O	bld	0.05	0.04	bld	0.03	0.05	bld	0.06	0.04
K_2O	bld	0.01	0.00	0.01	0.01	0.01	0.02	bld	0.01
V_2O_3	n.a.	0.16	0.14701	n.a.	n.a.	n.a.	n.a.	n.a.	n.a.
Total	100.93	99.54	100.14	99.95	98.77	99.94	98.40	99.38	99.25
Number of cations (apfu) on the basis of 3 oxygen atoms and 2 cations									
Nb	-	-	-	-	-	-	-	-	-
Si	0.003	-	-	0.021	0.015	0.003	0.031	0.006	0.002
Ti	0.355	0.575	0.506	0.478	0.486	0.470	0.472	0.506	0.499
Zn	-	-	-	0.001	0.002	0.001	0.002	0.001	0.002
Al	0.218	0.102	0.132	0.172	0.160	0.150	0.130	0.126	0.150
Cr	0.006	0.084	0.109	0.072	0.096	0.061	0.060	0.087	0.081
Fe^{2+}	0.852	0.654	0.587	0.816	0.853	0.843	0.908	0.927	0.904
Fe^{3+}	1.061	0.661	0.744	0.759	0.745	0.846	0.804	0.768	0.771
Ni	0.001	0.004	0.003	0.003	0.004	0.004	0.002	0.003	0.003
Mn	0.025	0.028	0.026	0.025	0.024	0.027	0.032	0.027	0.026
Mg	0.466	0.882	0.883	0.553	0.558	0.585	0.554	0.546	0.555
Ca	0.014	0.001	0.001	0.100	0.055	0.006	0.004	-	0.005
Ba	-	-	0.000	-	-	-	-	-	-
Na	-	0.001	0.001	-	0.000	0.001	-	0.001	0.001
K	-	0.000	0.000	0.000	0.000	0.000	0.000	-	0.000
V	-	0.004	0.004	-	-	-	-	-	-
sum	3.000	2.996	2.997	3.000	2.998	2.997	2.999	2.997	2.998

Table 8 continued

Intrusion	PK150	PK150	PK150	PK150	PK150	PK346	PK346	PK346	PK346
Sample	47517b-11	47517b-12	47517b-13	47517b-14	47517b-15	44864-1	44864-2	44864-3	44864-4
	ilm rim	ilm rim	ilm rim	ilm rim	ilm rim	g.m.	g.m.	g.m.	g.m.
Major element analysis (wt%)									
Nb_2O_5	bld	bld	bld	bld	bld	bld	bld	bld	bld
SiO_2	0.05	bld	0.56	0.23	0.02	0.06	0.07	0.09	0.07
TiO_2	18.98	18.87	19.94	18.55	19.91	18.16	17.85	10.24	9.85
ZnO	0.07	0.07	0.08	0.05	0.05	n.a.	n.a.	n.a.	n.a.
Al_2O_3	3.78	4.30	4.12	3.60	4.24	3.27	3.65	3.32	2.89
Cr_2O_3	3.38	3.76	2.84	2.13	2.98	4.21	3.68	1.00	0.52
FeO	29.65	29.13	30.71	29.06	32.23	27.95	28.49	26.98	27.99
Fe_2O_3	30.64	30.01	27.80	32.35	28.29	33.42	33.61	49.72	51.02
NiO	0.14	0.10	0.11	0.13	0.14	0.09	0.12	n.a.	0.07
MnO	1.02	1.00	0.98	1.05	0.79	0.89	0.93	0.90	0.89
MgO	11.85	12.08	12.19	11.86	10.97	12.96	12.40	8.82	7.82
CaO	0.24	0.09	0.05	0.25	0.06	0.08	0.05	0.16	0.15
BaO	bld	bld	bld	bld	bld	bld	bld	bld	bld
Na_2O	bld	0.04	0.05	0.04	0.03	bld	bld	bld	bld
K_2O	bld	0.02	bld	0.01	bld	bld	0.01	bld	0.01
V_2O_3	n.a.	n.a.	n.a.	n.a.	n.a.	n.a.	n.a.	n.a.	n.a.
Total	99.80	99.48	99.43	99.31	99.66	101.07	100.83	101.23	101.26
Number of cations (apfu) on the basis of 3 oxygen atoms and 2 cations									
Nb	-	-	-	-	-	-	-	-	-
Si	0.002	-	0.019	0.008	0.001	0.002	0.002	0.003	0.002
Ti	0.485	0.482	0.508	0.477	0.511	0.457	0.451	0.267	0.259
Zn	0.002	0.002	0.002	0.001	0.001	-	-	-	-
Al	0.151	0.172	0.164	0.145	0.170	0.129	0.145	0.136	0.119
Cr	0.091	0.101	0.076	0.058	0.080	0.111	0.098	0.027	0.014
Fe^{2+}	0.843	0.827	0.870	0.830	0.920	0.782	0.801	0.782	0.819
Fe^{3+}	0.784	0.767	0.709	0.832	0.727	0.842	0.850	1.297	1.344
Ni	0.004	0.003	0.003	0.004	0.004	0.002	0.003	0.000	0.002
Mn	0.029	0.029	0.028	0.030	0.023	0.025	0.026	0.026	0.026
Mg	0.600	0.611	0.616	0.604	0.559	0.646	0.621	0.456	0.408
Ca	0.009	0.003	0.002	0.009	0.002	0.003	0.002	0.006	0.006
Ba	-	-	-	-	-	-	-	-	-
Na	-	0.001	0.001	0.001	0.000	-	-	-	-
K	-	0.000	-	0.000	-	-	0.000	-	0.000
V	-	-	-	-	-	-	-	-	-
sum	3.000	2.997	2.998	2.998	2.999	3.000	3.000	3.000	3.000

Table 8 continued

Intrusion	PK346	PK346	PK346	PK346	PK346	PK346	PK346	PK346	PK346
Sample	44864-5	44864-6	44864-7	44864-8	44864-9	44864-10	44864-11	44864-12	44860-1
	g.m.	g.m.	g.m.	g.m.	g.m.	g.m.	g.m.	g.m.	g.m.
Major element analysis (wt%)									
Nb_2O_5	bld	bld	n.a.	n.a.	n.a.	n.a.	n.a.	n.a.	n.a.
SiO_2	0.05	0.05	0.04	0.05	0.03	0.03	0.05	0.02	n.a.
TiO_2	16.22	14.97	15.89	15.86	15.35	16.78	3.42	13.58	17.25
ZnO	n.a.	n.a.	0.01	0.01	0.01	0.02	n.a.	0.01	0.03
Al_2O_3	3.46	3.41	3.53	3.21	3.32	3.21	0.38	4.06	2.97
Cr_2O_3	2.87	3.18	1.94	1.40	3.24	2.41	0.15	0.47	3.79
FeO	28.52	28.74	27.29	28.34	27.48	26.44	18.60	25.49	23.93
Fe_2O_3	37.67	39.11	37.36	38.11	36.50	35.76	65.09	42.31	35.72
NiO	0.10	0.06	0.04	0.02	0.03	0.04	0.12	0.05	0.06
MnO	0.91	0.97	1.00	1.12	0.91	0.85	1.11	0.75	0.95
MgO	11.27	10.49	11.34	10.46	10.79	12.40	8.79	10.91	13.86
CaO	0.04	0.03	0.05	0.03	0.02	0.02	0.03	0.14	0.06
BaO	bld	bld	n.a.	0.02	0.03	n.a.	0.02	n.a.	n.a.
Na_2O	0.05	bld	0.04	0.08	0.05	0.04	0.03	0.11	0.22
K_2O	0.02	0.01	0.02	0.02	0.00	0.01	0.05	0.02	n.a.
V_2O_3	n.a.	n.a.	0.07	0.09	0.06	0.05	0.06	0.05	0.06
Total	101.18	101.02	98.62	98.81	97.83	98.06	97.91	97.98	98.91
Number of cations (apfu) on the basis of 3 oxygen atoms and 2 cations									
Nb	-	-	-	-	-	-	-	-	-
Si	0.002	0.002	0.002	0.002	0.001	0.001	0.002	0.001	-
Ti	0.413	0.385	0.414	0.415	0.405	0.436	0.094	0.357	0.440
Zn	-	-	0.000	0.000	0.000	0.000	-	0.000	0.001
Al	0.138	0.137	0.144	0.132	0.137	0.131	0.017	0.167	0.119
Cr	0.077	0.086	0.053	0.039	0.090	0.066	0.004	0.013	0.102
Fe^{2+}	0.807	0.821	0.790	0.825	0.806	0.764	0.568	0.744	0.679
Fe^{3+}	0.960	1.005	0.973	0.999	0.963	0.930	1.790	1.111	0.911
Ni	0.003	0.002	0.001	0.000	0.001	0.001	0.004	0.001	0.002
Mn	0.026	0.028	0.029	0.033	0.027	0.025	0.034	0.022	0.027
Mg	0.569	0.534	0.585	0.543	0.564	0.639	0.479	0.568	0.700
Ca	0.001	0.001	0.002	0.001	0.001	0.001	0.001	0.005	0.002
Ba	-	-	-	0.000	0.000	-	0.000	-	-
Na	0.001	-	0.001	0.001	0.001	0.001	0.001	0.002	0.004
K	0.000	0.000	0.000	0.000	0.000	0.000	0.001	0.000	-
V	-	-	0.002	0.002	0.002	0.002	0.002	0.001	0.002
sum	2.997	3.000	2.996	2.994	2.997	2.997	2.996	2.993	2.989

Table 8 continued

Intrusion	PK346 44860-	PK346 44860-	PK346 44860-	PK346 44860-	PK346 44860-	PK346 44860-	PK346 44860-	PK346 44860-	PK346 44860-
Sample	2	3	4	5	6	7	8	9	10
	g.m.	g.m.	g.m.	g.m.	g.m.	g.m.	g.m.	g.m.	g.m.
Major element analysis (wt%)									
Nb_2O_5	n.a.	n.a.	n.a.	n.a.	n.a.	n.a.	n.a.	n.a.	n.a.
SiO_2	0.01	n.a.	0.02	0.01	n.a.	0.01	n.a.	n.a.	0.02
TiO_2	12.51	11.27	10.07	13.67	11.00	11.75	16.10	12.36	13.74
ZnO	n.a.	n.a.	0.02	0.02	0.02	0.03	n.a.	0.02	0.02
Al_2O_3	2.03	2.17	1.52	2.39	1.68	1.97	3.55	2.30	2.42
Cr_2O_3	1.28	0.33	1.13	1.32	1.58	0.46	0.87	0.73	1.65
FeO	22.24	19.99	19.47	22.21	21.91	20.93	24.70	21.80	21.12
Fe_2O_3	47.35	50.66	52.30	45.26	50.27	50.06	39.62	48.42	44.53
NiO	0.08	0.08	0.10	0.06	0.07	0.09	0.06	0.08	0.08
MnO	0.77	0.84	0.77	0.85	0.77	0.84	0.90	0.80	0.86
MgO	12.23	12.99	12.59	12.96	11.71	12.72	12.79	12.64	13.52
CaO	0.06	0.05	0.05	0.07	0.07	0.05	0.06	0.04	0.21
BaO	n.a.	0.05	n.a.	n.a.	n.a.	n.a.	n.a.	0.02	n.a.
Na_2O	0.16	0.10	0.08	0.17	0.11	0.12	0.20	0.13	0.12
K_2O	0.00	0.01	n.a.	n.a.	0.01	n.a.	n.a.	n.a.	0.03
V_2O_3	0.03	0.04	0.05	0.06	0.05	0.05	0.05	0.06	0.07
Total	98.76	98.58	98.16	99.05	99.25	99.09	98.90	99.39	98.41
Number of cations (apfu) on the basis of 3 oxygen atoms and 2 cations									
Nb	-	-	-	-	-	-	-	-	-
Si	0.000	-	0.001	0.000	-	0.000	-	-	0.001
Ti	0.327	0.294	0.265	0.353	0.288	0.305	0.414	0.320	0.355
Zn	-	-	0.000	0.000	0.000	0.001	-	0.000	0.001
Al	0.083	0.089	0.063	0.097	0.069	0.080	0.143	0.093	0.098
Cr	0.035	0.009	0.031	0.036	0.043	0.013	0.023	0.020	0.045
Fe^{2+}	0.646	0.579	0.570	0.638	0.638	0.605	0.706	0.627	0.607
Fe^{3+}	1.237	1.321	1.378	1.170	1.317	1.302	1.018	1.253	1.152
Ni	0.002	0.002	0.003	0.002	0.002	0.002	0.002	0.002	0.002
Mn	0.023	0.025	0.023	0.025	0.023	0.025	0.026	0.023	0.025
Mg	0.633	0.671	0.657	0.663	0.608	0.655	0.651	0.648	0.693
Ca	0.002	0.002	0.002	0.003	0.003	0.002	0.002	0.001	0.008
Ba	-	0.001	-	-	-	-	-	0.000	-
Na	0.003	0.002	0.001	0.003	0.002	0.002	0.003	0.002	0.002
K	0.000	0.000	-	-	0.000	-	-	-	0.000
V	0.001	0.001	0.001	0.002	0.001	0.001	0.001	0.002	0.002
sum	2.992	2.994	2.995	2.991	2.994	2.993	2.989	2.993	2.992

Table 8 continued

Intrusion	PK346 44860-	PK346 44860-	PK346 44860-	PK346 44860-	PK346 44860-	PK346 44860-	PK346 44860-	PK346 44848a-	PK346 44848a-
Sample	11	12	13	14	15	16	17	1	2
	g.m.	g.m.	g.m.	g.m.	g.m.	g.m.	g.m.	ilm rim	ilm rim
Major element analysis (wt%)									
Nb_2O_5	n.a.	n.a.	n.a.	n.a.	n.a.	n.a.	n.a.	n.a.	n.a.
SiO_2	n.a.	0.01	0.01	n.a.	n.a.	0.04	0.04	0.06	0.08
TiO_2	10.93	13.80	17.19	12.71	14.98	13.44	11.73	17.41	18.84
ZnO	0.02	0.02	0.04	n.a.	0.03	0.02	0.03	0.05	0.08
Al_2O_3	3.05	2.11	2.73	1.98	3.12	2.36	2.33	3.45	3.48
Cr_2O_3	0.35	1.39	2.66	1.38	4.48	2.31	1.31	4.74	2.67
FeO	18.99	22.03	23.48	18.69	22.10	21.63	18.12	29.22	28.42
Fe_2O_3	50.55	44.93	37.48	48.55	38.90	44.62	49.00	32.44	32.84
NiO	0.08	0.07	0.05	0.07	0.06	0.06	0.08	0.06	0.07
MnO	0.81	0.89	0.93	0.81	0.93	0.88	0.89	0.76	0.92
MgO	13.50	12.97	14.21	14.94	13.93	13.30	14.39	11.42	12.67
CaO	0.29	0.10	0.03	0.09	0.05	0.17	0.09	0.04	0.08
BaO	0.02	0.02	n.a.	n.a.	0.01	n.a.	0.04	n.a.	n.a.
Na_2O	0.06	0.16	0.20	0.08	0.13	0.10	0.08	0.04	0.07
K_2O	0.01	0.01	0.00	n.a.	0.01	0.00	0.04	n.a.	n.a.
V_2O_3	0.03	0.06	0.08	0.06	0.08	0.07	0.06	n.a.	n.a.
Total	98.67	98.57	99.08	99.37	98.81	99.00	98.23	99.69	100.22
Number of cations (apfu) on the basis of 3 oxygen atoms and 2 cations									
Nb	-	-	-	-	-	-	-	-	-
Si	-	0.000	0.000	-	-	0.001	0.001	0.002	0.003
Ti	0.282	0.358	0.438	0.324	0.383	0.347	0.303	0.448	0.478
Zn	0.000	0.000	0.001	-	0.001	0.000	0.001	0.001	0.002
Al	0.123	0.086	0.109	0.079	0.125	0.095	0.094	0.139	0.138
Cr	0.009	0.038	0.071	0.037	0.120	0.063	0.036	0.128	0.071
Fe^{2+}	0.545	0.636	0.665	0.530	0.628	0.620	0.520	0.836	0.801
Fe^{3+}	1.306	1.168	0.954	1.238	0.995	1.151	1.266	0.835	0.834
Ni	0.002	0.002	0.001	0.002	0.002	0.002	0.002	0.002	0.002
Mn	0.023	0.026	0.027	0.023	0.027	0.025	0.026	0.022	0.026
Mg	0.691	0.668	0.717	0.755	0.706	0.680	0.736	0.582	0.637
Ca	0.011	0.004	0.001	0.003	0.002	0.006	0.003	0.001	0.003
Ba	0.000	0.000	-	-	0.000	-	0.001	-	-
Na	0.001	0.003	0.003	0.001	0.002	0.002	0.001	0.001	0.001
K	0.000	0.000	0.000	-	0.000	0.000	0.000	-	-
V	0.001	0.002	0.002	0.002	0.002	0.002	0.002	-	-
sum	2.996	2.991	2.989	2.995	2.992	2.994	2.994	2.998	2.997

Table 8 continued

Intrusion	PK346	PK346	PK346	PK346	PK346	PK346	PK346	PK346	PK346
Sample	44848b-1	44848b-2	44864-13	44864-14	44864-15	44864-16	44864-17	44860-18	44860-19
	ilm rim	ilm rim	ilm rim	ilm rim	ilm rim	ilm rim	ilm rim	ilm rim	ilm rim
Major element analysis (wt%)									
Nb_2O_5	n.a.	n.a.	n.a.	n.a.	n.a.	n.a.	n.a.	n.a.	n.a.
SiO_2	0.07	0.03	0.01	0.01	0.02	0.00	0.01	0.00	0.01
TiO_2	21.10	18.02	19.67	18.34	16.96	16.16	16.10	16.32	14.83
ZnO	0.06	0.07	0.02	0.02	0.02	0.03	0.02	0.02	0.02
Al_2O_3	3.42	3.70	2.90	3.70	3.58	3.04	2.97	2.71	2.28
Cr_2O_3	3.06	3.80	2.37	4.56	2.68	1.43	2.59	2.62	0.32
FeO	30.62	27.79	28.65	26.45	29.38	28.66	28.26	23.16	24.20
Fe_2O_3	28.40	32.85	30.86	31.49	34.40	37.97	36.55	39.44	43.85
NiO	0.07	0.06	0.05	0.05	0.05	0.05	0.04	0.07	0.08
MnO	0.88	0.87	0.87	0.86	0.87	1.00	0.99	0.94	0.88
MgO	12.61	12.80	12.58	13.64	10.80	10.53	10.77	13.89	12.24
CaO	0.10	0.05	0.02	0.02	0.03	0.05	0.02	0.13	0.16
BaO	n.a.	n.a.	n.a.	n.a.	0.02	n.a.	n.a.	n.a.	n.a.
Na_2O	0.09	bld	0.07	0.04	0.04	0.08	0.04	0.20	0.17
K_2O	n.a.	n.a.	0.01	0.01	n.a.	n.a.	0.00	n.a.	n.a.
V_2O_3	n.a.	n.a.	0.09	0.08	0.09	0.09	0.07	0.07	0.06
Total	100.48	100.04	98.18	99.27	98.94	99.09	98.43	99.59	99.10
Number of cations (apfu) on the basis of 3 oxygen atoms and 2 cations									
Nb	-	-	-	-	-	-	-	-	-
Si	0.002	0.001	0.000	0.000	0.001	0.000	0.000	0.000	0.000
Ti	0.533	0.458	0.510	0.465	0.442	0.422	0.423	0.415	0.385
Zn	0.001	0.002	0.000	0.001	0.001	0.001	0.001	0.001	0.001
Al	0.135	0.147	0.118	0.147	0.146	0.125	0.122	0.108	0.093
Cr	0.081	0.101	0.065	0.122	0.073	0.039	0.071	0.070	0.009
Fe^{2+}	0.860	0.784	0.825	0.746	0.850	0.833	0.825	0.654	0.698
Fe^{3+}	0.718	0.834	0.800	0.800	0.896	0.993	0.960	1.003	1.138
Ni	0.002	0.002	0.002	0.001	0.001	0.001	0.001	0.002	0.002
Mn	0.025	0.025	0.025	0.025	0.025	0.029	0.029	0.027	0.026
Mg	0.632	0.644	0.646	0.686	0.557	0.545	0.560	0.700	0.629
Ca	0.004	0.002	0.001	0.001	0.001	0.002	0.001	0.005	0.006
Ba	-	-	-	-	0.000	-	-	-	-
Na	0.001	-	0.001	0.001	0.001	0.001	0.001	0.003	0.003
K	-	-	0.000	0.000	-	-	0.000	-	-
V	-	-	0.002	0.002	0.002	0.003	0.002	0.002	0.002
sum	2.996	3.000	2.995	2.997	2.997	2.995	2.997	2.989	2.991

Table 8 continued

Intrusion	PK34644860-20	PK15147514-1	PK15147514-2	PK15147514-3	PK15147514-4	PK15147514-5	PK15147514-6	PK15147514-7	PK15147514-8
Sample	ilm rim	g.m.	g.m.	g.m.	g.m.	g.m.	g.m.	g.m.	g.m.
Major element analysis (wt%)									
Nb_2O_5	n.a.	n.a.	n.a.	n.a.	n.a.	bld	bld	bld	bld
SiO_2	0.01	0.40	0.04	0.02	0.50	0.44	0.63	0.37	0.15
TiO_2	16.36	14.05	8.82	10.10	14.85	10.61	19.41	13.06	17.22
ZnO	0.04	0.08	0.07	0.01	0.07	0.06	0.05	0.10	0.08
Al_2O_3	2.21	4.56	6.96	7.31	4.16	5.47	3.40	4.55	3.96
Cr_2O_3	1.50	9.67	25.83	22.26	5.84	0.22	1.11	0.80	1.74
FeO	23.02	31.22	24.14	24.74	36.25	27.50	35.03	33.59	32.43
Fe_2O_3	40.92	26.29	20.53	21.44	27.03	42.60	25.64	36.84	29.88
NiO	0.07	0.05	0.07	0.09	0.07	0.06	0.08	0.07	0.07
MnO	0.91	0.99	0.65	0.55	1.01	0.88	0.92	0.86	1.05
MgO	14.00	6.97	9.53	9.93	4.44	7.17	7.83	5.00	8.08
CaO	0.09	0.75	0.32	0.36	0.23	1.55	0.21	0.77	0.28
BaO	n.a.	n.a.	n.a.	n.a.	n.a.	bld	bld	bld	bld
Na_2O	0.18	0.03	0.01	0.01	0.03	bld	0.08	bld	bld
K_2O	n.a.	n.a.	n.a.	n.a.	n.a.	bld	0.03	0.01	bld
V_2O_3	0.05	0.09	0.18	0.20	0.11	n.a.	n.a.	n.a.	n.a.
Total	99.35	95.15	97.16	97.02	94.61	96.54	94.42	95.99	94.94
Number of cations (apfu) on the basis of 3 oxygen atoms and 2 cations									
Nb	-	-	-	-	-	-	-	-	-
Si	0.000	0.015	0.001	0.001	0.019	0.016	0.023	0.013	0.005
Ti	0.418	0.386	0.230	0.263	0.420	0.288	0.536	0.363	0.473
Zn	0.001	0.002	0.002	0.000	0.002	0.002	0.001	0.003	0.002
Al	0.088	0.196	0.285	0.298	0.184	0.232	0.147	0.198	0.171
Cr	0.040	0.279	0.709	0.610	0.173	0.006	0.032	0.023	0.050
Fe^{2+}	0.653	0.953	0.701	0.716	1.139	0.829	1.076	1.039	0.991
Fe^{3+}	1.045	0.722	0.536	0.559	0.764	1.155	0.709	1.025	0.822
Ni	0.002	0.001	0.002	0.003	0.002	0.002	0.002	0.002	0.002
Mn	0.026	0.031	0.019	0.016	0.032	0.027	0.029	0.027	0.032
Mg	0.708	0.379	0.493	0.513	0.249	0.385	0.429	0.275	0.440
Ca	0.003	0.029	0.012	0.013	0.009	0.060	0.008	0.030	0.011
Ba	-	-	-	-	-	-	-	-	-
Na	0.003	0.000	0.000	0.000	0.001	-	0.001	-	-
K	-	-	-	-	-	-	0.000	0.000	-
V	0.001	0.003	0.005	0.005	0.003	-	-	-	-
sum	2.991	2.997	2.997	2.997	2.997	3.000	2.995	3.000	3.000

Table 8 continued

Intrusion	PK151	PK151	PK151	PK151	PK151	PK151	PK151	PK312	PK312
Sample	47514-9	47514-10	47514-11	47514-12	47514-13	47514-14	47514-15	47553b-1	47553b-2
	ilm rim	ilm rim	ilm rim	ilm rim	ilm rim	ilm rim	ilm rim	g.m.	g.m.
Major element analysis (wt%)									
Nb_2O_5	n.a.	bld	bld	bld	bld	bld	bld	bld	bld
SiO_2	0.05	0.17	0.09	0.11	0.46	0.08	0.78	0.08	0.09
TiO_2	16.80	21.95	20.30	21.84	19.32	18.75	10.63	19.50	19.14
ZnO	0.02	0.08	0.09	0.13	0.05	0.08	0.08	n.a.	n.a.
Al_2O_3	4.01	2.82	3.19	3.12	3.60	3.62	4.19	4.29	4.41
Cr_2O_3	3.25	3.95	3.71	3.88	3.17	3.25	0.62	0.34	0.51
FeO	35.48	40.70	38.86	41.11	38.11	35.02	32.73	31.11	31.21
Fe_2O_3	28.05	18.41	21.72	18.55	23.63	25.10	42.95	32.97	33.17
NiO	0.05	0.09	0.09	0.11	0.09	0.08	0.07	0.10	0.16
MnO	0.89	1.03	1.14	1.00	0.90	0.99	0.88	0.82	0.77
MgO	5.76	5.63	5.57	5.35	6.28	7.20	5.07	11.54	11.41
CaO	0.34	0.08	0.22	0.04	0.14	0.12	0.36	0.52	0.34
BaO	0.02	bld	bld	bld	bld	bld	bld	bld	bld
Na_2O	0.03	bld	0.03	bld	bld	0.03	bld	bld	bld
K_2O	n.a.	bld	bld	bld	bld	bld	0.08	0.01	bld
V_2O_3	0.07	n.a.	n.a.	n.a.	n.a.	n.a.	n.a.	n.a.	n.a.
Total	94.84	94.90	94.98	95.24	95.76	94.30	98.43	101.25	101.19
Number of cations (apfu) on the basis of 3 oxygen atoms and 2 cations									
Nb	-	-	-	-	-	-	-	-	-
Si	0.002	0.006	0.003	0.004	0.017	0.003	0.028	0.003	0.003
Ti	0.470	0.615	0.569	0.611	0.533	0.522	0.290	0.492	0.484
Zn	0.001	0.002	0.002	0.004	0.001	0.002	0.002	-	-
Al	0.176	0.124	0.140	0.137	0.156	0.158	0.179	0.169	0.175
Cr	0.096	0.116	0.109	0.114	0.092	0.095	0.018	0.009	0.013
Fe^{2+}	1.103	1.268	1.210	1.279	1.169	1.084	0.992	0.873	0.877
Fe^{3+}	0.785	0.516	0.609	0.519	0.652	0.699	1.171	0.832	0.839
Ni	0.002	0.003	0.003	0.003	0.003	0.002	0.002	0.003	0.004
Mn	0.028	0.033	0.036	0.031	0.028	0.031	0.027	0.023	0.022
Mg	0.319	0.313	0.309	0.297	0.343	0.397	0.274	0.577	0.571
Ca	0.014	0.003	0.009	0.002	0.006	0.005	0.014	0.019	0.012
Ba	0.000	-	-	-	-	-	-	-	-
Na	0.001	-	0.000	-	-	0.000	-	-	-
K	-	-	-	-	-	-	0.001	0.000	-
V	0.002	-	-	-	-	-	-	-	-
sum	2.997	3.000	2.999	3.000	3.000	2.999	2.997	3.000	3.000

Table 8 continued

Intrusion	PK312	PK312	PK312	PK312	PK312	PK312	PK312	PK312	PK312
Sample	47553b-3	47553b-4	47553b-5	47553b-6	47553b-7	47553b-8	47553b-8	47553b-9	47553b-10
	g.m.	g.m.	g.m.	g.m.	g.m.	core	rim	g.m.	g.m.
Major element analysis (wt%)									
Nb_2O_5	bld	0.07	bld	bld	bld	bld	bld	bld	bld
SiO_2	0.07	0.08	0.18	0.09	0.11	0.05	1.10	0.08	0.05
TiO_2	19.30	18.50	18.69	19.53	18.84	3.87	18.46	18.82	17.46
ZnO	n.a.	n.a.	n.a.	n.a.	n.a.	n.a.	n.a.	n.a.	n.a.
Al_2O_3	4.12	4.50	4.44	4.40	5.22	0.22	5.22	4.40	4.49
Cr_2O_3	0.35	0.90	0.45	0.37	1.36	0.10	0.40	0.71	0.39
FeO	29.71	30.25	31.42	30.96	30.55	27.93	32.67	30.61	30.41
Fe_2O_3	33.72	33.79	33.26	32.48	30.45	64.18	29.26	33.86	35.66
NiO	0.11	0.13	0.14	0.13	0.17	0.11	0.17	0.16	0.19
MnO	0.82	0.78	0.86	0.82	0.81	0.93	0.94	0.79	0.94
MgO	12.16	11.46	10.82	11.69	11.42	3.78	10.41	11.65	10.15
CaO	0.63	0.54	0.45	0.30	0.23	0.35	0.36	0.19	0.94
BaO	bld	bld	bld	bld	bld	bld	bld	bld	bld
Na_2O	bld	bld	bld	bld	bld	bld	bld	bld	bld
K_2O	bld	0.03	0.02	0.03	bld	bld	0.02	0.04	0.02
V_2O_3	n.a.	n.a.	n.a.	n.a.	n.a.	n.a.	n.a.	n.a.	n.a.
Total	101.00	101.01	100.73	100.79	99.16	101.52	99.01	101.31	100.70
Number of cations (apfu) on the basis of 3 oxygen atoms and 2 cations									
Nb	-	0.001	-	-	-	-	-	-	-
Si	0.002	0.003	0.006	0.003	0.004	0.002	0.038	0.003	0.002
Ti	0.487	0.468	0.476	0.494	0.483	0.107	0.475	0.475	0.447
Zn	-	-	-	-	-	-	-	-	-
Al	0.163	0.178	0.177	0.174	0.210	0.010	0.211	0.174	0.180
Cr	0.009	0.024	0.012	0.010	0.037	0.003	0.011	0.019	0.010
Fe^{2+}	0.833	0.851	0.890	0.871	0.870	0.856	0.935	0.858	0.866
Fe^{3+}	0.850	0.855	0.847	0.822	0.781	1.770	0.754	0.854	0.913
Ni	0.003	0.004	0.004	0.004	0.005	0.003	0.005	0.004	0.005
Mn	0.023	0.022	0.025	0.023	0.023	0.029	0.027	0.022	0.027
Mg	0.607	0.574	0.546	0.586	0.580	0.207	0.531	0.582	0.515
Ca	0.023	0.019	0.016	0.011	0.008	0.014	0.013	0.007	0.034
Ba	-	-	-	-	-	-	-	-	-
Na	-	-	-	-	-	-	-	-	-
K	-	0.000	0.000	0.000	-	-	0.000	0.000	0.000
V	-	-	-	-	-	-	-	-	-
sum	3.000	2.999	2.999	2.999	3.000	3.000	2.999	2.999	2.999

Table 8 continued

Intrusion	PK312	PK312	PK312	PK312	PK314	PK314	PK314	PK314	PK314
Sample	47553b-11	47553b-12	47553b-13	47553b-14	47547-1	47547-2	47547-3	47547-4	47547-5
	xeno	ilm rim	ilm rim	ilm rim	g.m.	g.m.	g.m.	g.m.	g.m.
Major element analysis (wt%)									
Nb_2O_5	n.a.	bld	bld	bld	n.a.	bld	bld	bld	bld
SiO_2	0.11	0.06	0.15	0.07	0.10	0.15	0.23	0.18	0.25
TiO_2	0.03	20.05	20.04	19.62	7.02	6.74	8.24	7.45	8.05
ZnO	n.a.	n.a.	n.a.	n.a.	n.a.	n.a.	n.a.	n.a.	n.a.
Al_2O_3	0.03	5.04	4.58	4.28	16.46	14.43	14.65	12.77	12.51
Cr_2O_3	0.03	1.40	0.61	0.48	29.86	33.80	27.05	29.33	27.66
FeO	30.99	31.48	32.37	31.11	19.99	20.50	21.12	20.83	20.83
Fe_2O_3	68.49	30.43	30.81	32.86	12.09	11.81	15.32	16.71	17.19
NiO	0.00	0.11	0.12	0.13	0.17	0.14	0.14	0.11	0.16
MnO	0.09	0.80	0.84	0.82	0.36	0.35	0.31	0.48	0.51
MgO	0.03	12.06	11.40	11.87	13.17	12.85	13.25	12.75	12.69
CaO	0.01	0.17	0.08	0.21	0.02	0.02	0.15	0.05	0.28
BaO	bld	bld	bld	bld	bld	bld	bld	bld	bld
Na_2O	bld	bld	bld	bld	bld	bld	bld	bld	0.02
K_2O	bld	bld	0.01	bld	bld	0.01	bld	bld	0.03
V_2O_3	n.a.	n.a.	n.a.	n.a.	n.a.	n.a.	n.a.	n.a.	n.a.
Total	99.80	101.58	100.99	101.45	99.24	100.77	100.45	100.66	100.17
Number of cations (apfu) on the basis of 3 oxygen atoms and 2 cations									
Nb	-	-	-	-	-	-	-	-	-
Si	0.004	0.002	0.005	0.002	0.003	0.005	0.007	0.006	0.008
Ti	0.001	0.501	0.507	0.494	0.168	0.161	0.197	0.180	0.195
Zn	-	-	-	-	-	-	-	-	-
Al	0.001	0.197	0.181	0.169	0.617	0.539	0.548	0.482	0.475
Cr	0.001	0.037	0.016	0.013	0.751	0.848	0.679	0.743	0.704
Fe^{2+}	1.000	0.874	0.910	0.870	0.532	0.544	0.560	0.559	0.561
Fe^{3+}	1.988	0.761	0.779	0.827	0.289	0.282	0.366	0.403	0.417
Ni	0.000	0.003	0.003	0.003	0.004	0.003	0.004	0.003	0.004
Mn	0.003	0.022	0.024	0.023	0.010	0.009	0.008	0.013	0.014
Mg	0.002	0.597	0.571	0.592	0.625	0.608	0.627	0.609	0.609
Ca	0.000	0.006	0.003	0.008	0.001	0.001	0.005	0.002	0.010
Ba	-	-	-	-	-	-	-	-	-
Na	-	-	-	-	-	-	-	-	0.000
K	-	-	0.000	-	-	0.000	-	-	0.000
V	-	-	-	-	-	-	-	-	-
sum	3.000	3.000	3.000	3.000	3.000	3.000	3.000	3.000	2.998

Table 8 continued

Intrusion	PK314	PK314	PK314	PK314	PK314	PK314	PK314	PK314
Sample	47547-6	47547-7	47547-8	47547-9	47547-10	47547-11	47547-12	47547-13
	g.m.	g.m.	g.m.	g.m.	incl-ol	g.m.	incl-ilm	ilm rim
Major element analysis (wt%)								
Nb_2O_5	bld	bld	bld	bld	bld	bld	bld	bld
SiO_2	0.28	0.14	0.09	0.08	0.20	0.69	0.85	2.89
TiO_2	13.53	5.26	12.24	10.23	4.88	7.26	23.20	3.10
ZnO	n.a.	n.a.	n.a.	n.a.	n.a.	n.a.	n.a.	n.a.
Al_2O_3	10.22	21.39	10.53	8.42	20.22	0.91	1.36	0.10
Cr_2O_3	15.62	32.09	19.07	21.59	32.06	0.80	2.36	0.19
FeO	24.75	18.59	23.45	20.91	17.53	36.09	50.02	35.89
Fe_2O_3	22.08	9.53	21.08	23.48	11.03	51.05	17.54	54.10
NiO	0.18	0.18	0.15	0.13	0.18	0.04	0.20	n.a.
MnO	0.59	0.28	0.57	0.78	0.29	1.10	1.65	0.07
MgO	13.46	14.16	13.45	12.88	14.36	0.47	0.66	0.31
CaO	0.01	0.02	0.01	0.40	0.03	0.42	0.03	0.10
BaO	bld	bld	bld	bld	bld	bld	bld	bld
Na_2O	bld	bld	bld	bld	bld	bld	0.11	0.04
K_2O	bld	bld	bld	bld	bld	0.02	bld	0.03
V_2O_3	n.a.	n.a.	n.a.	n.a.	n.a.	n.a.	n.a.	n.a.
Total	100.70	101.62	100.64	98.90	100.76	98.85	97.98	96.82
Number of cations (apfu) on the basis of 3 oxygen atoms and 2 cations								
Nb	-	-	-	-	-	-	-	-
Si	0.009	0.004	0.003	0.003	0.006	0.026	0.032	0.113
Ti	0.329	0.120	0.297	0.256	0.113	0.208	0.658	0.091
Zn	-	-	-	-	-	-	-	-
Al	0.389	0.765	0.401	0.330	0.731	0.041	0.060	0.005
Cr	0.399	0.770	0.487	0.567	0.777	0.024	0.070	0.006
Fe^{2+}	0.669	0.472	0.633	0.581	0.450	1.152	1.577	1.170
Fe^{3+}	0.537	0.218	0.512	0.587	0.255	1.466	0.497	1.587
Ni	0.005	0.004	0.004	0.003	0.004	0.001	0.006	-
Mn	0.016	0.007	0.016	0.022	0.007	0.036	0.053	0.002
Mg	0.648	0.640	0.647	0.638	0.656	0.027	0.037	0.018
Ca	0.000	0.001	0.000	0.014	0.001	0.017	0.001	0.004
Ba	-	-	-	-	-	-	-	-
Na	-	-	-	-	-	0.000	0.002	0.001
K	-	-	-	-	-	0.000	-	0.000
V	-	-	-	-	-	-	-	-
sum	3.000	3.000	3.000	3.000	3.000	2.999	2.994	2.997

Table 9 – Apatite major and minor elements (wt%)

PK150	SiO_2	FeO	MnO	CaO	SrO	Na_2O	P_2O_5	SO_3	Cl	F	O=F	Total
44813a	0.39	0.07	bld	53.90	1.63	0.00	40.58	0.01	bld	2.77	1.17	98.18
44813a	0.24	0.00	bld	55.62	1.70	0.00	40.71	bld	bld	3.22	1.36	100.13
44813a	0.44	0.17	bld	54.37	1.60	0.00	40.40	0.03	bld	2.61	1.10	98.50
44813a	0.61	0.29	bld	52.65	1.34	0.00	40.51	0.05	bld	2.61	1.10	96.96
44813a	0.45	0.09	bld	54.42	1.55	0.10	40.21	0.02	0.02	2.91	1.23	98.52
44813a	0.22	0.11	bld	54.61	1.62	0.00	40.99	0.03	bld	2.90	1.22	99.24
44813a	0.25	0.09	bld	54.76	1.69	0.00	41.02	bld	bld	2.67	1.12	99.36
44813a	0.25	0.08	bld	54.65	1.63	0.00	40.89	0.01	bld	2.89	1.22	99.16
44813b	0.28	0.07	bld	54.29	1.64	0.00	40.41	0.02	bld	2.84	1.20	98.35
44813b	0.29	0.12	bld	54.20	1.67	0.00	40.82	0.02	bld	2.76	1.16	98.70
44813b	0.25	0.15	bld	54.41	1.66	0.00	40.76	0.02	bld	2.88	1.22	98.91
44813b	0.68	0.33	0.01	53.70	1.61	0.00	40.50	0.02	bld	2.56	1.08	98.31
44813b	0.41	0.06	bld	53.61	1.66	0.00	40.46	bld	bld	2.79	1.18	97.81
44813b	0.25	0.13	bld	54.05	1.62	0.00	40.74	bld	bld	2.67	1.13	98.33
44813b	0.26	0.12	bld	53.91	1.63	0.00	40.65	0.02	bld	2.67	1.12	98.12
44813b	0.31	0.07	bld	54.61	1.53	0.00	40.23	0.02	bld	2.69	1.13	98.33
44813b	1.03	2.27	0.02	51.93	1.60	0.00	38.90	0.02	0.01	2.59	1.09	97.26
44813b	0.31	0.25	bld	55.31	1.61	0.00	40.90	bld	bld	2.91	1.23	100.06
44813b	0.35	0.15	bld	54.63	1.64	0.00	40.84	0.01	bld	2.80	1.18	99.22
44813c	0.31	0.14	bld	54.04	1.65	n.a.	40.68	bld	bld	2.70	1.14	98.38
44813c	0.40	0.19	bld	54.75	1.68	n.a.	40.37	bld	bld	2.68	1.13	98.94
44813c	0.35	0.55	bld	54.02	1.63	n.a.	40.62	bld	bld	2.87	1.21	98.82
44813c	0.61	0.35	bld	53.75	1.53	n.a.	40.25	bld	bld	2.58	1.09	97.98
44813c	0.18	0.05	bld	54.59	1.63	n.a.	40.78	bld	bld	2.79	1.17	98.84
44813c	0.31	0.11	bld	54.48	1.67	n.a.	40.74	bld	bld	2.80	1.18	98.92
44813c	0.23	0.15	bld	55.08	1.66	n.a.	41.05	bld	bld	2.95	1.24	99.87
44813c	0.24	0.06	bld	54.04	1.63	n.a.	40.64	bld	bld	2.62	1.10	98.13
44813c	0.30	0.07	bld	54.44	1.62	n.a.	40.56	bld	bld	2.95	1.25	98.69
44813c	0.35	0.07	bld	53.66	1.68	n.a.	40.46	bld	bld	2.86	1.20	97.86
44813d	0.22	0.07	bld	53.86	1.65	n.a.	40.94	bld	bld	2.69	1.13	98.30
44813d	0.27	0.11	bld	54.41	1.67	n.a.	40.81	bld	bld	2.74	1.15	98.84
44813d	0.26	0.06	bld	53.97	1.67	n.a.	40.71	bld	bld	2.75	1.16	98.26
44813d	0.27	0.08	bld	53.62	1.65	n.a.	40.60	bld	bld	2.95	1.24	97.93
44813d	0.22	0.14	bld	53.45	1.60	n.a.	40.64	bld	bld	2.86	1.20	97.69

Table 10 – Ilmenite major and minor elements; rim = outermost margin of ilmenite with composition distinct from the core

Intrusion	PK150	PK150	PK150	PK150	PK150	PK150	PK150	PK150	PK150	PK150
Sample	47513	47513	47513	47513	47513	47513	47513	47513	44813a	44813a
Major element analysis (wt%)										
Nb_2O_5	0.11	0.11	0.12	0.12	0.06	0.10	0.16	0.10	n.a.	n.a.
SiO_2	0.01	0.01	bld	bld	0.01	0.01	bld	0.01	0.01	0.04
TiO_2	51.70	48.37	50.67	50.67	50.13	49.03	46.23	49.03	45.76	48.36
ZnO	bld	bld	bld	bld	bld	bld	bld	bld	0.05	0.23
Al_2O_3	0.57	2.56	0.37	0.37	0.71	0.51	0.41	0.51	0.78	0.62
Cr_2O_3	0.95	0.67	0.91	0.91	0.44	0.35	0.13	0.35	2.73	3.20
FeO	22.73	23.46	25.56	25.56	25.40	24.95	28.37	24.95	27.29	25.53
Fe_2O_3	8.41	12.56	9.03	9.03	10.12	11.98	15.46	11.98	12.68	8.28
NiO	0.06	0.11	0.08	0.08	0.09	0.06	0.02	0.06	0.10	0.11
MnO	0.49	0.27	0.38	0.38	0.28	0.32	0.25	0.32	0.34	1.74
MgO	12.94	11.02	10.96	10.96	10.81	10.44	7.25	10.44	9.08	10.28
CaO	0.07	0.02	0.03	0.03	0.02	0.02	0.01	0.02	0.04	0.04
BaO	0.04	0.03	bld	bld	0.03	0.02	0.06	0.02	n.a.	n.a.
Na_2O	0.04	0.02	0.02	0.02	0.02	0.05	0.03	0.05	bld	0.06
K_2O	bld	bld	bld	bld	bld	bld	bld	bld	n.a.	n.a.
V_2O_5	0.22	0.18	0.15	0.15	0.21	0.22	0.20	0.22	n.a.	n.a.
Total	98.36	99.39	98.27	98.27	98.34	98.06	98.59	98.06	98.84	98.49
Number of cations (apfu) on the basis of 3 oxygen atoms and 2 cations										
Nb	0.001	0.001	0.001	0.001	0.001	0.001	0.002	0.001	-	-
Si	0.000	0.000	-	-	0.000	0.000	-	0.000	0.000	0.001
Ti	0.906	0.845	0.903	0.903	0.892	0.879	0.847	0.879	0.829	0.869
Zn	-	-	-	-	-	-	-	-	0.001	0.004
Al	0.016	0.070	0.010	0.010	0.020	0.014	0.012	0.014	0.022	0.017
Cr	0.017	0.012	0.017	0.017	0.008	0.007	0.003	0.007	0.052	0.060
Fe^{2+}	0.443	0.456	0.506	0.506	0.503	0.497	0.578	0.497	0.550	0.510
Fe^{3+}	0.147	0.220	0.161	0.161	0.180	0.215	0.283	0.215	0.230	0.149
Ni	0.001	0.002	0.002	0.002	0.002	0.001	0.000	0.001	0.002	0.002
Mn	0.010	0.005	0.008	0.008	0.006	0.006	0.005	0.006	0.007	0.035
Mg	0.449	0.382	0.387	0.387	0.381	0.371	0.263	0.371	0.326	0.366
Ca	0.002	0.001	0.001	0.001	0.001	0.001	0.000	0.001	0.001	0.001
Ba	0.000	0.000	-	-	0.000	0.000	0.001	0.000	-	-
Na	0.000	0.000	0.000	0.000	0.000	0.001	0.000	0.001	-	0.001
K	-	-	-	-	-	-	-	-	-	-
V	0.004	0.003	0.003	0.003	0.004	0.004	0.004	0.004	-	-
sum	1.999	1.997	1.999	1.999	1.999	1.998	1.999	1.998	2.019	2.016

Table 10 continued

Intrusion	PK150	PK150	PK150	PK150	PK150	PK150	PK150	PK150	PK150
Sample	44813a	44813a	44813a	44813a	44813a	44813a	44813a	44813a	44813a
Major element analysis (wt%)									
Nb_2O_5	n.a.	n.a.	n.a.	n.a.	n.a.	n.a.	n.a.	n.a.	n.a.
SiO_2	0.02	bld	0.02	0.05	0.05	0.05	0.09	0.07	0.03
TiO_2	50.48	50.91	51.40	52.57	47.64	50.98	52.70	49.84	47.89
ZnO	0.03	bld	bld	0.03	0.07	0.05	0.09	bld	0.02
Al_2O_3	0.57	1.41	2.32	0.48	1.78	0.61	0.63	1.34	0.73
Cr_2O_3	1.70	1.24	1.91	2.32	1.05	2.07	2.17	0.20	0.24
FeO	22.96	17.13	15.32	17.65	23.26	21.63	16.10	16.99	26.29
Fe_2O_3	9.28	12.06	12.55	10.14	12.81	9.13	12.11	20.17	12.94
NiO	0.08	0.11	0.10	0.08	0.14	0.11	0.09	0.11	0.11
MnO	0.86	0.80	0.75	0.84	1.17	0.96	1.33	0.34	0.34
MgO	12.42	15.14	16.06	15.37	10.75	13.06	14.26	11.11	10.39
CaO	0.06	0.04	0.05	0.03	0.03	0.04	0.09	0.02	0.03
BaO	n.a.	n.a.	n.a.	n.a.	n.a.	n.a.	n.a.	n.a.	n.a.
Na_2O	0.035	0.07	0.06	0.05	0.03	0.06	bld	bld	0.015
K_2O	n.a.	n.a.	n.a.	n.a.	n.a.	n.a.	n.a.	n.a.	n.a.
V_2O_5	n.a.	n.a.	n.a.	n.a.	n.a.	n.a.	n.a.	n.a.	n.a.
Total	98.45	98.91	100.54	99.61	98.78	98.74	99.66	100.19	99.00
Number of cations (apfu) on the basis of 3 oxygen atoms and 2 cations									
Nb	-	-	-	-	-	-	-	-	-
Si	0.000	-	0.000	0.001	0.001	0.001	0.002	0.002	0.001
Ti	0.890	0.871	0.856	0.893	0.844	0.890	0.895	0.854	0.857
Zn	0.000	-	-	0.001	0.001	0.001	0.001	-	0.000
Al	0.016	0.038	0.061	0.013	0.049	0.017	0.017	0.036	0.020
Cr	0.031	0.022	0.033	0.041	0.020	0.038	0.039	0.004	0.004
Fe^{2+}	0.450	0.326	0.284	0.333	0.458	0.420	0.304	0.324	0.523
Fe^{3+}	0.164	0.206	0.209	0.172	0.227	0.159	0.206	0.346	0.232
Ni	0.001	0.002	0.002	0.001	0.003	0.002	0.002	0.002	0.002
Mn	0.017	0.015	0.014	0.016	0.023	0.019	0.025	0.007	0.007
Mg	0.434	0.513	0.530	0.518	0.378	0.452	0.480	0.377	0.368
Ca	0.002	0.001	0.001	0.001	0.001	0.001	0.002	0.000	0.001
Ba	-	-	-	-	-	-	-	-	-
Na	0.000	0.001	0.001	0.001	0.000	0.001	-	-	0.000
K	-	-	-	-	-	-	-	-	-
V	-	-	-	-	-	-	-	-	-
sum	2.004	1.995	1.991	1.992	2.006	2.001	1.973	1.951	2.015

Table 10 continued

Intrusion	PK150	PK150	PK150	PK150	PK150	PK150	PK150	PK150	PK150
Sample	44813a	44813a	44813a	44813a	44813a	44813a	44813a	44813a	44813a
Major element analysis (wt%)									
Nb_2O_5	n.a.	n.a.	n.a.	n.a.	n.a.	n.a.	n.a.	n.a.	n.a.
SiO_2	bld	0.03	0.05	0.04	0.07	0.05	0.05	0.02	0.03
TiO_2	50.61	51.22	52.00	51.00	49.94	48.89	51.37	51.44	50.48
ZnO	0.08	0.03	0.03	0.08	0.03	0.06	0.03	0.03	0.05
Al_2O_3	0.37	0.56	0.75	0.54	0.47	0.76	0.78	0.54	0.42
Cr_2O_3	2.68	2.18	2.43	0.71	0.69	0.20	1.70	1.91	3.30
FeO	17.92	21.97	20.40	21.52	24.61	25.17	22.03	18.32	15.23
Fe_2O_3	13.52	8.11	9.45	10.90	12.02	12.09	9.09	13.30	14.68
NiO	0.05	0.06	0.08	0.08	0.07	0.13	0.08	0.08	0.07
MnO	2.47	1.25	0.81	1.35	0.38	0.50	1.19	1.67	2.06
MgO	11.73	13.15	13.43	12.86	11.22	11.11	12.19	11.98	13.30
CaO	0.23	0.06	0.105	0.04	0.03	0.03	0.57	0.055	0.25
BaO	n.a.	n.a.	n.a.	n.a.	n.a.	n.a.	n.a.	n.a.	n.a.
Na_2O	bld	bld	0.055	0.05	bld	bld	0.04	0.03	0.04
K_2O	n.a.	n.a.	n.a.	n.a.	n.a.	n.a.	n.a.	n.a.	n.a.
V_2O_5	n.a.	n.a.	n.a.	n.a.	n.a.	n.a.	n.a.	n.a.	n.a.
Total	99.66	98.62	99.58	99.17	99.53	98.99	99.12	99.36	99.91
Number of cations (apfu) on the basis of 3 oxygen atoms and 2 cations									
Nb	-	-	-	-	-	-	-	-	-
Si	-	0.001	0.001	0.001	0.002	0.001	0.001	0.000	0.001
Ti	0.878	0.896	0.894	0.889	0.879	0.868	0.896	0.890	0.863
Zn	0.001	0.001	0.001	0.001	0.001	0.001	0.001	0.000	0.001
Al	0.010	0.015	0.020	0.015	0.013	0.021	0.021	0.015	0.011
Cr	0.049	0.040	0.044	0.013	0.013	0.004	0.031	0.035	0.059
Fe^{2+}	0.346	0.427	0.390	0.417	0.482	0.497	0.427	0.352	0.290
Fe^{3+}	0.235	0.142	0.163	0.190	0.212	0.215	0.159	0.230	0.251
Ni	0.001	0.001	0.001	0.001	0.001	0.002	0.001	0.001	0.001
Mn	0.048	0.025	0.016	0.027	0.008	0.010	0.023	0.033	0.040
Mg	0.403	0.456	0.458	0.444	0.391	0.391	0.421	0.411	0.451
Ca	0.006	0.001	0.003	0.001	0.001	0.001	0.014	0.001	0.006
Ba	-	-	-	-	-	-	-	-	-
Na	-	-	0.001	0.001	-	-	0.000	0.000	0.000
K	-	-	-	-	-	-	-	-	-
V	-	-	-	-	-	-	-	-	-
sum	1.976	2.005	1.991	2.000	2.001	2.011	1.997	1.969	1.975

Table 10 continued

Intrusion	PK150	PK150	PK150	PK150	PK150	PK150	PK150	PK150	PK150
Sample	44813a	44813a	44813a	44813a	44813a	44813b	44813b	44813b	44813b
Major element analysis (wt%)									
Nb_2O_5	n.a.	n.a.	n.a.	n.a.	n.a.	n.a.	n.a.	n.a.	n.a.
SiO_2	0.04	0.06	0.03	bld	0.04	0.04	0.09	bld	0.02
TiO_2	50.16	51.37	48.83	51.47	47.85	50.69	51.54	49.06	52.25
ZnO	0.10	0.04	bld	0.04	bld	n.a.	n.a.	n.a.	n.a.
Al_2O_3	0.52	0.69	0.51	0.65	0.42	0.50	0.33	0.42	0.79
Cr_2O_3	0.33	0.89	0.46	3.71	0.42	0.46	2.03	0.40	0.51
FeO	23.18	19.15	26.17	17.93	31.08	25.37	23.90	30.43	22.73
Fe_2O_3	12.14	14.55	12.93	12.38	9.82	11.00	8.29	11.11	10.37
NiO	0.10	0.09	0.11	0.08	0.06	0.09	0.07	0.10	0.09
MnO	1.01	1.02	0.22	0.65	0.26	0.33	2.35	0.48	0.73
MgO	11.62	12.11	10.21	12.92	8.77	11.12	11.09	7.34	13.09
CaO	0.17	0.22	0.02	0.04	0.015	0.03	0.085	0.02	0.11
BaO	n.a.	n.a.	n.a.	n.a.	n.a.	bld	bld	bld	bld
Na_2O	bld	bld	bld	0.04	0.015	bld	0.055	bld	bld
K_2O	n.a.	n.a.	n.a.	n.a.	n.a.	n.a.	n.a.	0.01	bld
V_2O_5	n.a.	n.a.	n.a.	n.a.	n.a.	n.a.	n.a.	n.a.	n.a.
Total	99.37	100.19	99.50	99.91	98.73	99.62	99.81	99.36	100.69
Number of cations (apfu) on the basis of 3 oxygen atoms and 2 cations									
Nb	-	-	-	-	-	-	-	-	-
Si	0.001	0.001	0.001	-	0.001	0.001	0.002	-	0.000
Ti	0.881	0.882	0.868	0.880	0.873	0.891	0.903	0.890	0.895
Zn	0.002	0.001	-	0.001	-	-	-	-	-
Al	0.014	0.019	0.014	0.017	0.012	0.014	0.009	0.012	0.021
Cr	0.006	0.016	0.009	0.067	0.008	0.008	0.037	0.008	0.009
Fe^{2+}	0.453	0.366	0.517	0.341	0.630	0.496	0.466	0.613	0.433
Fe^{3+}	0.213	0.250	0.230	0.212	0.179	0.193	0.145	0.202	0.178
Ni	0.002	0.002	0.002	0.001	0.001	0.002	0.001	0.002	0.002
Mn	0.020	0.020	0.004	0.013	0.005	0.007	0.046	0.010	0.014
Mg	0.405	0.412	0.360	0.438	0.317	0.387	0.385	0.264	0.445
Ca	0.004	0.005	0.001	0.001	0.000	0.001	0.002	0.001	0.003
Ba	-	-	-	-	-	-	-	-	-
Na	-	-	-	0.000	0.000	-	0.001	-	-
K	-	-	-	-	-	-	-	0.000	-
V	-	-	-	-	-	-	-	-	-
sum	2.001	1.974	2.005	1.971	2.027	2.000	1.998	2.000	2.000

Table 10 continued

Intrusion	PK150	PK150	PK150	PK150	PK150	PK150	PK150	PK150	PK150
Sample	44813b	44813b	44813b	44813b	44813b	44813b	44813c	44813c	44813c
Major element analysis (wt%)									
Nb_2O_5	n.a.	n.a.	n.a.	n.a.	n.a.	n.a.	n.a.	n.a.	n.a.
SiO_2	0.03	bld	0.06	0.05	0.06	0.045	bld	bld	0.01
TiO_2	39.38	47.51	48.56	51.91	51.35	50.85	51.79	43.40	51.15
ZnO	n.a.	n.a.	n.a.	n.a.	n.a.	n.a.	n.a.	n.a.	n.a.
Al_2O_3	0.32	0.32	0.54	0.62	0.57	0.52	0.62	0.43	0.53
Cr_2O_3	0.20	0.19	1.80	0.74	0.72	0.40	0.94	0.12	2.72
FeO	26.72	26.59	18.24	23.89	24.96	25.48	22.68	27.54	22.08
Fe_2O_3	27.08	15.09	15.47	8.79	9.50	10.45	9.39	21.65	8.34
NiO	0.00	0.00	0.10	0.13	0.12	0.11	0.09	0.03	0.11
MnO	0.18	0.92	1.91	1.04	0.33	0.27	1.17	0.34	2.37
MgO	4.76	8.39	13.04	12.15	11.68	11.18	12.67	6.21	11.93
CaO	0.00	0.02	0.12	0.04	0.03	0.02	0.04	0.01	0.07
BaO	bld	bld	bld	bld	bld	bld	bld	bld	bld
Na_2O	0.02	0.05	0.02	bld	bld	bld	bld	0.02	0.02
K_2O	bld	bld	bld	bld	bld	bld	bld	bld	bld
V_2O_5	n.a.	n.a.	n.a.	n.a.	n.a.	n.a.	n.a.	n.a.	n.a.
Total	98.67	99.08	99.84	99.34	99.30	99.31	99.39	99.73	99.32
Number of cations (apfu) on the basis of 3 oxygen atoms and 2 cations									
Nb	-	-	-	-	-	-	-	-	-
Si	0.001	-	0.001	0.001	0.001	0.001	-	-	0.000
Ti	0.739	0.858	0.841	0.907	0.901	0.896	0.901	0.795	0.895
Zn	-	-	-	-	-	-	-	-	-
Al	0.009	0.009	0.015	0.017	0.016	0.014	0.017	0.012	0.014
Cr	0.004	0.004	0.033	0.013	0.013	0.007	0.017	0.002	0.050
Fe^{2+}	0.557	0.534	0.351	0.464	0.487	0.499	0.439	0.561	0.430
Fe^{3+}	0.508	0.273	0.268	0.154	0.167	0.184	0.163	0.397	0.146
Ni	-	-	0.002	0.002	0.002	0.002	0.002	0.000	0.002
Mn	0.004	0.019	0.037	0.020	0.006	0.005	0.023	0.007	0.047
Mg	0.177	0.300	0.448	0.420	0.406	0.390	0.437	0.225	0.413
Ca	-	0.001	0.003	0.001	0.001	0.001	0.001	0.000	0.002
Ba	-	-	-	-	-	-	-	-	-
Na	0.000	0.001	0.000	-	-	-	-	0.000	0.000
K	-	-	-	-	-	-	-	-	-
V	-	-	-	-	-	-	-	-	-
sum	1.999	1.998	1.999	2.000	2.000	2.000	2.000	1.999	1.999

Table 10 continued

Intrusion	PK150	PK150	PK150	PK150	PK150	PK150	PK150	PK150	PK150
Sample	44813c	44813c	44813c	4813d	4813d	4813d	4813d	4813d	39249b
Major element analysis (wt%)									
Nb_2O_5	n.a.	n.a.	n.a.	n.a.	n.a.	n.a.	n.a.	n.a.	bld
SiO_2	0.02	0.03	0.05	0.04	0.06	0.04	0.04	bld	bld
TiO_2	53.65	53.11	53.10	51.02	52.86	51.67	53.53	52.03	52.47
ZnO	n.a.	n.a.	n.a.	n.a.	n.a.	n.a.	n.a.	n.a.	bld
Al_2O_3	1.42	0.76	0.55	0.52	0.44	0.45	0.87	0.51	1.31
Cr_2O_3	2.44	1.30	1.51	0.88	3.74	4.06	1.26	2.39	0.43
FeO	20.68	23.47	22.67	24.79	17.20	16.10	22.24	22.30	26.37
Fe_2O_3	5.58	7.35	7.00	9.61	7.68	8.96	6.30	7.75	6.78
NiO	0.09	0.13	0.08	0.12	0.07	0.08	0.12	0.09	0.12
MnO	0.79	0.53	2.42	0.35	0.71	1.16	0.89	1.80	0.33
MgO	14.78	13.26	12.60	11.58	16.57	16.01	13.95	12.56	11.41
CaO	0.18	0.05	0.04	0.03	0.08	0.50	0.06	0.05	0.03
BaO	bld	bld	bld	bld	bld	bld	bld	bld	n.a.
Na_2O	0.03	bld	0.03	bld	bld	bld	bld	0.03	bld
K_2O	bld	bld	bld	bld	bld	bld	bld	bld	bld
V_2O_5	n.a.	n.a.	n.a.	n.a.	n.a.	n.a.	n.a.	n.a.	n.a.
Total	99.66	99.97	100.02	98.94	99.41	99.03	99.25	99.52	99.25
Number of cations (apfu) on the basis of 3 oxygen atoms and 2 cations									
Nb	-	-	-	-	-	-	-	-	-
Si	0.000	0.001	0.001	0.001	0.001	0.001	0.001	-	-
Ti	0.912	0.914	0.918	0.899	0.895	0.880	0.922	0.904	0.919
Zn	-	-	-	-	-	-	-	-	-
Al	0.038	0.020	0.015	0.014	0.012	0.012	0.023	0.014	0.036
Cr	0.044	0.024	0.027	0.016	0.067	0.073	0.023	0.044	0.008
Fe^{2+}	0.391	0.449	0.436	0.486	0.324	0.305	0.426	0.431	0.513
Fe^{3+}	0.095	0.127	0.121	0.169	0.130	0.153	0.109	0.135	0.119
Ni	0.002	0.002	0.001	0.002	0.001	0.001	0.002	0.002	0.002
Mn	0.015	0.010	0.047	0.007	0.014	0.022	0.017	0.035	0.007
Mg	0.498	0.452	0.432	0.404	0.556	0.541	0.476	0.433	0.396
Ca	0.004	0.001	0.001	0.001	0.002	0.012	0.001	0.001	0.001
Ba	-	-	-	-	-	-	-	-	-
Na	0.000	-	0.000	-	-	-	-	0.000	-
K	-	-	-	-	-	-	-	-	-
V	-	-	-	-	-	-	-	-	-
sum	1.999	2.000	1.999	2.000	2.000	2.000	2.000	1.999	2.000

Table 10 continued

Intrusion	PK150	PK150	PK150	PK150	PK150	PK150	PK150	PK150	PK150
Sample	39249b	39249b	39249b	39249b	39249b	39249b	39249b	39249b	39249b
Major element analysis (wt%)									
Nb_2O_5	bld	bld	bld	bld	bld	bld	bld	bld	bld
SiO_2	0.06	0.14	bld	0.14	0.03	0.015	bld	0.11	0.04
TiO_2	50.87	51.87	53.43	49.54	53.53	50.72	51.71	51.16	51.19
ZnO	bld	bld	bld	bld	bld	bld	0.08	0.11	bld
Al_2O_3	0.47	1.05	0.80	1.26	1.06	0.66	0.40	0.33	1.33
Cr_2O_3	0.39	0.67	1.36	0.38	0.96	0.36	3.08	2.56	0.55
FeO	25.66	26.20	26.11	24.71	26.49	26.61	26.68	24.37	25.66
Fe_2O_3	10.08	7.38	4.70	11.45	4.95	10.04	5.13	7.07	8.94
NiO	0.12	0.11	0.09	0.10	0.14	0.10	0.06	0.08	0.11
MnO	0.21	0.40	0.59	0.29	0.35	0.32	1.65	2.08	0.38
MgO	11.12	11.04	11.79	10.74	11.88	10.42	10.06	10.47	11.13
CaO	0.02	0.05	0.09	0.20	0.03	0.03	0.08	0.51	0.03
BaO	n.a.	n.a.	n.a.	n.a.	n.a.	n.a.	n.a.	n.a.	n.a.
Na_2O	bld	0.08	0.03	0.05	bld	bld	bld	0.04	0.02
K_2O	bld	bld	bld	bld	bld	bld	bld	bld	bld
V_2O_5	n.a.	n.a.	n.a.	n.a.	n.a.	n.a.	n.a.	n.a.	n.a.
Total	99.00	98.99	98.99	98.86	99.42	99.27	98.93	98.89	99.35
Number of cations (apfu) on the basis of 3 oxygen atoms and 2 cations									
Nb	-	-	-	-	-	-	-	-	-
Si	0.001	0.003	-	0.003	0.001	0.000	-	0.003	0.001
Ti	0.899	0.913	0.936	0.876	0.933	0.898	0.920	0.907	0.898
Zn	-	-	-	-	-	-	0.001	0.002	-
Al	0.013	0.029	0.022	0.035	0.029	0.018	0.011	0.009	0.036
Cr	0.007	0.012	0.025	0.007	0.018	0.007	0.058	0.048	0.010
Fe^{2+}	0.504	0.513	0.508	0.486	0.513	0.524	0.528	0.480	0.500
Fe^{3+}	0.178	0.130	0.082	0.202	0.086	0.178	0.091	0.125	0.157
Ni	0.002	0.002	0.002	0.002	0.003	0.002	0.001	0.002	0.002
Mn	0.004	0.008	0.012	0.006	0.007	0.006	0.033	0.042	0.007
Mg	0.390	0.385	0.409	0.376	0.410	0.366	0.355	0.368	0.387
Ca	0.001	0.001	0.002	0.005	0.001	0.001	0.002	0.013	0.001
Ba	-	-	-	-	-	-	-	-	-
Na	-	0.001	0.000	0.001	-	-	-	0.000	0.000
K	-	-	-	-	-	-	-	-	-
V	-	-	-	-	-	-	-	-	-
sum	2.000	1.997	1.999	1.998	2.000	2.000	2.000	1.999	1.999

Table 10 continued

Intrusion	PK150	PK150	PK150	PK150	PK150	PK150	PK150	PK150	PK150
Sample	39249b	39249b	39249b	39249b	39249b	39249b	39249b	39249b	39249b
Major element analysis (wt%)									
Nb_2O_5	bld	bld	bld	bld	bld	bld	bld	bld	bld
SiO_2	bld	0.04	bld	0.03	0.04	bld	0.02	0.03	0.21
TiO_2	50.91	50.78	53.35	50.56	52.26	53.45	49.58	48.69	49.44
ZnO	bld	bld	0.03	bld	bld	bld	bld	bld	0.04
Al_2O_3	0.72	0.93	0.98	1.14	1.22	0.66	1.02	0.43	0.29
Cr_2O_3	4.57	0.40	1.41	0.31	0.92	2.39	0.56	0.36	2.96
FeO	25.53	25.56	26.12	25.91	26.00	26.43	25.39	27.85	25.44
Fe_2O_3	5.72	10.22	5.11	10.42	6.89	4.26	11.96	12.73	8.47
NiO	0.09	0.13	0.12	0.10	0.11	0.10	0.12	0.08	0.11
MnO	0.48	0.25	0.47	0.32	0.40	0.39	0.31	0.23	1.57
MgO	10.99	11.10	11.88	10.74	11.50	11.85	10.52	8.78	9.56
CaO	0.08	0.02	0.06	0.03	0.05	0.03	0.04	0.02	0.05
BaO	n.a.	n.a.	n.a.	n.a.	n.a.	n.a.	n.a.	n.a.	bld
Na_2O	bld	bld	bld	bld	bld	bld	bld	bld	0.03
K_2O	bld	bld	bld	bld	bld	bld	bld	bld	0.10
V_2O_5	n.a.	n.a.	n.a.	n.a.	n.a.	n.a.	n.a.	n.a.	n.a.
Total	99.09	99.40	99.53	99.56	99.37	99.56	99.52	99.20	98.28
Number of cations (apfu) on the basis of 3 oxygen atoms and 2 cations									
Nb	-	-	-	-	-	-	-	-	-
Si	-	0.001	-	0.001	0.001	-	0.000	0.001	0.005
Ti	0.897	0.893	0.929	0.889	0.914	0.932	0.875	0.875	0.889
Zn	-	-	0.001	-	-	-	-	-	0.001
Al	0.020	0.025	0.027	0.031	0.033	0.018	0.028	0.012	0.008
Cr	0.085	0.007	0.026	0.006	0.017	0.044	0.010	0.007	0.056
Fe^{2+}	0.500	0.500	0.506	0.507	0.505	0.512	0.498	0.557	0.509
Fe^{3+}	0.101	0.180	0.089	0.183	0.120	0.074	0.211	0.229	0.152
Ni	0.002	0.002	0.002	0.002	0.002	0.002	0.002	0.002	0.002
Mn	0.010	0.005	0.009	0.006	0.008	0.008	0.006	0.005	0.032
Mg	0.384	0.387	0.410	0.374	0.398	0.409	0.368	0.313	0.341
Ca	0.002	0.001	0.001	0.001	0.001	0.001	0.001	0.001	0.001
Ba	-	-	-	-	-	-	-	-	-
Na	-	-	-	-	-	-	-	-	0.000
K	-	-	-	-	-	-	-	-	0.001
V	-	-	-	-	-	-	-	-	-
sum	2.000	2.000	2.000	2.000	2.000	2.000	2.000	2.000	1.997

Table 10 continued

Intrusion	PK150	PK150	PK150	PK150	PK150	PK150	PK150	PK150	PK150
Sample	39249b	39249b	39249b	39249b	47517a	47517a	47517a	47517a	47517a
Major element analysis (wt%)									
Nb_2O_5	bld	bld	0.21	bld	bld	bld	bld	bld	bld
SiO_2	bld	0.03	bld	0.04	bld	0.12	1.10	0.04	0.05
TiO_2	51.27	50.43	50.19	49.64	51.66	49.34	50.29	48.75	51.70
ZnO	0.07	bld	0.10	0.11	bld	bld	bld	bld	bld
Al_2O_3	0.47	0.94	0.64	0.34	0.45	0.49	1.04	0.45	0.67
Cr_2O_3	2.39	0.98	1.90	2.60	2.04	3.81	2.49	0.51	1.30
FeO	25.17	24.31	27.13	26.17	23.70	22.33	22.37	25.24	24.51
Fe_2O_3	7.30	10.21	6.18	8.03	7.68	9.95	8.69	13.60	8.33
NiO	0.08	0.09	0.05	0.06	0.08	0.08	0.09	0.10	0.09
MnO	1.30	0.44	2.23	2.87	0.59	0.60	0.67	0.22	0.57
MgO	10.74	11.49	8.76	8.50	12.36	11.86	12.57	10.28	11.96
CaO	0.14	0.06	0.11	0.14	0.05	0.13	0.21	0.02	0.06
BaO	bld	bld	bld	bld	bld	bld	bld	bld	bld
Na_2O	0.04	bld	0.02	0.03	bld	0.05	0.16	bld	bld
K_2O	bld	bld	bld	bld	bld	bld	bld	bld	bld
V_2O_5	n.a.	n.a.	0.13	n.a.	n.a.	n.a.	n.a.	n.a.	n.a.
Total	98.95	98.98	97.66	98.53	98.61	98.73	99.68	99.19	99.23
Number of cations (apfu) on the basis of 3 oxygen atoms and 2 cations									
Nb	-	-	0.0023	-	-	-	-	-	-
Si	-	0.001	-	0.001	-	0.003	0.025	0.001	0.001
Ti	0.908	0.8874	0.9119	0.8976	0.9075	0.8687	0.8669	0.8672	0.9048
Zn	0.001	-	0.0018	0.0020	-	-	-	-	-
Al	0.013	0.026	0.018	0.010	0.012	0.014	0.028	0.013	0.018
Cr	0.044	0.018	0.036	0.049	0.038	0.070	0.045	0.009	0.024
Fe^{2+}	0.495	0.476	0.548	0.526	0.463	0.437	0.429	0.499	0.477
Fe^{3+}	0.129	0.180	0.112	0.145	0.135	0.175	0.150	0.242	0.146
Ni	0.002	0.002	0.001	0.001	0.002	0.002	0.002	0.002	0.002
Mn	0.026	0.009	0.046	0.058	0.012	0.012	0.013	0.004	0.011
Mg	0.377	0.401	0.315	0.305	0.430	0.414	0.429	0.362	0.415
Ca	0.004	0.002	0.003	0.004	0.001	0.003	0.005	0.001	0.001
Ba	-	-	-	-	-	-	-	-	-
Na	0.000	-	0.000	0.000	-	0.001	0.002	-	-
K	-	-	-	-	-	-	-	-	-
V	-	-	0.003	-	-	-	-	-	-
sum	1.999	2.000	1.999	1.999	2.000	1.998	1.995	2.000	2.000

Table 10 continued

Intrusion	PK150	PK150	PK150	PK150	PK150	PK150	PK150	PK150	PK150
Sample	47517a	47517a	47517a	47517a	47517a	47517a	47517a	47517a	47517a
Major element analysis (wt%)									
Nb_2O_5	bld	0.66	bld	bld	bld	bld	0.10	bld	bld
SiO_2	0.03	0.59	bld	0.045	0.05	bld	bld	0.03	0.04
TiO_2	50.22	50.69	50.14	51.40	50.84	48.00	47.46	50.14	51.79
ZnO	bld	bld	bld	bld	bld	bld	bld	bld	bld
Al_2O_3	0.78	0.12	0.40	0.69	0.70	0.23	0.68	0.64	0.72
Cr_2O_3	0.35	0.33	1.99	1.61	0.60	2.85	0.45	3.92	1.22
FeO	24.20	20.97	23.08	24.56	24.31	23.80	24.95	21.46	22.84
Fe_2O_3	11.44	8.55	10.87	8.29	9.94	12.81	14.95	8.87	8.68
NiO	0.11	0.04	0.07	0.10	0.09	0.08	0.11	0.09	0.06
MnO	0.35	0.60	0.60	0.50	0.49	0.49	0.29	0.58	0.61
MgO	11.51	8.49	11.84	11.75	11.68	10.52	9.78	12.80	12.92
CaO	0.03	7.33	0.13	0.05	0.06	0.04	0.03	0.04	0.07
BaO	bld	bld	bld	bld	bld	bld	bld	bld	bld
Na_2O	bld	0.19	0.02	0.03	bld	bld	bld	0.03	bld
K_2O	bld	bld	bld	bld	bld	bld	bld	bld	bld
V_2O_5	n.a.	n.a.	n.a.	n.a.	n.a.	n.a.	n.a.	n.a.	n.a.
Total	99.02	98.56	99.12	99.00	98.77	98.82	98.77	98.60	98.95
Number of cations (apfu) on the basis of 3 oxygen atoms and 2 cations									
Nb	-	0.007	-	-	-	-	0.001	-	-
Si	0.001	0.014	-	0.001	0.001	-	-	0.000	0.0009
Ti	0.885	0.899	0.881	0.903	0.896	0.856	0.851	0.878	0.902
Zn	-	-	-	-	-	-	-	-	-
Al	0.022	0.003	0.011	0.019	0.019	0.006	0.019	0.018	0.020
Cr	0.006	0.006	0.037	0.030	0.011	0.053	0.008	0.072	0.022
Fe^{2+}	0.474	0.413	0.451	0.479	0.476	0.472	0.497	0.417	0.442
Fe^{3+}	0.202	0.152	0.191	0.146	0.175	0.228	0.268	0.155	0.151
Ni	0.002	0.001	0.001	0.002	0.002	0.002	0.002	0.002	0.001
Mn	0.007	0.012	0.012	0.010	0.010	0.010	0.006	0.011	0.012
Mg	0.402	0.298	0.412	0.409	0.408	0.372	0.347	0.444	0.446
Ca	0.001	0.185	0.003	0.001	0.002	0.001	0.001	0.001	0.002
Ba	-	-	-	-	-	-	-	-	-
Na	-	0.002	0.000	0.000	-	-	-	0.000	-
K	-	-	-	-	-	-	-	-	-
V	-	-	-	-	-	-	-	-	-
sum	2.000	1.993	1.999	1.999	2.000	2.000	2.000	1.999	2.000

Table 10 continued

Intrusion	PK150	PK150	PK150	PK150	PK150	PK150	PK150	PK150	PK150
Sample	47517a	47517b	47517b	47517b	47517b	47517b	47517b	47517b	47517b
Major element analysis (wt%)									
Nb_2O_5	bld	bld	bld	bld	bld	bld	bld	0.19	bld
SiO_2	0.02	0.05	0.03	bld	0.04	bld	0.05	bld	0.05
TiO_2	50.55	49.81	52.79	50.03	51.36	50.92	51.86	48.39	51.38
ZnO	bld	bld	0.05	bld	bld	bld	bld	bld	bld
Al_2O_3	0.48	0.65	0.44	0.67	0.59	0.50	0.68	0.63	0.77
Cr_2O_3	1.84	0.38	1.42	4.06	2.21	1.61	1.87	0.96	0.88
FeO	22.83	24.71	23.23	22.91	23.38	25.55	22.96	23.75	23.58
Fe_2O_3	10.06	11.79	7.46	8.29	8.17	9.07	8.29	13.98	8.91
NiO	0.07	0.14	0.05	0.09	0.08	0.09	0.08	0.08	0.09
MnO	0.57	0.26	0.67	0.52	0.59	0.39	0.59	0.45	0.51
MgO	12.26	11.07	12.98	11.88	12.29	11.08	12.76	10.79	12.37
CaO	0.13	0.02	0.10	0.09	0.06	0.03	0.06	0.11	0.04
BaO	bld	bld	bld	bld	bld	bld	bld	bld	bld
Na_2O	bld	bld	0.05	0.04	0.05	bld	0.06	0.02	bld
K_2O	bld	bld	0.01	bld	bld	bld	bld	bld	bld
V_2O_5	n.a.	n.a.	n.a.	n.a.	n.a.	n.a.	n.a.	n.a.	n.a.
Total	98.81	98.88	99.28	98.58	98.81	99.22	99.24	99.33	98.56
Number of cations (apfu) on the basis of 3 oxygen atoms and 2 cations									
Nb	-	-	-	-	-	-	-	0.0020	-
Si	0.0005	0.001	0.001	-	0.001	-	0.001	-	0.001
Ti	0.888	0.882	0.917	0.881	0.900	0.898	0.902	0.856	0.902
Zn	-	-	0.001	-	-	-	-	-	-
Al	0.013	0.018	0.012	0.018	0.016	0.014	0.018	0.017	0.021
Cr	0.034	0.007	0.026	0.075	0.041	0.030	0.034	0.018	0.016
Fe^{2+}	0.446	0.486	0.448	0.449	0.456	0.501	0.444	0.467	0.460
Fe^{3+}	0.177	0.209	0.130	0.146	0.143	0.160	0.144	0.247	0.157
Ni	0.001	0.003	0.001	0.002	0.001	0.002	0.001	0.001	0.002
Mn	0.011	0.005	0.013	0.010	0.012	0.008	0.011	0.009	0.010
Mg	0.427	0.388	0.447	0.415	0.427	0.387	0.439	0.378	0.430
Ca	0.003	0.001	0.002	0.002	0.001	0.001	0.001	0.003	0.001
Ba	-	-	-	-	-	-	-	-	-
Na	-	-	0.001	0.000	0.001	-	0.001	0.000	-
K	-	-	0.000	-	-	-	-	-	-
V	-	-	-	-	-	-	-	-	-
sum	2.000	2.000	1.998	1.999	1.998	2.000	1.998	1.999	2.000

Table 10 continued

Intrusion	PK150	PK150	PK150	PK150	PK150	PK150	PK150	PK150	PK150	PK150
Sample	44803	44803	44803	44803	47513	47513	47513	47513	39249b	39249b
					rim	rim	rim	rim	rim	rim
Major element analysis (wt%)										
Nb_2O_5	0.04	0.14	0.04	0.10	n.a.	0.10	0.14	0.15	bld	bld
SiO_2	bld	0.01	bld	bld	0.04	0.02	0.10	0.06	0.08	0.03
TiO_2	52.60	50.43	53.08	53.19	41.45	42.11	43.46	43.31	50.44	51.61
ZnO	bld	bld	bld	bld	n.a.	n.a.	n.a.	n.a.	0.08	0.06
Al_2O_3	0.73	0.71	0.72	0.70	0.43	0.46	0.58	0.53	0.49	0.69
Cr_2O_3	2.19	0.63	1.75	1.65	0.93	0.58	0.69	1.10	1.72	2.31
FeO	24.58	24.11	25.10	25.60	25.70	27.83	29.52	29.42	27.16	26.93
Fe_2O_3	4.66	8.70	4.15	3.88	20.99	18.64	15.16	14.08	7.83	6.27
NiO	0.06	0.07	0.08	0.07	0.03	0.02	n.a.	n.a.	0.14	0.09
MnO	0.79	3.26	0.94	0.85	6.61	6.82	7.03	7.44	2.5	1.16
MgO	12.13	9.97	11.97	11.86	2.68	1.77	1.43	1.17	8.31	10.15
CaO	0.04	0.05	0.05	0.05	0.06	0.04	0.09	0.07	0.59	0.10
BaO	0.02	bld	0.03	0.02	0.02	n.a.	n.a.	0.06	n.a.	n.a.
Na_2O	0.05	0.05	0.06	0.05	0.01	0.01	0.02	0.01	bld	bld
K_2O	bld	0.00	bld	bld	n.a.	n.a.	n.a.	n.a.	bld	bld
V_2O_5	0.18	0.21	0.12	0.14	0.05	0.08	0.00	0.01	n.a.	n.a.
Total	98.05	98.32	98.08	98.15	99.01	98.48	98.21	97.42	99.34	99.40
Number of cations (apfu) on the basis of 3 oxygen atoms and 2 cations										
Nb	0.000	0.002	0.001	0.001	-	0.001	0.002	0.002	-	-
Si	-	0.000	-	-	0.001	0.000	0.003	0.002	0.002	0.001
Ti	0.927	0.902	0.936	0.939	0.784	0.806	0.834	0.840	0.905	0.913
Zn	-	-	-	-	-	-	-	-	0.001	0.001
Al	0.020	0.020	0.020	0.019	0.013	0.014	0.017	0.016	0.014	0.019
Cr	0.040	0.012	0.032	0.031	0.019	0.012	0.014	0.023	0.032	0.043
Fe^{2+}	0.481	0.479	0.492	0.502	0.540	0.592	0.630	0.634	0.542	0.529
Fe^{3+}	0.082	0.156	0.073	0.068	0.397	0.357	0.291	0.273	0.141	0.111
Ni	0.001	0.001	0.002	0.001	0.001	0.000	-	-	0.003	0.002
Mn	0.016	0.066	0.019	0.017	0.141	0.147	0.152	0.162	0.050	0.023
Mg	0.424	0.353	0.418	0.415	0.101	0.067	0.054	0.045	0.295	0.356
Ca	0.001	0.001	0.001	0.001	0.001	0.001	0.002	0.002	0.015	0.003
Ba	0.000	-	0.000	0.000	0.000	-	-	0.001	-	-
Na	0.001	0.001	0.001	0.001	0.000	0.000	0.000	0.000	-	-
K	-	0.000	-	-	-	-	-	-	-	-
V	0.003	0.004	0.002	0.003	0.001	0.001	0.000	0.000	-	-
sum	1.996	1.998	1.997	1.998	1.999	1.998	1.999	2.000	2.000	2.000

Table 10 continued

Intrusion	PK346	PK346	PK346	PK346	PK346	PK346	PK346	PK346	PK346
Sample	44848a	44848a	44848a	44848a	44848a	44848a	44848a	44848a	44848a
Major element analysis (wt%)									
Nb_2O_5	n.a.	n.a.	n.a.	n.a.	n.a.	n.a.	n.a.	n.a.	n.a.
SiO_2	0.03	bld	0.03	0.01	0.18	bld	bld	0.035	bld
TiO_2	50.73	51.05	46.30	46.26	50.32	46.80	49.68	46.65	52.33
ZnO	bld	bld	bld	0.01	bld	bld	bld	bld	bld
Al_2O_3	0.45	0.35	0.43	0.43	0.03	0.41	0.53	0.45	0.32
Cr_2O_3	0.15	0.15	0.14	0.15	0.03	0.16	0.14	0.14	0.14
FeO	24.74	24.07	32.44	27.45	45.12	30.41	22.87	28.12	20.58
Fe_2O_3	11.12	11.87	11.71	17.52	0.86	13.11	14.43	13.12	11.18
NiO	0.045	0.03	bld	0.03	bld	0.03	0.03	0.045	0.04
MnO	0.42	0.46	0.27	0.28	1.17	0.32	0.44	0.31	0.59
MgO	11.56	11.26	7.68	7.42	0.06	8.04	11.22	9.71	14.00
CaO	0.05	0.05	0.01	0.02	0.26	0.02	0.04	0.02	0.07
BaO	n.a.	n.a.	n.a.	n.a.	n.a.	n.a.	n.a.	n.a.	n.a.
Na_2O	0.04	0.08	0.04	0.02	0	0	0.06	0.015	0.08
K_2O	n.a.	n.a.	n.a.	n.a.	n.a.	n.a.	n.a.	n.a.	n.a.
V_2O_5	n.a.	n.a.	n.a.	n.a.	n.a.	n.a.	n.a.	n.a.	n.a.
Total	99.33	99.37	99.05	99.58	98.04	99.30	99.44	98.60	99.33
Number of cations (apfu) on the basis of 3 oxygen atoms and 2 cations									
Nb	-	-	-	-	-	-	-	-	-
Si	0.001	-	0.001	0.000	0.005	-	-	0.001	-
Ti	0.892	0.897	0.851	0.838	0.977	0.853	0.873	0.847	0.903
Zn	-	-	-	0.000	-	-	-	-	-
Al	0.012	0.010	0.012	0.012	0.001	0.012	0.015	0.013	0.009
Cr	0.003	0.003	0.003	0.003	0.001	0.003	0.003	0.003	0.003
Fe^{2+}	0.484	0.470	0.663	0.552	0.974	0.616	0.447	0.567	0.395
Fe^{3+}	0.196	0.209	0.215	0.317	0.017	0.239	0.253	0.238	0.193
Ni	0.001	0.001	-	0.001	-	0.001	0.001	0.001	0.001
Mn	0.008	0.009	0.006	0.006	0.026	0.007	0.009	0.006	0.011
Mg	0.403	0.392	0.280	0.266	0.002	0.290	0.391	0.349	0.478
Ca	0.001	0.001	0.000	0.000	0.007	0.001	0.001	0.001	0.002
Ba	-	-	-	-	-	-	-	-	-
Na	0.000	0.001	0.000	0.000	-	-	0.001	0.000	0.001
K	-	-	-	-	-	-	-	-	-
V	-	-	-	-	-	-	-	-	-
sum	2.001	1.992	2.033	1.996	2.009	2.021	1.991	2.026	1.994

Table 10 continued

Intrusion	PK346	PK346	PK346	PK346	PK346	PK346	PK346	PK346	PK346
Sample	44848a	44848a	44848a	44848a	44848a	44848a	44848a	44848a	44848a
Major element analysis (wt%)									
Nb_2O_5	n.a.	n.a.	n.a.	n.a.	n.a.	n.a.	n.a.	n.a.	n.a.
SiO_2	bld	0.07	0.05	0.06	0.06	0.03	0.06	0.03	0.06
TiO_2	49.21	48.42	51.99	51.04	49.82	49.46	50.44	49.24	52.53
ZnO	0.015	bld	bld	0.03	bld	0.02	bld	bld	bld
Al_2O_3	0.75	0.75	0.68	0.81	0.58	0.56	0.72	0.44	0.44
Cr_2O_3	0.63	0.86	1.31	0.40	0.31	0.30	0.50	0.31	1.71
FeO	23.29	24.03	22.61	23.92	22.35	23.51	22.22	24.85	20.06
Fe_2O_3	12.30	13.16	9.12	10.79	13.42	13.64	12.19	13.17	8.91
NiO	0.08	0.07	0.095	0.11	0.08	0.09	0.08	0.1	0.05
MnO	0.45	0.44	0.46	0.34	0.44	0.38	0.45	0.29	0.66
MgO	12.20	11.22	13.08	12.09	12.31	11.49	12.59	10.70	14.59
CaO	0.05	0.04	0.05	0.03	0.06	0.04	0.05	0.03	0.06
BaO	n.a.	n.a.	n.a.	n.a.	n.a.	n.a.	n.a.	n.a.	n.a.
Na_2O	0.04	0.08	0.06	0	0	0	0.04	0	0.1
K_2O	n.a.	n.a.	n.a.	n.a.	n.a.	n.a.	n.a.	n.a.	n.a.
V_2O_5	n.a.	n.a.	n.a.	n.a.	n.a.	n.a.	n.a.	n.a.	n.a.
Total	99.00	99.14	99.49	99.62	99.41	99.52	99.34	99.14	99.17
Number of cations (apfu) on the basis of 3 oxygen atoms and 2 cations									
Nb	-	-	-	-	-	-	-	-	-
Si	-	0.002	0.001	0.001	0.001	0.001	0.001	0.001	0.001
Ti	0.866	0.857	0.900	0.890	0.871	0.869	0.879	0.873	0.903
Zn	0.000	-	-	0.001	-	0.000	-	-	-
Al	0.021	0.021	0.018	0.022	0.016	0.015	0.020	0.012	0.012
Cr	0.012	0.016	0.024	0.007	0.006	0.006	0.009	0.006	0.031
Fe^{2+}	0.456	0.473	0.435	0.464	0.434	0.459	0.430	0.490	0.383
Fe^{3+}	0.217	0.233	0.158	0.188	0.235	0.240	0.212	0.234	0.153
Ni	0.002	0.001	0.002	0.002	0.001	0.002	0.001	0.002	0.001
Mn	0.009	0.009	0.009	0.007	0.009	0.008	0.009	0.006	0.013
Mg	0.425	0.393	0.449	0.418	0.426	0.400	0.435	0.376	0.497
Ca	0.001	0.001	0.001	0.001	0.001	0.001	0.001	0.001	0.001
Ba	-	-	-	-	-	-	-	-	-
Na	0.000	0.001	0.001	-	-	-	0.000	-	0.001
K	-	-	-	-	-	-	-	-	-
V	-	-	-	-	-	-	-	-	-
sum	2.009	2.006	1.998	2.000	2.000	2.000	1.999	2.000	1.997

Table 10 continued

Intrusion	PK346	PK346	PK346	PK346	PK346	PK346	PK346	PK346	PK346
Sample	44848b	44848b	44848b	44848b	44848b	44848b	44848b	44848b	44848b
Major element analysis (wt%)									
Nb_2O_5	n.a.	n.a.	n.a.	n.a.	n.a.	n.a.	n.a.	n.a.	n.a.
SiO_2	bld	0.05	0.11	0.02	bld	0.03	0.04	0.08	0.02
TiO_2	51.16	50.10	51.77	51.73	50.16	48.55	50.95	51.84	50.93
ZnO	bld	bld	bld	bld	bld	bld	bld	bld	bld
Al_2O_3	0.64	0.60	0.33	0.68	0.79	0.51	0.65	0.32	0.74
Cr_2O_3	1.05	0.69	3.68	2.11	0.51	0.28	0.36	1.99	1.25
FeO	23.37	24.88	18.19	23.20	21.75	23.93	22.90	20.36	22.53
Fe_2O_3	10.30	11.58	9.32	8.03	12.48	14.36	11.77	10.30	10.33
NiO	0.1	0.12	0.06	0.1	0.05	0.07	0.09	0.04	0.09
MnO	0.41	0.23	0.68	0.41	0.52	0.31	0.38	0.64	0.43
MgO	12.38	11.14	15.26	12.78	12.51	10.86	12.49	14.10	12.66
CaO	0.06	0.03	0.04	0.05	0.06	0.03	0.05	0.07	0.04
BaO	n.a.	n.a.	n.a.	n.a.	n.a.	n.a.	n.a.	n.a.	n.a.
Na_2O	0	0	0.11	bld	0.09	bld	0.04	0.1	0.04
K_2O	n.a.	n.a.	n.a.	n.a.	n.a.	n.a.	n.a.	n.a.	n.a.
V_2O_5	n.a.	n.a.	n.a.	n.a.	n.a.	n.a.	n.a.	n.a.	n.a.
Total	99.46	99.42	99.55	99.11	98.92	98.93	99.72	99.83	99.05
Number of cations (apfu) on the basis of 3 oxygen atoms and 2 cations									
Nb	-	-	-	-	-	-	-	-	-
Si	-	0.001	0.002	0.000	-	0.001	0.001	0.002	0.000
Ti	0.892	0.882	0.883	0.901	0.877	0.862	0.885	0.890	0.889
Zn	-	-	-	-	-	-	-	-	-
Al	0.017	0.017	0.009	0.019	0.022	0.014	0.018	0.009	0.020
Cr	0.019	0.013	0.066	0.039	0.009	0.005	0.007	0.036	0.023
Fe^{2+}	0.453	0.487	0.345	0.449	0.423	0.472	0.442	0.388	0.437
Fe^{3+}	0.180	0.204	0.159	0.140	0.218	0.255	0.205	0.177	0.180
Ni	0.002	0.002	0.001	0.002	0.001	0.001	0.002	0.001	0.002
Mn	0.008	0.005	0.013	0.008	0.010	0.006	0.007	0.012	0.008
Mg	0.428	0.389	0.516	0.441	0.434	0.382	0.430	0.480	0.438
Ca	0.001	0.001	0.001	0.001	0.001	0.001	0.001	0.002	0.001
Ba	-	-	-	-	-	-	-	-	-
Na	-	-	0.001	-	0.001	-	0.000	0.001	0.000
K	-	-	-	-	-	-	-	-	-
V	-	-	-	-	-	-	-	-	-
sum	2.000	2.000	1.996	2.000	1.997	2.000	1.999	1.997	1.999

Table 10 continued

Intrusion	PK346	PK346	PK346	PK346	PK346	PK346	PK346	PK346	PK346
Sample	44848b	44834a	44834a	44834b	44834b	44834b	44834b	44834b	44834b
Major element analysis (wt%)									
Nb_2O_5	n.a.	n.a.	n.a.	n.a.	n.a.	n.a.	n.a.	n.a.	n.a.
SiO_2	0.03	bld	0.04	bld	0.06	0.02	0.06	0.03	0.03
TiO_2	49.90	49.98	51.05	41.34	50.41	46.41	52.03	50.69	51.36
ZnO	bld	n.a.	n.a.	bld	bld	0.015	bld	bld	bld
Al_2O_3	0.765	0.53	0.515	0.375	0.68	0.61	0.87	0.695	0.67
Cr_2O_3	0.57	0.5	0.88	0.165	0.765	0.31	0.85	0.45	0.5
FeO	23.59	25.18	22.21	34.28	21.82	29.95	23.24	22.55	22.36
Fe_2O_3	12.10	12.18	11.45	16.31	13.58	12.33	9.56	12.23	11.76
NiO	0.12	0.08	0.07	bld	0.10	0.10	0.10	0.09	0.08
MnO	0.32	0.24	0.49	0.23	0.37	0.20	0.44	0.42	0.46
MgO	11.69	10.90	12.83	5.46	11.94	9.27	12.44	12.14	12.47
CaO	0.05	0.02	0.07	0.01	0.05	0.02	0.06	0.07	0.10
BaO	n.a.	bld	bld	n.a.	n.a.	n.a.	n.a.	n.a.	n.a.
Na_2O	bld	bld	0.055	bld	bld	bld	0.08	bld	0.035
K_2O	n.a.	n.a.	n.a.	n.a.	n.a.	n.a.	n.a.	n.a.	n.a.
V_2O_5	n.a.	n.a.	n.a.	n.a.	n.a.	n.a.	n.a.	n.a.	n.a.
Total	99.11	99.61	99.64	98.17	99.75	99.22	99.74	99.34	99.81
Number of cations (apfu) on the basis of 3 oxygen atoms and 2 cations									
Nb	-	-	-	-	-	-	-	-	-
Si	0.001	-	0.001	-	0.001	0.000	0.001	0.001	0.001
Ti	0.877	0.881	0.886	0.787	0.876	0.842	0.901	0.885	0.890
Zn	-	-	-	-	-	0.000	-	-	-
Al	0.021	0.015	0.014	0.011	0.019	0.017	0.024	0.019	0.018
Cr	0.011	0.009	0.016	0.003	0.014	0.006	0.015	0.008	0.009
Fe^{2+}	0.461	0.493	0.428	0.726	0.421	0.604	0.447	0.437	0.431
Fe^{3+}	0.213	0.215	0.199	0.311	0.236	0.224	0.166	0.213	0.204
Ni	0.002	0.002	0.001	-	0.002	0.002	0.002	0.002	0.001
Mn	0.006	0.005	0.010	0.005	0.007	0.004	0.009	0.008	0.009
Mg	0.407	0.381	0.441	0.206	0.411	0.333	0.427	0.420	0.428
Ca	0.001	0.001	0.002	0.000	0.001	0.001	0.001	0.002	0.002
Ba	-	-	-	-	-	-	-	-	-
Na	-	-	0.001	-	-	-	0.001	-	0.000
K	-	-	-	-	-	-	-	-	-
V	-	-	-	-	-	-	-	-	-
sum	2.000	2.000	1.998	2.052	1.988	2.035	1.994	1.994	1.993

Table 10 continued

Intrusion	PK346	PK346	PK346	PK346	PK346	PK346	PK346	PK346	PK346	PK346
Sample	44834b	44838	44838	44838	44838	44838	44838	44860	44860	44860
Major element analysis (wt%)										
Nb_2O_5	n.a.	0.15	0.48	0.26	0.17	0.18	0.17	0.26	0.23	0.16
SiO_2	bld	0.0076	bld	bld	0.00	0.001	0.26	bld	bld	0.05
TiO_2	50.08	49.78	42.36	47.03	49.64	48.87	48.76	47.48	52.47	49.71
ZnO	0.02	bld	bld	bld	bld	bld	bld	bld	bld	bld
Al_2O_3	0.58	0.62	0.37	0.52	0.80	0.98	0.55	0.45	0.27	0.56
Cr_2O_3	4.86	0.36	0.45	0.15	0.42	0.40	0.21	0.24	2.01	0.26
FeO	22.53	25.55	25.68	27.76	25.01	24.77	27.08	27.33	24.38	26.60
Fe_2O_3	8.82	10.96	21.32	14.41	10.80	12.12	11.55	14.01	6.58	10.40
NiO	0.09	0.10	0.04	0.02	0.07	0.09	0.05	0.05	0.03	0.06
MnO	0.35	0.25	0.21	0.27	0.33	0.21	0.27	0.25	0.59	0.30
MgO	11.93	10.63	7.06	8.10	10.83	10.66	9.43	8.54	11.75	9.98
CaO	0.04	0.02	0.00	0.01	0.04	0.02	0.02	0.01	0.06	0.02
BaO	n.a.	0.02	0.04	bld	0.03	bld	0.05	0.03	0.03	0.02
Na_2O	bld	0.02	0.02	0.02	0.02	0.01	0.02	0.03	0.31	0.04
K_2O	n.a.	bld	0.00	0.00	bld	bld	bld	bld	bld	bld
V_2O_5	n.a.	0.17	0.21	0.16	0.18	0.22	0.22	0.12	0.09	0.22
Total	99.28	98.63	98.25	98.72	98.35	98.53	98.66	98.78	98.81	98.37
Number of cations (apfu) on the basis of 3 oxygen atoms and 2 cations										
Nb	-	0.002	0.005	0.003	0.002	0.002	0.002	0.003	0.002	0.002
Si	-	0.000	-	-	0.000	0.000	0.006	-	-	0.001
Ti	0.875	0.886	0.783	0.854	0.884	0.869	0.875	0.859	0.922	0.891
Zn	0.000	-	-	-	-	-	-	-	-	-
Al	0.016	0.017	0.011	0.015	0.022	0.027	0.016	0.013	0.007	0.016
Cr	0.089	0.007	0.009	0.003	0.008	0.007	0.004	0.004	0.037	0.005
Fe^{2+}	0.438	0.505	0.528	0.560	0.495	0.490	0.540	0.550	0.476	0.530
Fe^{3+}	0.154	0.195	0.394	0.262	0.192	0.216	0.207	0.254	0.116	0.186
Ni	0.002	0.002	0.001	0.000	0.001	0.002	0.001	0.001	0.001	0.001
Mn	0.007	0.005	0.004	0.005	0.007	0.004	0.005	0.005	0.012	0.006
Mg	0.413	0.375	0.258	0.292	0.382	0.376	0.335	0.306	0.409	0.354
Ca	0.001	0.000	0.000	0.000	0.001	0.001	0.001	0.000	0.001	0.000
Ba	-	0.000	0.000	-	0.000	-	0.000	0.000	0.000	0.000
Na	-	0.000	0.000	0.000	0.000	0.000	0.000	0.000	0.003	0.000
K	-	-	0.000	0.000	-	-	-	-	-	-
V	-	0.003	0.004	0.003	0.003	0.004	0.004	0.002	0.002	0.004
sum	1.995	1.997	1.999	1.997	1.997	2.000	1.996	1.998	1.990	1.999

Table 10 continued

Intrusion	PK346	PK346	PK346	PK346	PK346	PK346	PK346	PK346	PK346
Sample	44860	44860	44860	44864	44864	44864	44864	44848a rim	44848a rim
Major element analysis (wt%)									
Nb_2O_5	0.19	0.09	0.19	0.21	0.08	0.15	0.20	n.a.	n.a.
SiO_2	bld	0.0342	bld	bld	0.07	0.04	bld	0.18	0.07
TiO_2	49.60	46.89	47.92	49.15	52.41	50.19	52.57	50.60	51.55
ZnO	bld	bld	bld	n.a.	n.a.	n.a.	bld	bld	bld
Al_2O_3	0.57	0.48	0.52	0.43	0.48	0.52	0.42	bld	bld
Cr_2O_3	0.61	0.13	0.49	0.46	1.13	0.36	1.95	0.05	0.42
FeO	25.06	25.37	26.02	24.70	20.45	24.75	20.16	43.12	45.25
Fe_2O_3	10.80	15.74	12.85	14.20	10.22	12.60	7.41	2.22	0.08
NiO	0.09	0.03	0.05	0.09	0.065	0.09	0.03	bld	bld
MnO	0.24	0.28	0.28	0.32	0.63	0.26	0.64	2.00	1.07
MgO	10.82	8.83	9.42	10.7	14.43	11.25	14.73	0.14	0.04
CaO	0.01	0.01	0.02	0.02	0.05	0.03	0.04	0.08	0.04
BaO	0.02	0.12	0.04	bld	bld	bld	0.07	n.a.	n.a.
Na_2O	0.03	0.17	0.03	bld	0.07	bld	0.07	0.05	bld
K_2O	bld	0.01	bld	bld	bld	bld	0.00	n.a.	n.a.
V_2O_5	0.15	0.19	0.20	n.a.	n.a.	n.a.	0.20	n.a.	n.a.
Total	98.19	98.37	98.03	100.28	100.08	100.24	98.49	98.44	98.52
Number of cations (apfu) on the basis of 3 oxygen atoms and 2 cations									
Nb	0.002	0.001	0.002	0.002	0.001	0.002	0.002	-	-
Si	-	0.001	-	-	0.002	0.001	-	0.005	0.002
Ti	0.885	0.849	0.867	0.863	0.895	0.877	0.909	0.975	0.993
Zn	-	-	-	-	-	-	-	-	-
Al	0.016	0.014	0.015	0.012	0.013	0.014	0.011	-	-
Cr	0.011	0.002	0.009	0.008	0.020	0.007	0.035	0.001	0.009
Fe^{2+}	0.497	0.511	0.523	0.482	0.388	0.481	0.387	0.923	0.969
Fe^{3+}	0.193	0.285	0.233	0.249	0.175	0.220	0.128	0.043	0.001
Ni	0.002	0.001	0.001	0.002	0.001	0.002	0.001	-	-
Mn	0.005	0.006	0.006	0.006	0.012	0.005	0.012	0.043	0.023
Mg	0.383	0.317	0.338	0.372	0.488	0.390	0.504	0.005	0.002
Ca	0.000	0.000	0.000	0.001	0.001	0.001	0.001	0.002	0.001
Ba	0.000	0.001	0.000	-	-	-	0.001	-	-
Na	0.000	0.002	0.000	-	0.001	-	0.001	0.001	-
K	-	0.000	-	-	-	-	0.000	-	-
V	0.003	0.004	0.004	-	-	-	0.004	-	-
sum	1.999	1.994	1.999	1.998	1.997	1.999	1.998	1.998	2.000

Table 10 continued

Intrusion	PK346	PK346	PK346	PK346	PK346	PK346	PK346	PK346	PK346
Sample	44848b	44848b	44848b	44834b	44834b	44834b	44834b	44838	44838
	rim	rim	rim	rim	rim	rim	rim	rim	rim
Major element analysis (wt%)									
Nb_2O_5	n.a.	n.a.	n.a.	n.a.	n.a.	n.a.	n.a.	0.55	0.27
SiO_2	0.10	0.10	0.19	0.29	0.11	0.24	0.04	n.a.	0.06
TiO_2	51.52	51.86	51.40	50.92	51.26	51.77	51.14	51.30	51.01
ZnO	bld	bld	bld	n.a.	bld	bld	bld	n.a.	n.a.
Al_2O_3	bld	bld	bld	bld	bld	bld	0.02	0.03	0.03
Cr_2O_3	0.32	0.45	0.06	0.06	0.35	0.37	0.46	0.97	0.66
FeO	44.80	45.22	45.08	43.71	43.82	44.65	44.68	44.00	43.65
Fe_2O_3	0.59	0.21	0.43	1.86	1.56	0.05	1.21	0.18	1.12
NiO	bld	bld	bld	n.a.	bld	bld	bld	n.a.	n.a.
MnO	1.20	1.10	1.08	1.01	1.77	1.07	1.14	1.35	1.95
MgO	0.05	0.06	0.03	0.06	0.07	0.17	0.12	0.54	0.05
CaO	0.03	0.04	0.04	0.63	0.31	0.06	bld	0.03	0.15
BaO	n.a.	n.a.	n.a.	0.58	n.a.	n.a.	n.a.	0.05	0.11
Na_2O	0.07	0.06	0.04	0.03	0.025	0.16	bld	0.08	0.05
K_2O	n.a.	n.a.	n.a.	0.03	n.a.	n.a.	n.a.	n.a.	0.01
V_2O_5	n.a.	n.a.	n.a.	n.a.	n.a.	n.a.	n.a.	0.02	n.a.
Total	98.68	99.10	98.35	99.19	99.25	98.55	98.81	99.08	99.11
Number of cations (apfu) on the basis of 3 oxygen atoms and 2 cations									
Nb	-	-	-	-	-	-	-	0.006	0.003
Si	0.003	0.003	0.005	0.007	0.003	0.006	0.001	-	0.002
Ti	0.990	0.992	0.991	0.975	0.980	0.994	0.982	0.980	0.978
Zn	-	-	-	-	-	-	-	-	-
Al	-	-	-	-	-	-	0.001	0.001	0.001
Cr	0.006	0.009	0.001	0.001	0.007	0.007	0.009	0.019	0.013
Fe^{2+}	0.957	0.962	0.967	0.931	0.931	0.953	0.954	0.935	0.930
Fe^{3+}	0.011	0.004	0.008	0.036	0.030	0.001	0.023	0.003	0.021
Ni	-	-	-	-	-	-	-	-	-
Mn	0.026	0.024	0.023	0.022	0.038	0.023	0.025	0.029	0.042
Mg	0.002	0.002	0.001	0.002	0.002	0.006	0.005	0.020	0.002
Ca	0.001	0.001	0.001	0.017	0.008	0.002	-	0.001	0.004
Ba	-	-	-	0.006	-	-	-	0.000	0.001
Na	0.001	0.001	0.000	0.000	0.000	0.002	-	0.001	0.001
K	-	-	-	0.000	-	-	-	-	0.000
V	-	-	-	-	-	-	-	0.000	-
sum	1.997	1.998	1.999	1.998	1.999	1.994	2.000	1.997	1.998

Table 10 continued

Intrusion	PK346	PK346	PK346	PK346	PK346	PK151	PK151	PK151	PK151	PK151
Sample	44838	44838	44838	44838	44838	47514	47514	47514	47514	47514
	rim	rim	rim	rim	rim					
Major element analysis (wt%)										
Nb_2O_5	0.48	0.02	0.41	0.51	0.67	0.23	0.01	0.01	0.02	0.13
SiO_2	0.03	0.01	0.00	0.18	0.06	bld	bld	bld	bld	bld
TiO_2	50.65	51.17	51.27	50.42	50.65	45.83	46.31	49.46	46.14	51.98
ZnO	n.a.	n.a.	n.a.	n.a.	n.a.	bld	bld	0.02	bld	0.09
Al_2O_3	0.04	0.02	0.02	0.04	0.03	0.66	0.61	0.85	0.68	0.69
Cr_2O_3	1.64	0.01	0.78	1.04	0.81	2.35	5.09	4.12	3.78	1.69
FeO	43.43	43.46	43.80	44.27	44.71	33.34	30.26	27.26	35.67	23.95
Fe_2O_3	0.54	2.09	0.10	0.24	0.04	10.47	8.51	6.07	7.44	7.23
NiO	n.a.	n.a.	n.a.	n.a.	n.a.	0.02	0.03	0.07	0.05	0.10
MnO	1.12	1.78	1.08	1.03	1.09	1.42	1.57	0.88	1.80	1.72
MgO	0.53	0.07	0.61	0.15	0.06	3.58	5.29	9.01	1.87	11.74
CaO	0.08	0.40	0.04	0.03	0.03	0.14	0.18	0.08	0.41	0.08
BaO	0.04	0.04	0.13	0.24	0.09	bld	0.03	bld	bld	bld
Na_2O	0.10	0.02	0.10	0.08	0.06	0.03	0.03	0.02	0.03	bld
K_2O	0.01	0.02	0.00	0.01	0.02	bld	bld	0.00	bld	bld
V_2O_5	0.03	n.a.	0.02	0.01	n.a.	0.16	0.11	0.15	0.13	n.a.
Total	98.72	99.10	98.35	98.25	98.32	98.21	98.02	98.01	98.01	99.40
Number of cations (apfu) on the basis of 3 oxygen atoms and 2 cations										
Nb	0.006	0.000	0.005	0.006	0.008	0.003	0.000	0.000	0.000	0.001
Si	0.001	0.000	0.000	0.005	0.001	-	-	-	-	-
Ti	0.971	0.980	0.986	0.975	0.980	0.863	0.861	0.892	0.880	0.910
Zn	-	-	-	-	-	-	-	0.000	-	0.002
Al	0.001	0.001	0.001	0.001	0.001	0.019	0.018	0.024	0.020	0.019
Cr	0.033	0.000	0.016	0.021	0.016	0.047	0.100	0.078	0.076	0.031
Fe^{2+}	0.925	0.925	0.936	0.951	0.961	0.698	0.625	0.547	0.756	0.466
Fe^{3+}	0.010	0.040	0.002	0.005	0.001	0.197	0.158	0.110	0.142	0.127
Ni	-	-	-	-	-	0.000	0.001	0.001	0.001	0.002
Mn	0.024	0.038	0.023	0.023	0.024	0.030	0.033	0.018	0.039	0.034
Mg	0.020	0.003	0.023	0.006	0.002	0.134	0.195	0.322	0.071	0.407
Ca	0.002	0.011	0.001	0.001	0.001	0.004	0.005	0.002	0.011	0.002
Ba	0.000	0.000	0.001	0.002	0.001	-	0.000	-	-	-
Na	0.001	0.000	0.001	0.001	0.001	0.000	0.000	0.000	0.000	-
K	0.000	0.000	0.000	0.000	0.000	-	-	0.000	-	-
V	0.001	-	0.000	0.000	-	0.003	0.002	0.003	0.003	-
sum	1.996	1.999	1.996	1.997	1.997	1.997	1.998	1.999	1.999	2.000

Table 10 continued

Intrusion	PK151	PK151	PK151	PK151	PK151	PK151	PK151	PK151	PK151	PK151
Sample	47514	47514	47514	47514	47514	47514	47514	47514	47514	47514
Major element analysis (wt%)										
Nb_2O_5	bld	bld	bld	bld	bld	bld	bld	bld	bld	bld
SiO_2	0.03	0.07	0.03	0.07	0.03	bld	0.06	0.03	bld	0.03
TiO_2	49.43	50.71	49.56	48.69	50.07	50.38	51.24	50.83	49.54	50.17
ZnO	bld	0.06	0.02	0.04	0.04	0.06	bld	bld	0.03	bld
Al_2O_3	0.61	0.60	0.84	0.51	0.55	0.62	0.89	0.56	0.52	0.66
Cr_2O_3	2.03	3.14	1.335	3.85	3.83	3.32	0.49	0.79	3.3	2.9
FeO	30.94	23.75	29.83	28.85	23.89	22.95	24.24	24.82	28.63	31.25
Fe_2O_3	7.91	7.65	8.10	7.63	8.17	7.74	9.75	10.39	7.40	5.72
NiO	0.06	0.09	0.07	0.06	0.09	0.10	0.14	0.13	0.06	0.11
MnO	1.58	1.61	1.84	1.80	1.33	2.70	0.31	0.26	1.56	1.28
MgO	6.54	11.04	7.085	7.17	10.98	10.86	11.99	11.52	7.96	6.97
CaO	0.14	0.21	0.10	0.12	0.11	0.10	0.03	0.03	0.06	0.07
BaO	bld	bld	bld	bld	bld	bld	bld	bld	bld	bld
Na_2O	0.02	0.05	0.02	0.04	bld	bld	0.02	bld	bld	bld
K_2O	bld	bld	bld	bld	bld	bld	bld	bld	bld	bld
V_2O_5	n.a.	n.a.	n.a.	n.a.	n.a.	n.a.	n.a.	n.a.	n.a.	n.a.
Total	99.27	98.98	98.81	98.82	99.10	98.83	99.14	99.34	99.06	99.16
Number of cations (apfu) on the basis of 3 oxygen atoms and 2 cations										
Nb	-	-	-	-	-	-	-	-	-	-
Si	0.001	0.002	0.001	0.002	0.001	-	0.001	0.001	-	0.001
Ti	0.900	0.895	0.901	0.886	0.884	0.892	0.897	0.893	0.895	0.910
Zn	-	0.001	0.000	0.001	0.001	0.001	-	-	0.001	-
Al	0.017	0.017	0.024	0.015	0.015	0.017	0.024	0.015	0.015	0.019
Cr	0.039	0.058	0.026	0.074	0.071	0.062	0.009	0.015	0.063	0.055
Fe^{2+}	0.626	0.466	0.603	0.583	0.469	0.452	0.472	0.485	0.575	0.630
Fe^{3+}	0.144	0.135	0.147	0.139	0.144	0.137	0.171	0.183	0.134	0.104
Ni	0.001	0.002	0.001	0.001	0.002	0.002	0.003	0.002	0.001	0.002
Mn	0.032	0.032	0.038	0.037	0.026	0.054	0.006	0.005	0.032	0.026
Mg	0.236	0.386	0.255	0.258	0.384	0.381	0.416	0.401	0.285	0.251
Ca	0.004	0.005	0.002	0.003	0.003	0.003	0.001	0.001	0.002	0.002
Ba	-	-	-	-	-	-	-	-	-	-
Na	0.000	0.001	0.000	0.000	-	-	0.000	-	-	-
K	-	-	-	-	-	-	-	-	-	-
V	-	-	-	-	-	-	-	-	-	-
sum	1.999	1.998	1.999	1.999	2.000	2.000	1.999	2.000	2.000	2.000

Table 10 continued

Intrusion	PK151	PK151	PK151	PK151	PK151	PK151	PK151	PK151	PK151	PK151
Sample	47514	47514	47514	47514	47514	47514	47514	47514	47514 rim	47514 rim
Major element analysis (wt%)										
Nb_2O_5	bld	bld	bld	bld	bld	0.09	0.23	bld	bld	bld
SiO_2	0.04	0.07	0.09	bld	bld	0.01	bld	bld	bld	bld
TiO_2	51.01	48.66	51.34	51.81	50.13	50.55	45.44	47.19	47.69	47.76
ZnO	bld	0.04	0.05	0.05	bld	0.06	bld	0.01	0.04	bld
Al_2O_3	1.11	0.51	0.94	0.54	0.57	0.47	0.65	0.87	0.47	0.47
Cr_2O_3	0.89	4.02	1.655	2.27	2.09	2.86	0.08	6.25	2.63	3.93
FeO	24.19	25.70	23.85	23.38	29.96	26.25	26.02	25.97	32.30	28.22
Fe_2O_3	9.81	8.86	7.89	7.19	7.39	7.37	16.13	7.50	9.02	9.22
NiO	0.12	0.06	0.10	0.09	0.09	0.07	0.07	0.09	0.07	0.06
MnO	0.35	2.47	1.54	1.86	1.68	1.77	0.31	1.14	1.79	2.03
MgO	11.92	8.54	11.49	11.81	7.28	9.72	8.21	8.44	4.58	7.02
CaO	0.02	0.08	0.11	0.07	0.07	0.08	0.01	0.10	0.15	0.09
BaO	bld	bld	bld	bld	bld	bld	bld	bld	bld	bld
Na_2O	bld	0.05	0.03	0.02	0.06	bld	0.02	0.02	0.07	bld
K_2O	bld	bld	bld	bld	bld	bld	bld	bld	bld	bld
V_2O_5	n.a.	n.a.	n.a.	n.a.	n.a.	n.a.	0.16	0.17	n.a.	n.a.
Total	99.46	99.07	99.07	99.07	99.32	99.28	97.32	97.74	97.91	97.88
Number of cations (apfu) on the basis of 3 oxygen atoms and 2 cations										
Nb	-	-	-	-	-	0.001	0.003	-	-	-
Si	0.001	0.002	0.002	-	-	0.000	-	-	-	-
Ti	0.890	0.875	0.901	0.909	0.907	0.900	0.836	0.858	0.885	0.871
Zn	-	0.001	0.001	0.001	-	0.001	-	0.000	0.001	-
Al	0.030	0.014	0.026	0.015	0.016	0.013	0.019	0.025	0.014	0.013
Cr	0.016	0.076	0.031	0.042	0.040	0.053	0.002	0.119	0.051	0.075
Fe^{2+}	0.469	0.514	0.465	0.456	0.602	0.519	0.532	0.525	0.667	0.572
Fe^{3+}	0.171	0.159	0.139	0.126	0.134	0.131	0.297	0.136	0.168	0.168
Ni	0.002	0.001	0.002	0.002	0.002	0.001	0.001	0.002	0.001	0.001
Mn	0.007	0.050	0.030	0.037	0.034	0.035	0.006	0.023	0.037	0.042
Mg	0.412	0.304	0.399	0.410	0.261	0.343	0.299	0.304	0.168	0.254
Ca	0.000	0.002	0.003	0.002	0.002	0.002	0.000	0.003	0.004	0.002
Ba	-	-	-	-	-	-	-	-	-	-
Na	-	0.001	0.000	0.000	0.001	-	0.000	0.000	0.001	-
K	-	-	-	-	-	-	-	-	-	-
V	-	-	-	-	-	-	0.003	0.003	-	-
sum	2.000	1.998	1.999	1.999	1.998	2.000	1.997	1.997	1.997	2.000

Table 10 continued

Intrusion	PK151	PK312	PK312	PK312	PK312	PK312	PK312	PK312	PK312
Sample	47514 rim	47553b	47553b	47553b	47553b	47553b	47553b	47553b	47553b
Major element analysis (wt%)									
Nb_2O_5	bld	n.a.	n.a.	n.a.	n.a.	n.a.	n.a.	n.a.	bld
SiO_2	0.13	0.04	0.045	0.03	0.04	0.03	0.05	0.035	0.38
TiO_2	46.68	49.50	50.92	50.73	50.81	48.20	49.44	49.49	51.54
ZnO	bld	n.a.	n.a.	n.a.	n.a.	n.a.	n.a.	n.a.	n.a.
Al_2O_3	0.38	0.43	0.89	0.71	0.68	0.57	0.62	0.42	0.87
Cr_2O_3	2.96	0.46	1.15	1.68	1.90	0.39	0.65	0.44	1.79
FeO	36.65	25.22	23.65	22.65	22.30	25.50	26.18	24.83	21.44
Fe_2O_3	6.84	13.42	10.74	10.26	10.77	14.85	13.32	14.48	10.18
NiO	0.05	0.12	0.13	0.06	0.05	0.08	0.08	0.11	0.08
MnO	1.85	0.26	0.42	0.51	0.54	0.32	0.27	0.26	0.59
MgO	1.92	10.63	12.12	12.54	12.76	9.80	10.08	10.86	13.20
CaO	0.12	0.02	0.05	0.07	0.04	0.03	0.03	0.02	0.23
BaO	bld	bld	bld	bld	bld	bld	bld	bld	bld
Na_2O	bld	bld	bld	bld	bld	bld	bld	bld	0.19
K_2O	bld	bld	bld	bld	bld	bld	bld	bld	bld
V_2O_5	n.a.	n.a.	n.a.	n.a.	n.a.	n.a.	n.a.	n.a.	n.a.
Total	96.89	100.09	100.10	99.25	99.89	99.74	100.71	100.93	100.49
Number of cations (apfu) on the basis of 3 oxygen atoms and 2 cations									
Nb	-	-	-	-	-	-	-	-	-
Si	0.003	0.001	0.001	0.001	0.001	0.001	0.001	0.001	0.009
Ti	0.896	0.871	0.883	0.885	0.880	0.856	0.867	0.863	0.881
Zn	-	-	-	-	-	-	-	-	-
Al	0.011	0.012	0.024	0.019	0.018	0.016	0.017	0.011	0.023
Cr	0.060	0.009	0.021	0.031	0.035	0.007	0.012	0.008	0.032
Fe^{2+}	0.782	0.493	0.456	0.439	0.429	0.504	0.511	0.481	0.407
Fe^{3+}	0.131	0.236	0.186	0.179	0.186	0.264	0.234	0.253	0.174
Ni	0.001	0.002	0.002	0.001	0.001	0.002	0.002	0.002	0.001
Mn	0.040	0.005	0.008	0.010	0.011	0.006	0.005	0.005	0.011
Mg	0.073	0.371	0.417	0.433	0.438	0.345	0.350	0.375	0.447
Ca	0.003	0.001	0.001	0.002	0.001	0.001	0.001	0.000	0.006
Ba	-	-	-	-	-	-	-	-	-
Na	-	-	-	-	-	-	-	-	0.002
K	-	-	-	-	-	-	-	-	-
V	-	-	-	-	-	-	-	-	-
sum	2.000	2.000	2.000	2.000	2.000	2.000	2.000	2.000	1.994

Table 10 continued

Intrusion	PK312	PK312	PK312	PK314	PK314	PK314	PK314	PK314	PK314
Sample	**47553b**	**47553b**	**47553b**	**47547**	**47547**	**47547**	**47547**	**47547**	**47547**
Major element analysis (wt%)									
Nb_2O_5	0.30	0.18	0.12	0.17	0.12	0.19	0.30	0.24	bld
SiO_2	0.03	0.035	0.03	0.03	0.03	bld	bld	0.03	0.05
TiO_2	51.01	48.45	49.30	51.15	50.22	48.50	53.60	51.28	53.48
ZnO	n.a.	n.a.	n.a.	n.a.	n.a.	n.a.	n.a.	n.a.	n.a.
Al_2O_3	0.88	0.55	0.52	1.56	0.79	1.25	1.20	0.84	0.89
Cr_2O_3	1.31	0.42	0.68	0.41	2.27	0.43	1.73	2.46	0.91
FeO	23.79	25.24	25.59	21.87	18.38	24.67	26.18	19.79	18.27
Fe_2O_3	10.70	15.41	14.01	9.38	10.74	13.82	2.63	10.38	8.75
NiO	0.06	0.07	0.09	0.10	0.11	0.09	0.14	0.10	0.13
MnO	0.51	0.33	0.24	2.28	5.75	0.32	0.60	2.16	3.41
MgO	12.25	10.19	10.41	12.28	11.71	10.49	11.87	13.48	14.71
CaO	0.04	0.02	0.03	0.05	0.07	0.04	0.03	0.05	0.08
BaO	bld	bld	bld	bld	bld	bld	bld	bld	bld
Na_2O	bld	bld	bld	bld	bld	bld	bld	bld	bld
K_2O	n.a.	bld	bld	bld	bld	bld	bld	bld	bld
V_2O_5	n.a.	n.a.	n.a.	n.a.	n.a.	n.a.	n.a.	n.a.	n.a.
Total	100.87	100.87	101.02	99.28	100.19	99.80	98.28	100.81	100.68
Number of cations (apfu) on the basis of 3 oxygen atoms and 2 cations									
Nb	0.003	0.002	0.001	0.002	0.001	0.002	0.003	0.002	-
Si	0.001	0.001	0.001	0.001	0.001	-	-	0.001	0.001
Ti	0.879	0.850	0.862	0.890	0.873	0.854	0.942	0.875	0.905
Zn	-	-	-	-	-	-	-	-	-
Al	0.024	0.015	0.014	0.043	0.022	0.034	0.033	0.022	0.024
Cr	0.024	0.008	0.012	0.007	0.041	0.008	0.032	0.044	0.016
Fe^{2+}	0.456	0.492	0.497	0.423	0.355	0.483	0.512	0.376	0.344
Fe^{3+}	0.184	0.270	0.245	0.163	0.187	0.243	0.046	0.177	0.148
Ni	0.001	0.001	0.002	0.002	0.002	0.002	0.003	0.002	0.002
Mn	0.010	0.007	0.005	0.045	0.113	0.006	0.012	0.042	0.065
Mg	0.418	0.354	0.360	0.423	0.403	0.366	0.414	0.456	0.493
Ca	0.001	0.000	0.001	0.001	0.002	0.001	0.001	0.001	0.002
Ba	-	-	-	-	-	-	-	-	-
Na	-	-	-	-	-	-	-	-	-
K	-	-	-	-	-	-	-	-	-
V	-	-	-	-	-	-	-	-	-
sum	2.000	2.000	2.000	2.000	2.000	2.000	1.997	1.998	2.000

Table 10 continued

Intrusion	PK314	PK314	PK314	PK314	PK314
Sample	47547	47547	47547	47547	47547
Major element analysis (wt%)					
Nb_2O_5	0.27	bld	n.a.	0.03	0.09
SiO_2	bld	0.03	0.23	bld	0.02
TiO_2	47.46	51.60	50.62	52.93	47.09
ZnO	n.a.	n.a.	n.a.	bld	bld
Al_2O_3	1.06	0.50	0.47	1.36	0.45
Cr_2O_3	0.41	0.28	0.23	2.84	0.74
FeO	22.21	25.95	27.27	23.93	28.06
Fe_2O_3	18.61	8.53	8.60	2.26	12.88
NiO	0.13	0.10	0.06	0.14	0.03
MnO	0.20	0.78	0.25	0.31	0.26
MgO	11.27	10.99	10.16	13.00	7.85
CaO	0.01	0.02	0.01	0.03	0.01
BaO	bld	bld	bld	bld	bld
Na_2O	bld	bld	bld	0.01	0.03
K_2O	bld	bld	bld	bld	bld
V_2O_5				0.22	0.15
Total	101.64	98.78	97.90	97.05	97.67
Number of cations (apfu) on the basis of 3 oxygen atoms and 2 cations					
Nb	0.003	-	-	0.000	0.001
Si	-	0.001	0.005	-	0.001
Ti	0.819	0.914	0.909	0.932	0.865
Zn	-	-	-	-	-
Al	0.029	0.014	0.013	0.037	0.013
Cr	0.007	0.005	0.004	0.053	0.014
Fe^{2+}	0.426	0.511	0.545	0.468	0.573
Fe^{3+}	0.321	0.151	0.154	0.040	0.236
Ni	0.002	0.002	0.001	0.003	0.001
Mn	0.004	0.016	0.005	0.006	0.005
Mg	0.385	0.386	0.362	0.454	0.285
Ca	0.000	0.001	0.000	0.001	0.000
Ba	-	-	-	-	-
Na	-	-	-	0.000	0.000
K	-	-	-	-	-
V	-	-	-	0.004	0.003
sum	1.998	2.000	1.999	2.000	1.999

Table 11 – Garnet major and minor elements (wt%)

Intrusion	PK150	PK150	PK150	PK150	PK150
Sample	39249b-1	44813c-1	44813c-2	44813c-3	47513-1
Nb_2O_5	bld	n.a.	n.a.	n.a.	bld
SiO_2	40.47	41.57	41.20	42.09	41.81
TiO_2	bld	0.99	1.26	0.68	0.71
ZnO	bld	n.a.	n.a.	n.a.	bld
Al_2O_3	22.65	16.69	20.93	18.21	20.10
Cr_2O_3	0.11	6.93	0.72	5.66	4.52
FeO_T	18.21	7.27	12.10	6.65	7.42
NiO	bld	bld	bld	bld	0.01
MnO	0.52	0.31	0.39	0.30	0.29
MgO	12.39	21.15	18.63	21.80	21.16
CaO	6.36	5.17	5.45	4.81	4.69
BaO	n.a.	bld	bld	bld	bld
Na_2O	bld	0.09	0.08	0.08	0.08
K_2O	bld	bld	bld	bld	0.00
V_2O_3	n.a.	n.a.	n.a.	n.a.	0.04
Total	100.71	100.14	100.76	100.28	100.84

Table 12 – Perovskite major and minor elements (wt%)

Intrusion	PK150	PK150	PK150	PK150	PK150	PK150	PK150	PK150	PK150	PK150	PK150	PK150
Sample	47517a-1	47517a-2	47517a-3	47517a-4	47517a-5	47517a-6	47517b-1	47517b-2	47517b-3	47517b-4	47517b-5	47517b-6
Nb_2O_5	2.14	2.53	1.32	2.26	0.84	1.61	1.39	1.13	1.43	2.19	2.19	1.71
SiO_2	0.06	1.22	0.31	2.06	0.13	0.25	bld	0.02	1.77	0.42	0.53	0.07
TiO_2	53.28	54.35	54.93	56.19	53.78	54.89	55.03	55.22	51.71	54.10	53.18	54.22
ZnO	bld	bld	bld	bld	bld	bld	bld	bld	bld	bld	bld	bld
Al_2O_3	0.16	0.19	0.14	0.15	0.23	0.15	0.15	0.14	0.14	0.18	0.18	0.16
Cr_2O_3	0.04	bld	0.06	bld	bld	bld	0.07	0.05	0.07	0.08	bld	0.09
FeO_T	1.58	1.57	1.19	1.63	1.23	1.80	1.31	1.46	1.57	1.32	1.45	1.26
NiO	bld	bld	bld	bld	bld	bld	bld	bld	bld	bld	bld	bld
MnO	0.04	0.05	0.04	0.03	0.02	0.03	0.05	0.07	0.03	0.03	0.03	0.03
MgO	0.08	0.98	0.21	1.83	0.13	0.31	0.05	0.07	1.29	0.37	0.51	0.08
CaO	37.69	32.08	38.87	27.57	40.35	36.31	39.56	39.81	36.50	36.45	36.16	38.94
BaO	bld	0.29	bld	0.17	bld	bld	bld	bld	bld	0.32	0.40	bld
Na_2O	0.80	0.80	0.54	0.62	0.59	0.62	0.62	0.57	0.64	0.77	0.78	0.65
K_2O	0.02	0.01	0.02	0.06	0.10	0.04	0.02	0.02	0.02	0.04	0.02	0.08
Total	95.89	94.07	97.63	92.57	97.40	96.01	98.25	98.56	95.17	96.27	95.43	97.29

Table 13 – Rutile major and minor elements (wt%)

Intrusion	**PK150**	**PK150**	**PK150**	**PK150**	**PK150**	**PK150**	**PK150**	**PK150**	**PK150**	**PK150**	**PK150**
Sample	**47513-2**	**44803-1**	**44813a-1**	**44813a-1**	**44813a-2**	**44813a-3**	**44813a-4**	**44813a-4**	**44813a-5**	**44813a-6**	**44813a-7**
	ilm rim	ilm rim	g.m.	g.m.	g.m.	g.m.	g.m.	g.m.	g.m.	ilm rim	g.m.
Nb_2O_5	3.44	0.02	n.a.	n.a.	n.a.	n.a.	n.a.	n.a.	n.a.	n.a.	n.a.
SiO_2	0.02	0.03	0.05	0.10	0.15	0.09	0.11	0.07	0.86	0.10	0.19
TiO_2	89.90	97.90	94.72	95.44	92.65	95.89	92.73	94.61	91.59	93.61	92.23
ZnO	bdl	bdl	n.a.	n.a.	n.a.	n.a.	n.a.	n.a.	n.a.	n.a.	n.a.
Al_2O_3	0.07	0.08	0.02	0.02	bld	0.02	bld	bld	0.02	bld	bld
Cr_2O_3	0.20	0.23	bld	bld	bld	bld	bld	bld	bld	bld	bld
FeO_T	3.22	0.74	2.13	1.50	3.09	1.80	3.01	2.04	1.98	2.87	3.12
NiO	bdl	bdl	n.a.	n.a.	n.a.	n.a.	n.a.	n.a.	n.a.	n.a.	n.a.
MnO	0.08	0.01	bld	bld	bld	bld	bld	bld	0.03	bld	bld
MgO	0.08	0.02	0.04	0.04	0.06	0.04	0.05	0.02	1.46	0.03	0.17
CaO	0.33	0.04	0.05	0.08	0.17	0.1	0.35	0.24	0.16	0.31	0.21
BaO	0.12	bdl	0.34	0.33	0.39	0.38	0.4	0.35	0.4	0.42	0.46
Na_2O	0.02	0.01	bld	bld	bld	bld	bld	bld	bld	bld	bld
K_2O	0.01	bdl	bld	bld	0.01	0.02	bld	0.01	0.01	bld	0.01
V_2O_3	0.05	bdl	n.a.	n.a.	n.a.	n.a.	n.a.	n.a.	n.a.	n.a.	n.a.
Total	97.91	99.17	97.35	97.51	96.52	98.34	96.65	97.34	96.51	97.34	96.39

Table 13 continued

Intrusion	PK150	PK150	PK150	PK150	PK150	PK150	PK150	PK150	PK150	PK150	PK150
Sample	44813a-8	44813a-9	44813a-10	44813a-10	44813a-10	44813a-11	44813a-12	44813a-13	44813a-14	44813a-15	44813b-1
	g.m.	g.m.	ilm rim	ilm rim	ilm rim	ilm rim	ilm rim	g.m.	g.m.	ilm rim	ilm rim
Nb_2O_5	n.a.	n.a.	n.a.	n.a.	n.a.	n.a.	n.a.	n.a.	n.a.	n.a.	n.a.
SiO_2	0.08	0.08	0.10	bdl	0.09	0.05	0.08	0.12	0.06	0.16	0.04
TiO_2	93.36	95.08	94.32	97.39	95.86	98.18	92.63	91.38	93.11	93.96	98.34
ZnO	n.a.	n.a.	bdl	bdl	bdl	bdl	bdl	bdl	bdl	bdl	n.a.
Al_2O_3	bld	0.02	0.02	bdl	0.02	bdl	bdl	bdl	0.00	0.02	bld
Cr_2O_3	bld	bld	0.06	0.05	0.15	0.07	bdl	bdl	bdl	bdl	0.13
FeO_T	2.18	1.82	3.17	0.80	2.27	0.48	2.29	2.69	1.88	1.35	0.92
NiO	n.a.	n.a.	0.06	bdl	0.03	bdl	bdl	bdl	bdl	bdl	bld
MnO	bld	bld	0.03	bdl	0.02	bdl	bdl	bdl	bdl	bdl	bld
MgO	0.04	0.04	0.04	bdl	0.05	bdl	0.03	0.05	0.03	0.05	bld
CaO	0.47	0.07	0.40	0.08	0.05	0.11	0.20	0.34	0.10	0.19	0.14
BaO	0.36	0.335	n.a.	n.a.	n.a.	n.a.	n.a.	n.a.	n.a.	n.a.	bld
Na_2O	bld	0	bdl	bdl	bdl	bdl	bdl	bdl	0.06	bdl	0.03
K_2O	0.01	bld	n.a.	n.a.	n.a.	n.a.	n.a.	n.a.	n.a.	n.a.	bld
V_2O_3	n.a.	n.a.	n.a.	n.a.	n.a.	n.a.	n.a.	n.a.	n.a.	n.a.	n.a.
Total	96.50	97.63	98.55	98.41	98.79	98.94	95.48	94.88	95.45	95.88	99.60

Table 13 continued

Intrusion	PK150	PK150	PK150	PK150	PK150	PK150	PK150	PK150	PK150	PK150	PK346
Sample	44813b-1	44813b-1	44813b-2	44813b-3	44813c-1	44813c-2	44813d-1	44813d-2	44813d-3	44813d-3	44864-1
	ilm rim	ilm rim	ilm rim	g.m.	g.m.	g.m.	g.m.	ilm rim	ilm rim	ilm rim	ilm rim
Nb_2O_5	n.a.	n.a.	n.a.	n.a.	n.a.	n.a.	n.a.	n.a.	n.a.	n.a.	1.13
SiO_2	0.03	0.16	0.08	0.25	0.06	0.04	0.07	0.08	0.05	0.03	0.1
TiO_2	96.35	90.07	95.06	93.37	97.32	97.21	92.59	95.01	94.99	98.51	93.16
ZnO	n.a.	n.a.	n.a.	n.a.	n.a.	n.a.	n.a.	n.a.	n.a.	n.a.	n.a.
Al_2O_3	bld	bld	bld	bld	bld	bld	bld	bld	bld	bld	bld
Cr_2O_3	bld	bld	bld	bld	0.09	bld	bld	bld	bld	0.14	bld
FeO_T	1.00	3.31	1.91	2.34	0.71	1.02	2.67	1.80	1.92	0.62	1.26
NiO	bld	bld	bld	bld	bld	bld	bld	bld	bld	bld	bld
MnO	bld	bld	bld	bld	bld	bld	bld	bld	bld	bld	0.03
MgO	bld	0.07	bld	0.08	0.03	bld	bld	bld	bld	bld	0.03
CaO	0.09	0.22	0.04	0.12	0.16	0.05	0.11	0.21	0.08	0.13	0.14
BaO	bld	bld	bld	bld	bld	bld	bld	bld	bld	bld	bld
Na_2O	0.05	0.04	bld	bld	bld	bld	bld	0.03	0.03	bld	bld
K_2O	bld	bld	bld	0.01	bld	bld	bld	0.01	0.01	bld	0.01
V_2O_3	n.a.	n.a.	n.a.	n.a.	n.a.	n.a.	n.a.	n.a.	n.a.	n.a.	n.a.
Total	97.52	93.87	97.09	96.17	98.37	98.32	95.44	97.14	97.08	99.43	95.86

Table 13 continued

Intrusion	PK346	PK346	PK346	PK346	PK346	PK346	PK346	PK151	PK151	PK151	PK151
Sample	44864-1	44864-2	44864-3	44860-1	44860-2	44860-3	44860-4	47514-1	47514-1	47514-2	47514-3
	ilm rim	ilm rim	ilm rim	ilm rim	alt	alt	ilm rim	ilm rim	ilm rim	ilm rim	ilm rim
Nb_2O_5	1.45	1.40	1.18	0.89	1.34	1.44	0.97	2.14	2.75	2.48	2.40
SiO_2	0.07	0.03	bdl	0.07	0.04	0.07	0.04	0.34	0.40	0.18	0.27
TiO_2	94.89	92.98	95.49	96.31	96.10	96.21	96.00	93.03	90.90	91.88	90.61
ZnO	n.a.	bdl	bdl	bdl	bdl	bdl	bdl	bld	bld	bld	bld
Al_2O_3	bld	0.06	0.06	0.07	0.06	0.07	0.06	bld	bld	bld	bld
Cr_2O_3	bld	0.02	0.03	0.26	bdl	0.03	0.16	bld	0.07	0.05	0.10
FeO_T	0.99	0.86	1.46	1.08	0.87	0.58	0.72	1.17	2.39	1.75	3.18
NiO	bld	bdl	bdl	bdl	bdl	bdl	bdl	bld	bld	bld	bld
MnO	bld	0.01	0.00	bdl	0.01	0.02	0.02	0.04	bld	0.05	bld
MgO	0.05	0.04	0.01	0.01	0.03	0.03	0.02	0.33	0.16	0.10	0.87
CaO	0.09	1.90	0.15	0.30	0.46	0.67	0.59	0.50	0.78	0.38	1.19
BaO	bld	bdl	0.03	0.06	0.06	bdl	0.02	bld	bld	bld	bld
Na_2O	bld	0.01	0.01	0.01	0.01	0.01	0.01	bld	bld	bld	0.04
K_2O	0.03	bdl	0.01	0.00	0.00	0.01	0.00	0.01	bld	0.01	bld
V_2O_3	n.a.	bdl	bdl	0.04	bdl	0.04	0.06	n.a.	n.a.	n.a.	n.a.
Total	97.57	97.41	98.59	99.22	99.08	99.24	98.75	97.56	97.45	96.88	98.66

Table 13 continued

Intrusion	**PK151**	**PK151**	**PK151**	**PK151**	**PK314**	**PK314**	**PK314**	**PK314**
Sample	**47514-3**	**47514-5**	**47514-6**	**47514-7**	**47547-1**	**47547-2**	**47547-3**	**47547-4**
	ilm rim	ilm rim	ilm rim	g.m.	rilm rim	ilm rim	ilm rim	ilm rim
Nb_2O_5	2.86	3.10	1.98	2.16	0.07	1.87	1.76	2.44
SiO_2	0.18	0.01	0.03	0.05	0.30	0.15	0.09	0.08
TiO_2	91.67	93.74	90.20	88.65	95.56	95.38	96.43	95.50
ZnO	bld	bdl	bdl	bdl	n.a.	n.a.	n.a.	n.a.
Al_2O_3	bld	0.07	0.05	0.05	0.01	bld	bld	bld
Cr_2O_3	0.06	0.04	0.38	0.09	1.56	0.13	0.11	0.07
FeO_T	1.76	0.99	2.41	1.75	2.41	1.20	1.06	1.55
NiO	bld	bdl	bdl	bdl	bld	bld	bld	bld
MnO	0.02	bdl	bdl	bdl	0.05	0.02	bld	bld
MgO	0.03	0.03	0.95	0.17	0.04	0.13	bld	bld
CaO	0.38	0.52	1.38	1.65	0.25	0.79	0.62	0.29
BaO	bld	0.02	bdl	0.03	bld	bld	bld	bld
Na_2O	0.03	0.01	0.01	0.00	bld	bld	bld	bld
K_2O	0.01	0.03	bdl	0.02	0.01	0.02	0.01	0.02
V_2O_3	n.a.	bdl	bdl	0.03	n.a.	n.a.	n.a.	n.a.
Total	97.00	98.69	97.66	94.85	100.23	99.66	100.08	99.95

Table 14 – Pseudorutile major and minor elements (wt%)

Sample	47547-1	47547-1	47547-2	47547-2	47547-2	47547-3	47547-3	47547-4	47547-5	47547-5	47547-6
Nb_2O_5	0.91	0.89	0.95	0.66	0.92	1.65	1.09	0.09	1.00	0.09	0.12
SiO_2	0.37	0.32	0.28	0.87	0.38	0.68	0.53	0.05	0.07	0.08	0.16
TiO_2	57.30	56.90	56.72	52.99	55.97	55.91	56.26	52.54	55.62	52.65	52.76
ZnO	0.00	0.00	0.02	0.03	0.00	0.00	0.00	0.50	0.00	0.36	0.49
Al_2O_3	0.31	0.52	0.64	0.71	0.51	0.23	0.24	3.03	1.25	3.84	0.32
Cr_2O_3	31.50	32.14	32.17	34.13	27.46	31.99	30.70	27.50	34.26	26.68	31.87
FeO_T	0.04	0.00	0.00	0.00	0.00	0.00	0.00	0.08	0.00	0.06	0.14
NiO	2.86	2.79	2.88	1.88	6.88	2.53	3.31	5.92	2.04	5.48	3.80
MnO	0.13	0.09	0.20	0.15	0.09	0.14	0.10	3.04	0.24	4.32	0.85
MgO	0.03	0.03	0.08	0.18	0.25	0.12	0.09	0.07	0.07	0.04	0.03
CaO	0.00	0.00	0.00	0.00	0.00	0.00	0.00	0.00	0.00	0.00	0.00
Na_2O	0.05	0.07	0.08	0.13	0.07	0.07	0.15	0.06	0.00	0.04	0.00
K_2O	0.01	0.03	0.01	0.04	0.02	0.03	0.06	0.00	0.02	0.00	0.00
Total	93.51	93.78	94.03	91.77	92.55	93.35	92.53	92.88	94.57	93.64	90.54

Table 15 – Apatite trace elements (ppm) from PK150

PK150	44813a_1	44813a_1	44813a_2	44813a_3	44813a_5	44813a_7	44813a_8	44813a_9
Si	bld	bld	bld	206000*	bld	bld	120000	bld
Ca	402500	406000	401500	409000	400000	408200	407400	405900
Ti	63.9	32.1	27.9	1720	27*	15*	49	46
V	729	572	774	1600	1530	575	1310	609
Cr	bld	13.6	21.3	490	bld	178	370	1040
Ni	96.3	94	38.6	333	21.9	44.7	188	441
Rb	0.6*	bld	bld	26.9	1.7*	bld	bld	bld
Sr	11470	12390	12310	13030	8830	13520	13060	13270
Y	19.7	19.8	31	26.2	12.7	21.1	50	25
Zr	9.18	10.56	10.33	62	5.55	12.7	17.7	20.6
Nb	0.19	0.264	0.674	10.5	0.047	0.297	1.2	0.66
Ba	121.2	138.9	129.8	201	90.7	160.1	138.8	159.4
La	121	128.7	101.9	102.4	57.6	119.6	90.6	127
Ce	138.4	131.7	100.9	135.1	49.9	105.1	68.9	98.8
Pr	18.58	17.3	12.42	17.46	5.56	12.4	7.45	11.2
Nd	70.5	65.1	47	67.3	20.4	46.2	27	43.3
Sm	13.61	12.46	9.5	13.8	4.04	8.8	5.38	8
Eu	3.81	3.45	2.87	3.74	1.38	2.87	2.16	2.76
Gd	9.66	8.75	7.81	10	3.37	7.3	7.12	7.5
Tbm	1.045	1.01	0.903	1.22	0.472	0.837	1.01	0.9
Dy	4.35	4.22	4.75	5.06	2.44	4.02	5.64	4.06
Ho	0.658	0.631	0.842	0.869	0.456	0.663	1.24	0.74
Er	1.307	1.277	1.861	1.93	0.88	1.4	2.81	1.59
Tm	0.123	0.118	0.179	0.17	0.084	0.133	0.289	0.186
Yb	0.618	0.621	0.792	0.89	0.44	0.66	1.03	0.75
Lu	0.066	0.067	0.086	0.107	bld	0.077	0.134	0.088
Hf	bld	bld	bld	1.52	bld	0.11*	0.33	0.41
Ta	bld	0.005*	bld	0.33	bld	bld	0.055	0.03
Pb204	bld	bld	bld	9.6	bld	bld	bld	6.5*
Pb208	0.606	0.534	0.608	15.8	0.626	0.721	0.87	0.83
Th	7.91	7.19	6.02	11.4	2.34	8.1	3.99	6.3
U238	0.176	0.183	0.18	0.95	0.085	0.207	0.461	0.64

*Analyses was above LOD, but below LOQ

Table 15 continued

PK150	44813b_1	44813b_2	44813b_7	44813b_11	44813b_11	44813c_4	44813c_5	44813c_8
Si	bld	bld	bld	bld	bld	550000*	bld	33000*
Ca	407800	413300	400200	403600	411600	405800	407000	402200
Ti	75	6.6	36*	39.9	58	11000	67.8	22.6
V	977	550	73	705	767	2190	748	832
Cr	740	183	bld	bld	bld	4290	bld	13.5
Ni	300	41.7	74	42	233	2760	174	43.2
Rb	bld	bld	bld	bld	bld	33.1	1.1*	bld
Sr	12310	13080	6600	12290	13170	11990	13020	11420
Y	34.4	17.8	2	22.6	24.1	72	65.9	25.9
Zr	27	11.06	2.16	9.78	11.68	484	19.7	9.15
Nb	1.35	0.295	0.043	0.357	0.241	131	1.66	0.286
Ba	133.1	154.8	27.5	138.2	136.8	1450	130.9	125.6
La	109.5	119.6	11.1	100.6	105.3	140.4	129.5	104.3
Ce	144.8	101.1	12.9	93.8	108.6	198	156	117.7
Pr	19.9	11.64	1.35	11.7	13.3	27.8	20.7	15.4
Nd	77.5	44.7	3.64	42.8	49.6	109	77.8	58.6
Sm	14.9	8.5	0.76	8.44	9.6	22.9	15.4	10.9
Eu	4.37	2.59	0.26	2.67	3	7.58	4.93	3.34
Gd	11.24	6.13	0.62	6.85	8.11	19.2	13.2	8.08
Tbm	1.28	0.758	0.097	0.813	0.92	2.68	1.65	1.002
Dy	6.18	3.44	0.5	4.07	4.49	12.8	8.7	4.54
Ho	1.13	0.557	0.105	0.676	0.724	2.2	1.69	0.774
Er	2.18	1.31	0.3	1.39	1.55	5.24	3.96	1.71
Tm	0.239	0.116	0.04	0.143	0.173	0.59	0.447	0.157
Yb	0.92	0.65	0.184	0.645	0.83	3.07	1.82	0.777
Lu	0.093	0.073	bld	0.06	0.061	0.524	0.205	0.072
Hf	0.6	bld	0.08*	0.043	0.133	13.2	0.36	0.04*
Ta	0.131	bld	bld	0.007*	bld	5.78	0.062	0.007*
Pb204	bld	5.4*	bld	bld	bld	54	bld	bld
Pb208	3.1	0.599	0.52	1.126	0.84	58	0.767	0.561
Th	10.56	7.53	0.4	7.48	8.6	26.2	12.3	7.81
U238	0.54	0.176	0.08	0.212	0.29	9.45	0.617	0.171

*Analyses was above LOD, but below LOQ

Table 15 continued

PK150	44813c_9	44813c_10	44813d_1	44813d_2	44813d_3	44813d_5
Si	bld	bld	40000*	200000*	280000*	bld
Ca	405000	406600	404500	408000	409400	405300
Ti	42	50.7	52.5	79	97	44.1
V	475	672	560.3	763	606	468
Cr	21.6	3.4*	bld	bld	bld	bld
Ni	141	98.5	42.2	177	356	42.2
Rb	bld	0.7*	bld	bld	bld	bld
Sr	10933	11989	11985	12460	13340	12010
Y	16.84	22.5	21.64	27.8	20.7	23.1
Zr	10.19	11.84	10.76	14.43	16.5	12.17
Nb	0.168	0.353	0.287	0.626	0.55	1.02
Ba	134.5	146.2	139.7	134.4	159.8	146.7
La	124.1	122.2	114.2	141.2	135.5	145.4
Ce	110.9	91.4	92.5	186	77	142.9
Pr	13.64	10.44	10.83	24.8	7.6	16.34
Nd	50	38.6	41.1	91.7	29	59
Sm	8.93	7.32	7.87	17.5	5.3	10.76
Eu	2.64	2.257	2.47	5.01	1.86	3.29
Gd	6.51	6.05	6.08	12.13	5.2	8.18
Tbm	0.724	0.732	0.731	1.33	0.63	0.929
Dy	3.33	3.5	3.79	6.13	3.53	4.53
Ho	0.508	0.624	0.63	0.896	0.65	0.731
Er	1.107	1.4	1.349	1.96	1.28	1.54
Tm	0.117	0.13	0.125	0.145	0.134	0.126
Yb	0.512	0.599	0.593	0.82	0.5	0.77
Lu	0.0474	0.087	0.0655	0.066	0.076	0.087
Hf	0.04*	0.05*	0.05*	0.12*	0.198	0.07*
Ta	bld	0.009*	0.008*	bld	bld	0.018*
Pb204	bld	bld	bld	bld	bld	bld
Pb208	0.497	0.489	0.519	0.92	0.69	1.41
Th	4.96	4.83	6.88	21	5.4	11.62
U238	0.17	0.169	0.147	0.345	0.428	0.262

*Analyses was above LOD, but below LOQ

Table 16 – Ilmenite trace elements (ppm); spot size in µm

Body	Sample	Spot Size	Sc	Ti	V	Mn	Co	Ni	Zn	Ga	Zr	Nb	Hf	Ta	W	U
PK150	**44813a**	193	18	286700	1273	1710	138	355	86	8.0	216	934	8.0	115	0.17	0.023
PK150	**44813a**	193	17	288300	1269	1714	138	359	85	7.9	215	948	8.1	116	0.18	0.023
PK150	**44813a**	193	22	314800	1399	1837.4	152	590	81	10.1	323	999	12.3	107	0.15	0.044
PK150	**44813a**	50	32	320400	1820	3118	135	835	259	16.7	253	919	9.6	94	0.14	0.054
PK150	**44813a**	50	47	401900	2222	6800	194	975	742	10.7	293	424	13.2	63	0.81	0.19
PK150	**44813a**	50	31	318000	1738	10270	146	892	683	11.0	354	1062	12.6	88	12.5	3.4
PK150	**44813b**	193	19	327900	1666	1958	158	657	79	9.4	182	629	7.1	82	0.13	0.087
PK150	**44813b**	130	29	366200	1693	4324	173	973	197	11.9	316	779	11.0	84	2.52	0.98
PK150	**44813b**	130	19	179000	1546	1172	82	86	88	9.4	491	1744	17.7	186	0.46	0.045
PK150	**44813b**	50	39	388800	2179	5830	156	874	347	9.3	295	852	11.6	85	1.14	0.27
PK150	**44813b**	50	30	275000	1381	3210	118	530	246	14.4	518	1856	18.0	171	1.51	0.42
PK150	**44813c**	130	17	217200	1082	1701	113	144	332	7.6	426	1548	13.4	150	0.45	0.66
PK150	**44813c**	90	36	371700	2383	4680	178	1155	536	15.8	239	336	10.5	49	0.39	0.16
PK150	**44813c**	90	33	409500	2435	3750	162	1030	208	11.8	275	2094	16.7	272	0.22	0.15
PK150	**44813d**	90	23	305800	1422	1646	139	721	79	13.2	332	1159	10.8	118	0.28	0.056
PK150	**44813d**	50	29	182200	2210	6040	85	667	273	28.5	1022	2466	23.9	200	0.36	3.3
PK150	**44813d**	50	30	348100	1904	3422	148	958	453	12.0	232	651	8.7	65	0.13	0.030
PK150	**44813d**	50	39	424200	2463	7300	176	964	826	9.7	179	516	8.1	74	0.77	0.15

Table 16 continued

Body	Sample	Spot Size	Sc	Ti	V	Mn	Co	Ni	Zn	Ga	Zr	Nb	Hf	Ta	W	U
PK346	**44834a**	130	27	322700	1196	1754	164	624	79	10.7	407	1621	13.9	188	0.28	0.041
PK346	**44834a**	130	23	312300	1538	1859	155	542	87	9.9	363	1292	13.0	132	0.35	0.036
PK346	**44834b**	193	28	208100	1479	1297.5	96	124	59	9.4	825	2661	28.3	258	0.39	0.10
PK346	**44834b**	130	22	272500	1480	1761	139	637	66	10.4	256	857	8.8	79	1.5	0.42
PK346	**44834b**	50	21	270800	1579	1661	135	637	90	10.6	247	904	8.6	73	0.37	0.078
PK346	**44834b**	50	38	340500	1684	4147	114	517	85	5.4	420	1801	13.6	126	5.2	7.8
PK346	**44813b**	50	28	336600	1410	2669	145	794	104	9.0	327	1079	11.9	100	0.32	0.040
PK346	**44848a**	193	21	263400	1199	1769	116	157	83	8.1	440	1497	15.3	163	0.259	0.050
PK346	**44848a**	193	22	273600	1241	1897	122	210	72	8.1	452	1544	15.4	166	0.271	0.053
PK346	**44848a**	193	24	315500	1572	1906	150	436	77	9.4	405	1508	14.2	156	0.347	0.043
PK346	**44848a**	130	41	262400	779	5180	550	3400	520	12.2	607	1646	14.0	118	35	13.6
PK346	**44848a**	50	26	276000	699	5400	121	517	67	5.3	782	2186	16.8	121	59	21.2
PK346	**44848a**	50	37	317000	1306	4710	116	508	134	6.3	417	1817	14.7	129	8.7	5.3
PK346	**44848a**	50	31	314200	1524	2900	131	586	86	7.8	435	1564	14.4	141	3.7	1.7
PK346	**44848b**	130	20	339200	1717	1896	175	908	84	10.5	251	824	8.9	87	0.31	0.037
PK346	**44848b**	130	28	323600	1273	1900	157	759	70	8.8	400	1417	10.6	149	0.31	0.053
PK346	**44848b**	90	42	384900	2090	3176	149	828	95	7.0	498	1375	18.1	131	0.42	0.041
PK346	**44848b**	50	31	326200	1552	2695	141	752	101	10.4	453	2237	15.2	216	0.55	0.051
PK346	**44848b**	50	40	383000	2326	7970	184	856	511	9.5	211	548	9.0	82	0.64	0.32

Table 17 – Apatite U-Pb geochronology isotopic data for PK150; no val = no value

Sample	U	Pb	$^{206}Pb/^{238}U$	2σ	$^{207}Pb/^{206}Pb$	2σ	$^{206}Pb/^{204}Pb$	2σ	^{204}Pb	^{206}Pb	^{207}Pb	^{238}U
	ppm	ppm							cps	cps	cps	cps
44813_1	0.223	no val	0.043	0.046	0.691	0.022	18	2.4	510	7860	5380	14240
44813_2	0.173	no val	0.046	0.051	0.692	0.019	21	2.7	482	8550	5900	10890
44813_3	0.270	no val	0.057	0.060	0.737	0.017	18	2.2	661	10310	7550	17020
44813_4	0.243	no val	0.029	0.033	0.705	0.019	28	7.4	399	8210	5740	15190
44813_5	0.187	no val	0.048	0.052	0.716	0.021	17	26	335	7770	5450	11620
44813_6	0.206	no val	0.039	0.043	0.676	0.021	20	3.4	540	9150	6140	12760
44813_7	0.208	no val	0.065	0.071	0.747	0.021	23	2.3	634	13430	10000	12750
44813_8	0.206	no val	0.061	0.071	0.650	0.015	23	1.9	770	16750	10790	12620
44813_9	0.185	no val	0.074	0.079	0.722	0.018	22	2.9	549	10190	7420	11290
44813_10	0.248	no val	0.025	0.029	0.694	0.019	23	4.2	463	8260	5720	15070
44813_11	0.257	no val	0.035	0.038	0.698	0.022	17	12	369	7570	5230	15560
44813_12	0.178	no val	0.048	0.052	0.655	0.019	31	11	299	7740	5050	10790
44813_13	0.490	no val	0.160	0.160	0.661	0.022	22	5.2	1170	31000	19100	30000
44813_14	0.220	no val	0.049	0.053	0.676	0.019	20	2.4	524	9260	6170	13340
44813_15	0.176	no val	0.052	0.057	0.669	0.018	23	4.6	417	8780	5820	10650
44813_16	0.203	no val	0.053	0.057	0.696	0.020	34	8.9	443	9020	6160	12290
44813_17	0.255	no val	0.030	0.035	0.719	0.017	19	2.2	596	9570	6850	15490
44813_18	0.291	no val	0.039	0.041	0.687	0.025	32	8.2	392	8260	5597	17700

Table 18 – Perovskite U-Pb geochronology isotopic data for PK150; used decay constants of 1.55125E-10 for ^{238}U and 9.8485E-10 for ^{235}U

	Spot Size	U	Pb	$^{238}U/^{206}Pb$	2σ	$^{207}Pb/^{206}Pb$	2σ	$^{204}Pb/^{206}Pb$	2σ	^{204}Pb	^{206}Pb	^{207}Pb	^{238}U
	µm	ppm	ppm							cps	cps	cps	cps
47517a-1	23	354	39	12.626	0.478	0.117	0.002	0.0029	0.0009	179	39420	4600	4.41E+05
47517a-2**	23	262	24	13.587	0.517	0.133	0.004	-0.0143	0.0388	128	26100	3380	3.26E+05
47517a-3	23	282	30	13.333	0.480	0.144	0.014	0.0043	0.0014	166	29000	3740	3.50E+05
47517a-7	23	260	26	13.021	0.509	0.151	0.015	0.0034	0.0014	158	23800	3340	3.18E+05
47517a-9	23	333	31	11.148	0.534	0.132	0.003	0.0100	0.0310	178	37400	4940	4.08E+05
47517b-2	23	249	21	10.331	0.566	0.170	0.007	0.0053	0.0020	245	29600	5030	3.05E+05
47517b-4	23	395	62	12.937	0.452	0.126	0.004	0.0040	0.0012	221	42800	5380	4.77E+05
47517b-4b**	23	237	13	10.893	0.380	0.181	0.025	-0.0059	0.0170	185	27200	4570	2.85E+05
47517b-7	23	330	42	11.834	0.392	0.150	0.010	0.0054	0.0011	255	37500	5190	3.97E+05
47517b-9	23	312	31	13.141	0.483	0.148	0.004	0.0088	0.0058	221	29000	4290	3.74E+05
47517a-5	33	163	16	11.905	0.581	0.195	0.018	0.0070	0.0015	234	31100	4870	3.97E+05
47517a-6	33	251	29	13.123	0.586	0.170	0.008	0.0057	0.0017	400	48600	8030	6.17E+05
47517a-8	33	212	24	12.240	0.554	0.149	0.004	0.0044	0.0012	288	44000	6440	5.23E+05
47517a-10	33	251	23	11.696	0.561	0.157	0.013	0.0053	0.0008	307	53500	7340	6.20E+05
47517a-11	33	91	5	9.681	0.572	0.239	0.008	0.0100	0.0025	260	21700	5160	2.27E+05
47517a-12	33	254	40	11.364	0.529	0.158	0.003	0.0067	0.0008	464	62000	9680	7.11E+05
47517b-6	33	212	16	11.025	0.693	0.188	0.018	0.0065	0.0015	412	49400	8710	5.87E+05
47517b-8	33	348	46	12.920	0.618	0.155	0.008	0.0073	0.0007	603	76200	11590	9.90E+05
47517b-10*	33	190	35	13.089	0.720	0.205	0.016	0.0076	0.0015	338	38900	6990	5.41E+05
47517b-11	33	220	27	12.739	0.730	0.177	0.010	0.0068	0.0015	358	42900	7560	6.26E+05
47517a-13	33	291	47	13.123	0.534	0.155	0.003	0.0057	0.0009	429	63000	9640	8.18E+05
47504-2	23	42	9	4.274	0.603	0.395	0.039	0.0238	0.0085	339	15900	5200	9.50E+04
47504-4	23	131	19	8.403	0.847	0.243	0.017	0.0111	0.0027	409	30700	6950	2.90E+05

*Omitted from final age calculation on basis of 2σ error envelope for both semi-total and total Pb approaches

**Omitted from final age calculation for total Pb approach only due to negative $^{204}Pb/^{206}Pb$ ratios

Table 18 continued

Sample	Spot Size	U	Pb	$^{238}U/^{206}Pb$	2σ	$^{207}Pb/^{206}Pb$	2σ	$^{204}Pb/^{206}Pb$	2σ	^{204}Pb	^{206}Pb	^{207}Pb	^{238}U
	µm	ppm	ppm							cps	cps	cps	cps
47504-5	23	204	43	11.494	0.846	0.207	0.005	0.0102	0.0017	464	39800	8240	4.50E+05
47504-6	23	136	10	11.173	0.512	0.208	0.008	0.0085	0.0022	396	32300	6670	2.99E+05
47517b-12	23	165	12	10.352	0.482	0.192	0.012	0.0069	0.0018	400	44100	8390	3.59E+05
47517b-13	23	57	10	5.910	0.384	0.341	0.011	0.0109	0.0046	450	21900	7280	1.24E+05
47517b-14*	23	124	5	8.333	1.319	0.196	0.033	0.0116	0.0035	340	26900	5000	2.58E+05
47517b-15	23	23	3	4.926	0.388	0.416	0.015	0.0200	0.0088	228	9900	4260	4.66E+04
47517b-16	23	274	29	13.072	0.632	0.172	0.007	0.0068	0.0011	411	49500	8350	5.64E+05
47517b-18	23	185	11	8.197	0.873	0.230	0.029	0.0098	0.0021	414	39800	8140	3.78E+05
47517b-19	23	244	11	9.009	0.974	0.195	0.021	0.0058	0.0020	361	48400	9070	4.90E+05
47517b-20	23	248	13	10.173	0.890	0.205	0.022	0.0081	0.0034	440	44800	9090	4.98E+05
47517b-22	23	372	94	13.038	0.663	0.148	0.016	0.0061	0.0015	390	54700	7830	6.87E+05
47517b-23	23	389	67	11.173	0.986	0.130	0.012	0.0083	0.0493	259	62700	8040	7.07E+05
47517b-24	23	246	50	11.587	0.483	0.138	0.003	0.0040	0.0012	261	44200	6060	4.39E+05
47517b-27	23	241	45	9.785	0.527	0.173	0.008	0.0060	0.0021	307	46000	7840	4.25E+05
47517b-28	23	296	44	11.390	0.649	0.164	0.006	0.0057	0.0010	335	46400	7480	5.15E+05
47517b-29	23	213	7	10.776	0.708	0.184	0.018	0.0050	0.0040	268	29400	5320	3.64E+05
47517b-37	23	221	12	10.965	0.625	0.189	0.015	0.0098	0.0023	330	31500	5790	3.53E+05
47517b-39	23	152	8	9.083	0.511	0.260	0.022	0.0159	0.0028	449	26600	6480	2.42E+05
47517b-40	23	271	16	10.341	0.749	0.188	0.026	0.0057	0.0022	331	39700	6730	4.32E+05
47517b-42	23	295	13	10.246	0.945	0.169	0.025	0.0500	0.6250	310	42900	7000	4.69E+05
47517b-43	23	294	49	12.019	0.506	0.176	0.010	0.0045	0.0023	371	46000	7750	4.68E+05
47517b-44	23	204	15	9.132	0.801	0.187	0.020	0.0031	0.0023	239	33400	5780	3.21E+05

*Omitted from final age calculation on basis of 2σ error envelope for both semi-total and total Pb approaches

Table 18 continued

Sample	Spot Size	U	Pb	$^{238}U/^{206}Pb$	2σ	$^{207}Pb/^{206}Pb$	2σ	$^{204}Pb/^{206}Pb$	2σ	^{204}Pb	^{206}Pb	^{207}Pb	^{238}U
	µm	ppm	ppm							cps	cps	cps	cps
47517b-47	23	185	19	8.953	0.665	0.202	0.010	0.0079	0.0024	330	30900	6230	2.90E+05
47517b-48	23	237	24	11.641	0.515	0.144	0.008	0.0052	0.0010	212	34800	4780	3.70E+05
47517b-49	23	182	16	10.870	0.721	0.151	0.004	0.0064	0.0018	208	26200	4010	2.83E+05
47517b-50	23	150	16	7.937	0.693	0.244	0.020	0.0096	0.0033	329	27000	6070	2.33E+05
47517b-51	23	189	19	8.757	0.537	0.198	0.006	0.0083	0.0048	334	34400	6750	2.93E+05
47517b-53	23	308	17	10.604	1.035	0.143	0.009	0.0049	0.0017	294	43200	6040	4.86E+05
47517b-55	23	162	15	6.993	0.782	0.319	0.027	0.0147	0.0026	572	35100	10900	2.58E+05
47517b-61	23	376	50	12.285	0.724	0.139	0.005	0.0040	0.0021	272	50700	6980	6.07E+05

Table 19 – Perovskite Sm-Nd isotopic data for PK150

Sample	Nd ppm	Sm ppm	$^{147}Sm/^{144}Nd$	2σ	$^{143}Nd/^{144}Nd$	2σ	$^{143}Nd/^{144}Nd$ (t)	εNd (t)	2σ
47504_3	2390	278	0.0711	0.0001	0.51246	0.00008	0.51226	3.28	1.54
47504_7	2260	281	0.0761	0.0005	0.51231	0.00014	0.51210	0.15	2.74
47517b_17	5500	650	0.0728	0.0013	0.51232	0.00015	0.51212	0.52	2.94
47517b_21	8800	970	0.0682	0.0005	0.51234	0.00006	0.51215	1.17	1.27
47517b_26	2450	307	0.0775	0.0007	0.51240	0.00013	0.51219	1.83	2.55
47517b_30	7000	810	0.0719	0.0013	0.51219	0.00013	0.51199	-1.97	2.55
47517b_31b	7400	844	0.0698	0.0004	0.51235	0.00008	0.51216	1.32	1.50
47517b_33	6300	730	0.0733	0.0019	0.51221	0.00011	0.51201	-1.66	2.16
47517b_36	6600	760	0.0719	0.0011	0.51223	0.00013	0.51203	-1.19	2.55
47517b_41	8100	900	0.0695	0.0009	0.51224	0.00011	0.51205	-0.87	2.16
47517b_54	5550	620	0.0692	0.0001	0.51234	0.00009	0.51215	1.08	1.77
47517b_58	4500	540	0.0757	0.0021	0.51215	0.00012	0.51194	-2.96	2.35
47517b_63	4400	520	0.0757	0.0012	0.51222	0.00012	0.51201	-1.59	2.35
47517b_65	9100	1040	0.0709	0.0003	0.51224	0.00005	0.51205	-0.87	1.08
47517a_15	4500	520	0.0723	0.0017	0.51223	0.00016	0.51203	-1.21	3.13

Appendix B – Figures

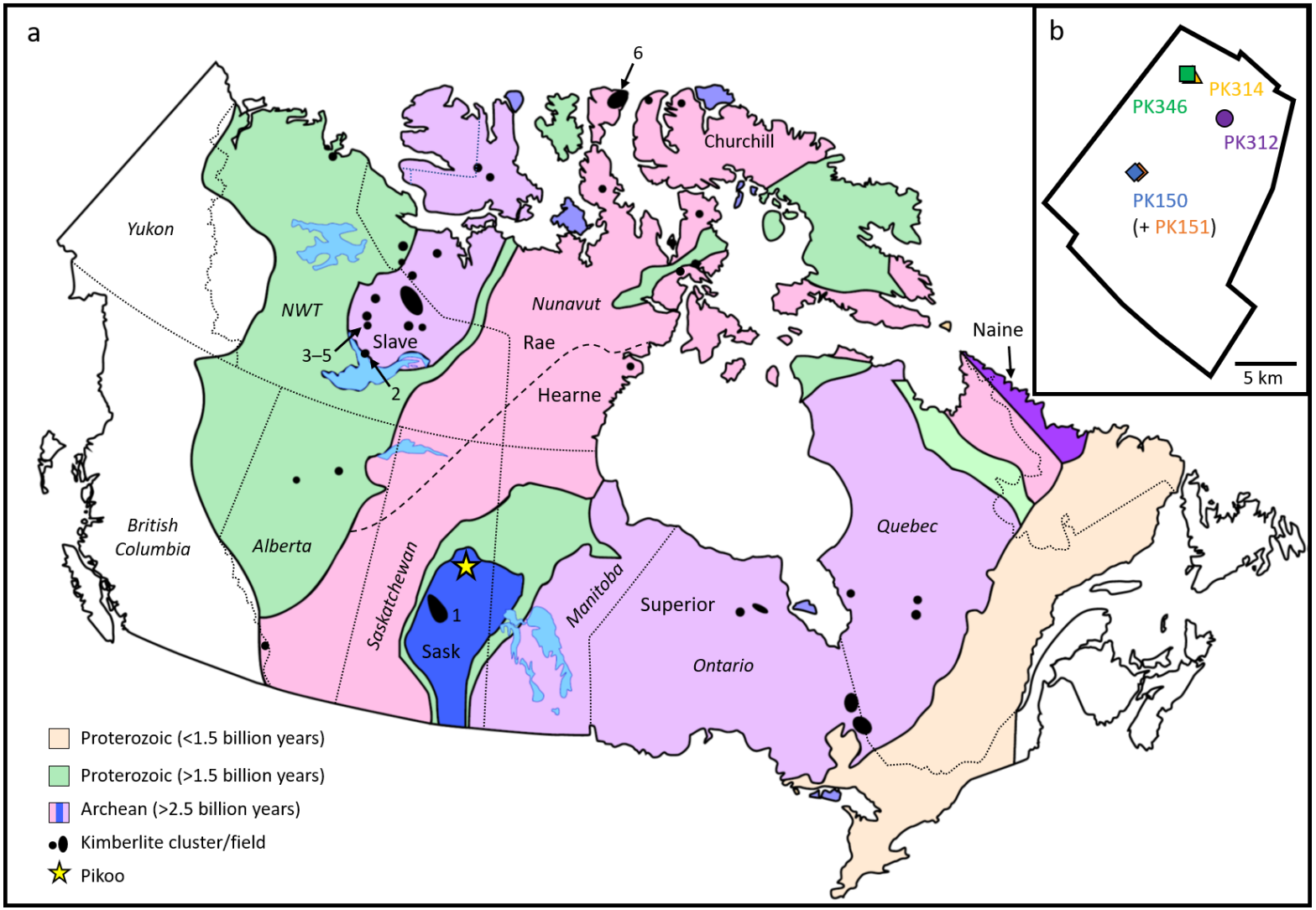

Fig. 1 – a) Schematic map of Canada showing distribution of cratons and kimberlites; b) outline of the Pikoo property and the distribution of the Pikoo kimberlites. 1 = FALC, 2 = DryBones Bay, 3 – 5 = Cross, Orion, Ursa, 6 = Somerset Island.

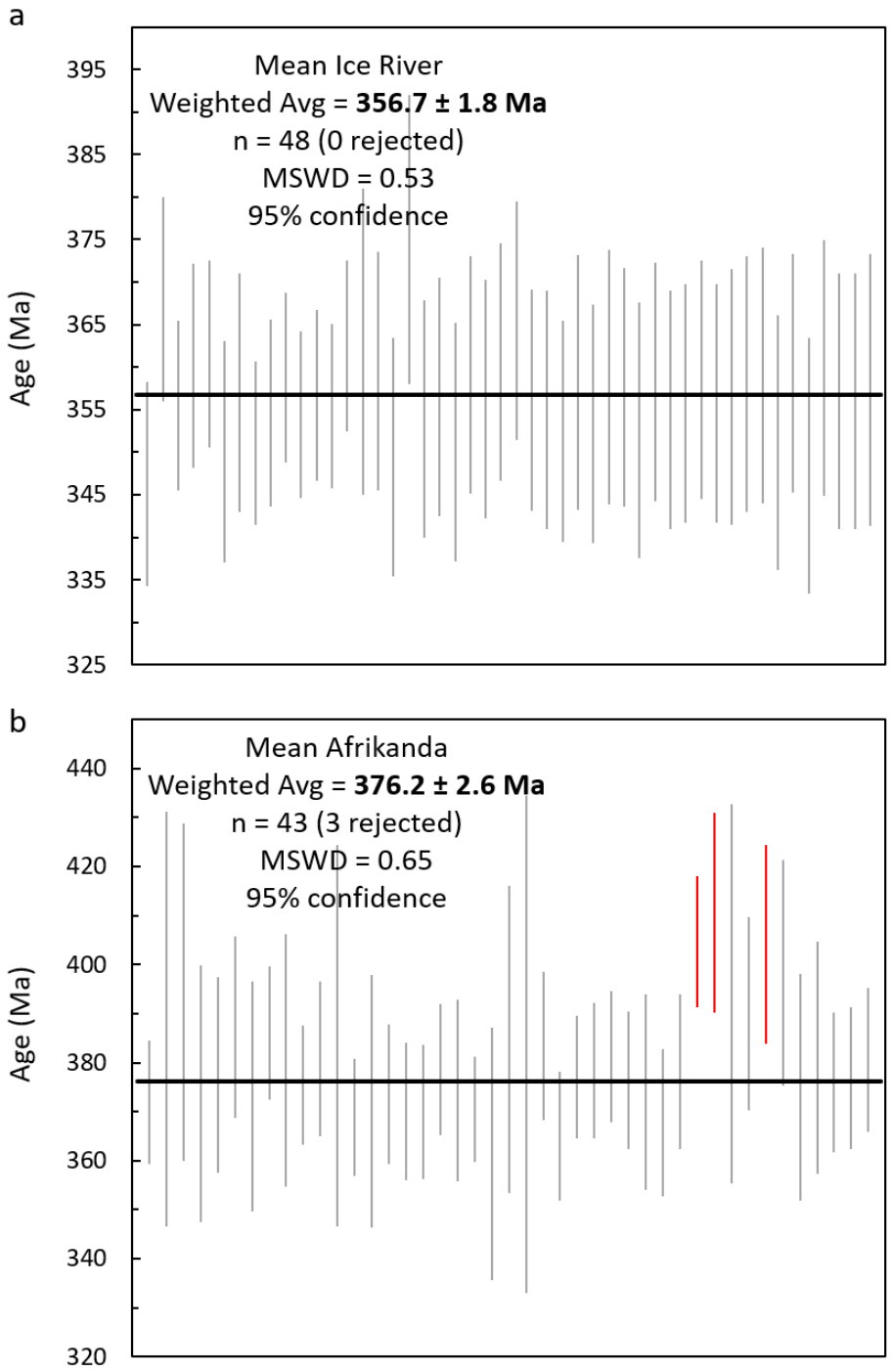

Fig. 2 – Weighted average $^{206}Pb/^{238}U$ results for perovskite geochronology standards a) Ice River and b) Afrikanda. Red lines = rejected points.

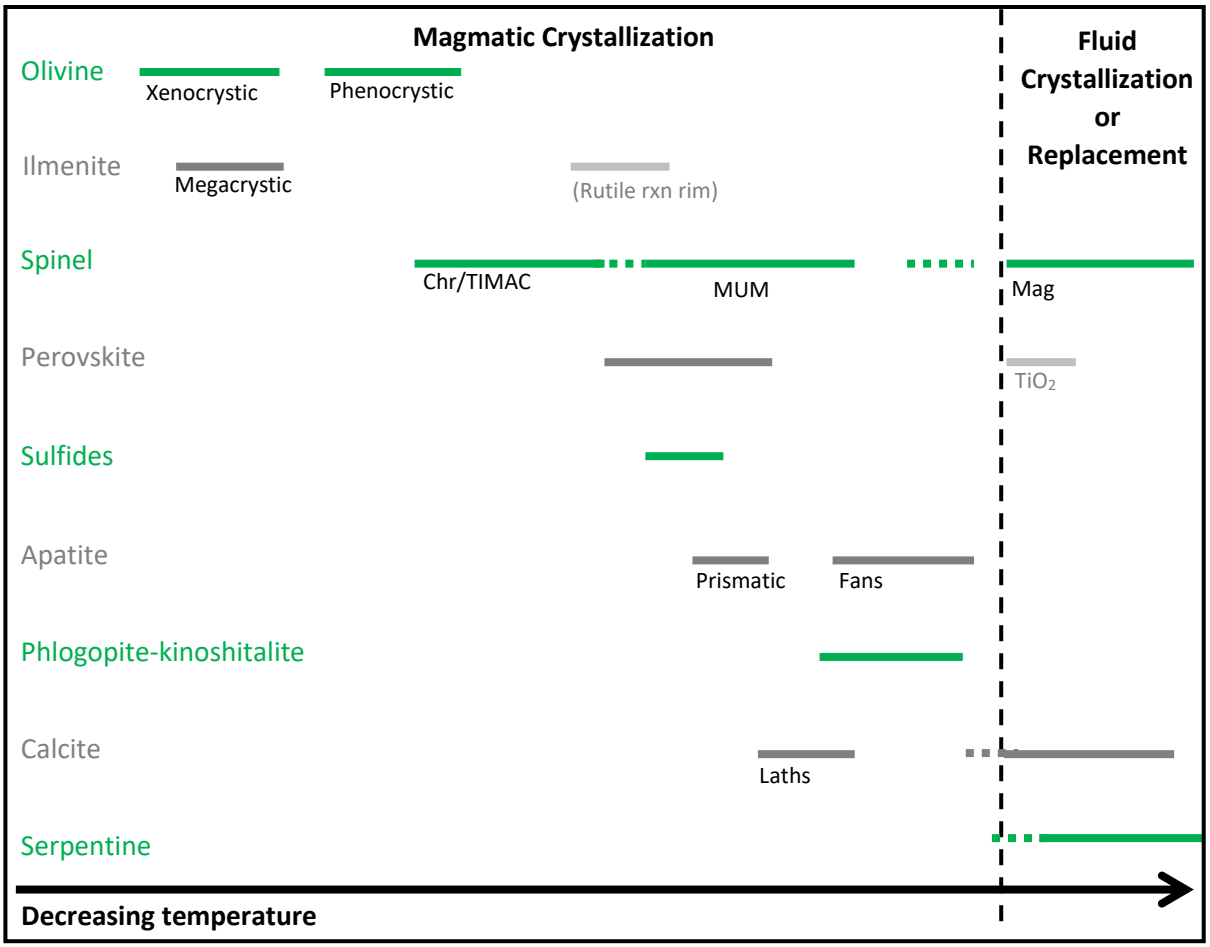

Fig. 3 – Pikoo crystallization sequence determined from petrographic analysis of polished thin sections and BSE images (based on mineral textures, relationships, and inclusions). Rutile forms in rims on some ilmenite megacrysts at contacts with the kimberlite magma. Perovskite is often pseudomorphed by high TiO_2 phases after crystallization. Sulfides are only definitively identified in a small subset of PK346 samples.

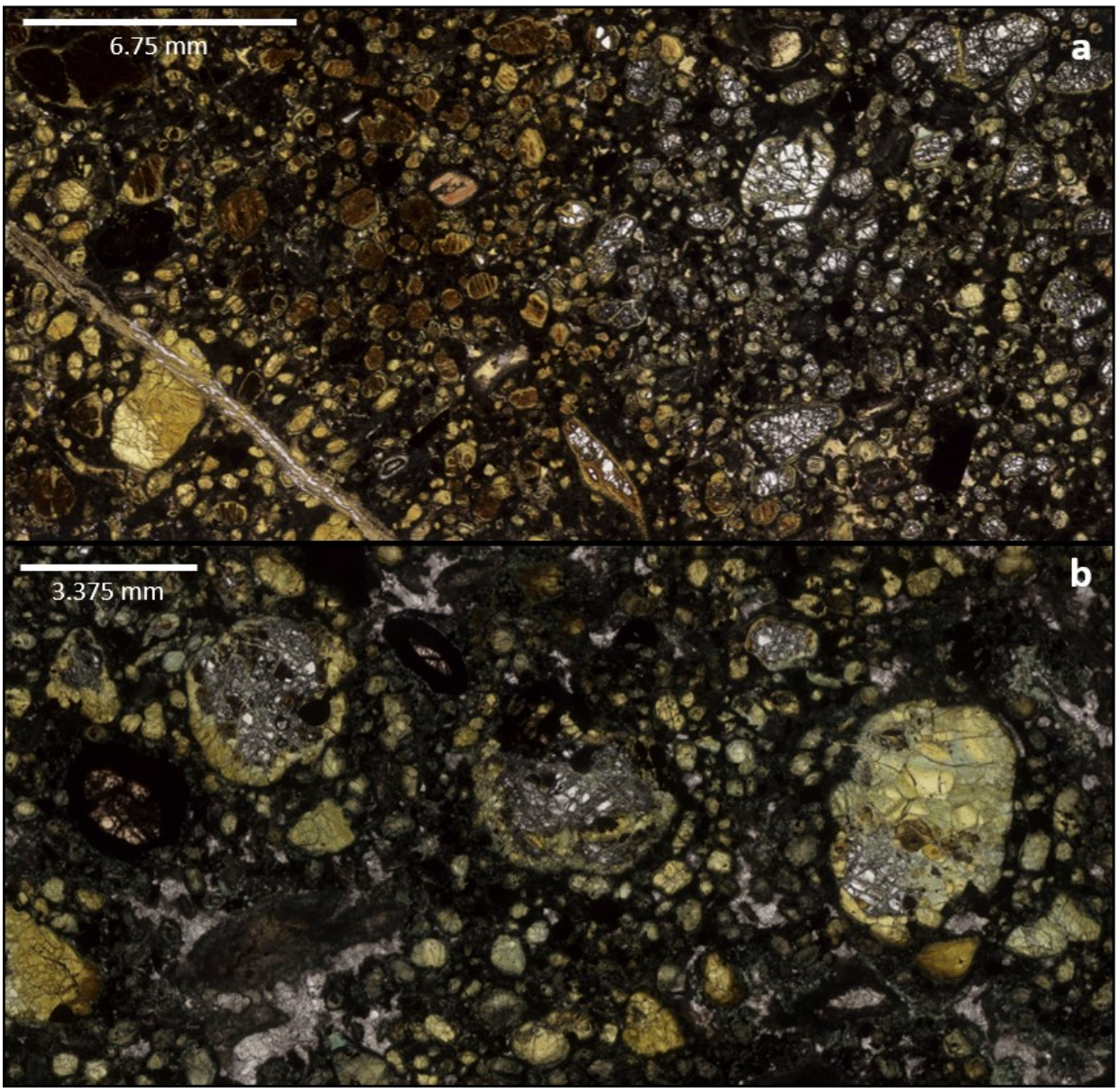

Fig. 4 – Photomicrographs depicting unaltered olivine in PK150; a) a thin section of 47517b contains a pool of partially fresh material (on right), including olivine (colourless) and perovskite (not visible at this scale), adjacent to the typical heavily serpentinized appearance of the majority of PK150 (left); b) olivine macrocrysts in 47504 with partially fresh areas (colourless) and variable amounts of serpentinization (pale green to yellow-green).

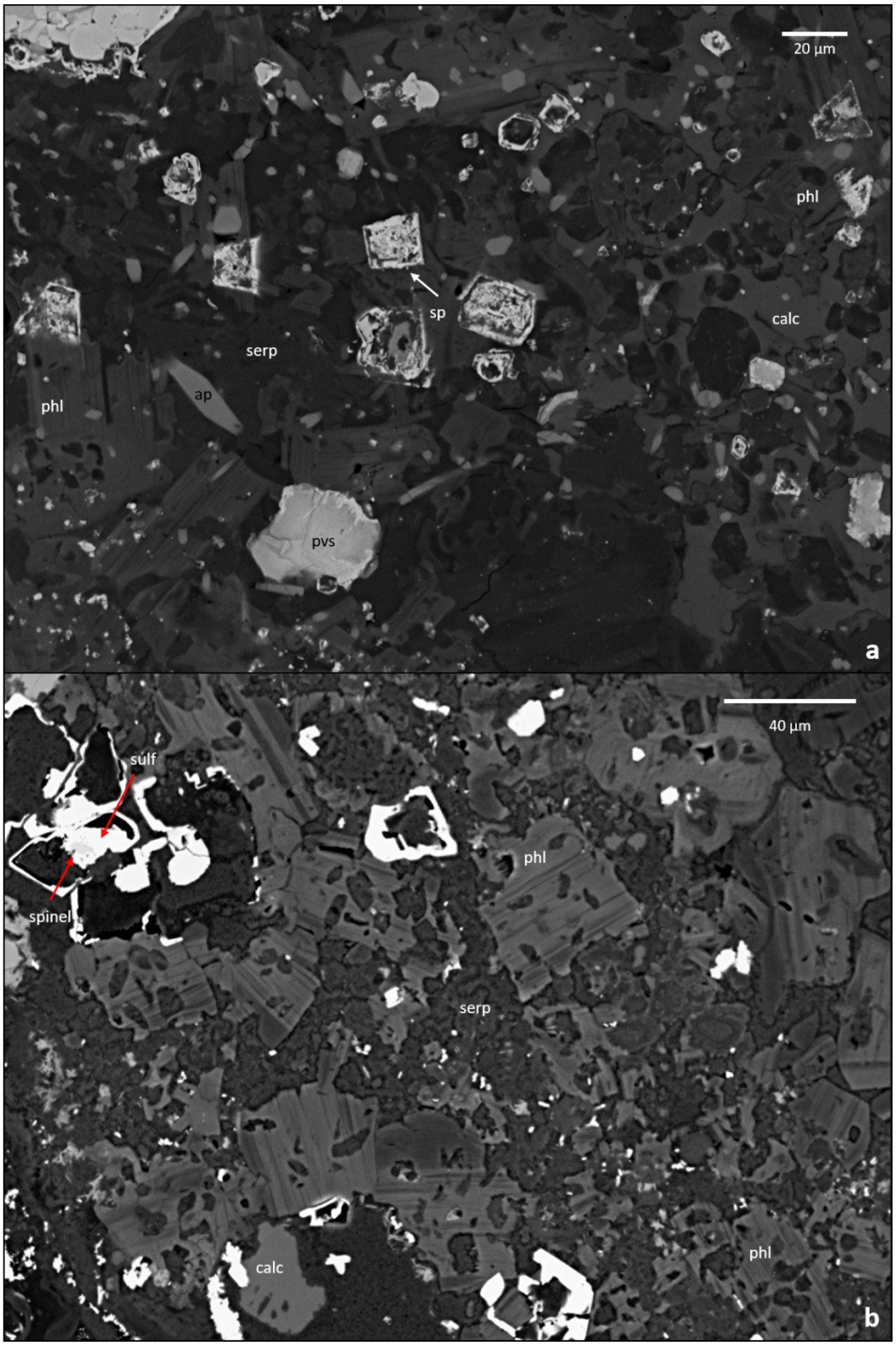

Fig. 5 – Representative BSE images of the groundmass assemblage for a) PK150 and b) PK346. Note: fine prisms of apatite of similar texture to PK150 is present in some portions of PK346 but are present in this area. Ap = apatite, pvs = perovskite, sp = spinel, phl = phlogopite, calc = calcite, serp = serpentine, sulf = sulfide.

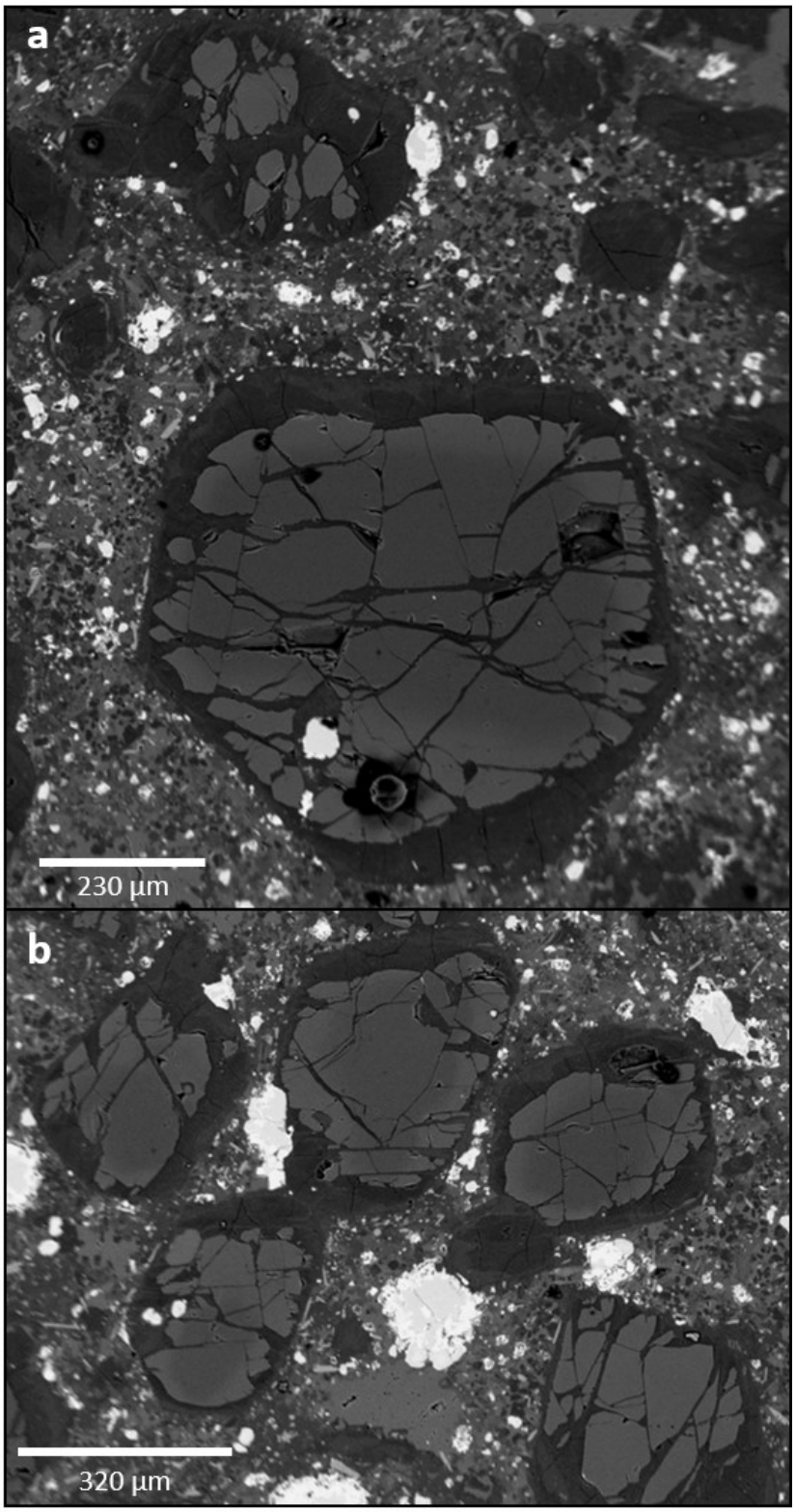

Fig. 6 – BSE images of olivine in PK150 a) large olivine macrocryst with distinct rim and only minor serpentinization with a heavily serpentinized olivine above; b) multiple olivines with distinct (asymmetric) rims and adjacent unrimmed olivine (bottom right corner).

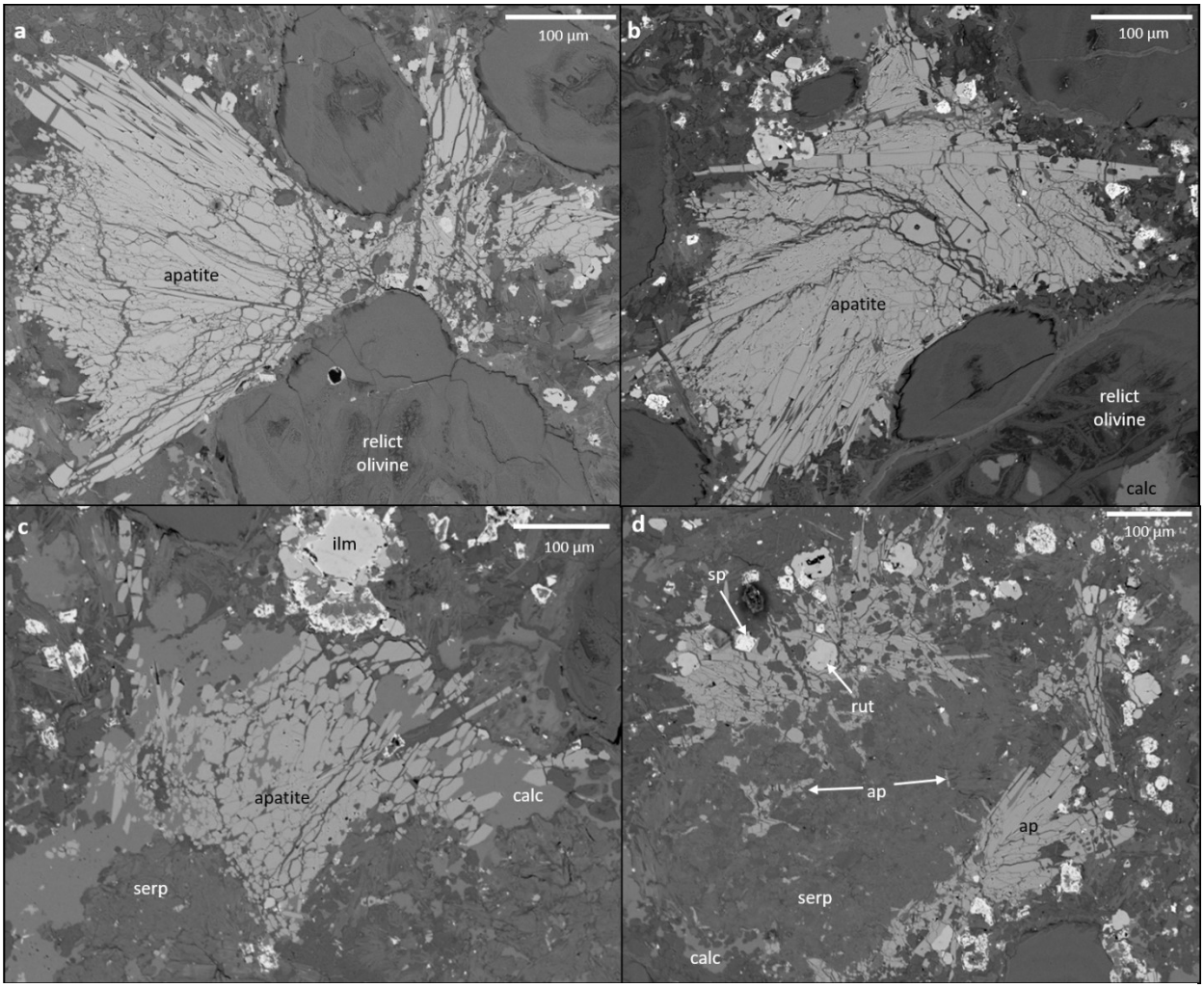

Fig. 7 – Representative BSE images of large apatite textures; a and b) acicular radial apatite crystallizing around adjacent olivine; c) large apatite intergrown with calcite; d) large apatite overgrown by serpentine; ap = apatite, sp = spinel group mineral, calc = calcite, rut = rutile, ilm = ilmenite.

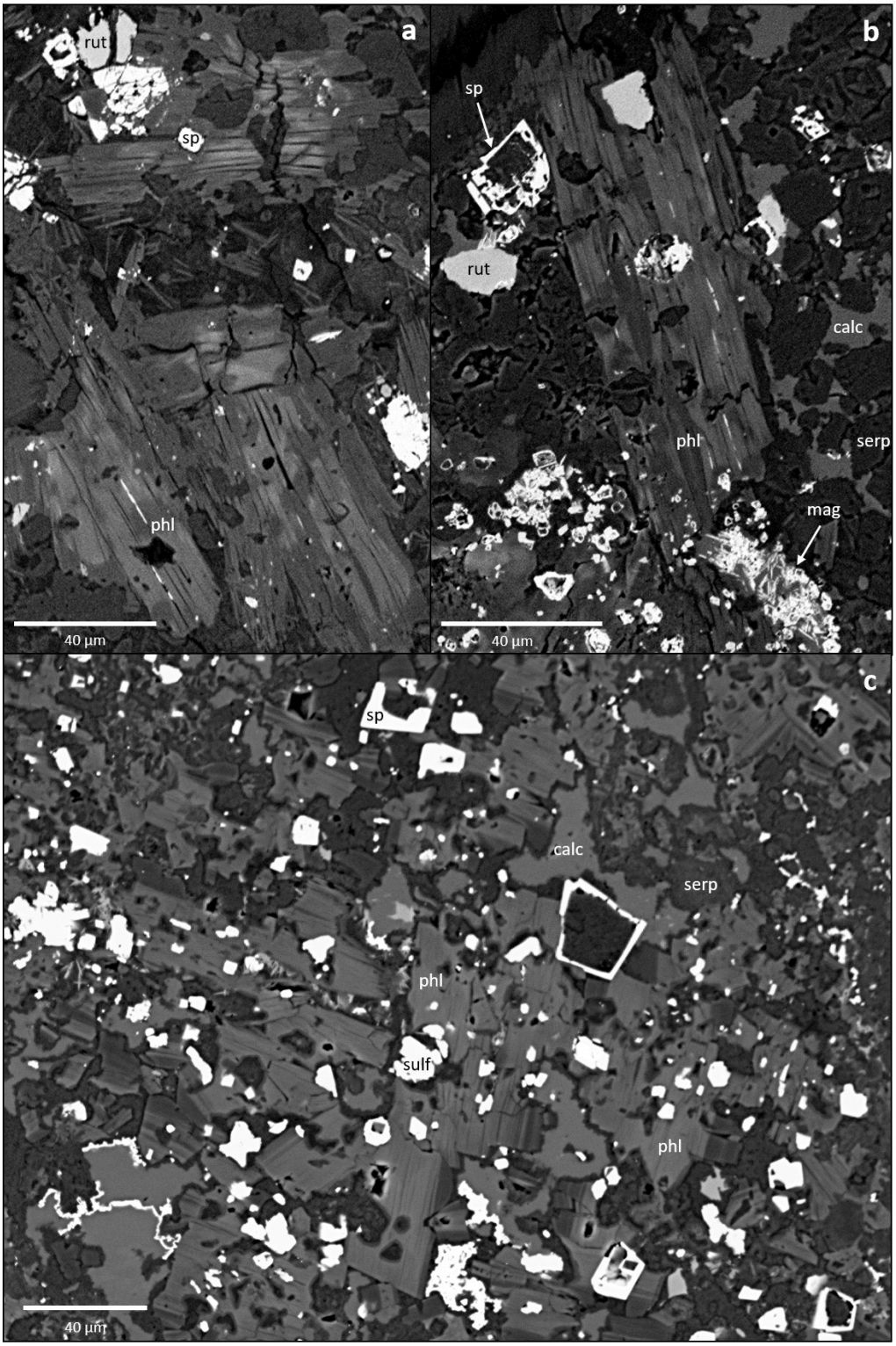

Fig. 8 – BSE images of range in groundmass phlogopite morphology between PK150 and PK346; a and b) elongate laths of phlogopite in PK150 (contrast to emphasize compositional variation) and fine secondary magnetite; c) ragged, poikilitic plate variety of phlogopite in PK346 in which sulfide droplets and spinel are common chadacrysts; phl = phlogopite, rut = rutile, sp = spinel, calc = calcite, serp = serpentine, mag = magnetite, sulf = sulfide.

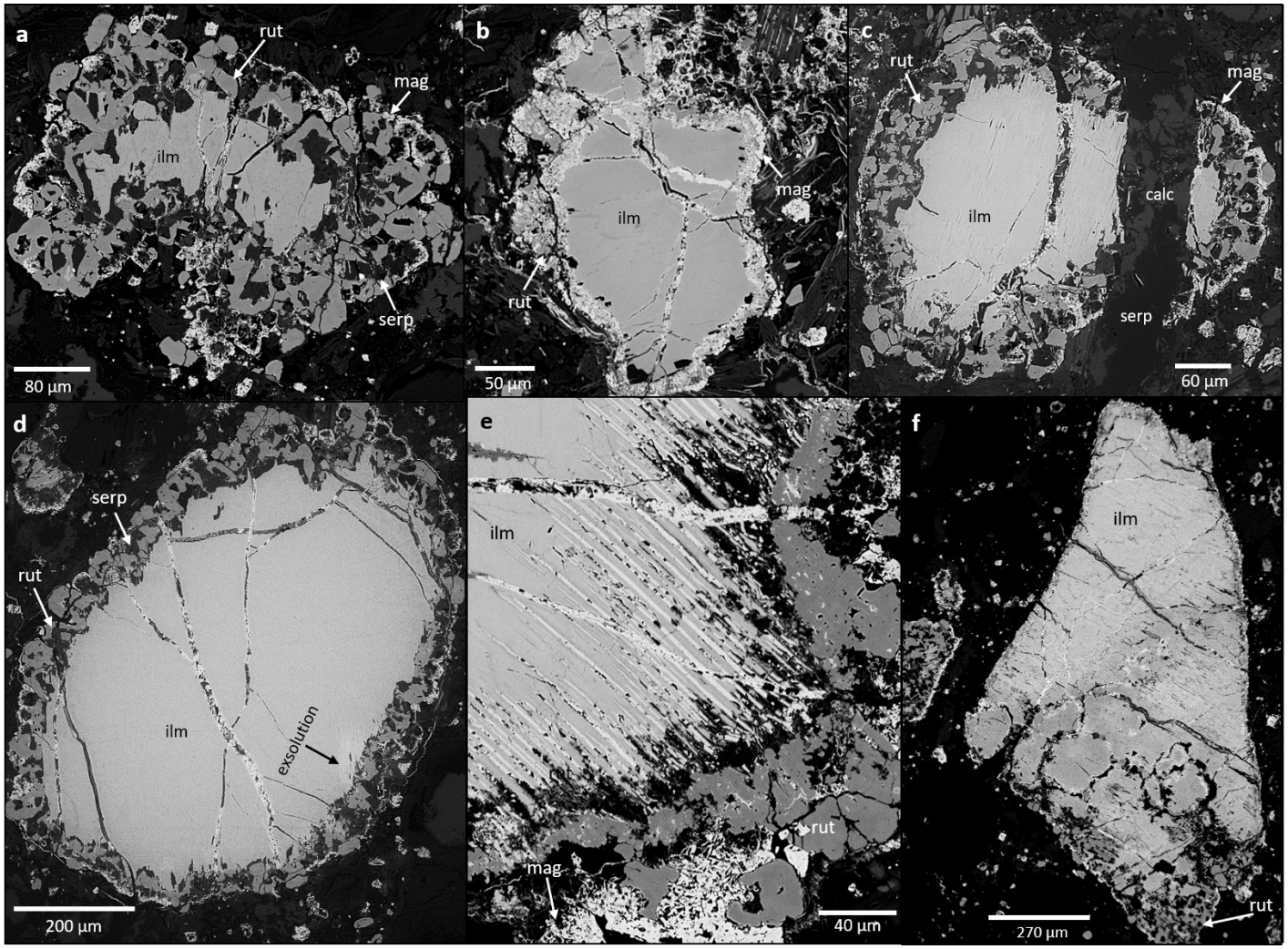

Fig. 9 – Representative BSE images of ilmenite in PK150; a) ilmenite with only minor development of exsolution on the right edge and a rim of rutile, serpentine, and fine flecks of magnetite; b) rim containing greater magnetite than rutile; c) thick rutile rim relative to ilmenite core, significant serpentine content as well; d) ilmenite crosscut by calcite and serpentine; e) exsolution of Fe-rich phase (brighter lamellae); f) large ilmenite with minor exsolution and patchy Mg enrichment (medium grey in lower and middle portions of the grain); ilm = ilmenite, rut = rutile, mag = magnetite, serp = serpentine, calc = calcite.

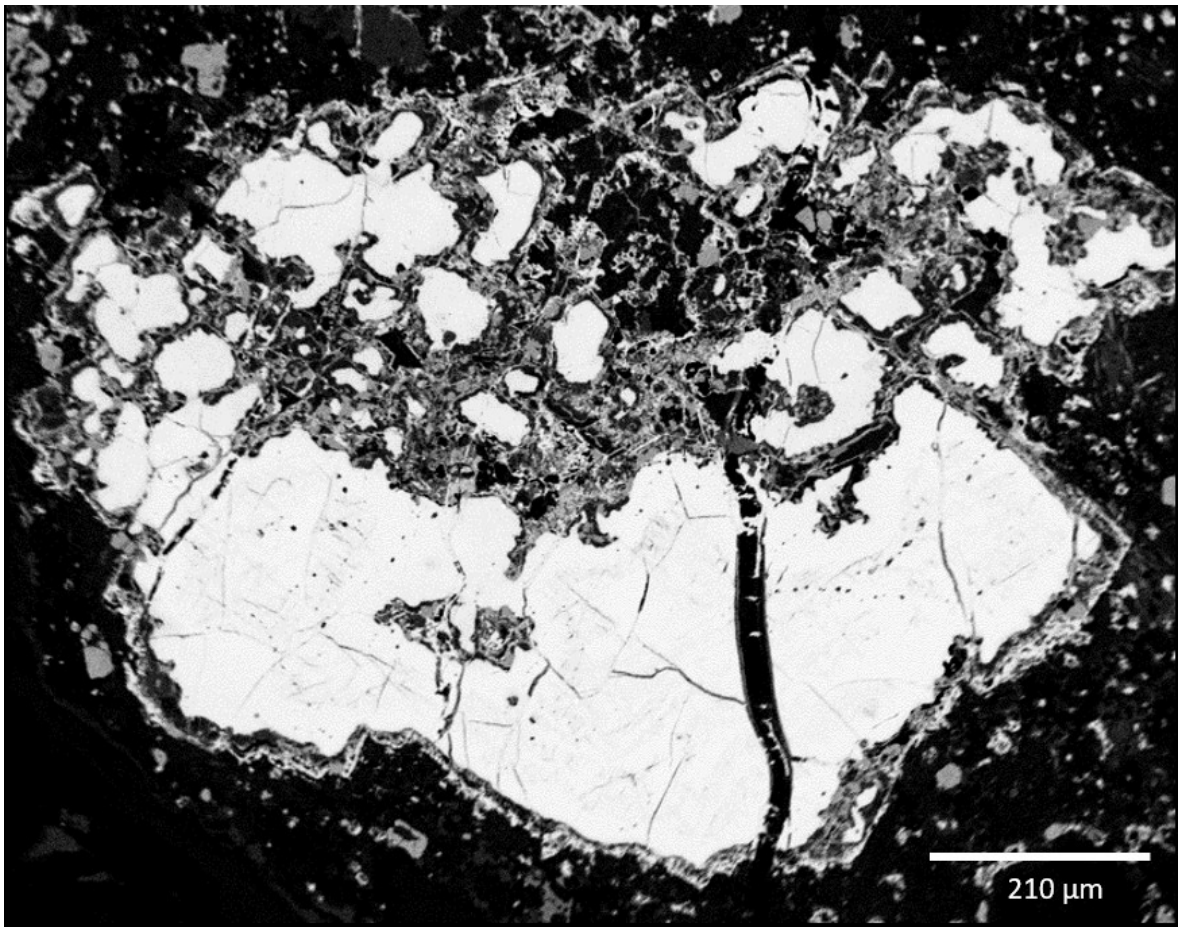

Fig. 10 – BSE image of xenocrystic magnetite in PK150 with extensive degradation in the upper half of the grain.

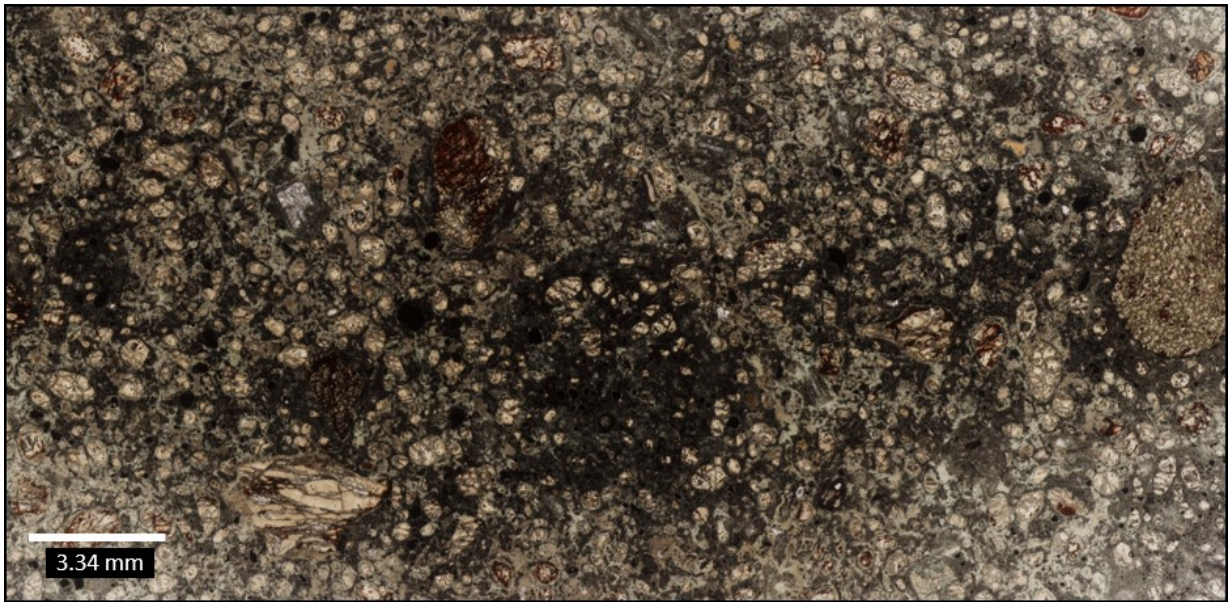

Fig 11 – Representative photomicrograph of a pseudomagmaclast in PK150 arising from serpentine alteration

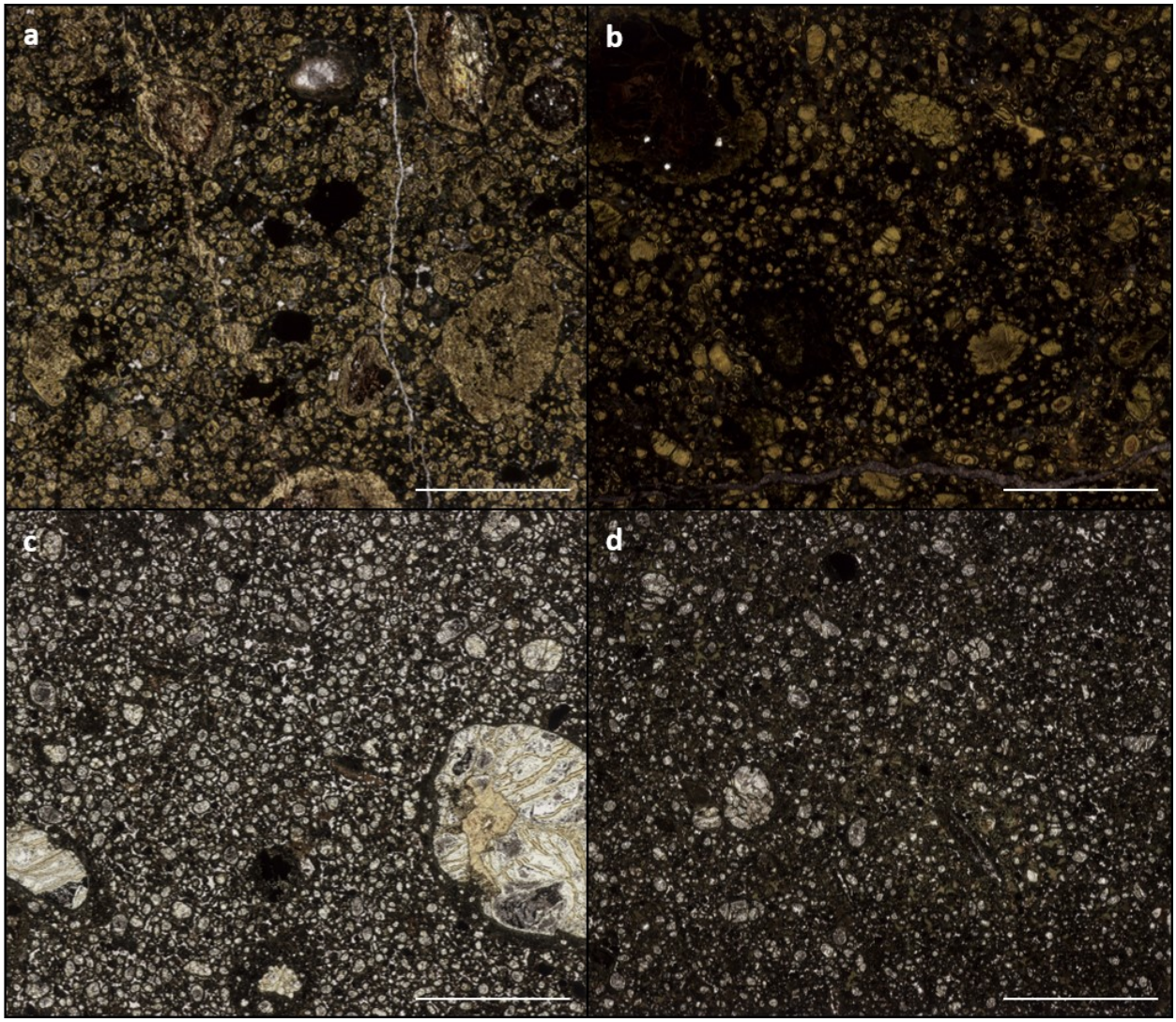

Fig. 12 – Photomicrographs depicting the distinct differences between PK150 (a and b) and PK346 (c and d) in terms of alteration and grain size. PK150 is dominated by serpentinization and is richer in macrocrysts, PK346 is overall more fine-grained and the olivine is largely replaced by carbonate. Scalebar is 6.75 mm.

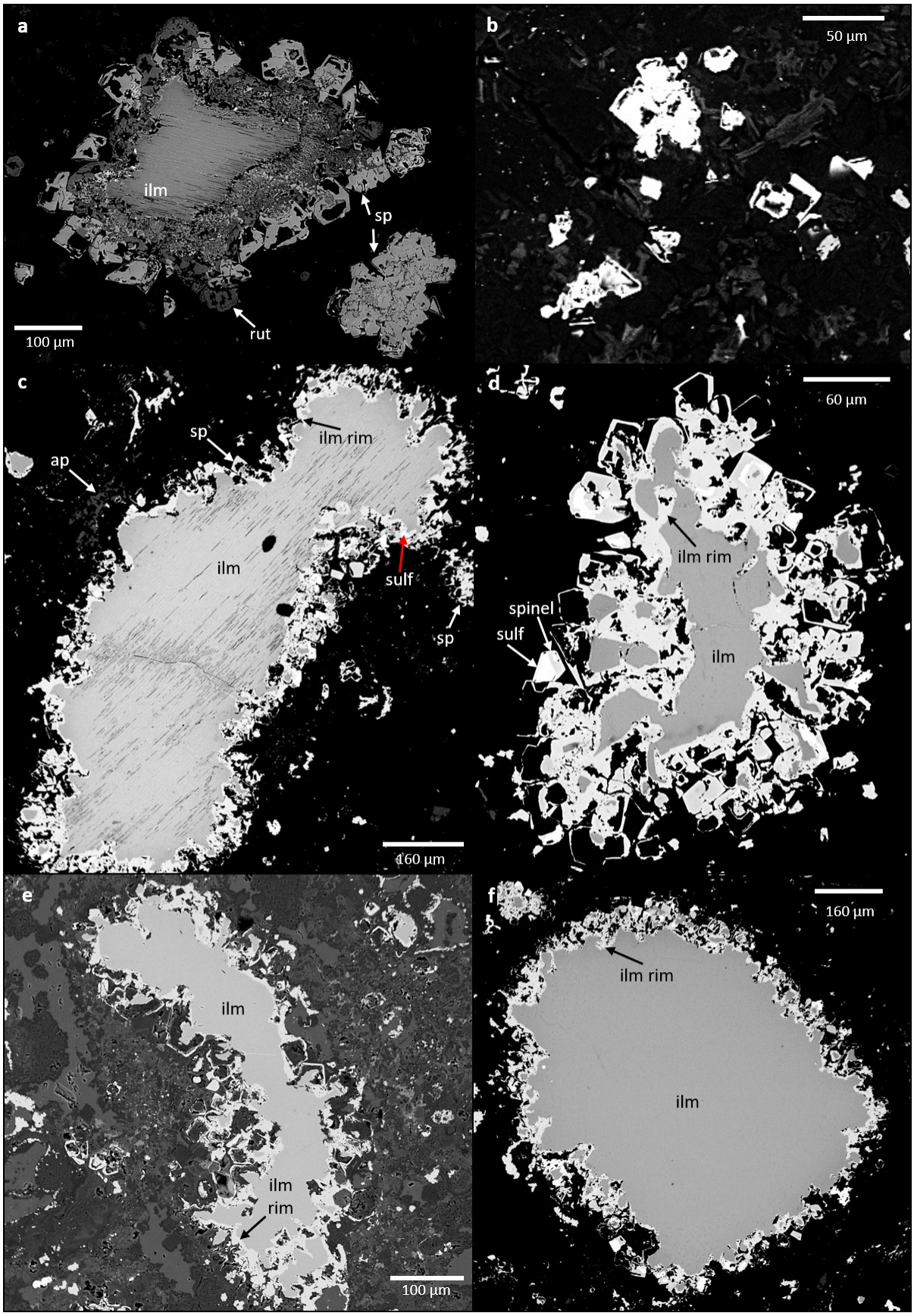
a
ilm
sp
rut
100 µm
b
50 µm
c
sp
ilm rim
ap
ilm
sulf
sp
160 µm
d
60 µm
ilm rim
spinel
sulf
ilm
e
ilm
ilm
rim
100 µm
f
160 µm
ilm rim
ilm

Fig. 13 – Representative BSE images of ilmenite textures in PK346; a) rare example of ilmenite in PK346 with rutile and exsolution lamellae, euhedral grains of titanomagnetite rim the ilmenite and cluster in the groundmass; b) cluster of spinel in groundmass with atoll texture; c) ilmenite with uncommon exsolution lamellae, rim of low MgO/high FeO ilmenite plus spinel and sulfide; d) relatively homogeneous main composition with low MgO/high FeO ilmenite rim, also containing spinel and sulfide droplets in the rim; e) heavily resorbed ilmenite and spinel pseudomorphed by serpentine (texture preserved) set in intergrown serpentine and calcite with bounding calcite segregations; f) large ilmenite macrocryst with homogeneous composition and lack of texture in main body but typical PK346 rim material, margins appear corroded; ilm = ilmenite, ilm rim = low Mg/high FeO ilmenite rim; sp = spinel, rut = rutile, ap = apatite, sulf = sulfide.

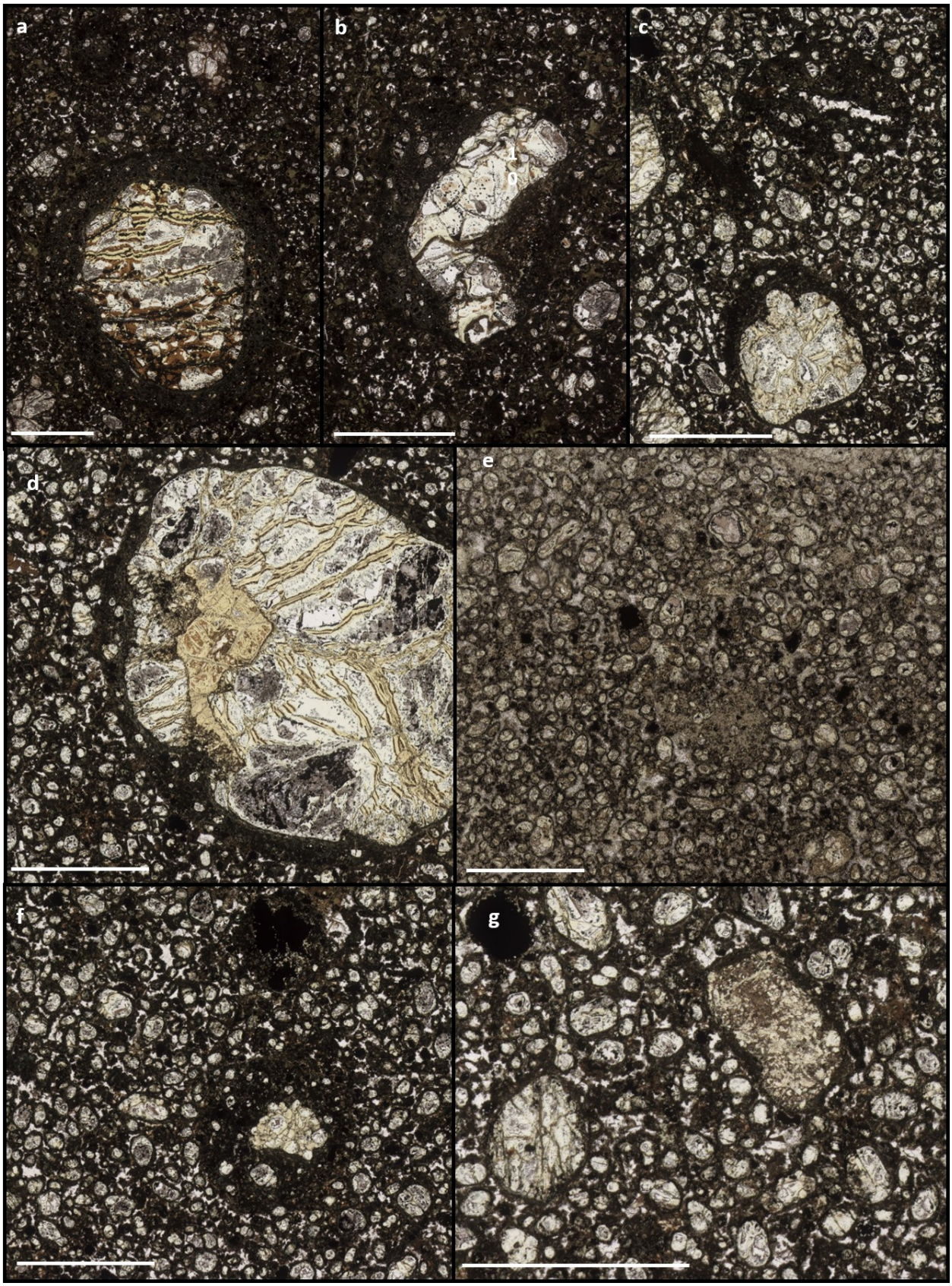
a
b
c
d
e
f
g

Fig. 14 – Representative photomicrographs of magmaclasts in PK346; a) complete, symmetrical, thick selvage of melt on heavily altered olivine core, components in the selvage have a faint tangential orientation; b) irregular, subangular olivine core with incomplete melt selvage; c) incomplete asymmetric selvage on irregular olivine core (bottom), pocket of dark serpentine of ambiguous origin (center left), and elliptical uncored magmaclast with irregular-shaped calcite strip and olivine microcrysts; d) incomplete selvage on serpentinized olivine macrocryst (alteration distinctly different from olivine microcrysts); e) thinly cut section emphasizing irregularity of serpentine distribution; f) complete selvage on broken ilmenite (top) and elliptical melt surrounding irregular olivine; g) characteristic coating of serpentine on all olivine micro- and macrocrysts, distinct from the abundant calcite segregations. Scale bar = 3.375 mm.

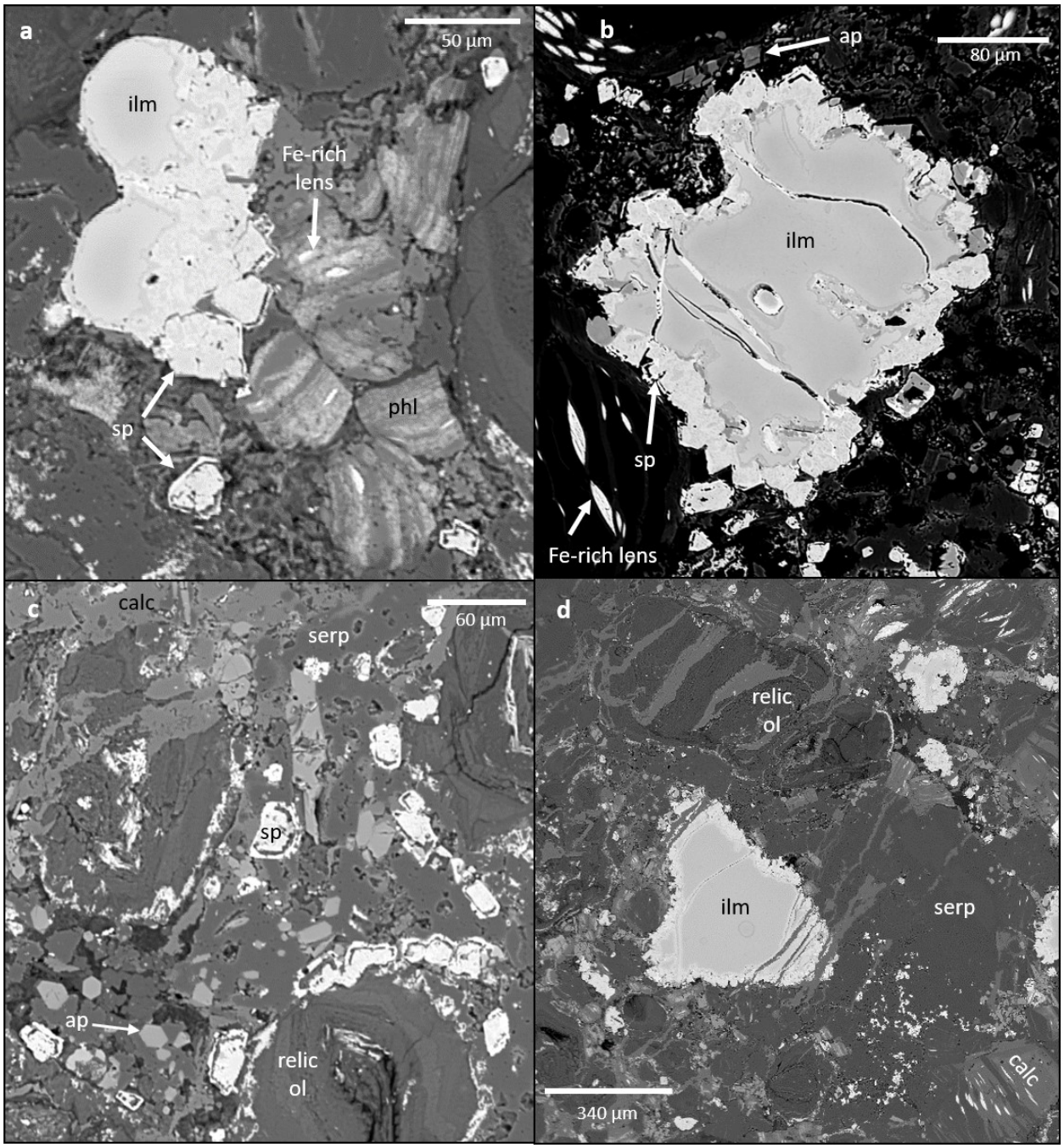

Fig. 15 – Representative BSE image of PK151's most peculiar textural characteristics; a) altered phlogopite with Fe-rich lenses adjacent to partially resorbed ilmenite; b) spinel bordering ilmenite with Mn-rich rim and olivine with Fe-rich lenses; c) prisms of apatite in serpentine-rich groundmass with atoll spinel; d) ilmenite with Mn-rich rim and relict olivine with swaths of calcite; ilm = ilmenite, sp = spinel, phl = phlogopite, ap = apatite, serp = serpentine, calc = calcite.

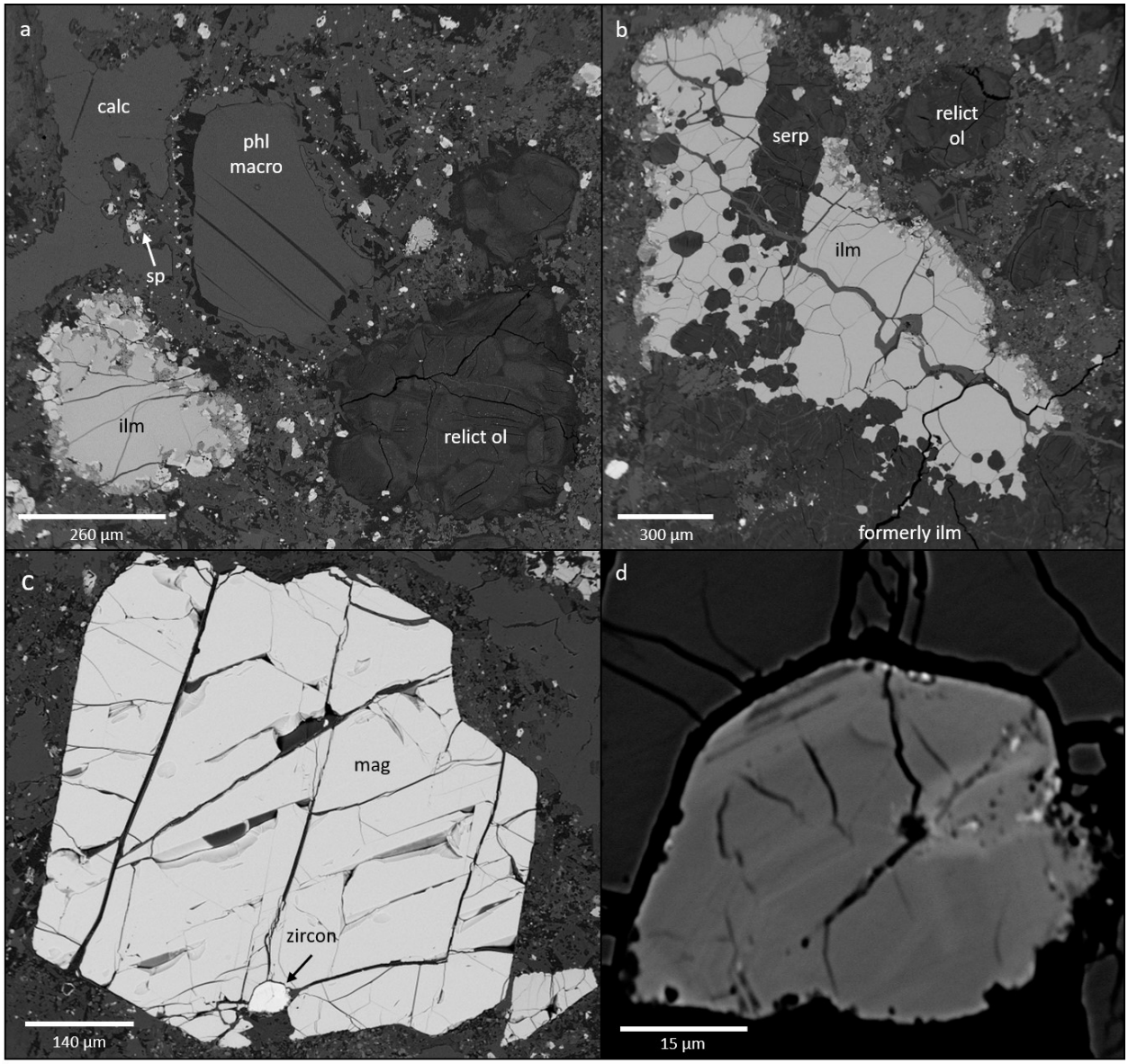

Fig. 16 – BSE images of PK312; a) pristine amoeboid calcite segregation (top left), rounded phlogopite macrocryst (center), ilmenite with bounding spinel (bottom left), and relict olivine (bottom right); b) ilmenite significantly overgrown by serpentine; c) magnetite with associated zircon (faintly zoned and surrounding calcite segregations; d) faintly-zoned zircon shown from c; ilm = ilmenite, calc = calcite, phl = phlogopite macrocrysts; ol = olivine, mag = magnetite.

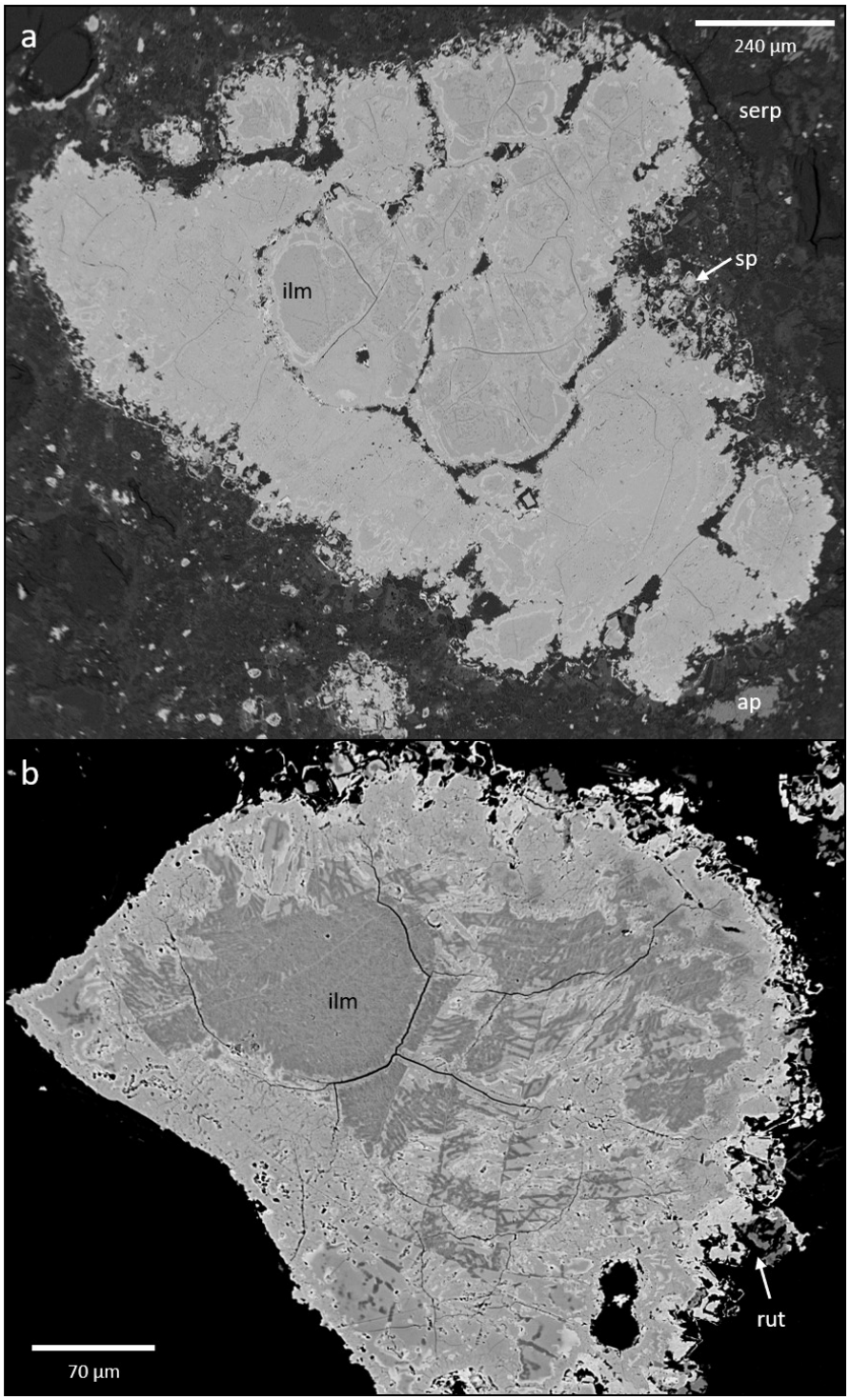

Fig. 17 – Representative BSE images of PK314; a) ilmenite with compositional variations throughout the grain (darker grey areas have higher Mg) and trails of serpentine replacement; ilmenite edges are resorbed with atoll spinel, apatite has many small patches of serpentine, and the groundmass in this areas is dominantly composed of intergrown serpentine and calcite; b) heavily textured PK314 ilmenite with compositional variations throughout the grain with minorly resorbed edges and rutile within the rim.

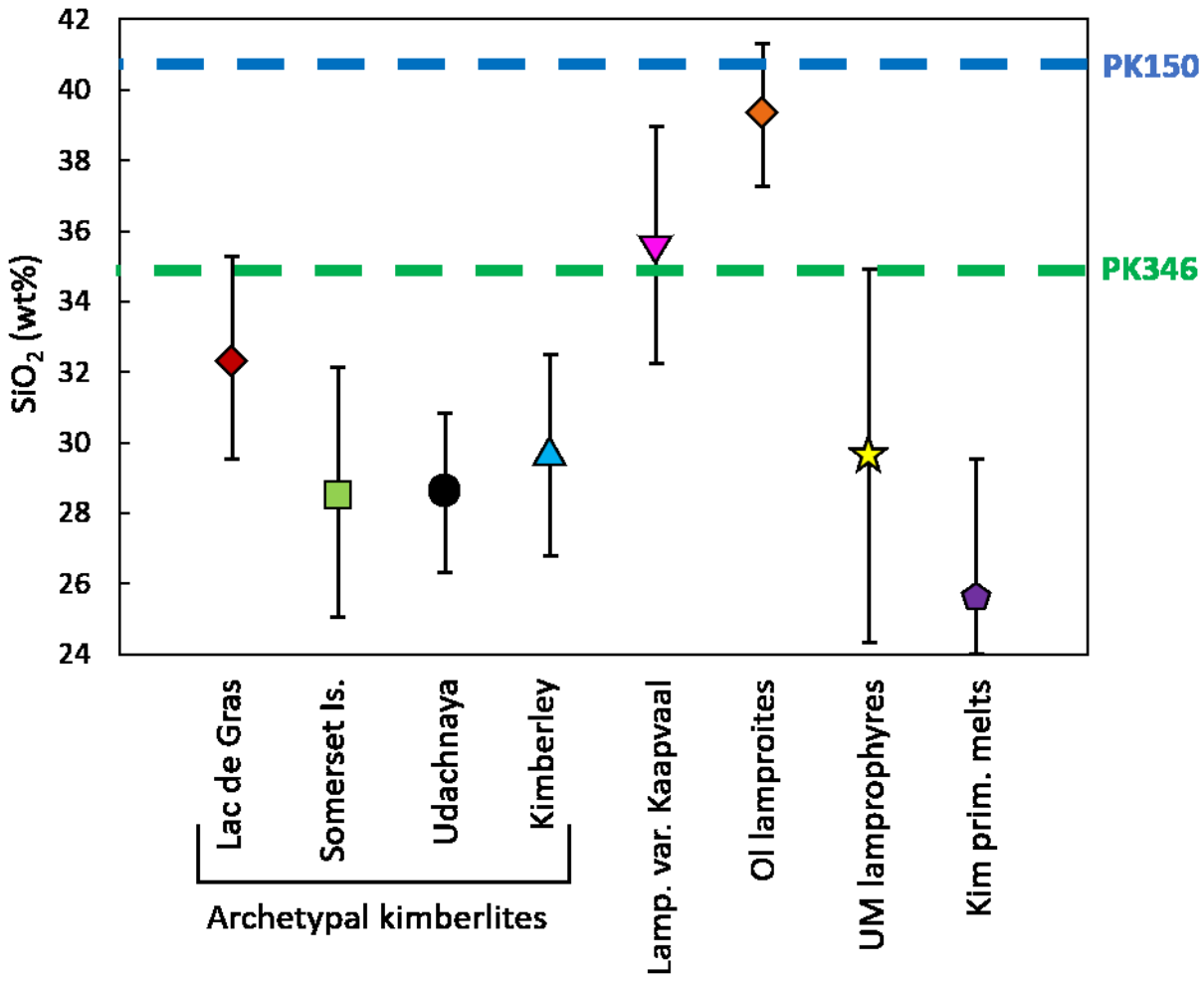

Fig. 18 – Comparison of Pikoo whole rock SiO_2 contents to various rock types including a selection of archetypal kimberlites, lamproites var. Kaapvaal (previously known as orangeites), olivine lamproites (Ol lamproites), ultramafic lamprophyres (UM lamprophyres), and kimberlite primitive melts. The high SiO_2 of Pikoo in comparison to other archetypal kimberlites is likely the result of serpentinization. Adapted from Pearson et al. (in press).

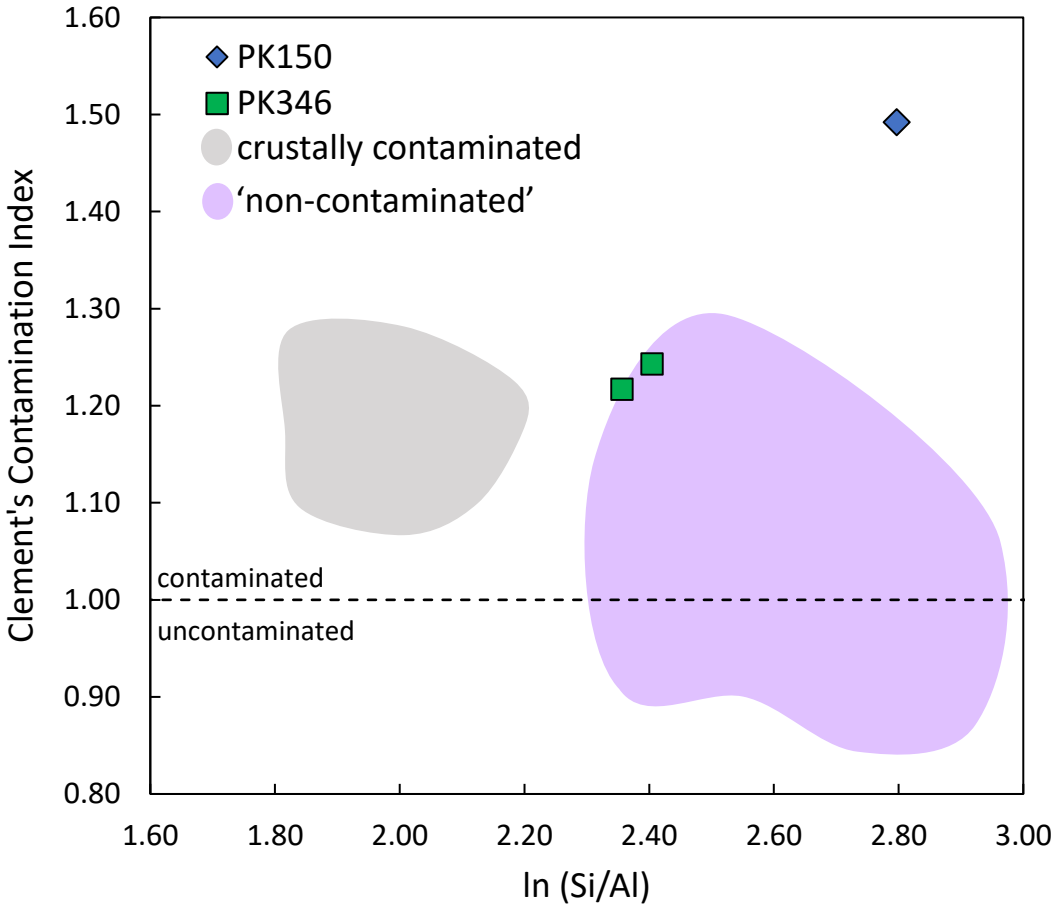

Fig. 19 – C.I. vs ln(Si/Al) for Pikoo samples; crustally contaminated and 'non-contaminated' fields from Kjarsgaard et al. (2009b) based on Lac de Gras samples.

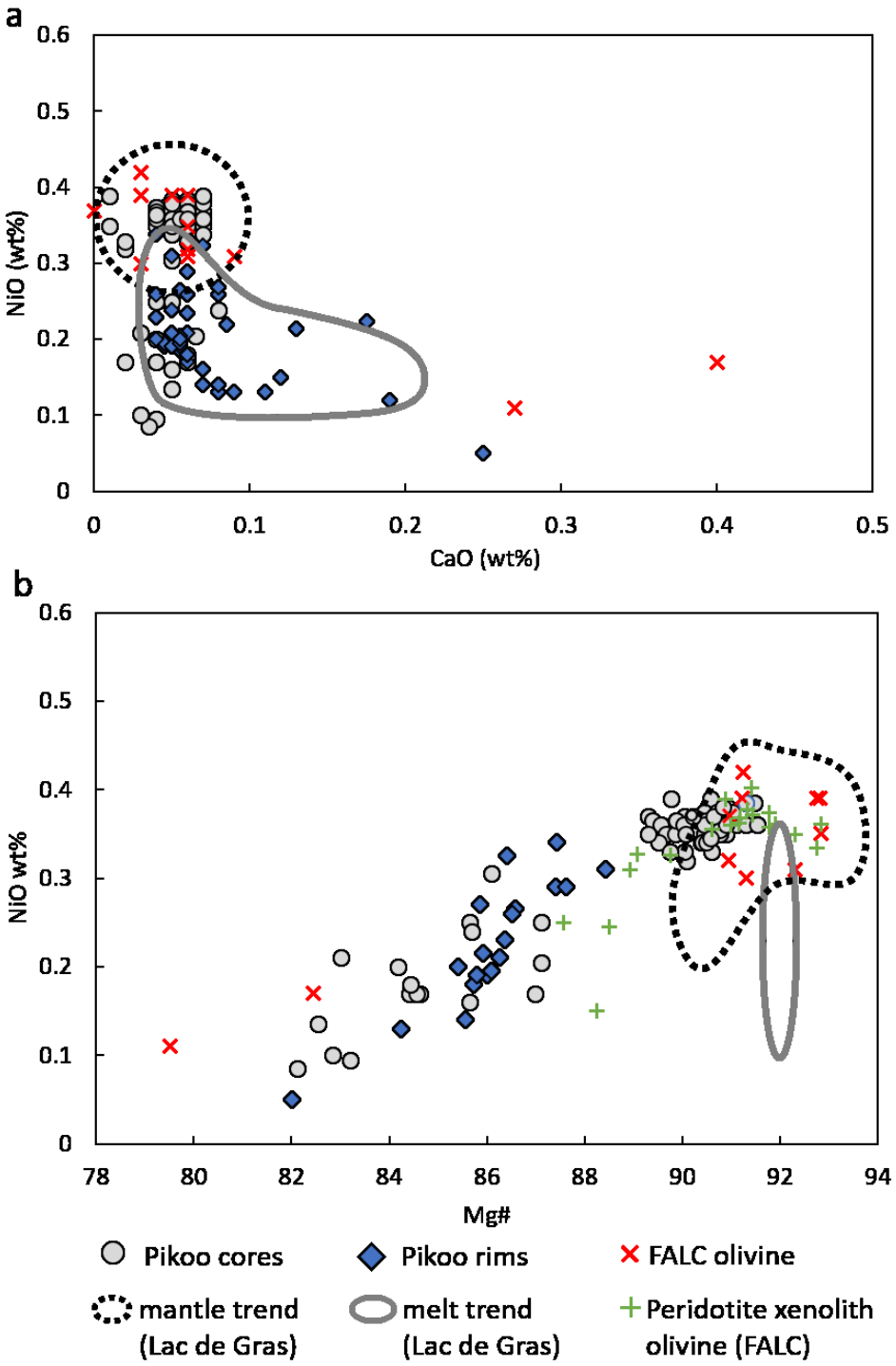

Fig. 20 – Olivine from PK150 exhibits rim chemistry that falls well within the melt trend in NiO vs CaO space (a) but displays a decrease in NiO over a much larger range in Mg# than the typical melt trend (b). Many core analyses fall within the mantle trend but a quarter overlap well with the rim values. Lac de Gras olivine mantle and melt trends from Bussweiler et al. (2015), olivine from peridotite mantle xenoliths from FALC from Czas et al. (submitted) and FALC olivine data from Leahy (1996).

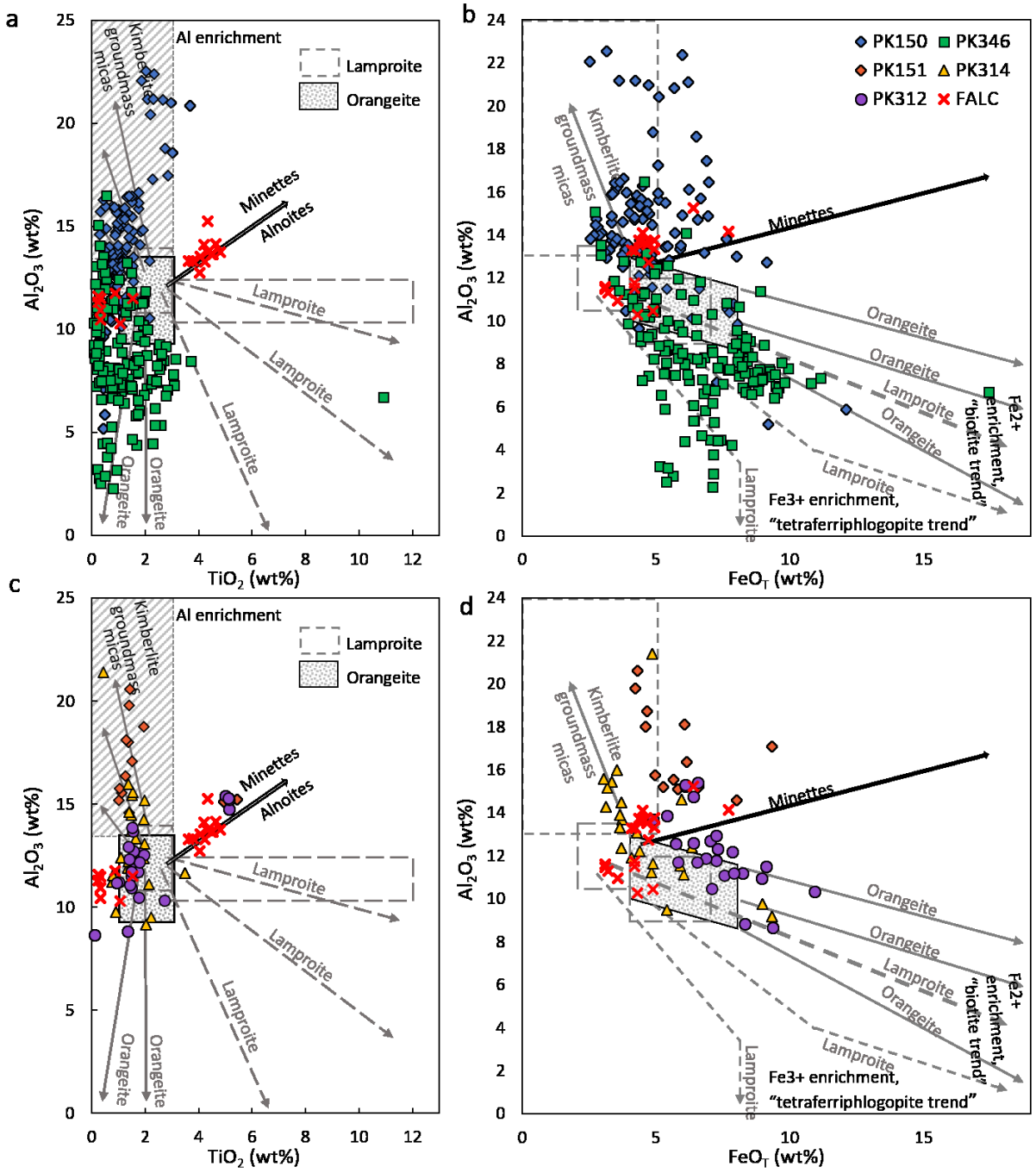

Fig. 21 – Compositional variation in groundmass phlogopite from Pikoo; a and b) PK150 falls along the typical kimberlite trend, PK346 overlaps with PK150 within the kimberlite box but extends to lower TiO_2 and higher FeO_T; c and d) PK151 and PK314 appear to follow a similar trend to PK150 but to lesser degrees of enrichment/depletion; the dataset for PK312 is insufficient to determine whether the data is more akin to the tetraferriphlogopite or biotite trend. FALC analyses plotted for reference (Leahy, 1996; Chalapathi Rao et al., 2017) and compositional trends from Mitchell (1995). It should be noted that it is now recommended that the term orangeite be replaced with lamproite var. Kaapvaal (Scott Smith et al., 2018).

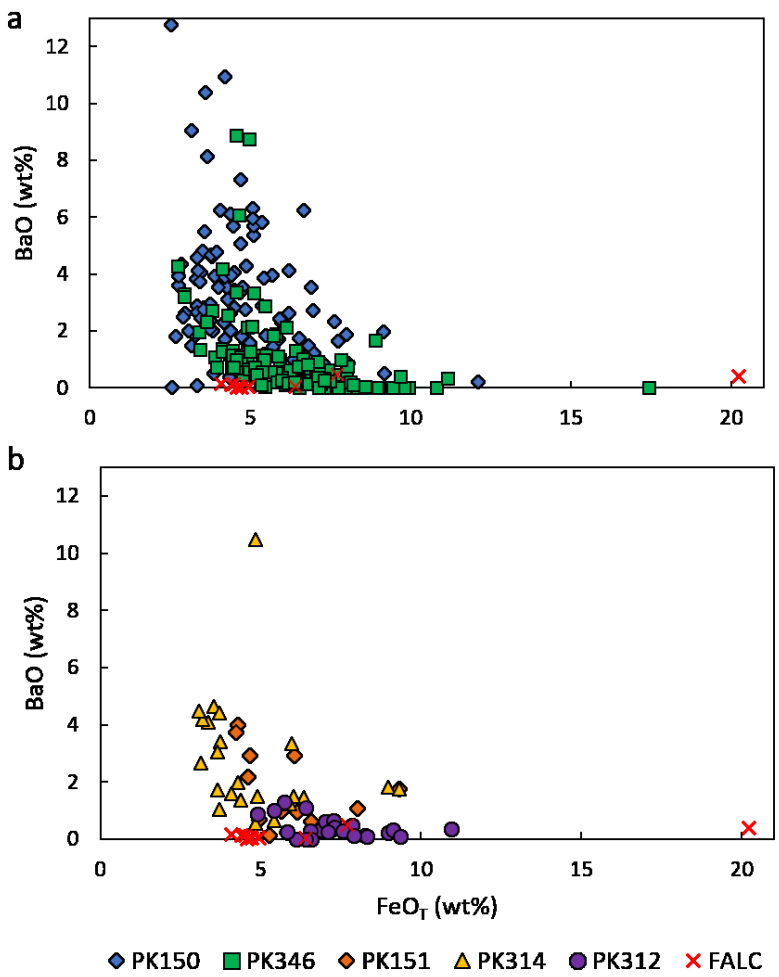

Fig 22 – Groundmass phlogopite can exhibit considerable Ba enrichment in some samples; a) depicts PK150 and PK346, b) depicts PK151, PK312, and PK314; FALC analyses from Chalapathi Rao et al. (2017).

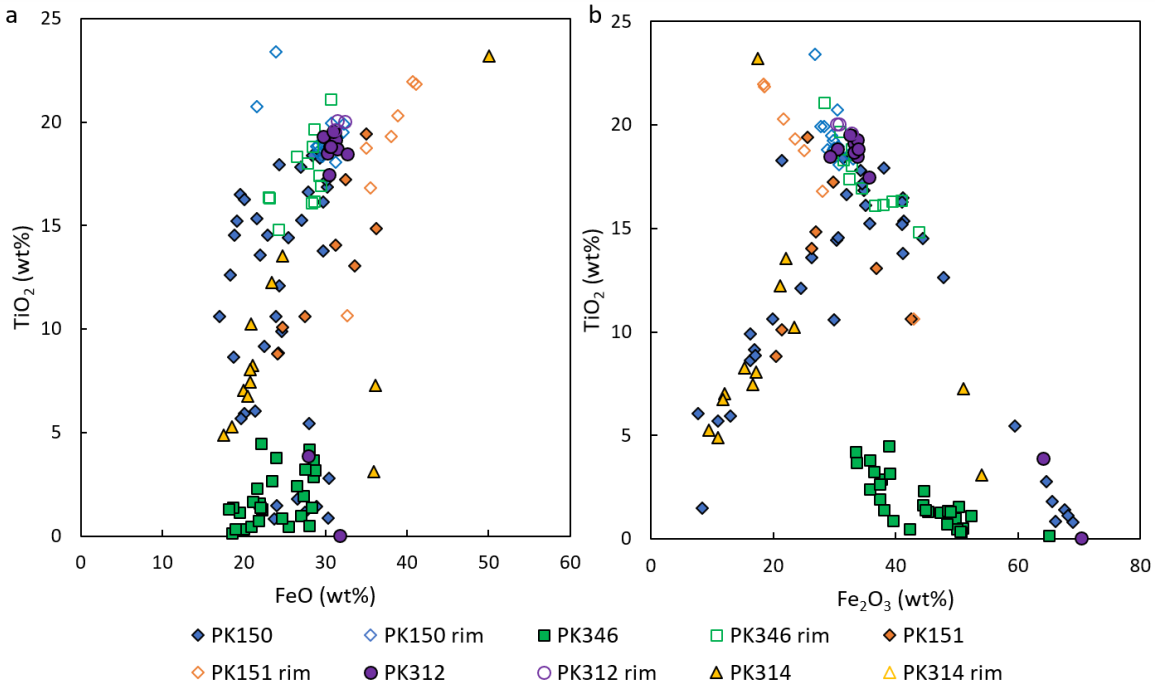

Fig. 23 – Spinel analyses plotted in terms of a) TiO_2 vs FeO and b) TiO_2 vs Fe_2O_3. Labels of "rim" indicate spinel intergrown with ilmenite reaction rims, which plot at high TiO_2. Analyses plotting in the lower left corner of b) are reflective of magnetite (infilling fractures, within the groundmass, or disaggregated components of xenocrysts).

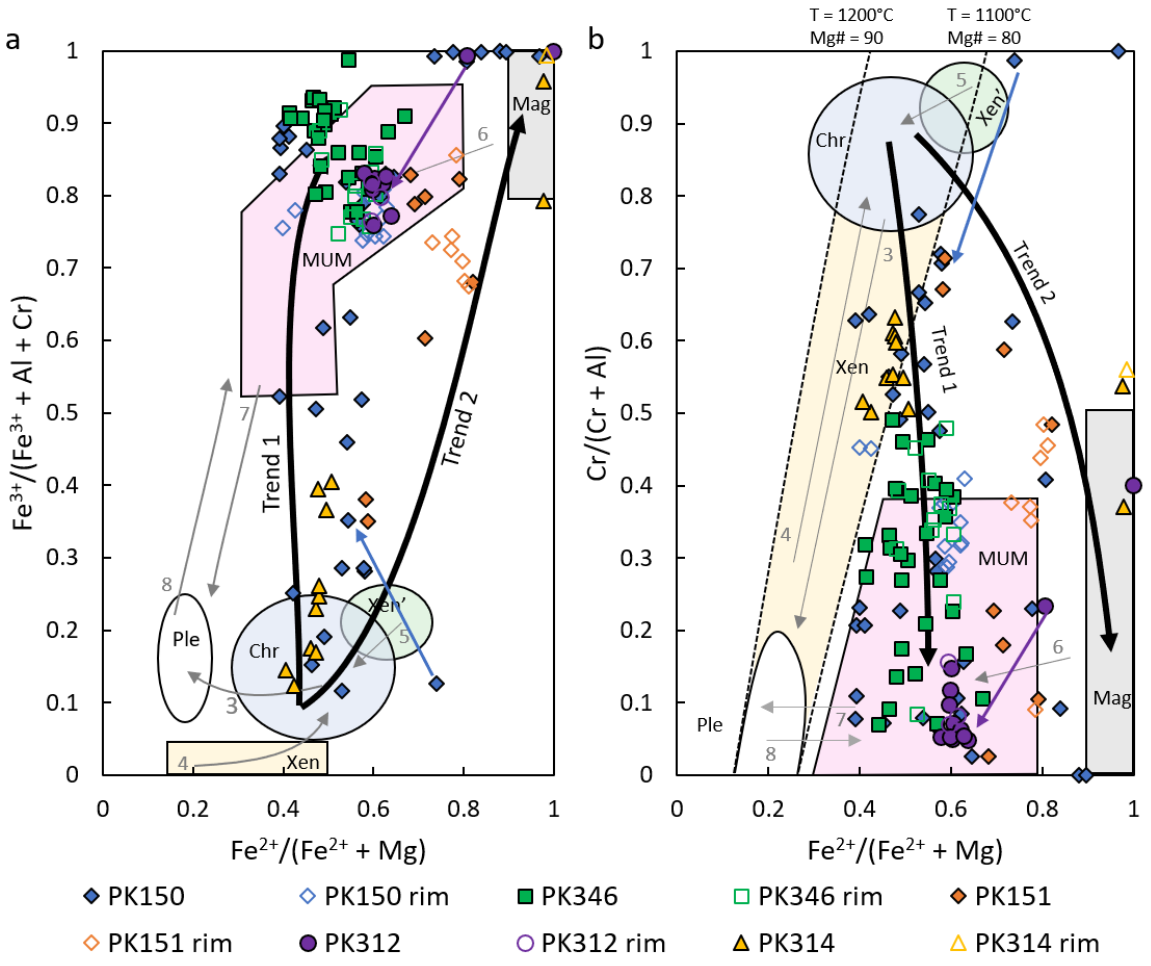

Fig. 24 – Plots of a) $Fe^{3+}/(Fe^{3+} + Al + Cr)$ vs $Fe^{2+}/(Fe^{2+} + Mg)$ and b) $Cr/(Cr + Al)$ vs $Fe^{2+}/(Fe^{2+} + Mg)$ for Pikoo spinel group minerals; 'rim' indicates spinel in ilmenite reaction rims. Curves for Trend 1 and 2 after Mitchell (1986), arrows for Trends 3—8 after Roeder and Schulze (2008). Mag = magnetite, MUM = magnesian ulvöspinel—ulvöspinel—magnetite, Chr = chromite, Ple = pleonaste, Xen = xenolith, Xen' = metasomatized xenolith.

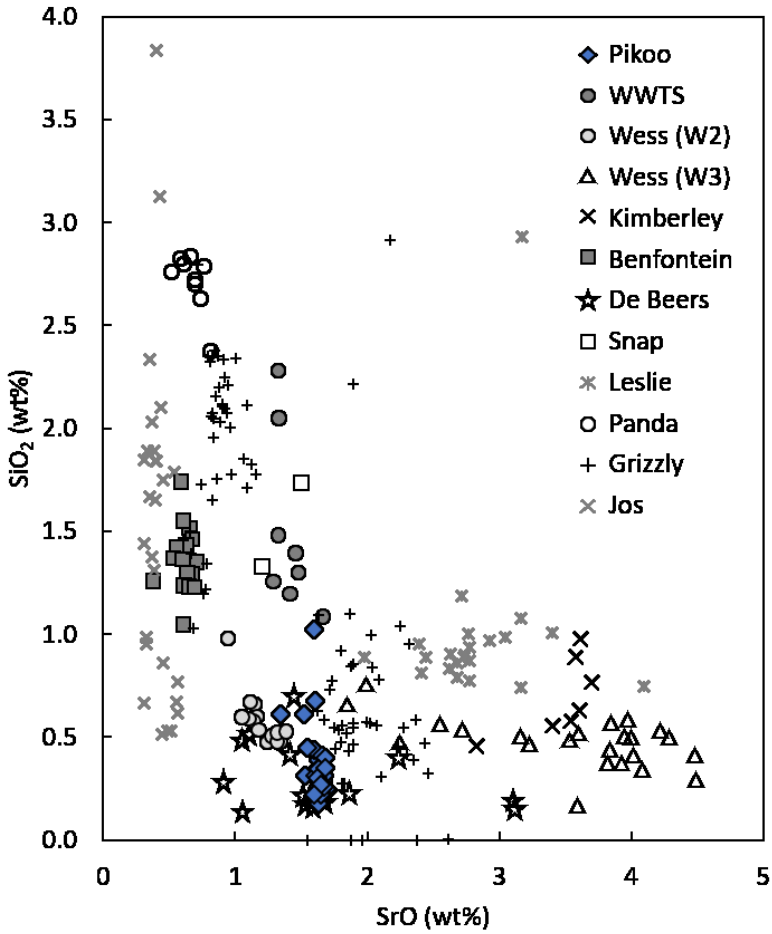

Fig. 25 – SiO_2 vs SrO (wt%) for apatite from Pikoo (PK150) compared to apatite from other kimberlites. Benfentein, Wesselton (W2 and W3), Wesselton water tunnel sills, and Kimberley Mine from Soltys et al. (2017); Leslie, Panda, Grizzly, and Snap (Type 1, 2 and 3) from Milligan (2017); Jos from Malarkey et al. (2010).

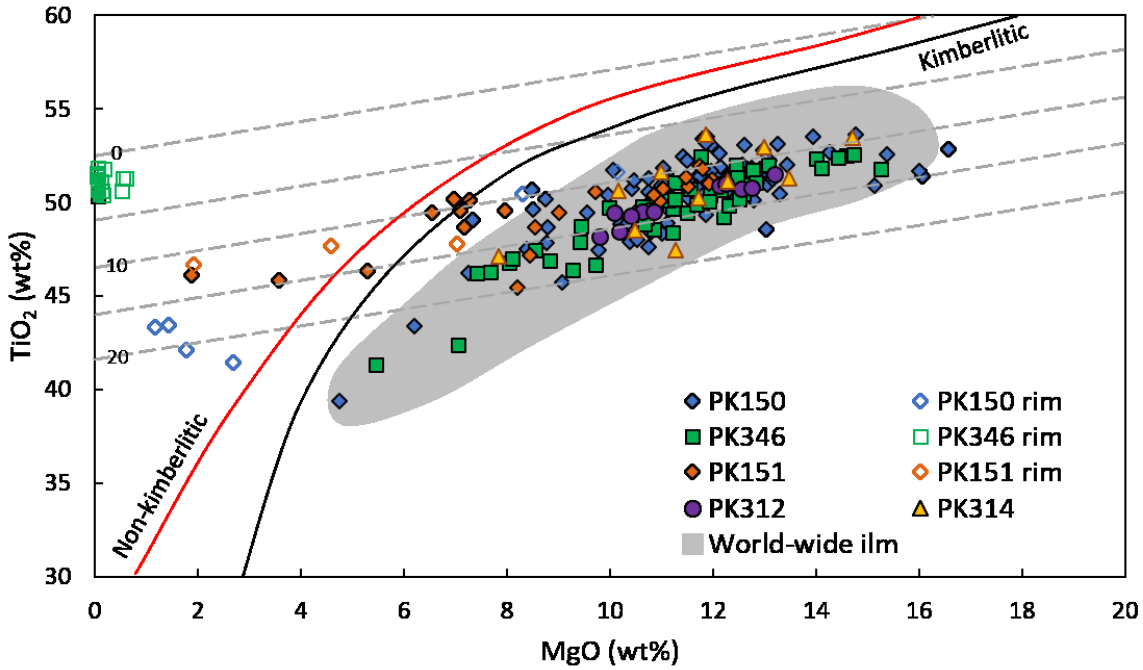

Fig. 26 – Plot of TiO_2 vs MgO showing classification of kimberlitic (black bounding line) and non-kimberlitic (red) ilmenite (Wyatt et al., 2004). Pikoo ilmenite plots firmly within the kimberlitic field and with good overlap with worldwide kimberlitic ilmenite, except for the ilmenite rim composition of PK346 and a portion of PK150. Dashed lines represent contours of Fe_2O_3, grey field of world-wide ilmenite from Kaminsky et al. (2004).

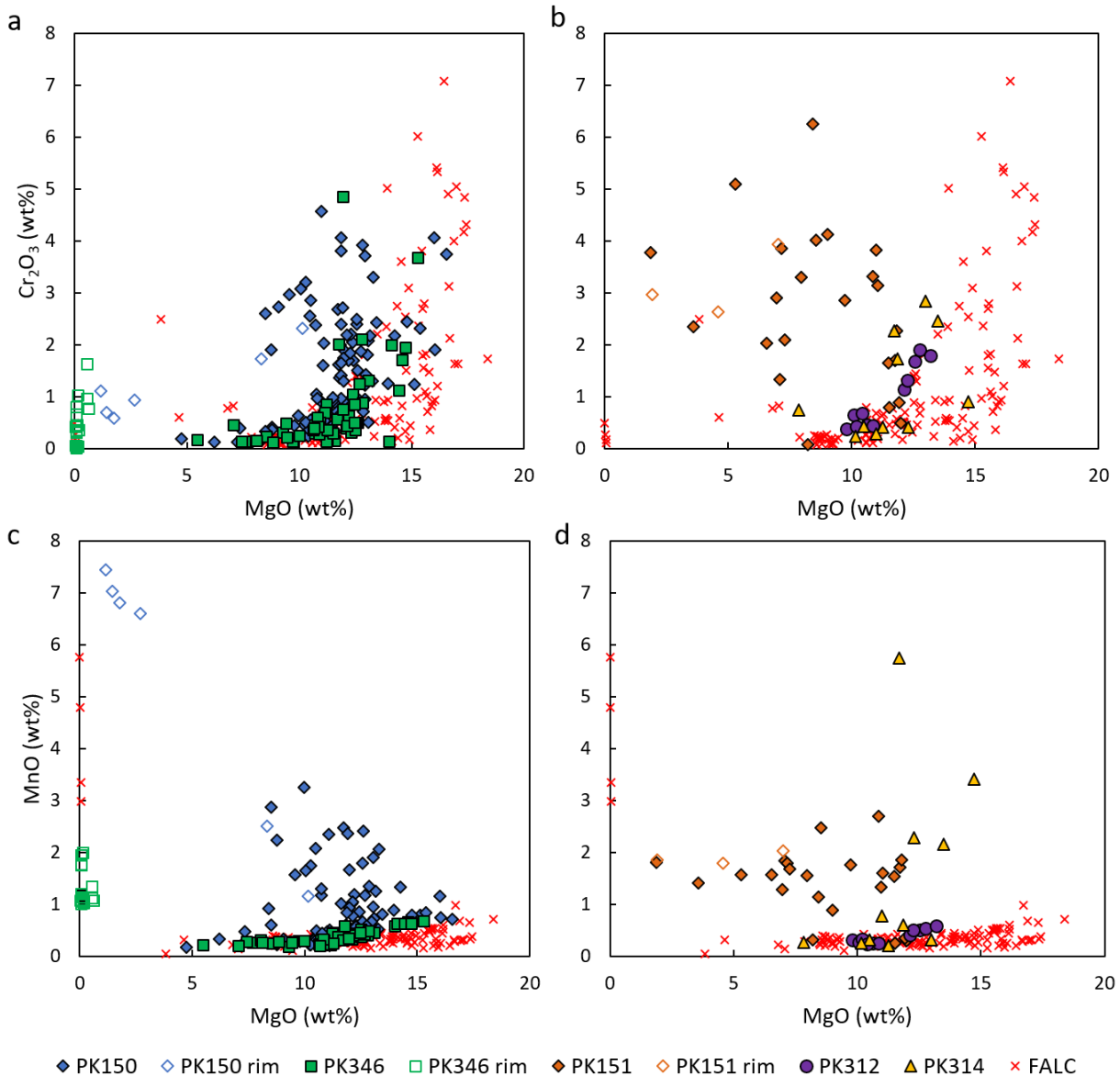

Fig. 27 – Ilmenite minor element chemistry of MnO (a and b) and Cr_2O_3 (c and d). PK150, PK151, and PK314 show significantly greater enrichment in Mn. 'Rim' indicates the ilmenite composition of the outermost margin, distinct from the core composition. FALC analyses from Leahy (1996) and Chalapathi Rao et al., (2017).

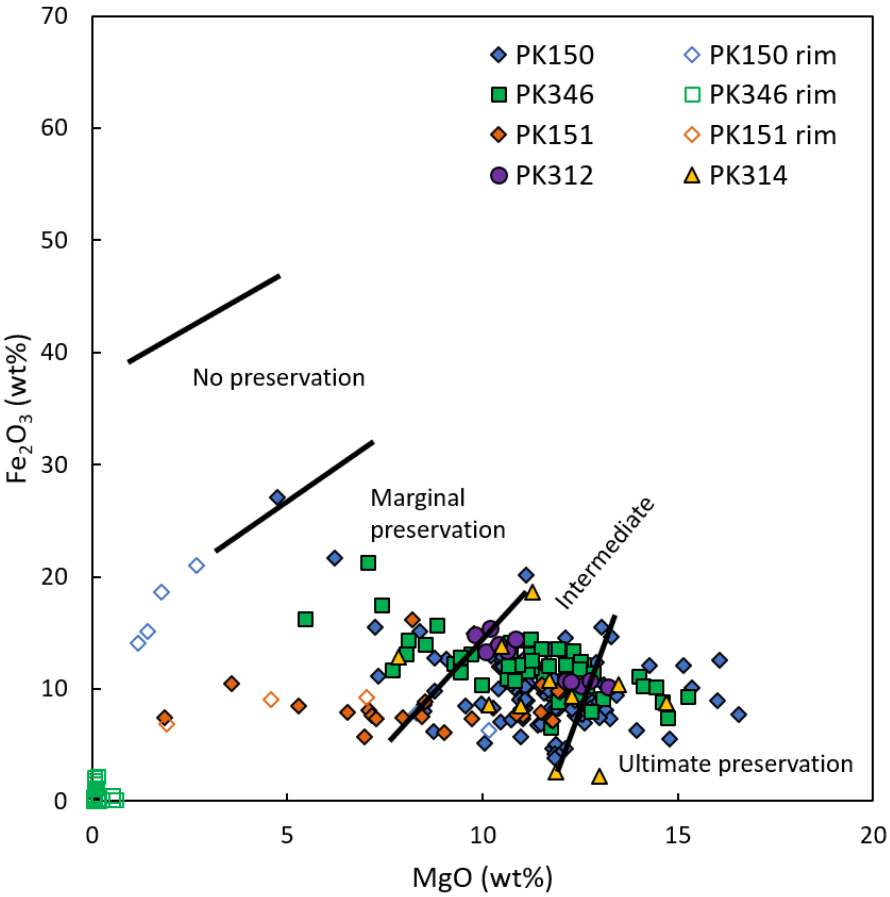

Fig. 28 – Plot of Fe_2O_3 vs MgO for Pikoo ilmenite. A negative correlation between ilmenite composition and the preservation potential of diamond as higher oxygen fugacity leads to greater resorption. Pikoo ilmenite plots dominantly in the intermediate to ultimate preservation fields. 'Rim' indicates the ilmenite composition of the outermost margin, distinct from the core composition. Classifications from Gurney and Zweistra (1995) are based on South African kimberlites and should only be taken as an indication of diamond preservation.

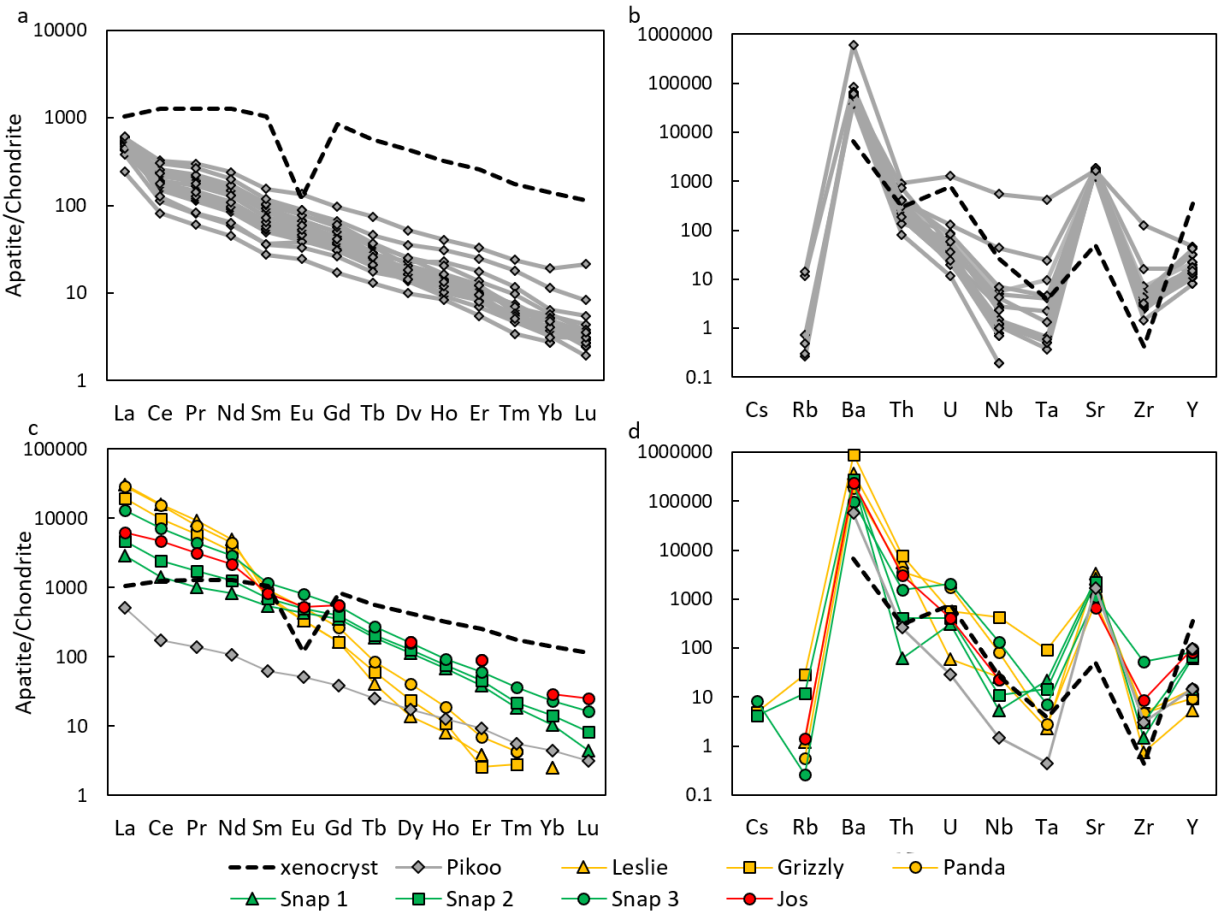

Fig. 29 – REE and spider diagrams of trace elements for apatite normalized to CI chondrites (McDonough and Sun, 199) in Pikoo (a and b); c and d) comparison of median Pikoo values to representative compositions of other kimberlitic apatite from Ekati (Leslie, Grizzly, and Panda; Milligan, 2017), Snap Lake (Snap Type 1, Type 2, and Type 3; Milligan, 2017), and Jos (Malarkey et al., 2010). Representative crustal xenolith apatite from Leslie plotted for reference (dashed black line; Milligan, 2017).

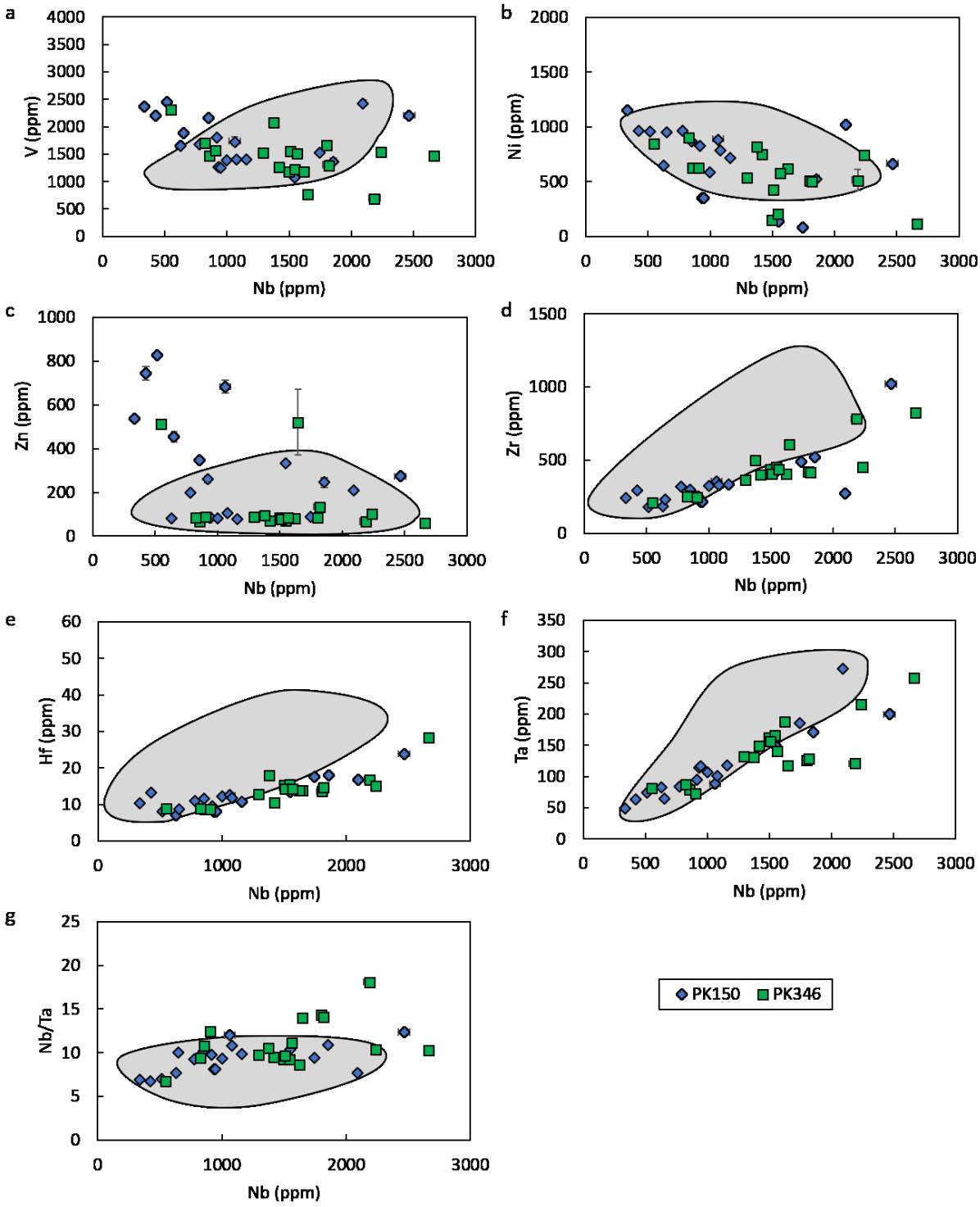

Fig. 30– Subset of ilmenite trace elements for Pikoo. Fields for ilmenite found in kimberlite and related secondary ilmenite shown in grey from Castillo-Oliver et al. (2017) and references therein. Note: the variety Castillo-Oliver et al. (2017) termed "symplectic ilmenite" can reach HFSE levels significantly higher than Mg-enriched nodular ilmenite, xenocrysts, tabular ilmenite, and secondary Mn-rich ilmenite (varieties included in the grey field) and thus could not be displayed adequately.

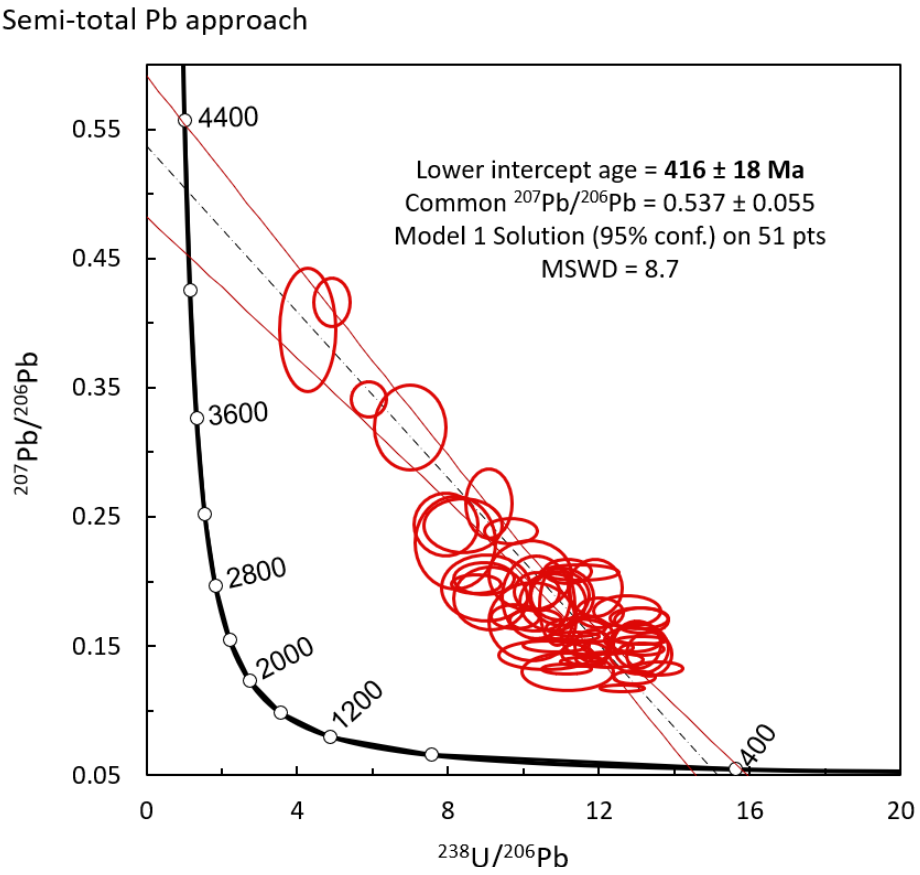

Fig. 31 –Tera-Wasserburg diagram for semi total Pb approach with uncorrected perovskite data from Pikoo. Common Pb composition derived by intersection with the y-axis ($^{207}Pb/^{206}Pb$), lower intercept age from intersection with thick solid black concordia line. Decay constant errors are included. Red lines represent error envelope on extrapolation (dashed line). Data point error ellipses are 95% confidence.

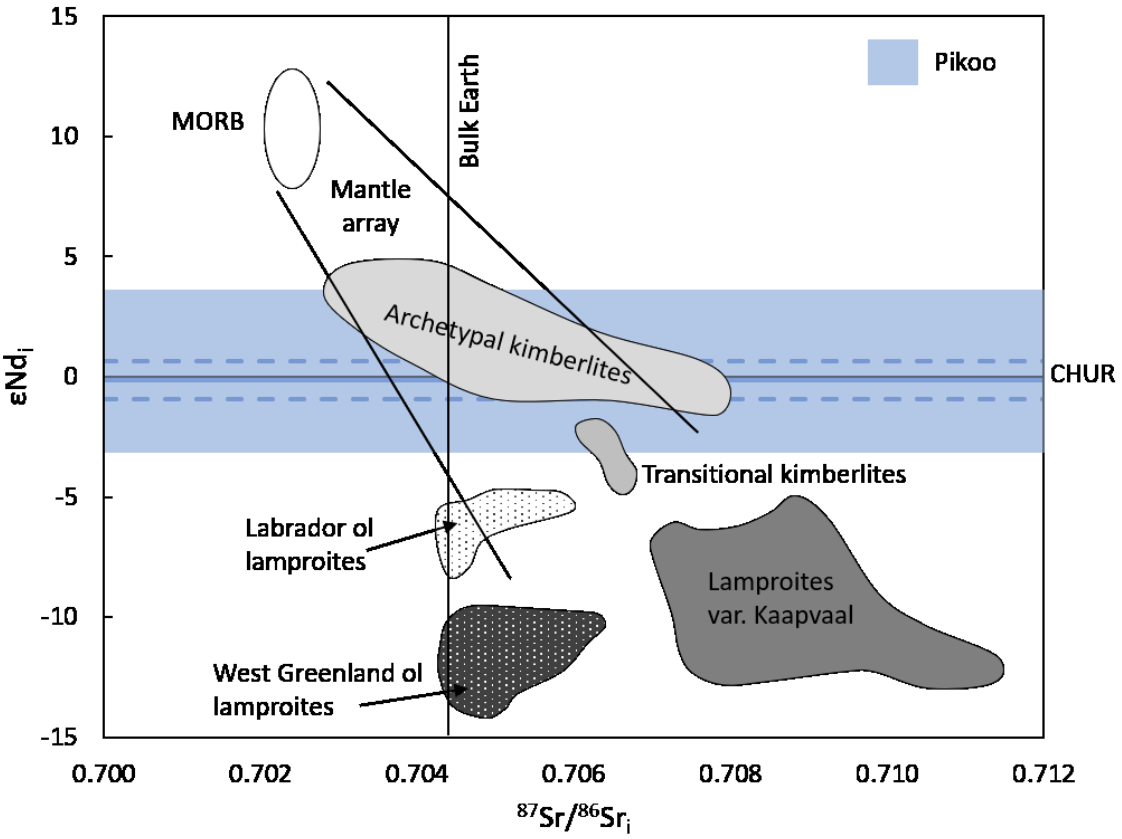

Fig. 32 – εNd_{417} of Pikoo calculated from PK150 perovskite (blue band; Sr composition unknown) overlaying εNd_i vs $^{87}Sr/^{86}Sr_i$ for archetypal kimberlites in comparison to lamproites var. Kaapvaal. Weighted mean εNd_i for Pikoo is -0.18 ± 0.80, represented by the solid blue and dashed blue lines. Adapted from Nowell et al. (2004) with fields for Labrador and West Greenland olivine lamproites adapted from Sarkar et al. (2018).

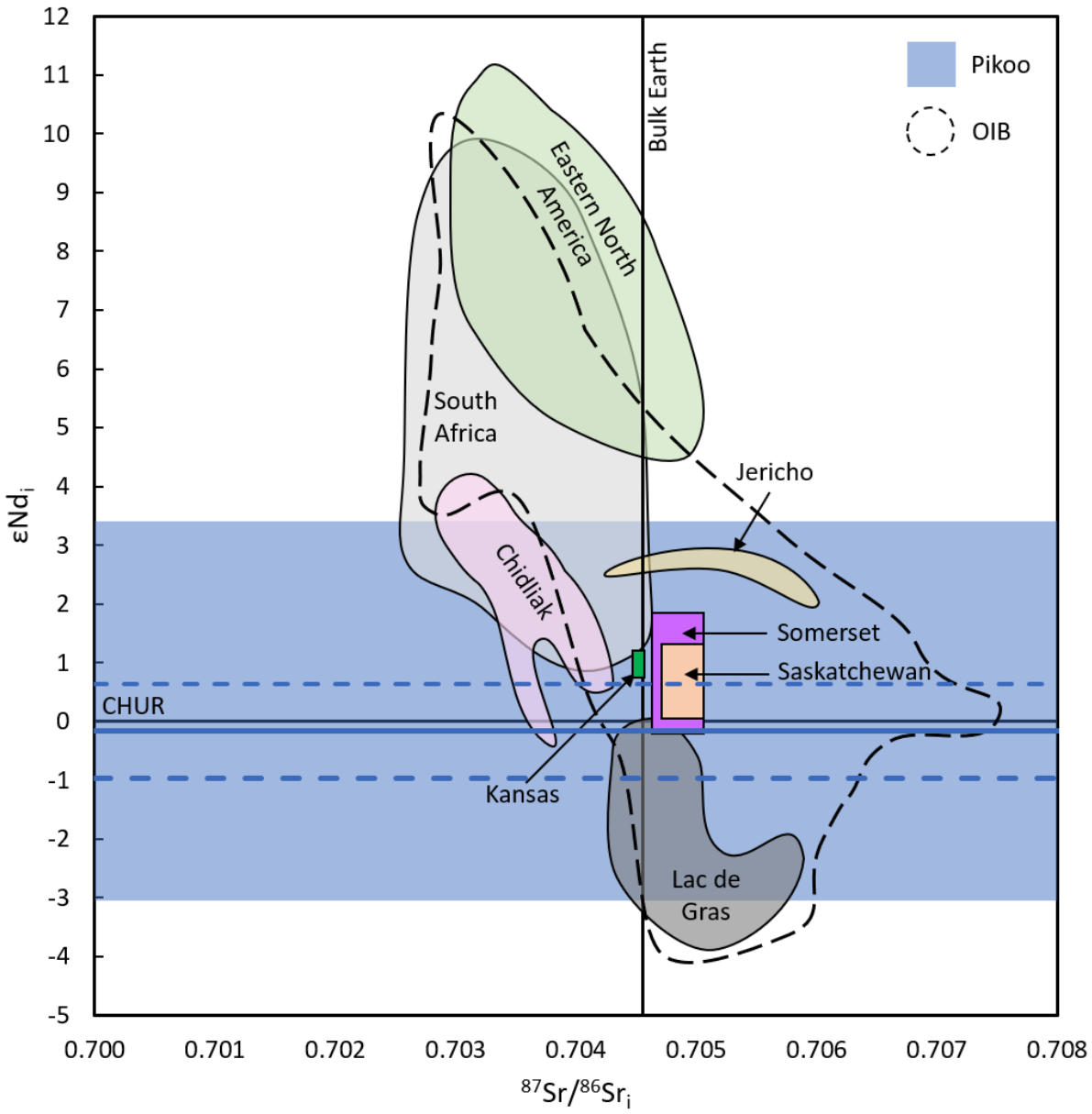

Fig. 33 – Plot of εNd_i versus $^{87}Sr/^{86}Sr_i$ with fields for kimberlites of the mid-Cretaceous corridor and other regions with archetypal kimberlites. The range for εNd_{417} of Pikoo calculated from PK150 perovskite (blue band; Sr composition unknown) overlaps with Saskatchewan perovskite results. Weighted mean εNd_i for Pikoo is -0.18 ± 0.80, represented by the solid blue and dashed blue lines. Fields analyzed determined from perovskite (Eastern North America, South Africa, Chidliak), whole rock (Jericho, Lac de Gras), or a combination of components (using Sr from perovskite and Nd from whole rock + perovskite for Saskatchewan and Somerset; using Sr_i from phlogopite isochron and εNd_i from whole rock for Kansas). Adapted from Kjarsgaard et al. (2017) and references therein.

Appendix C – Ilmenite Standard

In anticipation of an extensive ilmenite LA-ICP-MS trace element study, efforts where made to identify a suitable homogeneous, matrix-matched secondary ilmenite standard. Ilmenite from PHN5814 was liberated from hand sample and then crushed into small fragments using a rock hammer. Fragments of PHN5814 were chosen from two areas of the hand sample, ten centimeters apart (PHN5814a and PHN5814b). Ilmenite concentrate from Sverdrup Basin (99-19-146 and 99-18-122-9) was previously isolated and available for analysis. The fragments were scrutinized with a hand lens and the purest those with minimal contamination were selected for further study. The fragments were separated into clean plastic vials and repeatedly run through an ultrasonic bath until no more surface contaminants could be removed. The fragments were placed in a mount, encased in epoxy, and then exposed through polishing. As an initial assessment of homogeneity, the ilmenite mounts were analyzed by WDS on a CAMECA SX100 EPMA in the same method described in section 4.3 (analytical settings for this session reported in Table 20). Major and minor oxides of Nb_2O_5, SiO_2, ZrO_2, TiO_2, ZnO, Al_2O_3, V_2O_3, Cr_2O_3, FeO_T, NiO, MnO, MgO, Ca, Na_2O, and K_2O were analyzed. Two approximately perpendicular transects (each consisting of 23 to 26 points) were plotted on each of the samples to asses the compositional variation throughout the grain (Fig. 34). Each transect consisted of 23 to 26 points of approximate even spacing, though fractures or dust specks required some points to be offset slightly. The exposed portion of PHN5814b was irregular and much narrower so one approximately north-south transect was plotted with four shorter east-west transects (n = 5 for each) plotted at regular intervals along the length of the exposed area (Fig. 34b). The major and minor element chemistry is reported in Table 21 and a summary of statistical variation is

provided in Table 22. Also included is data from the NMNH ilmenite standard as a comparison to a reasonably homogeneous sample.

The ideal chemical formula for ilmenite is $FeTiO_2$. While the intended purpose for the ilmenite standard is ultimately for trace element work, it is important to first asses the Fe and Ti content as both Fe and Ti are used as internal standards when processing ilmenite trace elements with Iolite (version 3.32). The most significant component is TiO_2, comprising roughly 50 % of the total oxide content. Ilmenite 99-18-122-9 has a range of 1.21 wt% TiO_2 across 1 mm though the range is smaller in 99-19-146 at 0.4 wt%. Ilmenites 99-19-146 and 99- have FeO ranges of approximately 0.7 and 1 wt%, respectively.

The difference in the mean value of TiO_2 between the two PHN5814 fragments is almost 2 wt%, with appreciable variations within each grain as well (Fig. 34). Unfortunately, there is often a greater variation in Fe content. The internal standard chosen for processing the preliminary trace element results (see 4.4) was ^{57}Fe as it generally performed more accurately for repeated analyses of the secondary standard BIR-1G (Fig. 35), which has more similar trace element contents to the Pikoo ilmenite than the secondary standard GSC. There was a broad increase in Fe moving towards the right of PHN5814a, though obvious zoning was immediately apparent using BSE imaging. The disparity in FeO between the fragments of PHN5814 is quite high at 5.3 wt%. The large variation in major element composition in ilmenite from the PHN5814 hand specimen is not suitable for widespread use. There does appear to be a better overlap in minor element composition (e.g., Nb_2O_5, V_2O_5) for the PHN5814 fragments, though this may reflect the smaller values and instrument sensitivity. However, the minor elements can exhibit much higher relative standard deviations (RSD) in all four samples (e.g., 23 to 35 % for Nb_2O_5, 17 to 23 % for V_2O_3).

The variability of Fe and Ti contents (the elements used as internal standards during data processing) and high relative standard deviations in minor elements over small areas are not desirable characteristics for an ilmenite standard for trace element studies. As such, no further analyses (i.e. LA-ICP-MS) were performed in assessment of the potential use for ilmenite standards.

Table 20 – EPMA analytical settings for potential ilmenite standards (CAMECA)

Element Line	Crystal	Standard	On-Peak Time	Background	Accelerating Voltage	Beam Current	Beam Size
			s	s	kV	nA	um
Si ka	LTAP	Frank Smith pyrope garnet	30	30	20	20	0 – 3
Na ka	TAP	NaAlSi3O8 albite VA 131705	30	30	20	20	0
K ka	LPET	KAlSi3O8 sanidine Itrongay	30	30	20	20	0
Cr ka	PET	Cr2O3 chromium oxide Alfa	30	30	20	20	0
Fe ka	LLIF	FeTiO3 Ilmenite 96189	30	30	20	20	0
Mg ka	LTAP	Frank Smith pyrope garnet	30	30	20	20	0
Al ka	TAP	ZnAl2O4 gahnite H111989	30	30	20	20	0
Ca ka	LPET	CaMgSi2O6 diopside Wakefield	30	30	20	20	0
Ti ka	PET	FeTiO3 Ilmenite 96189	30	30	20	20	0
Mn ka	LLIF	(Mn,Fe)3Al2Si3O12 spessartine, Navegadora Mine	30	30	20	20	0
Zr la	LPET	ZrSiO4 Zircon JH block	30	30	20	20	0
Nb lb	PET	Niobium, Nb - ESPI	30	30	20	20	0
V ka	PET	V vanadium Alfa	30	30	20	20	0
Ni ka	LLIF	Ni nickel Alfa	30	30	20	20	0
Zn ka	LLIF	ZnAl2O4 gahnite H111989	30	30	20	20	0

Table 21 – Major and minor element chemistry for potential ilmenite standards

Sample (NW – SE)	**Nb_2O_5**	**SiO_2**	**ZrO_2**	**TiO_2**	**ZnO**	**Al_2O_3**	**V_2O_3**	**Cr_2O_3**	**FeO_T**	**NiO**	**MnO**	**MgO**	**CaO**	**Na_2O**	**K_2O**	**Total**
PHN5814a	bld	bld	bld	51.13	bld	0.52	0.16	2.37	29.52	0.17	0.28	13.04	bld	bld	bld	97.19
PHN5814a	0.77	0.03	bld	51.29	bld	0.51	0.18	2.39	29.53	0.18	0.27	13.00	0.01	bld	bld	98.16
PHN5814a	0.72	0.02	0.05	51.38	bld	0.50	0.17	2.38	29.58	0.17	0.27	13.14	0.02	bld	bld	98.40
PHN5814a	0.59	0.02	bld	51.12	bld	0.53	0.18	2.40	29.67	0.19	0.26	13.09	0.01	bld	bld	98.06
PHN5814a	0.74	0.02	bld	51.44	bld	0.50	0.18	2.40	29.52	0.19	0.25	13.05	0.02	bld	bld	98.31
PHN5814a	0.60	bld	bld	51.20	bld	0.51	0.17	2.40	29.62	0.18	0.26	13.09	0.01	bld	bld	98.04
PHN5814a	1.11	0.03	0.05	51.36	bld	0.52	0.14	2.37	29.55	0.18	0.27	13.06	0.02	bld	bld	98.66
PHN5814a	0.63	bld	bld	51.17	bld	0.52	0.20	2.43	29.57	0.20	0.28	13.12	0.02	bld	bld	98.14
PHN5814a	0.41	0.03	bld	51.25	bld	0.52	0.20	2.36	29.54	0.18	0.29	13.06	0.01	bld	bld	97.85
PHN5814a	0.47	0.03	bld	51.35	bld	0.52	0.20	2.37	29.69	0.18	0.27	13.09	0.01	bld	bld	98.18
PHN5814a	0.35	0.02	bld	51.41	bld	0.55	0.15	2.42	29.68	0.18	0.29	13.05	0.02	bld	bld	98.12
PHN5814a	0.71	0.03	bld	51.13	bld	0.53	0.23	2.42	29.70	0.18	0.26	12.96	0.01	bld	bld	98.16
PHN5814a	0.90	0.03	bld	51.16	bld	0.53	0.28	2.35	29.57	0.19	0.27	13.03	0.02	bld	bld	98.33
PHN5814a	0.79	0.02	bld	51.34	bld	0.56	0.21	2.40	29.64	0.19	0.27	13.07	0.01	bld	bld	98.50
PHN5814a	0.49	0.02	0.04	51.14	bld	0.50	0.20	2.38	29.60	0.17	0.27	13.05	0.02	bld	bld	97.88
PHN5814a	0.67	0.02	bld	51.43	bld	0.53	0.22	2.36	29.55	0.16	0.27	13.05	0.03	bld	bld	98.29
PHN5814a	0.59	bld	bld	51.17	bld	0.55	0.20	2.43	29.58	0.18	0.28	13.11	0.02	bld	bld	98.11
PHN5814a	1.01	bld	bld	51.18	bld	0.53	0.21	2.38	29.52	0.20	0.26	13.09	0.01	bld	bld	98.39
PHN5814a	0.42	bld	bld	51.13	bld	0.53	0.22	2.40	29.66	0.17	0.27	13.14	0.01	bld	bld	97.95
PHN5814a	1.26	bld	bld	51.10	bld	0.52	0.23	2.32	29.57	0.17	0.27	13.11	0.02	bld	bld	98.57
PHN5814a	0.76	0.03	0.05	51.31	bld	0.49	0.22	2.35	29.70	0.18	0.29	13.09	0.02	bld	bld	98.49
PHN5814a	0.98	bld	bld	51.21	bld	0.51	0.24	2.33	29.65	0.17	0.28	13.10	0.02	bld	bld	98.49
PHN5814a	0.78	0.03	0.06	51.28	bld	0.51	0.16	2.39	29.74	0.18	0.27	13.08	0.02	bld	bld	98.50

Table 21 continued

Sample (SW – NE)	Nb_2O_5	SiO_2	ZrO_2	TiO_2	ZnO	Al_2O_3	V_2O_3	Cr_2O_3	FeO_T	NiO	MnO	MgO	CaO	Na_2O	K_2O	Total
PHN5814a	0.54	0.02	bld	51.57	bld	0.50	0.14	2.42	29.49	0.19	0.28	13.15	0.02	bld	bld	98.32
PHN5814a	1.19	0.03	0.05	51.64	bld	0.51	0.18	2.38	29.42	0.19	0.26	13.05	0.02	bld	bld	98.92
PHN5814a	0.61	0.02	bld	51.34	bld	0.52	0.21	2.36	29.41	0.17	0.29	13.07	0.01	bld	bld	98.01
PHN5814a	1.01	0.03	0.05	51.47	bld	0.54	0.20	2.42	29.46	0.19	0.26	13.15	0.02	bld	bld	98.80
PHN5814a	0.76	0.03	0.05	51.39	bld	0.52	0.21	2.39	29.57	0.18	0.28	13.06	0.02	bld	bld	98.46
PHN5814a	1.09	0.02	bld	51.39	bld	0.52	0.19	2.36	29.66	0.16	0.27	13.11	0.02	bld	bld	98.79
PHN5814a	0.54	bld	bld	51.48	bld	0.51	0.12	2.40	29.64	0.18	0.26	13.02	bld	bld	bld	98.15
PHN5814a	1.07	0.03	0.04	51.33	bld	0.54	0.17	2.36	29.59	0.18	0.27	13.06	0.02	bld	bld	98.66
PHN5814a	0.52	0.03	bld	51.46	bld	0.57	0.18	2.40	29.36	0.18	0.26	12.95	bld	bld	bld	97.91
PHN5814a	0.90	0.02	bld	51.27	0.02	0.51	0.18	2.37	29.53	0.16	0.27	13.01	0.01	bld	bld	98.25
PHN5814a	1.13	bld	bld	51.20	bld	0.53	0.20	2.38	29.59	0.19	0.27	13.03	0.01	bld	bld	98.53
PHN5814a	0.49	0.03	0.04	51.29	bld	0.53	0.18	2.42	29.62	0.17	0.27	13.07	0.01	bld	bld	98.12
PHN5814a	0.67	0.03	bld	51.25	0.03	0.51	0.19	2.39	29.54	0.17	0.28	13.04	0.01	bld	bld	98.11
PHN5814a	0.80	bld	bld	51.11	0.03	0.55	0.18	2.40	29.71	0.19	0.28	13.03	0.02	bld	bld	98.30
PHN5814a	0.79	bld	bld	51.42	bld	0.53	0.16	2.40	29.67	0.19	0.26	13.09	0.01	bld	bld	98.52
PHN5814a	1.19	0.02	bld	51.13	bld	0.52	0.19	2.38	29.65	0.19	0.26	13.06	0.02	bld	bld	98.61
PHN5814a	1.04	0.03	bld	51.40	bld	0.52	0.18	2.34	29.67	0.17	0.25	13.09	0.01	bld	bld	98.70
PHN5814a	0.85	0.03	bld	51.35	bld	0.52	0.14	2.38	29.79	0.18	0.27	13.10	0.02	bld	bld	98.63
PHN5814a	0.66	0.04	bld	51.32	bld	0.53	0.20	2.39	29.78	0.18	0.26	13.09	0.01	bld	bld	98.46
PHN5814a	0.46	bld	bld	51.42	bld	0.54	0.18	2.38	29.71	0.17	0.26	13.08	0.01	bld	bld	98.21
PHN5814a	0.75	0.04	bld	51.12	bld	0.52	0.22	2.41	29.76	0.18	0.28	13.10	0.02	bld	bld	98.40
PHN5814a	0.88	0.02	bld	51.36	bld	0.50	0.16	2.44	29.66	0.18	0.28	13.13	0.01	bld	bld	98.62
PHN5814a	0.98	0.03	bld	51.44	bld	0.54	0.27	2.40	29.79	0.18	0.29	13.12	0.02	bld	bld	99.06

Table 21 continued

Sample (N – S)	Nb_2O_5	SiO_2	ZrO_2	TiO_2	ZnO	Al_2O_3	V_2O_3	Cr_2O_3	FeO_T	NiO	MnO	MgO	CaO	Na_2O	K_2O	Total
PHN5814b	1.42	bld	bld	49.37	bld	0.46	0.35	1.28	34.65	0.11	0.30	10.78	0.01	bld	bld	98.73
PHN5814b	0.98	bld	bld	49.22	bld	0.46	0.23	1.23	34.77	0.12	0.29	10.81	0.02	bld	bld	98.13
PHN5814b	1.31	bld	bld	49.33	bld	0.47	0.25	1.26	34.79	0.10	0.29	10.79	0.02	bld	bld	98.61
PHN5814b	1.16	bld	bld	49.41	bld	0.45	0.27	1.26	34.79	0.10	0.28	10.84	bld	bld	bld	98.56
PHN5814b	0.93	0.03	bld	49.38	bld	0.43	0.22	1.28	34.84	0.12	0.27	10.81	0.02	bld	bld	98.33
PHN5814b	1.22	0.02	bld	49.42	bld	0.44	0.23	1.28	34.93	0.11	0.29	10.83	0.01	bld	bld	98.78
PHN5814b	0.89	bld	bld	49.36	bld	0.46	0.21	1.27	34.84	0.11	0.28	10.93	0.01	bld	bld	98.36
PHN5814b	0.70	bld	bld	49.01	bld	0.44	0.14	1.26	34.84	0.11	0.30	10.86	0.02	bld	bld	97.68
PHN5814b	0.73	bld	bld	49.21	bld	0.45	0.21	1.29	34.93	0.11	0.29	10.84	0.01	bld	bld	98.07
PHN5814b	1.37	bld	bld	49.41	bld	0.46	0.25	1.26	34.87	0.10	0.28	10.84	0.02	bld	bld	98.86
PHN5814b	1.29	bld	bld	49.36	0.02	0.44	0.28	1.31	34.85	0.09	0.28	10.78	0.02	bld	bld	98.72
PHN5814b	0.72	bld	bld	49.17	bld	0.45	0.25	1.28	34.84	0.11	0.32	10.83	0.02	bld	bld	97.99
PHN5814b	0.95	bld	bld	49.48	0.02	0.44	0.22	1.26	34.88	0.11	0.31	10.79	0.03	bld	bld	98.49
PHN5814b	1.21	bld	0.04	49.35	bld	0.46	0.25	1.28	34.86	0.11	0.30	10.77	0.02	bld	bld	98.65
PHN5814b	1.28	0.02	bld	49.43	0.03	0.47	0.27	1.30	34.92	0.11	0.29	10.75	0.02	bld	bld	98.89
PHN5814b	1.35	bld	bld	49.42	bld	0.45	0.23	1.26	34.77	0.12	0.30	10.75	0.02	bld	bld	98.67
PHN5814b	0.75	bld	0.04	49.28	bld	0.46	0.22	1.25	34.92	0.11	0.30	10.86	0.01	bld	bld	98.20
PHN5814b	0.97	bld	bld	49.30	0.03	0.48	0.21	1.27	35.06	0.13	0.30	10.87	0.02	bld	bld	98.64
PHN5814b	0.59	0.02	bld	49.45	0.02	0.44	0.19	1.27	34.99	0.10	0.29	10.83	0.02	bld	bld	98.21
PHN5814b	0.73	bld	bld	49.43	bld	0.46	0.16	1.28	34.84	0.11	0.29	10.79	0.02	bld	bld	98.11
PHN5814b	0.56	bld	bld	49.32	bld	0.43	0.16	1.26	34.86	0.11	0.28	10.86	bld	bld	bld	97.84
PHN5814b	1.16	bld	bld	49.36	bld	0.43	0.18	1.26	34.99	0.11	0.30	10.80	0.01	bld	bld	98.60
PHN5814b	0.97	bld	bld	49.29	0.03	0.48	0.20	1.25	34.96	0.12	0.30	10.77	0.03	bld	bld	98.40
PHN5814b	0.96	bld	bld	49.36	bld	0.46	0.23	1.28	34.95	0.10	0.30	10.76	0.02	bld	bld	98.42
PHN5814b	0.54	bld	0.05	49.66	0.03	0.46	0.20	1.29	35.14	0.12	0.29	10.82	0.01	bld	bld	98.61
PHN5814b	1.44	0.02	bld	49.43	bld	0.45	0.22	1.25	34.89	0.10	0.31	10.82	0.01	bld	bld	98.94

Table 21 continued

Sample (E – W 1)	Nb_2O_5	SiO_2	ZrO_2	TiO_2	ZnO	Al_2O_3	V_2O_3	Cr_2O_3	FeO_T	NiO	MnO	MgO	CaO	Na_2O	K_2O	Total
PHN5814b	0.85	0.02	bld	49.37	0.02	0.43	0.18	1.20	34.83	0.08	0.29	10.84	0.01	bld	bld	98.12
PHN5814b	0.61	0.02	bld	49.20	bld	0.47	0.18	1.25	34.89	0.11	0.29	10.89	0.01	bld	bld	97.92
PHN5814b	0.50	bld	bld	49.04	bld	0.45	0.27	1.28	34.80	0.11	0.30	10.82	0.01	bld	bld	97.58
PHN5814b	1.01	bld	0.05	49.28	bld	0.44	0.27	1.25	34.76	0.10	0.31	10.81	bld	bld	bld	98.28
PHN5814b	1.23	bld	bld	49.20	bld	0.46	0.27	1.27	34.66	0.10	0.28	10.84	0.02	bld	bld	98.33
(E – W 2)																
PHN5814b	0.65	bld	bld	49.36	bld	0.43	0.25	1.24	34.88	0.13	0.29	10.75	0.02	bld	bld	98.00
PHN5814b	1.06	0.04	0.05	49.00	bld	0.44	0.20	1.26	35.07	0.10	0.28	10.81	0.02	bld	bld	98.33
PHN5814b	1.12	bld	bld	49.20	bld	0.44	0.20	1.28	34.90	0.11	0.29	10.87	0.01	bld	bld	98.42
PHN5814b	0.75	bld	bld	49.36	bld	0.45	0.21	1.28	34.87	0.10	0.31	10.87	0.01	bld	bld	98.21
PHN5814b	0.51	bld	bld	49.41	bld	0.45	0.23	1.26	35.01	0.11	0.28	10.93	bld	bld	bld	98.19
(E – W 3)																
PHN5814b	0.89	bld	bld	49.45	bld	0.42	0.17	1.30	35.02	0.09	0.28	10.71	0.01	bld	bld	98.34
PHN5814b	1.30	bld	bld	49.40	0.03	0.48	0.23	1.26	34.93	0.10	0.28	10.79	0.01	bld	bld	98.81
PHN5814b	1.07	0.03	bld	49.57	0.03	0.46	0.20	1.29	34.85	0.10	0.31	10.78	0.02	bld	bld	98.71
PHN5814b	0.97	bld	0.05	49.27	0.03	0.46	0.23	1.27	34.90	0.10	0.28	10.82	0.01	bld	bld	98.39
PHN5814b	0.84	bld	bld	49.33	bld	0.44	0.23	1.28	34.91	0.11	0.29	10.87	0.02	bld	bld	98.32
(E – W 4)																
PHN5814b	1.18	0.02	bld	49.57	0.03	0.44	0.19	1.25	34.86	0.10	0.32	10.72	0.01	bld	bld	98.69
PHN5814b	1.46	0.02	0.06	49.33	0.03	0.45	0.28	1.26	34.74	0.10	0.27	10.81	0.01	bld	bld	98.82
PHN5814b	0.95	bld	bld	49.32	0.03	0.47	0.25	1.27	34.78	0.11	0.31	10.80	0.02	bld	bld	98.31
PHN5814b	1.46	bld	bld	49.25	bld	0.48	0.29	1.26	34.72	0.10	0.29	10.81	0.02	bld	bld	98.68
PHN5814b	0.78	bld	0.04	49.24	bld	0.45	0.21	1.27	34.87	0.10	0.29	10.94	0.02	bld	bld	98.21

Table 21 continued

Sample (N – S)	Nb_2O_5	SiO_2	ZrO_2	TiO_2	ZnO	Al_2O_3	V_2O_3	Cr_2O_3	FeO_T	NiO	MnO	MgO	CaO	Na_2O	K_2O	Total
99-19-146	1.25	bld	bld	47.78	bld	0.44	0.19	bld	43.71	bld	0.26	4.84	0.02	bld	bld	98.49
99-19-146	1.38	bld	0.05	47.99	bld	0.40	0.13	bld	43.71	bld	0.25	4.85	0.02	bld	bld	98.78
99-19-146	1.03	bld	bld	47.61	0.04	0.42	0.09	bld	43.89	bld	0.25	4.86	bld	bld	bld	98.19
99-19-146	0.90	0.02	0.06	47.78	0.03	0.42	0.13	bld	43.99	bld	0.27	4.88	bld	bld	bld	98.48
99-19-146	1.22	bld	bld	47.76	0.04	0.42	0.11	bld	43.88	bld	0.26	4.89	0.02	bld	bld	98.60
99-19-146	1.07	bld	bld	47.75	bld	0.42	0.12	bld	43.88	bld	0.28	4.92	0.01	bld	bld	98.45
99-19-146	0.74	bld	bld	47.71	0.03	0.40	0.18	bld	43.96	bld	0.24	4.88	0.01	bld	bld	98.15
99-19-146	0.88	bld	bld	47.68	bld	0.40	0.11	bld	43.84	bld	0.25	4.88	bld	bld	bld	98.04
99-19-146	1.01	bld	bld	47.60	bld	0.42	0.11	bld	44.06	bld	0.26	4.94	bld	bld	bld	98.40
99-19-146	1.38	bld	0.06	47.84	0.03	0.41	0.15	bld	43.83	bld	0.27	4.90	0.02	bld	bld	98.89
99-19-146	0.99	bld	0.06	47.73	0.03	0.42	0.18	bld	43.92	bld	0.26	4.91	0.01	bld	bld	98.51
99-19-146	1.24	bld	bld	47.70	bld	0.43	0.12	bld	43.90	bld	0.25	4.89	bld	bld	bld	98.53
99-19-146	0.90	bld	0.05	47.72	0.03	0.42	0.14	0.03	43.69	bld	0.24	4.94	bld	bld	bld	98.16
99-19-146	0.57	bld	0.05	47.83	bld	0.41	0.13	bld	43.75	bld	0.26	4.90	bld	bld	bld	97.90
99-19-146	1.09	bld	bld	47.67	bld	0.40	0.21	bld	43.78	bld	0.26	4.91	0.02	bld	bld	98.34
99-19-146	0.57	bld	0.05	47.59	bld	0.42	0.20	bld	43.84	bld	0.25	4.98	0.01	bld	bld	97.91
99-19-146	1.49	bld	bld	47.73	0.03	0.45	0.22	bld	43.74	bld	0.26	4.94	0.01	bld	bld	98.87
99-19-146	1.02	bld	0.05	47.66	0.02	0.43	0.20	bld	43.72	bld	0.25	4.95	bld	0.04	bld	98.34
99-19-146	1.28	bld	0.07	47.76	0.04	0.42	0.09	bld	43.86	bld	0.24	4.99	0.01	bld	bld	98.76
99-19-146	1.36	bld	0.05	47.87	bld	0.42	0.18	bld	43.65	bld	0.27	5.03	0.02	bld	bld	98.85
99-19-146	1.16	bld	0.08	47.85	0.04	0.43	0.20	bld	43.53	bld	0.25	5.02	0.01	bld	bld	98.57
99-19-146	1.18	bld	bld	47.82	bld	0.44	0.18	bld	43.71	bld	0.25	4.97	0.02	bld	bld	98.57
99-19-146	1.31	bld	bld	47.79	0.03	0.42	0.13	bld	43.70	bld	0.27	5.04	0.02	bld	bld	98.71

Table 21 continued

Sample (E – W)	Nb_2O_5	SiO_2	ZrO_2	TiO_2	ZnO	Al_2O_3	V_2O_3	Cr_2O_3	FeO_T	NiO	MnO	MgO	CaO	Na_2O	K_2O	Total
99-19-146	0.90	bld	bld	47.68	bld	0.41	0.10	bld	44.00	bld	0.27	4.86	0.01	bld	bld	98.23
99-19-146	1.30	bld	bld	47.77	0.03	0.41	0.15	bld	43.78	bld	0.26	4.87	0	bld	bld	98.57
99-19-146	1.22	bld	bld	47.89	0.03	0.40	0.18	bld	43.93	bld	0.27	4.89	0.01	bld	bld	98.82
99-19-146	1.21	bld	0.09	47.70	bld	0.40	0.16	bld	43.71	bld	0.24	4.85	0.01	bld	bld	98.37
99-19-146	1.57	bld	bld	47.78	0.04	0.43	0.18	bld	43.86	bld	0.26	4.93	0	bld	bld	99.05
99-19-146	0.61	bld	0.07	47.65	0.03	0.42	0.11	bld	43.83	bld	0.24	4.89	0.01	bld	bld	97.86
99-19-146	1.13	bld	0.04	47.64	bld	0.42	0.17	bld	43.83	bld	0.25	4.90	0.01	bld	bld	98.39
99-19-146	0.70	bld	0.06	47.94	0.04	0.41	0.12	bld	43.84	bld	0.24	4.91	0.02	bld	bld	98.28
99-19-146	1.18	bld	0.05	47.67	bld	0.43	0.11	0.03	44.01	bld	0.26	4.88	0.01	bld	bld	98.63
99-19-146	0.87	bld	0.06	47.73	0.02	0.44	0.09	bld	43.87	bld	0.28	4.92	0.01	bld	bld	98.29
99-19-146	0.97	bld	bld	47.77	0.04	0.39	0.14	bld	43.99	bld	0.25	4.93	0.01	0.03	bld	98.52
99-19-146	0.99	bld	0.06	47.93	0.03	0.43	0.14	bld	43.93	bld	0.26	4.94	0.01	bld	bld	98.72
99-19-146	1.17	bld	0.05	47.93	bld	0.42	0.16	bld	43.83	bld	0.25	4.91	0.01	bld	bld	98.73
99-19-146	1.93	bld	0.04	47.84	0.03	0.44	0.17	bld	43.79	bld	0.26	4.92	0.02	bld	bld	99.44
99-19-146	1.32	bld	bld	47.76	bld	0.44	0.12	bld	43.86	bld	0.26	4.89	bld	bld	bld	98.65
99-19-146	1.15	bld	0.06	47.81	0.04	0.42	0.11	bld	43.79	bld	0.25	4.99	0.02	bld	bld	98.64
99-19-146	1.25	bld	0.07	47.91	bld	0.40	0.13	bld	43.87	bld	0.25	4.98	bld	bld	bld	98.86
99-19-146	1.14	bld	0.06	47.68	0.03	0.44	0.15	bld	43.82	bld	0.26	5.01	0.02	bld	bld	98.61
99-19-146	1.25	bld	bld	47.74	bld	0.42	0.22	bld	43.52	bld	0.26	4.93	0.02	bld	bld	98.36
99-19-146	1.04	bld	0.06	47.84	bld	0.41	0.14	bld	43.65	bld	0.25	5.03	bld	bld	bld	98.42
99-19-146	1.12	bld	0.09	47.72	bld	0.44	0.16	bld	43.70	0.02	0.25	5.09	0.01	bld	bld	98.60
99-19-146	1.83	bld	0.05	47.82	bld	0.43	0.26	bld	43.36	bld	0.24	5.09	bld	bld	bld	99.08
99-19-146	1.16	bld	bld	47.75	bld	0.46	0.17	bld	43.35	bld	0.24	5.25	0.02	bld	bld	98.40

Table 21 continued

Sample (NW – SE)	Nb_2O_5	SiO_2	ZrO_2	TiO_2	ZnO	Al_2O_3	V_2O_3	Cr_2O_3	FeO_T	NiO	MnO	MgO	CaO	Na_2O	K_2O	Total
99-18-122-9	1.21	bld	bld	46.78	bld	0.25	0.15	bld	44.04	bld	0.28	5.47	0.02	bld	bld	98.20
99-18-122-9	1.16	bld	bld	47.74	bld	0.32	0.15	bld	43.08	bld	0.28	5.62	0.03	bld	bld	98.38
99-18-122-9	1.26	bld	0.04	47.92	0.05	0.39	0.19	0.03	43.14	bld	0.26	5.54	0.03	0.04	bld	98.89
99-18-122-9	1.39	bld	bld	47.88	0.03	0.42	0.21	bld	43.10	bld	0.26	5.50	0.03	bld	bld	98.82
99-18-122-9	1.6	bld	0.04	47.86	bld	0.46	0.18	bld	43.24	bld	0.27	5.42	0.03	0.04	bld	99.14
99-18-122-9	0.85	bld	bld	47.59	bld	0.48	0.16	bld	43.30	bld	0.25	5.30	0.02	bld	bld	97.95
99-18-122-9	1.37	bld	bld	47.46	bld	0.50	0.20	bld	43.32	bld	0.25	5.29	0.03	bld	bld	98.42
99-18-122-9	1.66	bld	0.05	47.64	bld	0.53	0.13	bld	43.27	bld	0.25	5.22	0.02	bld	bld	98.77
99-18-122-9	0.88	bld	bld	47.76	0.02	0.55	0.19	bld	43.36	bld	0.25	5.25	0.03	bld	bld	98.29
99-18-122-9	1.51	bld	bld	47.83	0.03	0.54	0.16	bld	43.58	bld	0.27	5.09	0.03	bld	bld	99.04
99-18-122-9	1.23	bld	bld	47.99	bld	0.53	0.21	bld	43.46	bld	0.25	5.11	0.03	bld	bld	98.81
99-18-122-9	1.57	bld	bld	47.80	bld	0.55	0.24	bld	43.33	bld	0.25	5.13	0.03	bld	bld	98.90
99-18-122-9	1.17	bld	bld	47.94	bld	0.55	0.18	bld	43.65	bld	0.26	5.06	0.03	bld	bld	98.84
99-18-122-9	1.15	bld	bld	47.68	bld	0.55	0.20	bld	43.66	bld	0.25	5.11	0.03	bld	bld	98.63
99-18-122-9	1.15	bld	bld	47.75	0.04	0.52	0.12	bld	43.68	bld	0.25	5.07	0.04	bld	bld	98.62
99-18-122-9	1.23	bld	bld	47.74	bld	0.53	0.26	bld	43.52	bld	0.25	5.08	0.03	bld	bld	98.64
99-18-122-9	1.3	bld	bld	47.72	bld	0.53	0.20	bld	43.54	bld	0.27	5.04	0.03	bld	bld	98.63
99-18-122-9	1.23	bld	bld	47.61	0.03	0.53	0.17	bld	43.63	bld	0.25	5.00	0.02	0.05	bld	98.52
99-18-122-9	1.31	bld	bld	47.74	0.04	0.53	0.12	bld	43.48	bld	0.25	5.04	0.02	bld	bld	98.53
99-18-122-9	1.79	bld	bld	47.66	0.04	0.50	0.19	bld	43.40	bld	0.25	5.06	0.03	bld	bld	98.92
99-18-122-9	1.26	bld	0.05	47.82	bld	0.51	0.20	bld	43.44	bld	0.26	5.03	0.03	0.04	bld	98.64
99-18-122-9	1.55	bld	bld	47.68	0.06	0.50	0.21	bld	43.48	bld	0.26	5.07	0.02	bld	bld	98.83
99-18-122-9	0.94	bld	0.05	47.67	bld	0.56	0.27	bld	43.40	bld	0.24	5.04	0.02	bld	bld	98.19

Table 21 continued

Sample (SW – NE)	Nb_2O_5	SiO_2	ZrO_2	TiO_2	ZnO	Al_2O_3	V_2O_3	Cr_2O_3	FeO_T	NiO	MnO	MgO	CaO	Na_2O	K_2O	Total
99-18-122-9	0.84	bld	bld	47.43	0.03	0.25	0.09	bld	43.80	bld	0.24	5.35	0.03	bld	bld	98.06
99-18-122-9	0.97	bld	bld	47.57	0.04	0.29	0.15	bld	43.60	bld	0.27	5.34	0.04	bld	bld	98.27
99-18-122-9	1.19	bld	0.04	47.77	bld	0.34	0.16	bld	43.64	bld	0.27	5.33	0.03	bld	bld	98.77
99-18-122-9	1.30	bld	bld	47.84	bld	0.37	0.14	bld	43.54	bld	0.26	5.28	0.04	0.04	bld	98.81
99-18-122-9	1.11	bld	bld	47.79	0.03	0.46	0.10	bld	43.48	bld	0.26	5.18	0.04	bld	bld	98.45
99-18-122-9	0.79	bld	bld	47.68	0.03	0.49	0.13	bld	43.47	bld	0.24	5.19	0.03	0.04	bld	98.09
99-18-122-9	0.58	0.02	bld	47.72	bld	0.49	0.15	bld	43.47	bld	0.25	5.20	0.03	bld	bld	97.91
99-18-122-9	1.21	bld	0.05	47.54	bld	0.52	0.12	bld	43.44	bld	0.26	5.18	0.03	bld	bld	98.35
99-18-122-9	1.21	bld	bld	47.62	0.03	0.51	0.15	bld	43.31	bld	0.25	5.21	0.02	bld	bld	98.31
99-18-122-9	1.27	bld	bld	47.75	0.03	0.54	0.16	bld	43.49	bld	0.24	5.17	0.02	bld	bld	98.67
99-18-122-9	1.34	bld	bld	47.52	bld	0.55	0.12	bld	43.40	bld	0.26	5.21	0.02	bld	bld	98.42
99-18-122-9	1.50	bld	0.07	47.64	bld	0.58	0.17	bld	43.47	bld	0.25	5.20	0.02	bld	bld	98.90
99-18-122-9	1.51	bld	bld	47.76	0.05	0.54	0.16	bld	43.35	bld	0.25	5.18	0.02	bld	bld	98.82
99-18-122-9	1.72	bld	bld	47.71	bld	0.53	0.18	bld	43.48	bld	0.27	5.15	0.03	0.04	bld	99.11
99-18-122-9	0.47	bld	0.05	47.70	0.03	0.54	0.14	bld	43.43	bld	0.25	5.19	0.03	bld	bld	97.83
99-18-122-9	1.51	bld	bld	47.76	0.03	0.55	0.16	bld	43.52	bld	0.24	5.17	0.02	bld	bld	98.96
99-18-122-9	1.06	bld	0.08	47.57	0.03	0.54	0.14	bld	43.52	bld	0.25	5.14	0.02	bld	bld	98.35
99-18-122-9	1.23	bld	bld	47.64	bld	0.51	0.13	bld	43.45	bld	0.25	5.16	0.03	bld	bld	98.40
99-18-122-9	1.24	bld	bld	47.85	bld	0.50	0.17	bld	43.45	bld	0.24	5.13	0.03	bld	bld	98.61
99-18-122-9	1.02	bld	bld	47.92	bld	0.50	0.14	bld	43.41	bld	0.25	5.16	0.02	bld	bld	98.42
99-18-122-9	1.40	bld	bld	47.64	0.05	0.51	0.15	bld	43.43	bld	0.25	5.09	0.02	bld	bld	98.54
99-18-122-9	1.00	bld	bld	47.81	bld	0.52	0.17	bld	43.40	bld	0.23	5.15	0.02	bld	bld	98.30
99-18-122-9	1.39	bld	0.06	47.92	bld	0.48	0.19	bld	43.33	bld	0.24	5.15	0.03	bld	bld	98.79

Table 21 continued

Sample	Nb_2O_5	SiO_2	ZrO_2	TiO_2	ZnO	Al_2O_3	V_2O_3	Cr_2O_3	FeO_T	NiO	MnO	MgO	CaO	Na_2O	K_2O	Total
NMNH ilmenite	2.32	bld	0.04	45.82	0.07	bld	0.15	bld	46.29	bld	4.68	0.33	bld	bld	bld	99.70
NMNH ilmenite	2.76	bld	bld	45.84	0.07	0.02	0.12	bld	46.04	bld	4.67	0.32	bld	bld	bld	99.84
NMNH ilmenite	2.25	bld	bld	45.77	0.04	bld	0.14	bld	46.04	bld	4.64	0.31	bld	bld	bld	99.19
NMNH ilmenite	2.92	bld	bld	45.56	0.06	bld	0.14	bld	45.98	bld	4.61	0.30	bld	bld	bld	99.57
NMNH ilmenite	2.14	0.02	bld	45.70	0.03	bld	0.13	bld	46.11	bld	4.63	0.32	bld	bld	bld	99.08

Table 22 – Compositional statistical variation of major contributing oxides

		Nb_2O_5	TiO_2	Al_2O_3	V_2O_3	Cr_2O_3	FeO_T	NiO	MnO	MgO	Total
PHN5814a	mean	0.75	51.30	0.52	0.19	2.39	29.61	0.18	0.27	13.07	98.29
n = 46	std dev	0.26	0.13	0.02	0.03	0.03	0.10	0.01	0.01	0.04	0.32
	RSD	34.6%	0.26%	3.20%	16.7%	1.12%	0.34%	5.37%	3.88%	0.34%	0.32%
	max	1.26	51.64	0.57	0.28	2.44	29.79	0.20	0.29	13.15	99.01
	min	0.00	51.10	0.49	0.12	2.32	29.36	0.16	0.25	12.95	97.19
	range	1.26	0.54	0.08	0.16	0.12	0.43	0.04	0.04	0.20	1.82
PHN5814b	mean	0.99	49.33	0.45	0.23	1.27	34.87	0.11	0.29	10.82	98.36
n = 46	std dev	0.28	0.13	0.01	0.04	0.02	0.10	0.01	0.01	0.05	0.32
	RSD	28.5%	0.27%	3.32%	17.7%	1.51%	0.29%	9.06%	4.18%	0.47%	0.32%
	max	1.46	49.66	0.48	0.35	1.31	35.14	0.13	0.32	10.94	98.91
	min	0.50	49.00	0.42	0.14	1.20	34.65	0.08	0.27	10.71	97.57
	range	0.96	0.66	0.06	0.21	0.11	0.49	0.05	0.05	0.23	1.34
99-19-146	mean	1.13	47.76	0.42	0.15	0.00	43.80	0.00	0.26	4.94	98.46
n = 46	std dev	0.28	0.09	0.02	0.04	0.01	0.15	0.00	0.01	0.08	0.31
	RSD	24.6%	0.20%	3.58%	26.2%	474%	0.35%	14.7%	4.18%	1.56%	0.32%
	max	1.93	47.99	0.46	0.26	0.03	44.06	0.02	0.28	5.25	99.35
	min	0.57	47.59	0.39	0.09	0.00	43.35	0.00	0.24	4.84	97.75
	range	1.36	0.40	0.07	0.17	0.03	0.71	0.02	0.04	0.41	1.60
99-18-122-9	mean	1.23	47.70	0.49	0.17	0.00	43.46	0.00	0.25	5.20	98.50
n = 46	std dev	0.28	0.19	0.08	0.04	0.00	0.17	0.00	0.01	0.14	0.32
	RSD	22.5%	0.39%	16.8%	22.9%	14.7%	0.39%	-	4.35%	2.71%	0.32%
	max	1.79	47.99	0.58	0.27	0.03	44.04	0.00	0.28	5.62	99.04
	min	0.47	46.78	0.25	0.09	0.00	43.08	0.00	0.23	5.00	97.72
	range	1.32	1.21	0.33	0.18	0.03	0.96	0.00	0.05	0.62	1.32
NMNH	mean	2.48	45.74	0.00	0.14	0.00	46.09	0.00	4.65	0.32	99.41
n = 5	std dev	0.34	0.11	0.01	0.01	0.00	0.12	0.00	0.03	0.01	0.31
	RSD	13.8%	0.25%	44.7%	8.38%	-	0.26%	-	0.62%	3.61%	0.31%
	max	2.92	45.84	0.02	0.15	0.00	46.29	0.00	4.68	0.33	99.77
	min	2.14	45.56	0.00	0.12	0.00	45.98	0.00	4.61	0.30	99.03
	range	0.78	0.28	0.02	0.03	0.00	0.31	0.00	0.07	0.03	0.74

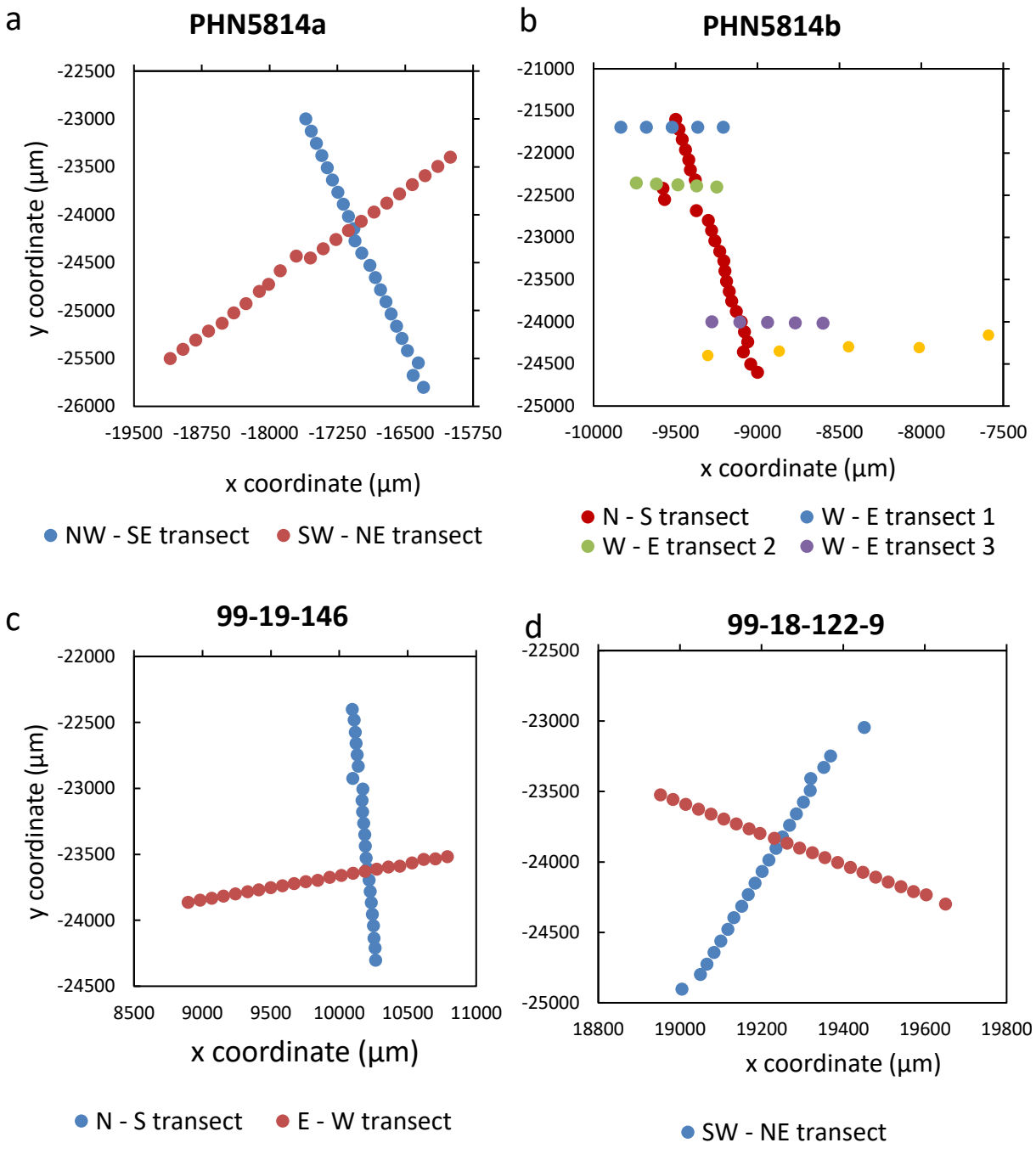

Fig. 34 – X and Y coordinates of the approximately perpendicular transects plotted on the potential ilmenite standards of a) PHN5814a; b) PHN5814b; c) 99-19-146; d) 99-18-122-9

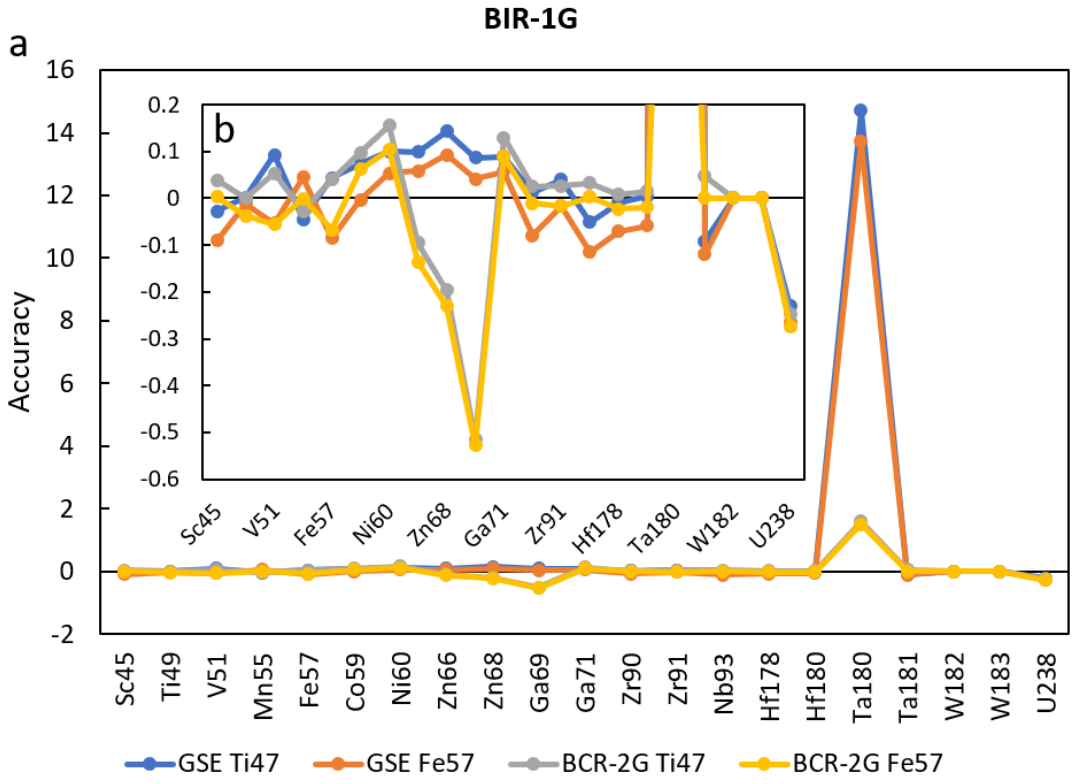

Fig. 35 – Comparison of the accuracy of BIR-1G when processed with combinations of reference materials (GSE and BCR-2G) and internal standards (^{47}Ti and ^{57}Fe)